Fault Detection and Isolation in Centrifugal Pumps

1 author:

Carsten Skovmose Kallesøe
Grundfos Holding and Aalborg University
96 PUBLICATIONS **729** CITATIONS

Fault Detection and Isolation
in
Centrifugal Pumps

Ph.D. Thesis

Carsten Skovmose Kallesøe
Grundfos Management A/S

Aalborg University
Institute of Elec. Systems
Dept. of Control Eng.

ATV
The Danish Academy of Technical Sciences

GRUNDFOS
BE > THINK > INNOVATE

ISBN 87-90664-22-1
March 2005

Printing: Budolfi tryk ApS

To my wife Susanne
and
my three sons Emil, Mikkel and Andreas.

Preface and Acknowledgements

This thesis is submitted as partly fulfillment of the requirements for the Doctor of Philosophy at the Department of Control Engineering at the Institute of Electronic Systems, Aalborg University, Denmark. The work has been carried out in the period January 2002 to January 2005 under the supervision of Associate Professor Henrik Rasmussen, Associate Professor Roozbeh Izadi-Zamanabadi, and Chief Engineer Pierré Vadstrup.

The subject of the thesis is fault detection and identification in centrifugal pumps. The thesis is mainly aimed to investigate the newest accomplishments in fault detection and identification, in order to obtain robust and realiable detection schemes for the centrifugal pump. Even though the main focus is on the application, a number of theoretical contributions are also obtained. These are mainly in the area of robustness analysis in event based detection schemes, and the realization of subsystems identified using Structural Analysis.

I would like to thank my supervisors Associate Professor Henrik Rasmussen, Associate Professor Roozbeh Izadi-Zamanabadi, and Chief Engineer Pierré Vadstrup for their good and constructive criticism during the whole project. A special thank should be given to Roozbeh Izadi-Zamanabadi for many valuable and inspiring discussions during the project. Furthermore, I would like to thank Karen Drescher for her help in transforming the thesis into readable english. Also, I would like to thank my wife Susanne for her patience and support during the whole project period, and for her help with my english writing.

A sincere thanks goes to Dr. Vincent Cocquempot at the USTL-LAIL in Lille, France, for letting me visit the university, and our inspiring discussions during my stay there. I am also grateful to the staff at the Department of Control Engineering, and my colleagues at Grundfos for providing a pleasant and inspiring working environment, and their helpfulness throughout the whole project.

Finally, I want to acknowledge the financial support from The Danish Academy of Technical Sciences (ATV) and Grundfos Management A/S.

Aalborg University, January 2005
Carsten Skovmose Kallesøe

Summary

The main subject of this thesis is Fault Detection and Identification (FDI) in centrifugal pumps. Here, it is assumed that an induction motor is driving the centrifugal pump, and that only electrical and hydraulic quantities are measured. A state of the art analysis of the topic has shown that signal-based approaches are the most used approaches for FDI in centrifugal pumps. Robustness is seldom considered in these approaches. However, robustness is a very important aspect when it comes to implementation in real life applications. Therefore, special focus is put on robustness in this thesis.

The signal-based approaches are utilizing signal processing and/or artificial intelligence to obtain knowledge about the faults in the pump. To analyse robustness in these systems, a combination of the Failure Mode and Effect Analysis (FMEA) and the Fault Propagation Analysis (FPA) is proposed. To enable robustness analysis using the FMEA and FPA a so-called disturbing event is introduced. Moreover, one of the manual steps in the FPA is automated, using an algorithm developed in this thesis. The proposed analysis method is used to identify a set of signal events, which can be used for robust FDI in the centrifugal pump. This shows the usability of the proposed method, not only for analysis purpose, but also as a part of the design of signal-based fault detection schemes.

The most common fault in submersible pump applications is stator burnout. In the state of the art analysis it is argued that this kind of fault is often initiated by an inter-turn short circuit inside the stator. To understand the impact of this short circuit, a model of an induction motor, including an inter-turn short circuit, is derived. This model is utilized in the design of an adaptive observer, which can estimate the states of the motor, the speed, and the inter-turn short circuit simultaneously. The observer is incorporated in a detection scheme, by which the size of the inter-turn short circuit and the phase, affected by the short circuit, can be found. The detection scheme is tested on an industrial test-bench showing the capabilities of the detection scheme on a real application.

Structural Analysis (SA) is utilized in the design of residual generators for FDI in the mechanical and hydraulic part of the centrifugal pump. The use of the SA is two folded. Firstly, it is used to divide the centrifugal pump model into two cascade-connected sub-parts, enabling the design of residual generators. Secondly, it is used to identify subsystems, which can be used in the derivation of residual generators.

Traditionally, the results of the SA are used in the derivation of Analytical Redundant

Relations (ARR). However, here a novel realization approach is proposed. With this approach the subsystems, found using SA, are transformed into nonlinear state space descriptions suitable for observer designs. All unknown variables, except for the states, are eliminated in this state space description, leaving only the stability problem to be considered in the observer design.

The proposed realization approach is used in the derivation of three residual generators for FDI in the mechanical and hydraulic parts of the pump. The obtained residual observers are tested on an industrial test-bench, showing that the observers are robust, with respect to changes in the operating conditions of the pump. Likewise, the tests shows that the observers are able to detect and identify 5 different faults in the mechanical and hydraulic part of the pump.

In many real life centrifugal pump applications, only slow bandwidth sensors are available. This means that FDI schemes, based on dynamic models of the system, are not usable. Therefore, a detection scheme, based on the steady state model of the centrifugal pump, is proposed. This detection scheme is derived using SA to obtain ARR's. Robustness, with respect to parameter variation, is incorporated in the detection scheme, with the utilization of the set-valued approach. This algorithm is also tested on an industrial test-bench, and is also shown to be able to detect 5 different faults in the mechanical and hydraulic part of the centrifugal pump. Moreover, the algorithm is shown to be robust to the operating conditions of the pump, but not to transient changes in these operating conditions.

Sammenfatning

Hovedemnet for denne afhandling er Fejl Detektering og Identifikation (FDI) i centrifugalpumper. Her antages det, at centrifugalpumperne er drevet af induktionsmotorer og at kun elektriske og hydrauliske værdier måles. En state of the art analyse af området har vist, at signalbaserede metoder er de mest brugte til fejl detektering i centrifugalpumper. Der tages sjældent hensyn til robusthed i designet af disse metoder. Imidlertid er robusthed et meget vigtigt aspekt, når FDI algoritmer skal implementeres i de færdige produkter. Derfor vil der blive lagt specielt vægt på robusthed i denne afhandling.

I designet af de signalbaserede metoder, benyttes signalbehandling og/eller kunstig intelligens til at uddrage fejlinformation fra pumpen. Til analyse af robusthed i disse metoder, foreslås en kombination af en "Failure Mode and Effect Analysis" (FMEA) og en "Fault Propagation Analysis" (FPA). For at gøre det muligt at bruge FMEA'en og FPA'en til analyse af robusthed, er et såkaldt forstyrrelses event foreslået. Derudover er en af de manuelle opgaver i FPA'en automatiseret via en algoritme opbygget i projektet. Den foreslåede metode er benyttet til identifikation af en række signal events, som kan benyttes til robust FDI i centrifugalpumper. Dette viser brugbarheden af den foreslåede metode i såvel analyse som design af signalbaserede FDI algoritmer.

En af de mest almindelige fejl i dykpumpeapplikationer er stator sammenbrud. I state of the art analysen argumenteres der for, at en stor del af disse fejl starter som kortslutninger mellem enkelte vindinger i statoren. For at forstå betydningen af sådanne kortslutninger, er der opbygget en model af en induktionsmotor med denne type kortslutning i statoren. Denne model er efterfølgende benyttet i designet af en adaptiv observer, som på samme tid kan estimere de elektriske tilstande, hastigheden og kortslutningen i motoren. Denne observer er indbygget i en FDI algoritme, som både kan estimere kortslutningen og identificere fasen, som er påvirket af denne. Brugbarheden af FDI algoritmen er påvist på en testopstilling, opbygget til dette formål.

I designet af residualgeneratorer til detektering af fejl i den mekaniske og hydrauliske del af pumpen, er Struktur Analyse (SA) benyttet. Brugen af SA har to formål. Det første formål er at opdele modellen af centrifugal pumpen i to cascade-koblede systemer. Denne opdeling er foretaget for at muliggøre design af residualgeneratorer. Det andet formål er identifikation af delsystemer, som kan bruges i designet af residualgeneratorer.

Traditionelt bruges resultaterne af SA'en til at udlede Analytiske Redundante Relationer (ARR). Imidlertid benyttes her i stedet en ny realisationsmetode udviklet i projektet. Med denne metode kan de delsystemer, der er fundet via SA, omskrives til tilstandsmodeller, som er velegnede til observer design. De eneste ukendte signaler i disse tilstandsmodeller er tilstandene i modellen. Det betyder, at kun stabilitetsproblemet skal behandles i observer designet.

Den udviklede realisationsmetode er i afhandlingen brugt til design af tre residual observere til FDI i den mekaniske og hydrauliske del af pumpen. De udviklede residual observere er testet på en industriel testopstilling, hvormed det er vist, at observerne er robuste overfor ændringer i pumpens driftspunkt. Derudover er det vist, at observerne kan bruges til identifikation af 5 forskellige fejl i den mekaniske og hydrauliske del af pumpen.

I mange industrielle applikationer forefindes der kun sensorer med en lav båndbredde. Det betyder, at FDI algoritmer, opbygget på baggrund af dynamiske modeller, ikke kan bruges. Derfor er der i denne afhandling udviklet en algoritme baseret på en ligevægts model af pumpen. Til udvikling af denne algoritme er SA brugt til at finde tre ARR'er. Robusthed er inkorporeret i algoritmen ved brug af en "set-valued" metode. Herved er algoritmen gjort robust overfor parametervariationer i pumpen. Denne algoritme er også testet på en industriel testopstilling, hvor det er vist, at algoritmen kan detektere 5 forskellige fejl i den mekaniske og hydrauliske del af pumpen. Ydermere, er det vist, at algoritmen er robust overfor driftspunktet for pumpen, men ikke overfor transiente ændringer i driftspunktet.

Contents

Nomenclature

Symbols

In this thesis all matrices and vectors are written with bold letters, to distinguish these from scalar values.

Symbols and parameters used in connection with the motor model

$\mathbf{v}_{tdq}$	dq-transformed voltages at the terminals of the induction motor, $\mathbf{v}_{tdq} = (v_{td} \;\; v_{tq})^T$.
$\mathbf{i}_{tdq}$	dq-transformed currents at the terminals of the induction motor, $\mathbf{i}_{tdq} = (i_{td} \;\; i_{tq})^T$.
$\mathbf{v}_{sdq}$	dq-transformed stator voltages of the induction motor, $\mathbf{v}_{sdq} = (v_{sd} \;\; v_{sq})$.
$\mathbf{i}_{sdq}$	dq-transformed stator currents of the induction motor, $\mathbf{i}_{sdq} = (i_{sd} \;\; i_{sq})$.
$\mathbf{i}'_{sdq}$	Derived dq-transformed stator current, $\mathbf{i}'_{sdq} = \mathbf{i}_{sdq} - \mathbf{T}_{dq}\boldsymbol{\gamma} i_f$.
$\mathbf{i}_{rdq}$	dq-transformed rotor currents of the induction motor, $\mathbf{i}_{rdq} = (i_{rd} \;\; i_{rq})$.
$\boldsymbol{\gamma}$	Among of turns involved in the stator short circuit, $\boldsymbol{\gamma} = (\gamma_a \;\; \gamma_b \;\; 0)^T$.
i_f	Current in the short circuit loop of the stator.
T_e	Torque generated by the electrical circuit of the motor.
$\mathbf{T}_{dq0}(\theta)$	Transformation matrix given by $\mathbf{x}_{dq0} = \mathbf{T}_{dq0}(\theta)\mathbf{x}_{abc}$, where $\mathbf{T}_{dq0}(\theta) = \frac{2}{3}\begin{bmatrix} \cos(\theta) & \cos(\theta + \frac{2}{3\pi}) & \cos(\theta + \frac{4}{3\pi}) \\ \sin(\theta) & \sin(\theta + \frac{2}{3\pi}) & \sin(\theta + \frac{4}{3\pi}) \\ \frac{1}{2} & \frac{1}{2} & \frac{1}{2} \end{bmatrix}$.
$\mathbf{T}_{dq0}$	Transformation matrix given by $\mathbf{T}_{dq0} = \mathbf{T}_{dq0}(0)$.
$\mathbf{T}_{dq}$	Matrix consisting of the two first rows of $\mathbf{T}_{dq0}$.
$\mathbf{T}_{dq}^{-1}$	Matrix consisting of the two first columns of $\mathbf{T}_{dq0}^{-1}$.
$\mathbf{J}$	2×2 skew symmetrical matrix given by $\mathbf{J} = \begin{bmatrix} 0 & -1 \\ 1 & 0 \end{bmatrix}$.

$\mathbf{I}$	Identity matrix.
r_s	Stator resistance.
r_r	Rotor resistance.
l_{sl}	Leakage inductance in the stator.
l_{rl}	Leakage inductance in the rotor.
l_m	Mutual inductance in the induction motor.
z_p	Number of pole pairs in the motor.
$\mathbf{R}_s$	Stator resistance matrix, $\mathbf{R}_s = \text{diag}\{r_s, r_s\}$.
$\mathbf{R}_r$	Rotor resistance matrix, $\mathbf{R}_r = \text{diag}\{r_r, r_r\}$.
$\mathbf{L}_s$	Strator inductance matrix, $\mathbf{L}_s = \text{diag}\{\frac{3}{2}l_m + l_{ls}, \frac{3}{2}l_m + l_{ls}\}$.
$\mathbf{L}_r$	Rotor inductance matrix, $\mathbf{L}_r = \text{diag}\{\frac{3}{2}l_m + l_{lr}, \frac{3}{2}l_m + l_{lr}\}$.
$\mathbf{L}_m$	Mutual inductance matrix, $\mathbf{L}_m = \text{diag}\{\frac{3}{2}l_m, \frac{3}{2}l_m\}$.
$\mathbf{R}'_r$	derived rotor resistance matrix, $\mathbf{R}'_r = \mathbf{L}_m\mathbf{L}_r^{-1}\mathbf{R}_r\mathbf{L}_r^{-1}\mathbf{L}_m$.
$\mathbf{L}'_s$	derived stator inductance matrix, $\mathbf{L}'_s = \mathbf{L}_s - \mathbf{L}_m\mathbf{L}_r^{-1}\mathbf{L}_m$.
$\mathbf{L}'_m$	derived mutual inductance matrix, $\mathbf{L}'_s = \mathbf{L}_m\mathbf{L}_r^{-1}\mathbf{L}_m$.
$\mathbf{B}_v$	Transformation from voltages at the terminals of the motor to phase voltages at the stator, $\mathbf{v}_{sdq} = \mathbf{B}_v\mathbf{v}_{tdq}$.
$\mathbf{C}_i$	Transformation from the phase current in the stator to the current at the terminals of the motor, $\mathbf{i}_{tdq} = \mathbf{C}_i\mathbf{i}_{sdq}$.

Symbols and parameters used in connection with the pump model

H_p	Pressure across the pump.
H_e	Head calculated from Eulers pump equation.
Q_p	Flow through the pump.
Q_i	Flow through the impeller.
T_p	Shaft torque of the pump.
ω_r	Shaft speed of the pump.
J	Moment of inertia of the rotor and the impeller.
B	Linear friction.
a_{hi}	Parameters in the pressure model of the pump, $i \in \{1, 2, 3\}$.
a_{ti}	Parameters in the torque model of the pump, $i \in \{1, 2, 3\}$.
g	Gravity constant.
ρ	Density of the liquid in the system.
K_l	Leakage fault inside the centrifugal pump.
K_f	Clogging faul inside the centrifugal pump.
ΔB	Rub impact fault.
f_c	Cavitation fault.
f_d	Dry running fault.

Symbols used in connection with the FMEA and FPA

$\mathcal{F}$	Finite set of all event vectors in the system.
$\mathcal{F}_i$	Finite set of all event vectors in the i^{th} component in the system.
$\mathcal{F}_f$	Finite set of all fault event vectors.
$\mathcal{F}_d$	Finite set of all disturbing event vectors.
$\mathcal{I}_f$	Finite set of all fault event vectors with only one non zero element.
$\mathbf{f}$	Vector of fault events.
$\mathbf{d}$	Vector of disturbing events.
$\mathbf{A}^j_{f_i}$	Propagation matrix from the faults defined in the i^{th} component to the effects defined in the j^{th} component.
$\mathbf{A}^j_i$	Propagation matrix from the effects defined in the i^{th} component to the effects defined in the j^{th} component.
$\mathbf{A}_f$	Propagation matrix from the faults to the end-effects in the system.
$\mathbf{A}_d$	Propagation matrix from the disturbing events to the end-effects in the system.
G_f, D_f	Graph G_f and corresponding adjacency matrix D_f describing the connection between faults and components in the FPA diagram.
G_e, D_e	Graph G_e and corresponding adjacency matrix D_e describing the structure of the effect propagation in the FPA diagram.

Symbols used in connection with the SA and realization

$\mathcal{S}$	Dynamic system.
$\mathcal{O}$	Observer design based on the dynamic system $\mathcal{S}$.
$\mathcal{C}$	Set of constraints.
$\mathcal{Z}$	Set of variables.
$\mathcal{S}$	System composed of a set of constraints and a set of variables, i.e. $\mathcal{S} = (\mathcal{C}, \mathcal{Z})$.
$\mathcal{K}$	Set of known variables, i.e. $\mathcal{K} \subset \mathcal{Z}$.
$\mathcal{X}$	Set of unknown variables, i.e. $\mathcal{X} \subset \mathcal{Z}$.
$\mathbf{x}_d$	State vector of the dynamic system $\mathcal{S}$.
$\mathbf{x}_a$	Algebraic variables of the dynamic system $\mathcal{S}$.
c	Constraint which links a subset of the variables in $\mathcal{Z}$.
d	Constraint on the form $\dot{x}_d = \frac{dx_d}{dt}$, where $\dot{x}_d, x_d \in \mathcal{X}$.
$\mathbf{f}_x, \mathbf{m}_x, \mathbf{h}_x$	Vector field, algebraic constraints, and output maps of the dynamic system $\mathcal{S}$.
$\mathbf{f}_o, \mathbf{h}_o$	Vector field and output maps of an output transformed system.
$\mathbf{f}_z, \mathbf{h}_z$	Vector field and output maps of a state transformed system.

Symbols used in connection with the steady state FDI

V_{rms}	RMS value of the supply voltage.
I_{rms}	RMS value of the supply current.
ω_e	Frequency of the supply voltage.
ϕ	Angle between the supply voltage and supply current.
V_{sd}^e	Stator voltage used in the steady state model of the motor.
V_{sq}^e	Stator voltage used in the steady state model of the motor.
I_{sq}^e	Stator current used in the steady state model of the motor.
I_{md}^e	Magnetizing current used in the steady state model of the motor.
I_{mq}^e	Magnetizing current used in the steady state model of the motor.
r	Residual.
$\mathcal{R}$	Set of residual values.

Mathematical Symbols

$\succ, \prec$	Positive and negative definit respectively.
$>, <$	Larger than and smaller than respectively.
$\rightarrow$	Logical expression to the left implies logical expression to the right.
$\vee$	Logical or operator.
$\wedge$	Logical and operator.
$\overline{x}$	Maximum value of x.
$\underline{x}$	Minimum value of x.
R	The reals.
R_+	The positive reals including zero, i.e. $R_+ = \{x \in R \mid x \geq 0\}$.

Abbreviations

FDI	Fault Detection and Identification.
SA	Structural Analysis.
ARR	Analytical Redundant Relation.
FMEA	Failure Mode and Effect Analysis.
FPA	Fault Propagation Analysis.
Model-based FDI	FDI approaches based on mathematical models of the application.
Signal-based FDI	FDI approaches based on signal processing and classifing techniques.

Chapter 1

Introduction

This thesis considers the analysis and design of algorithms for Fault Detection and Identification (FDI) in centrifugal pumps. The aim has been to investigate methods for FDI in centrifugal pumps, with special focus on the robustness and usability of the obtained algorithms. This means that the algorithms must be able to detect faults under changing operating conditions, and should be robust with respect to disturbances in the system.

1.1 Background and Motivation

This project was founded by Grundfos, which is a multi-national company with production and sale facilities in around 50 different countries all over the world. Grundfos is producing pumps for a variety of different applications. Still, most of the produced pumps are for use in water treatment and aqueous solutions. In these applications the centrifugal pump is the most used pump type. This is due to its simple construction with few moving parts, making it very reliable and robust. In this thesis especially centrifugal pumps for use in industrial applications, submersible applications, water supply applications, and sewage applications are of interest.

In many of these applications it is crucial that the pumps are working all the time. Moreover, the size of the pumps makes maintenance costly, in many cases. In addition to that, the applications are often situated in remote places, when it comes to water supply and sewage treatment. This means that maintenance becomes even more costly. Therefore, in these applications supervision, including fault detection and in specially fault prediction, is very interesting. Equally interesting is supervision in industrial applications. Here, the need is initiated by the ongoing demand for production improvement, meaning that it is crucial that the pumps are only stopped when absolutely necessary. Therefore, the use of a monitoring system, which includes supervision of the pumps, would be beneficial in many of these applications. This implies, that monitoring systems can be expected to be a growing competition parameter in the following years.

This project was initiated by a growing need, inside Grundfos, for knowledge about the newest methods for detection of events and faults in pumps and pump systems. This need is based on the expectation that monitoring and control systems will be commonly used for supervision and control, of especially larger pumps, in the future. Besides that, pumps are sometimes returned on warranty where it has been impossible to reproduce the fault. In these cases it would be of great interest to know what the pump has been exposed to before it is returned. This knowledge could be used to improve the construction of the pumps and user manuals to avoid unnecessary returns on warranty, and thereby unnecessary inconveniencies for the costumer.

The most common maintenance problems and faults expected in centrifugal pumps can be divided into three main categories,

- Maintenance, such as cleaning of the pump.
- Faults which demands maintenance, such as bearing faults, and leakage due to sealing faults.
- Severe faults, which demand replacement, such as stator burnouts, and damaged impeller.

The first item covers normal maintenance, which, to some extend, is necessary in any application. Likewise, the second item covers replacement of wearing parts, which also should be expected in any pump setup, when running for long time periods. The last item covers severe damages, normally caused by unexpected faults or by lack of maintenance.

A well designed monitoring system will be able to help a user, exposed to faults, in any of the three mentioned categories. Traditionally, the first two categories are, in large pump applications, handled by doing scheduled maintenance on the plant. At these scheduled maintenance procedures, a set of predetermined wearing parts are often exchanged to avoid future breakdowns. When using a monitoring system, maintenance can be done on demand, which will save costs for unnecessary replacement parts, and more important, the pump only has to be stopped for maintenance when really necessary. For the last category, a monitoring system would be able to detect and stop the pump before a given fault causes total breakdown of the pump. In larger pumps this would make repair possible, meaning that a replacement of the whole pump is saved.

Different sets of sensors could be used as inputs to such a monitoring system. For centrifugal pumps the following sensors are interesting; vibration sensors, current and voltage sensors, absolute pressure and pressure difference sensors, flow sensors, and temperature sensors. Of these, the current and voltage sensors, and the flow and pressure difference sensors have been considered in this project. These sensors are all reasonably cheep and are often already mounted in a pump system. Therefore, by using only these sensors, no additional hardware is needed for the proposed algorithms to work. Therefore, the implementation costs for the system is reduced considerably.

1.2 Objectives

The aim of the Thesis is to investigate different methods for their usability in analyzing and designing FDI algorithms for centrifugal pumps. In the investigation, special emphasis is layed on the robustness and practical usability of the obtained algorithms.

In (Åström et al., 2001) it is argued that methods for FDI can be divided into two main groups, namely the model-based and signal-based approaches. Here, the signal-based approaches are approaches, in which signal processing and/or artificial intelligence are utilized to obtain knowledge about faults in a given system. The model-based approaches are, on the other hand, utilizing system theory to obtain knowledge about the faults. In this thesis special focus will be put on the use of the model-based approaches, as these approaches have inherent methods for handling disturbances. Hereby, increased robustness of the algorithms can be obtained. However, signal-based approaches have been widely used for fault detection in centrifugal pumps and their applications. See Chapter 2 concerning the state of the art of the area. In most of these cases robustness has not been considered. Therefore, a method for analyzing robustness in signal-based FDI systems, is also considered.

1.3 Contributions

The contributions of the Thesis can be divided into two groups. The first group contains contributions to FDI in the centrifugal pumps. The second group contains theoretical contributions, mainly on robustness analysis of signal-based fault detection schemes and the realization of subsystems found using Structural Analysis. In this section, first the theoretical contributions are listed, followed by the contribution to FDI in centrifugal pumps.

The main contributions in the theoretical areas are:

- A new algorithm for cutting loops in a Fault Propagation Analysis (FPA) graph is proposed in Chapter 4. With this algorithm and a theorem also proposed in this thesis, the FPA is automated. This means that the only manual step is to setup the event model.

- A disturbing event is introduced as a part of the FPA in Chapter 4. With this event it is possible to analyse the robustness of signal-based fault detection algorithms. Two theorems are formulated, aimed to analyse robustness, based on this idea.

- A new adaptive observer, for a particular kind of bilinear system, is proposed in Chapter 5. With this observer it is possible to explore the parameter structure in the system. Observability of the known part of the system is not necessary. The gain matrix of the observer can be analysed, and in some cases calculated, using the proposed Linear Matrix Inequalities (LMI).

- A novel transformation method is proposed in Chapter 6. With this transformation, minimal over-constraint subsystems, identified using Structural Analysis (SA), can be transformed into state space descriptions. The method includes two transformations; an output transformation, and a state transformation. These are formulated in two theorems. The state transformation is submitted for publication (Kallesøe and Izadi-Zamanabadi, 2005).

- As a part of the derivation of a set-valued residual expression, the Taylor Series expantion is proposed in Chapter 7. The Taylor Series expantion is used on the parameter expression to include a linear approximation of the nonlinear dependency of the parameters. This has been submitted for publication (Kallesøe et al., 2004a).

The main contributions to FDI in the centrifugal pumps are:

- A fault propagation model of the faults, expected to happen in centrifugal pumps, is derived in Chapter 4. This model has been used to analyse different sensor combinations aimed for robust signal-based fault detection.

- A new model of an inter-turn short circuit in the stator of an induction motor is derived in Chapter 5. The model is derived for both $\mathbf{Y}$- and Δ-connected motors, and has a nice structure, which has similarities to models of motors not affected by inter-turn short circuits. The model of the $\mathbf{Y}$-connected motor has been published in (Kallesøe et al., 2004c).

- An adaptive observer for estimating inter-turn short circuit faults in the stator of an induction motor is proposed in Chapter 5. This has been published in (Kallesøe et al., 2004c).

- An example of using SA to divide a complex system into two cascade-connected, less complex, subsystems is shown in Chapter 6. This enables possibilities for easy observer designs. The idea has been used for solving the nonlinear FDI problem in the centrifugal pump, using only electrical and hydraulic measurements. This has been submitted for publication (Kallesøe et al., 2004a).

- A model-based FDI scheme, for FDI in centrifugal pumps, is proposed in Chapter 6. The FDI scheme is based on measurements of the electrical quantities and the hydraulic quantities only. Here, the electrical quantities are the motor voltages and currents, and the hydraulic quantities are the pressure and volume flow. Parts of the approach have been published in (Kallesøe et al., 2004b).

- A robust FDI scheme, based on the steady state model of the pump and set-valued algebra, is derived in Chapter 7. The obtained algorithm depends on steady state measurements only, making it useful in cost sensitive products.

1.4 Outline of the Thesis

The thesis is organized as follows,

Chapter 1: Introduction

Chapter 2: Fault Detection and Isolation in Pump Systems

The purpose of this chapter is two-folded. Firstly, the most important ideas and terms used in the area of Fault Detection and Identification (FDI) are introduced. Secondly, state of the art on FDI in centrifugal pumps, as well as in induction motors, is considered. This includes contributions from the academic world and products already on the market.

Chapter 3: Model of the Centrifugal Pump

This chapter introduces the mathematical model of the centrifugal pump. This includes a model of the induction motor driving the pump, and models of the mechanical and hydraulic parts of the pump. The presented models are lumped parameter models, which especially are suitable for use in model-based FDI design. Special emphasize is put on the dynamics of the hydraulic part. Here, it is shown that the energy conversion from mechanical to hydraulic energy, is described by a purely algebraic equation. Moreover, it is shown that the pump dynamics can be described by adding extra mass to the rotating parts of the pump, i.e. increasing the moment of inertia of the rotating parts of pump. The derived model is valid under two assumptions, also stated in the chapter.

Chapter 4: System Analysis and Fault Modelling

In this chapter the use of Failure Mode and Effect Analysis (FMEA) and Fault Propagation Analysis (FPA) in the design of signal-based fault detection algorithms is explored. The FMEA and the FPA are well known analysis tools, and have been proposed as an analysis tool in the design Fault Tolerant Control, as well as in FDI algorithms. A new algorithm for automating parts of the FPA is proposed in this chapter. Moreover, by introducing a so-called disturbing event in the FPA, it is shown that the robustness of signal-based FDI algorithms can be analysed.

The chapter includes an FMEA of a general centrifugal pump, meaning that the conceptual faults, expected in centrifugal pumps, are identified and analyzed. The outcome of the FMEA is a list of possible faults in centrifugal pumps. 11 of these faults are grouped into 7 fault groups. These 7 faults found the basis for the FDI algorithms designed in this thesis. Using the FPA, different sensor combinations are analysed, aimed to find a set of signals, which can be used in a signal-based fault detection scheme. One of these sensor configurations is proven to work on a special designed test setup.

Chapter 5: A New Approach for Stator Fault Detection in Induction Motors

This chapter introduces a new approach for inter-turn short circuit detection in the stator of an induction motor. In the design, an adaptive observer approach is used, utilizing only electrical measurements. The observer is based on a model of the induction motor, in which a description of the inter-turn short circuit is included. This model is derived in the beginning of the chapter. With the designed observer it is possible to estimate the states of the motor, the speed, and the inter-turn short circuit simultaneously. The observer is shown to work on a special designed motor, where it is possible to simulate inter-turn short circuit faults. Likewise, it is shown that it is possible to identify the phase, affected by the inter-turn short circuit. The adaptive observer, used in the proposed design, is formulated in general terms, and could therefore be used in a number of other applications.

Chapter 6: A New Approach for FDI in Centrifugal Pumps

The topic of this chapter is FDI on the hydraulic and mechanical parts of the centrifugal pump. The model-based approach is used for this purpose. This means that residual generators are developed, based on the model of the centrifugal pump, presented in Chapter 3. In the design of the residual generators, subsystems, which are robust with respect to disturbances and unknown model parts, are identified using Structural Analysis (SA) (Blanke et al., 2003). These subsystems are then transformed into state space form, enabling residual observer designs. The transformation from subsystems, identified using SA, into state space descriptions is novel, and is described in general terms in the beginning of the chapter.

Chapter 7: FDI on the Centrifugal Pump: A Steady State Solution

In this chapter a FDI algorithm, based on a steady state model of the pump, is developed. The FDI algorithm is developed using Structural Analysis, in order to obtain three Analytical Redundant Relations, each used in the calculation of a residual. The algorithm is shown to enable detection and identification of five different faults in the hydraulic part of the pump. Robustness of the algorithm is insured using a set-valued approach, making it possible to in-count parameter variations in the FDI algorithm.

Chapter 8: Conclusion and Recommendations

Chapter 2

Fault Detection and Isolation in Pump Systems

The purpose of this chapter is two-folded. Firstly, a short introduction to the most important ideas and terms used in the area of Fault Detection and Identification (FDI) is included. Secondly, a state of the art analysis on FDI in centrifugal pump applications is presented. The first part is included to lighten readers of the thesis not familiar with the concept of FDI. The second part includes both a state of the art analysis of FDI in the centrifugal pump itself, and on the induction motor drive by which centrifugal pump is driven. Moreover, the analysis includes contributions from both the academic world and products already on the market.

In Section 2.1, where the concept of FDI is introduced, three different approaches to FDI are considered. First of all, distinguishing between model-based and signal-based FDI is considered (Åström et al., 2001), and the main ideas behind both methods are described. This is followed by an introduction of the parameter adaptation approach, and finally the concept of residual evaluation is introduced.

In Sections 2.2 and 2.3 state of the art of FDI in respectively induction motors and centrifugal pumps is considered. A number of different faults and detection methods have been treated in both the induction motor and in the centrifugal pump. However, considerable more work is done in the area of FDI on induction motors compared to the work done on centrifugal pumps. This is mainly because of the widespread use of the motor type. The state of the art analysis is followed by some concluding remarks, which end the chapter.

2.1 Fault Detection and Isolation

To understand the concept of FDI, first it has to be defined what is meant by faults, and which information is expected to be available for detection of these. To explain this, let the structure of a system with inputs $\mathbf{u}(t) \in R^m$, outputs $\mathbf{y}(t) \in R^d$ be defined as shown in Fig. 2.1. Here, a fault affecting the system is symbolized by f. This

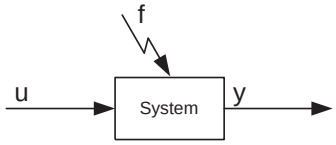

Figure 2.1: System with inputs $\mathbf{u}$, outputs $\mathbf{y}$ and a fault f affecting the system.

fault is interpreted as an unwanted event creating abnormal operation of the system. Faults can affect the operation of a system in different ways. Normally, these fault effects are divided into two sub-groups, which are denoted *multiplicative faults* and *additive faults* respectively. Multiplicative faults influence the system as a product, like for example parameter variations, and additive faults influence the system by an added term (Isermann and Balle, 1997).

As an example of a system affected by faults, consider the following linear system, which is affected by both multiplicative and additive faults.

$$\begin{aligned} \tfrac{d\mathbf{x}}{dt} &= \mathbf{A}(\boldsymbol{\theta}_f)\mathbf{x} + \mathbf{B}(\boldsymbol{\theta}_f)\mathbf{u} + \mathbf{E}_1\mathbf{d} + \mathbf{F}_1\mathbf{f} \\ \mathbf{y} &= \mathbf{C}(\boldsymbol{\theta}_f)\mathbf{x} + \mathbf{D}(\boldsymbol{\theta}_f)\mathbf{u} + \mathbf{E}_2\mathbf{d} + \mathbf{F}_2\mathbf{f} \ . \end{aligned} \tag{2.1}$$

In this system $\mathbf{x}(t) \in R^n$ contains the states, $\mathbf{u}(t) \in R^p$ contains the inputs, $\mathbf{y}(t) \in R^d$ contains the outputs, and $\mathbf{d}(t) \in R^l$ contains disturbances, which can be interpreted as unknown or unmeasurable inputs. This system is affected by the faults $\mathbf{f}(t) \in R^h$ affecting the system by an added term, and the parameters $\boldsymbol{\theta}_f \in R^k$ affecting the system in multiplicative manner. Here the multiplicative faults are seen as changes of the parameter values in the system. Besides the multiplicative and additive fault effects, a fault can change the structure of a system, meaning that the system becomes a so-called hybrid system, where the state change is caused by the given fault.

Having the above described system in mind the fault detection problem is the task of detecting that a fault $f \in \mathcal{F}$ has occurred in a given system, where $\mathcal{F}$ is the set of all possible faults in the system, i.e. it contains all faults in $\mathbf{f}$ and $\boldsymbol{\theta}_f$. The solution to the fault detection problem is based on the set of measurements $\mathbf{y}$ and possibly the set of known input signals $\mathbf{u}$. When a fault is detected it is possible to state that something is wrong in the system but not what is wrong. However, sometimes it is possible to isolate the fault, meaning that fault f_i can be distinguished for the set of possible faults $\mathcal{F}$ in the system. When a fault is isolated it is possible to state where and what is wrong in

the system (Chen and Patton, 1999; Gertler, 1998). The problem of both detection and isolation of a fault is called the Fault Detection and Isolation (FDI) problem. If it is not only possible to isolate the fault f_i in the set $\mathcal{F}$, but also possible to estimate the size of this fault f_i, the fault is said to be estimated. The three levels of complexity in the fault detection problem, described above, are summarized below.

Fault Detection: An abnormality in a system is detected, but the type and size are unknown.

Fault Isolation: The fault f_i is identified in the set of all possible faults $\mathcal{F}$. Hereby the type of the fault is known but the size remains unknown.

Fault Estimation: The size of the fault $f_i \in \mathcal{F}$ is estimated.

Different methods can be used for detecting a fault $f \in \mathcal{F}$. The choice of method should be based on the type of fault, which has to be detected, and which measurements are available. Below three main groups of approaches are described.

2.1.1 Signal-Based Approach

In the Signal-Based approach, characteristics in the measured signals $\mathbf{y}$ containing information about the health of the system are utilized (Åström et al., 2001). A block diagram of a FDI system based on the signal-based approach is shown in Fig. 2.2. From

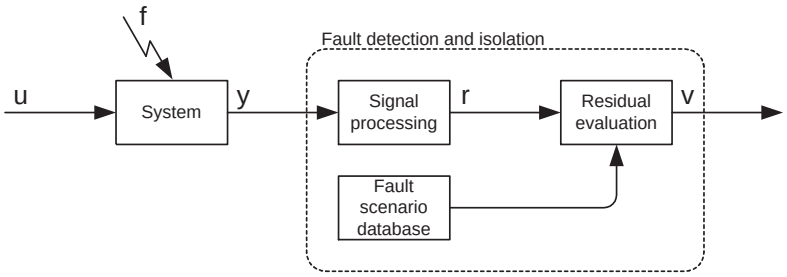

Figure 2.2: Structure of a signal based fault detection and isolation system (Åström et al., 2001).

this figure it is seen that the fault detection algorithm consists of three blocks. In the first block, *signal processing*, methods from signal processing theory are utilized to extract information about the health of the system from the measured signals. The output from the signal-processing block is sent to a unit consisting of a database and some sorts of artificial intelligence. In Fig. 2.2 this is the *residual evaluation* block and the *fault scenario database* block. This part of the algorithm compares the output from the

signal-processing block with predefined data sets from the database, each describing the characteristics of a given fault. From this comparison the FDI algorithm decides if the system is affected by a fault and if so, which one it is.

The signal-processing block often consists of frequency spectrum analysis such as FFT-algorithms, wavelets, or higher order statistic (HOS) tools. However, it could also be a simple limit check on the measured signal. In the decision unit, i.e. the fault scenario database and the residual evaluation block, all kinds of methods for data evaluation are used. Of these clustering techniques, neural networks, and fuzzy logic should be mentioned. All of these are sophisticated methods for data mining. However, in most real applications simple forms of decision logic are used.

Now considering the advantages and disadvantages of the signal-based method as the author see it. First of all, a mathematical model is not used in this approach, which is a huge advantage, as such a model can be difficult and even in some cases impossible to derive. However, the drawback is the need for data from the system when it is affected by faults, as these data should be used in the development of the fault scenario database. Moreover, it can be difficult to ensure robustness of the FDI algorithm, as in theory all possible operation conditions should be tested, before robustness is ensured. Of course, simulations can solve some of these problems, but then a model is needed, undermining one of the advantages of the approach. Considering these characteristics, this approach must be considered most suitable for systems, which are difficult or in particular cases impossible to describe with a mathematical model.

2.1.2 Model-Based Approach

The model-based approach utilizes analytical redundancy to extract information about faults in the system. When using analytical redundancy one utilizes physical bindings between inputs and outputs and between different outputs of the system to describe normal operation conditions. The physical bindings are here denoted analytical relations. Faults are then detected when the analytical relation is not fulfilled. When this is the case the system is operating under abnormal operation conditions, which are exactly the definition of a fault. The analytical relations, utilized in this approach, are described using mathematical models. The relations described by these models are compared to the physical relations in the real system, revealing abnormal operation if a difference exists.

In Fig. 2.3 a block diagram of a model-based fault detection algorithm is shown. The first block *model based residual filter* uses the mathematical redundancy to generate a so-called residual signal. This residual signal is defined in the following definition.

Definition 2.1.1 *This residual signal is a signal with the following characteristics,*

$$|r(t)| > \kappa \geq 0 \qquad \textit{for} \quad f \neq 0$$
$$\lim_{t\to\infty} r(t) = 0 \qquad \textit{for} \quad f = 0$$

where f is a fault in the system and r is the residual signal.

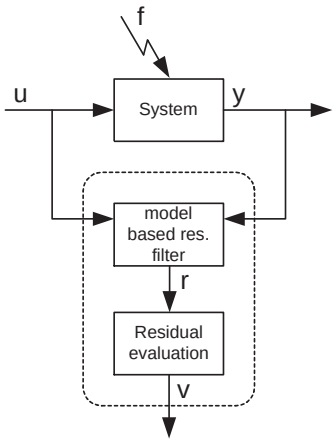

Figure 2.3: Structure of a model based fault detection and isolation system.

The model-based residual filter is also called a residual generator. For linear systems the residual generator is well established, and is well described in the literature. Here, only two books will be mentioned, these are (Gertler, 1998) in which the parity equation approach is treated, and (Chen and Patton, 1999) in which observer based approaches are considered. Else, see for example (Patton and Chen, 1997; Frank and Ding, 1997) and references included. The aim in the design of the residual generator is to be able to create residuals with properties as defined in Definition 2.1.1, where the residuals are not influenced by the disturbance on the system $\mathbf{d}$, see (2.1). When this is possible the residual generator is said to be robust. Different design approaches have been used to obtain robustness. Of these should be mentioned, the unknown input observer approach (Chen and Patton, 1999, Chap. 3), the eigenvalue assignment approach (Chen and Patton, 1999, Chap. 4), the geometric approach (Massoumnia et al., 1989), and the standard formulation approach (Stoustrup and Niemann, 2002).

It was stated before that the residual generator for linear systems is well established. This is not the case for non-linear systems in fact a lot of research is going on in this field. In (Garcia and Frank, 1997) an overview is given. To mention some newer results, for example, the geometric approach is extended to the design of residual filters for non-linear systems in (De Persis and Isidori, 2001), and in (Stoustrup and Niemann, 1998, 2002) the internal model control approach is used to handle the non-linear parts of the system. Moreover, the derivation of analytical redundant relations, based on structure analysis, is described in (Blanke et al., 2003). This approach can be seen as an extension of the parity equation approach to nonlinear systems.

2.1.3 Parameter Estimation Approach

In the parameter estimation approach parameters are estimated, which contains fault information. The estimated parameter values are then compared to the expectation values of these parameters, resulting in a set of residuals, as shown below,

$$\mathbf{r} = \boldsymbol{\theta}_0 - \hat{\boldsymbol{\theta}} \ ,$$

where $\boldsymbol{\theta}_0$ are the expected parameter values and $\hat{\boldsymbol{\theta}}$ are the estimated values. The parameters can either be estimated by an extended Kalman filter (Del Gobbo et al., 2001) or by means of adaptive observers (Xu and Zhang, 2004; Jiang and Staroswiecki, 2002). With both of these approaches the states of the system and the parameters containing fault information are estimated simultaneously. System identification, as it is presented in (Ljung, 1999), can also be used to estimate the parameter values of the system online. This approach is explored in for example (Isermann, 1997).

2.1.4 Residual Evaluation

From the definition of the residual signal given in Definition 2.1.1 the residual r should be smaller than a predefined threshold value κ, when no fault has happened in the system. However, it can be difficult or even impossible to find a κ, which is smaller than $|r|$ if a fault has happened and larger then $|r|$ at all times in the no fault case. This is because the residual r will be corrupted by model errors, un-modelled disturbances, and noise in real life application. To overcome this problem different methods are developed. Two of these are mentioned here.

To overcome the model error problem it is possible to derive an adaptive threshold $\kappa(t)$ on the residual signal. If for example the model is poor under transient phases, the threshold could be increased during this phase. This is called adaptive residual evaluation (Frank and Ding, 1997). To overcome the noise problem statistical test can be used. Especially the CUSUM algorithm is often used for testing changes in the residual signals when it is affected by noise (Basseville and Nikiforov, 1998).

2.2 FDI in the Induction Motors

Fault detection and identification in induction motors have gained a lot of attention in the resent years. Here all kind of faults in induction motors are considered. However, in (Kliman et al., 1996) it is argued that the main causes of faults in induction motors can be divided into the following three groups,

40-50% Bearing faults.

30-40% Stator faults.

5-10% Rotor faults.

Even though most faults fall into one of these three groups, mechanical faults such as miss alignment and rub impact between stator and rotor are also considered. In the following two sections detection of mechanical faults are considered first, followed by an analysis of the used method in detection of electrical faults.

2.2.1 Mechanical Faults in the Motor

As stated before, most mechanical breakdowns of motors are due to bearing faults. This is especially a problem if a voltage inverter supplies the motor. If this is the case, large high frequency voltage components will cause circulating current through the bearings. This current will eventually destroy the bearings. Even though bearing faults are the most common mechanical faults, also other kind of faults such as for example bend shaft or rub impact between stator and rotor can happen. For the whole group of mechanical faults the most used detection schemes fall into two groups,

- Spectrum analysis of motor currents.
- Spectrum analysis of vibration signals.

The current spectrum analysis is explored in (Eren and Devaney, 2001; Schoen et al., 1995; Benbouzid, 2000). In (Eren and Devaney, 2001) Wavelets are used for analysing the stator current at start up, to detect bearing faults, and in (Schoen et al., 1995) the current spectrum, during steady state operation, is used for the same purpose. In (Benbouzid, 2000) an overview is given over different signal analysis methods for current spectrum analysis. Here such different methods as the FFT, wavelets, and Higher Order Spectrum (HOS) analyses are considered. The obtained current spectrums are used in the detection of bearing faults and other mechanical faults.

The spectrum analysis of vibrations is explored in (Li et al., 2000; Chow and Tan, 2000; Stack et al., 2002). In (Li et al., 2000) the signal of vibrations is transformed into a frequency spectrum, creating attributes used as input to a neural network. The neural network is then used to map the attributes into fault types. In (Chow and Tan, 2000; Stack et al., 2002) Higher Order Spectrum (HOS) analysis is used to extract fault information from the signal of vibrations. Also model-based methods have been used in the detection of mechanical faults. This is explored in (Loparo et al., 2000) where a mathematical model of the mechanical part of the motor is developed, and used in a FDI scheme.

In commercial products the analysis of the vibration spectrum is the mostly used approach for detection of mechanical faults. Companies such as *SKF*, and *Brüel & Kjær* offer hand held or stationary vibration analysers, for use by the maintenance staff. Here the spectrum of vibrations is shown, leaving it to the user to interpret the signal, and thereby conclude if there is a fault in the motor or not. To help the maintenance staff supervising the frequency spectrum, it is normally possible to set alarm thresholds on parts of this spectrum.

Even though, analysis of vibration signals is considered the most used method for detection of mechanical faults in electrical motors, advanced motor protection units can detect mechanical faults to some extend too. Such motor protection units are offered by for example *Siemens*, *Rockwell Automation*, and *ABB*. With these motor protection units it is possible to detect faults such as blocked rotor, and high temperature, which could be caused by mechanical faults.

2.2.2 Electrical Faults in the Motor

Both stator and rotor faults are denoted electrical faults. These faults are responsible for around 35-50% of the faults in induction motors. The only referred electrical fault in the rotor is broken rotor bar. However, in the stator three main fault groups are considered. These are; inter-turn short circuits, phase to phase short circuits, and phase to ground faults. Of these the inter-turn short circuit fault has gained most attention. This could be explained by referring to (Bonnett and Soukup, 1992; Kliman et al., 1996), where it is argued that phase to phase or phase to ground faults often start by an inter-turn short circuit in one of the stator phases.

The detection of inter-turn short circuits in a stator is explored in a large number of papers. In (García et al., 2004) the voltage between line neutral and the star point of the motor is used for detection. This is shown theoretical using a model of the motor in (Tallam et al., 2002). An inter-turn short circuit will cause imbalance in the stator. This imbalance is used in the detection schemes proposed in (Trutt et al., 2002; Lee et al., 2003), where the negative sequence impedance is estimated, and used as fault indicator. When there is an imbalance in the motor a negative sequence current will be created. This current is used for fault detection in (Kliman et al., 1996; Arkan et al., 2001; Tallam et al., 2003). In (Arkan et al., 2001) robustness, with respect to imbalanced voltage supply, is added to the approach by using an estimate of the negative impedance in the motor. Oscillations in the Park transformed current, due to the motor imbalance are used for detection in (Cruz and Cardoso, 2001), and in (Kostic-Perovic et al., 2000) the so-called space vector fluctuations of the current are used.

Also frequency spectrum approaches have be proposed for the detection of inter-turn short circuit faults (Joksimovic and Penman, 2000; Perovic et al., 2001). In these FFT as well as Wavelet Package transformations have be used together with some sort of classifier. Higher Order Statistics (HOS) has also be used for extracting knowledge about faults in the stator (Chow and Tan, 2000; Arthur and Penman, 2000). In both the frequency spectrum based methods, and in the HOS based methods steady state conditions are assumed on the motor. This assumption is relaxed in (Nandi and Toliyat, 2002) where the frequency spectrum of the voltage after having the supply switched off is used to extract fault information. In (Backir et al., 2001) a parameter estimation approach is used, also relaxing the steady state assumption.

All the references mentioned until now have been dealing with stator faults, but also the detection of rotor faults is considered in the literature. For example in (Trzynad-

lowski and Ritchie, 2000) and in (Bellini et al., 2001) the FFT of the Park transformed current, is used to extract fault information. However, not only the FFT is used in signal-based detection of rotor faults. For example in (Ye et al., 2003; Ye and Wu, 2001; Cupertino et al., 2004) the discrete Wavelet and the Wavelet Package transforms are used for analysing the motor current.

In industry intelligent motor protection units are commercial available. These Motor protection units can detect ground faults and overcurrent, which again can be initiated by inter-turn short circuits. These kinds of motor protection units are available from for example *Siemens*, *Rockwell Automation*, and *ABB*. Moreover, offline analysis tools are available from for example *Baker Instrument Company*, which is able to detect inter-turn short circuits in stators of electrical machines, directly.

2.3 FDI in Centrifugal Pumps

The most referred fault in the hydraulic part of centrifugal pumps is cavitation. Cavitation is the phenomenon, that cavities are created in the liquid if the pressure, at some points inside the pump, decreases below the vapor pressure of the liquid. When this phenomenon occurs the impeller erodes and in extreme cases it vanishes totally after just a short time of duty.

Even though cavitation is the most referred fault other faults are also treated in the literature. The most important of these are mentioned here,

- Obstruction inside the pump or in the inlet or outlet pipe.
- Leakage from the pump or from the inlet or outlet pipe.
- Leakage flow inside the pump.
- Bloked impeller.
- Defect impeller.
- Bearing faults.

In the two following subsections, detection of caviation is considered first, followed by an overview of the most interesting approaches for detection of the faults listed above.

2.3.1 Detection of Caviation

The cavitation phenomenon has been known for decades, and is treated in most books dealing with centrifugal pumps, see for example (Stepanoff, 1957) and (Sayers, 1990). Even though the phenomenon has been known for a long time it is still a topic of research. Especially detecting cavitation and designing pumps to avoid cavitation has achieved attention. Here, only the problem of detecting the phenomenon is addressed.

As described before cavitation is the phenomenon of cavities created by vaporization of the liquid, due to local pressure drops below the vapor pressure inside the pump. When the cavities, due to the vaporization, implode large pressure shocks are created. These pressure shocks will destroy the pump over time. Cavitation has traditional been defined at the point where the pressure delivered by the pump has dropped 3%. However, the degradation of the pump has started long before this point. Therefore, only methods aimed to detect cavitation before the 3% limit are considered here. Different approaches are proposed for cavitation detection. These are based on different signals, such as; mechanical vibrations, high frequency pressure vibrations, high frequency current oscillations, acoustic noise, and vision.

The mechanical vibration signal is investigated in (Lohrberg et al., 2002; Lohrberg and Stoffel, 2000), and the power spectrum of the signal of mechanical vibrations is compared to the power spectrum of the high frequency pressure signal in (Parrondo et al., 1998). Here it is argued that the pressure signal has the favour of the signal of vibrations. The high frequency pressure signal is also considered in (Friedrichs and Kosyna, 2002), where a connection between cavitation inside the pump and pressure vibrations is established based on experiments presented in the paper. The same is obtained in (Neill et al., 1997) where controlled cavitation tests, in a special designed pipeline, are explored. More sophisticated methods are considered in (Cudina, 2003; Baldassarre et al., 1998). In (Cudina, 2003) audio microphones are placed around the pump, collecting the audio noise created by cavitation, and in (Baldassarre et al., 1998) a vision camera is placed inside the pump filming the bobbles created during cavitations.

In the following subsection references, which treat the fault detection and identification problem in a more general framework, are presented. However, in almost all of these references, the problem of cavitation detection has also been considered.

2.3.2 Performance Monitoring and Fault Detection

In the start of this section a number of possible faults in a centrifugal pump application are listed. These faults can be as important as cavitation to detect in real life applications. Therefore, the detection and identification of these faults have also be considered in the literature. Some of the references concerned with this fault detection and identification problem are presented in this subsection.

The signal of mechanical vibration has been proposed for general fault detection in centrifugal pumps in (Surek, 2000; Bleu Jr. and Xu, 1995; Kollmar et al., 2000b). In (Surek, 2000) it is argued that a change in the level of vibrations of the pump can be used as an indication for need of maintenance. In (Bleu Jr. and Xu, 1995) a so-call spick energy approach is proposed for signal processing, and in (Kollmar et al., 2000b) the FFT spectrum of the vibration signals is used as input to a classifier for fault identification. In this case the classification is based on machine learning techniques.

The current signal has also been used for detection and identification of a number of faults in centrifugal pumps (Perovic et al., 2001; Müller-Petersen et al., 2004;

Kenull et al., 1997). In (Perovic et al., 2001) the current spectrum is used as input to a fuzzy Logic based classifier. This classifier is used for identification of cavitation, clogging, and damaged impeller. In (Müller-Petersen et al., 2004; Kenull et al., 1997) fault detection in submersible pumps is considered, based on different signal processing philosophies.

Also the model-based approach has been used for fault detection in centrifugal pumps (Dalton et al., 1996; Liu and Si, 1994; Wolfram et al., 2001). In (Liu and Si, 1994) a linearised model of the pump is used in the design, and the considered faults are; motor faults and the efficiency of the pump hydraulic. In (Dalton et al., 1996) also a linearised model of the pump is used. In this case a two-pump system is treated. Clogging faults and faults in connection with the valves in the two pump system are considered. In (Wolfram et al., 2001) a nonlinear model of the pump, described by a Neuro-Fuzzy model, is used in the design. Here, faults such as various sensor faults, leakage, clogging, cavitation, bearings faults, and impeller faults are considered.

Different protection units are commercial available. For example the monitoring unit *CU3* for protection of submersible application is offered by *Grundfos*. However, this is not the only commercial available monitoring unit, as both *KSB* and *ITT* offer monitoring units, too. *KSB* has just launched the *PumpExpert* unit, which enables detection of cavitation, bearing faults and worn impeller. Moreover, dry running protection is included. The identification approach is based on a fault tree as described in (Kollmar et al., 2000a). Likewise, *ITT* has launched a set of monitoring units with the brand *PumpSmart*. This monitoring unit is based on power level protection, and does not include adjustment to different operating points of the pump. With the adjusted alarm levels it is only possible to detect faults with major impact on the power level. Beside these advanced monitoring units, *ABB* offers a system for data collection in pump application. With this system data measured at any given application location is made available on a website, and evaluations of trend curves are performed.

Also special sensors for seal protection exist. *Burgmann*, a seal producing company, offers a life protection system for their special designed seals, and *Grundfos* offers the humidity sensor *LiqTec*, for protecting water lubricated seals. The company *Wilo* is also working in this area, as the publication (Greitzke and Schmidthals, 2000) describes a proposed seal protection system.

Beside the products mentioned above, most centrifugal pumps with imbedded electronic control units, do offer some kind of fault detection and protection. Likewise, for larger pump systems customized designed monitoring systems can be available.

2.4 Discussion

In this chapter the FDI problem is introduced. Two different approached are considered, these are the signal-based fault detection approach and the model-based fault detection approach. It is argued that the signal-based approach has its advantages when a model of the system is not available. However, robustness properties are difficult to establish.

For the model-based approach it is argued that the advantages are in its ability to obtain robustness from theoretical consideration, and the drawback is the need for reasonable good models.

This introduction is followed by a state of the art analysis of Fault Detection and Identification (FDI) in centrifugal pump applications. Centrifugal pumps are mostly driven by induction motors, therefore state of the art in the area of FDI in induction motors is also considered. Here, it is stated that the most common faults in induction motors are bearing faults. However, from internal data at Grundfos it is known that stator burnouts are one of the main reason for faults in submersible pumps. Both signal-based and model-based approaches have been used for detecting stator faults. The signal-based approaches are mostly concerned in finding fault signatures in the stator current. The model-based approaches are mostly based on steady state impedance models of the machine. This basically means that robustness with respect to dynamic changes in the motor speed and motor current is not considered.

From the state of the art analysis of FDI in centrifugal pumps it is seen that different centrifugal pump faults are considered, and that different methods are used for their detection. However, the model-based approach is fare less used than signal-based methods. This might be due to the nonlinear nature of the centrifugal pump model. It is well known that frequency converters, making it possible to optimize the operating point of the pump, are used more and more often as drives for centrifugal pumps. However, this means that the detection algorithms should not only be robust with respect to changes in the hydraulic resistance, i.e. the flow through the pump, but also to speed changes. This has not be considered in any of the presented papers.

Chapter 3

Model of the Centrifugal Pump

In this chapter the mathematical model of the centrifugal pump is presented. The chapter starts by describing the mechanical construction of a standard centrifugal pump. Here it is argued that the model of the pump can be divided into three subparts,

- The induction motor driving the pump.
- The hydraulics of the pump.
- The mechanical parts of the pump.

The induction motor is modelled using a so-called dq-model of the motor dynamics. This type of model is extensively described in the literature. The description presented here is based on (Krause et al., 1994; Kazmierkowski, 1994; Novotny and Lipo, 1996).

The steady state performance of the hydraulics of the centrifugal pump is extensively described in the literature too, (Sayers, 1990; Stepanoff, 1957) and others. Here this steady state description is extended to cover the dynamics of the centrifugal pump as well as the steady state operation, making it particular suitable in model based FDI algorithms. The same approach is in (Gravdahl and Egeland, 1999) used for modelling a centrifugal compressor, but here the dynamics are neglected. Dynamics of centrifugal pumps are treated in for example (Bóka and Halász, 2002).

In this work the model is derived using the control volume approach (Roberson and Crowe, 1993). The derived model expresses the theoretical performance of the impeller. To obtain a model describing the performance of a real pump extra pressure losses are added to the theoretical model (Sayers, 1990; Stepanoff, 1957). The obtained model describes the performance of a single impeller. However, it is shown that the same model structure also describes the performance of a multi stage pump.

The mechanical part of the pump is modelled using simple considerations based on Newton's second law. The frictions losses in the bearing and seals are modelled by a simple linear friction term, as the friction losses are very small compared to the torque necessary the drive the pump, and therefore are not important in the model.

The first section of this chapter contains a description of the mechanical construction of the centrifugal pump. The second section describes the induction motor model, and the third section contains the derivation of the model modelling the hydraulics of the centrifugal pump. The fourth section presents the mechanical model, and in the fifth section each of the submodels, derived in the previous sections, are composed into the final nonlinear state space model of the centrifugal pump. Finally, concluding remarks end the chapter.

3.1 The Construction of the Centrifugal Pump

In this section the mechanical components of the centrifugal pump are described. This is done in order to give an overview over the construction of the pump. This description is included to help the reader to follow the model derivations presented in the following parts of this chapter.

In Fig. 3.1 a CR5-10 Grundfos centrifugal pump is shown. This centrifugal pump contains the same set of components as almost all other centrifugal pumps, and is in this section used as an example of a standard centrifugal pump. In Fig. 3.1 the pump is sliced revealing the inside of the pump. The CR5-10 pump is a multistage centrifugal pump, meaning that the pressure is increased using a set of identical impellers, see Fig. 3.1. The impellers are the rotating part of the pump, which increase the pressure by the utilization of the centrifugal force induced by the rotation. This effect is formalized in section 3.3.

The pump is driven by an 1.5 [KW] induction motor, which is connected to the pump by a shaft connection, see Fig. 3.1. This is a typical way to drive centrifugal pumps in the rang from 50 [W] up till several hundreds [KW]. The pumps considered in this thesis have the same structure as the one shown in Fig. 3.1.

A signal flow diagram of such a centrifugal pump is shown in Fig. 3.2. Here the pump is divided into four subsystems. These subsystems are,

- The electrical part of the induction motor. This part converts electrical energy into mechanical energy.
- The mechanical part of the induction motor and the pump. This part connects the impeller to the rotor of the induction motor.
- The hydraulic part of the pump. This part converts mechanical energy into hydraulic energy.
- The hydraulic application. This part absorbs the hydraulic energy delivered by the pump.

The first three of these are parts of the centrifugal pump itself, and the last part is the application in which the pump is placed. As the topic of this thesis is FDI on centrifugal pumps only the first three parts are considered in the following.

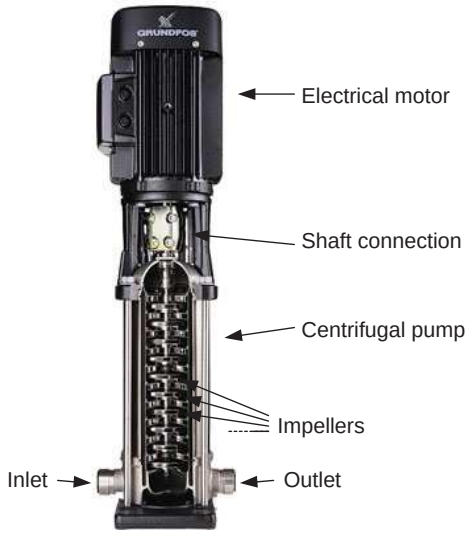

Figure 3.1: A multistage centrifugal pump driven by an induction motor.

3.2 Model of the Electrical Motors

In this section modelling of the energy conversion from electrical to mechanical energy in the induction motor is considered. The presented model is described in the so-called $dq0$-coordinates as it is shown in (Krause et al., 1994), but with the coordinate system oriented as in (Leonhard, 1996; Kazmierkowski, 1994; Novotny and Lipo, 1996). These four references contain good descriptions of the induction motor model and form the foundation for the model presented in this section. Only the stator fixed $dq0$-coordinates are treated in this work. This is so because the observer designs, for which the model is used in this work, are all based on stator fixed models.

In the model derivations described in this section the following set of assumptions are used, (Kazmierkowski, 1994),

- The motor is symmetrical and contains three phases.
- Only the basic harmonic is considered, while higher harmonics in the field distribution and in the magnetomotive force are neglected.
- The distributed windings in the stator and the rotor cage are replaced by concentrated coils.
- The permeability of the iron parts are assumed infinite, meaning that the effect of magnetic saturation is neglected, hereby the magnetic circuit becomes linear.

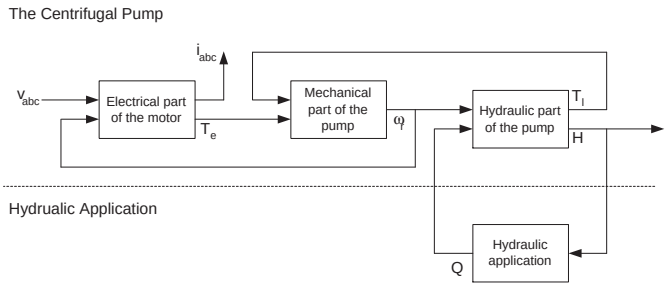

Figure 3.2: Blockdiagram depicting the connection between the different parts of the centrifugal pump.

- Iron losses and eddy current losses are neglected.

It is possible to avoid the assumptions about the harmonics and the winding distributions by using higher order models. This is done in (Vadstrup, 2002; Toliyat et al., 1991). However, this leads to complicated high order models. As the electrical faults, under consideration in this work, mainly affect the fundamental harmonics in the induction motor, these high order models introduce unnecessary complexity.

Likewise it is possible to include magnetic saturation in the model (Sullivan and Sanders, 1995). This effect is neglected in this model, as it is expected, that the motor is controlled, such that the level of magnetization is almost constant in all operating points under consideration. This is in fact often the case in induction motor control schemes.

3.2.1 The Induction Motor Model in abc-coordinates

Using the assumptions given above the electrical circuit of an induction motor is given by the circuit shown in Fig. 3.3. In this figure the stator circuits are supplied with three voltages v_{sa}, v_{sb} and v_{sc} and the rotor circuits are short circuited. The coils in both the rotor and stator are magnetic connected meaning that all coils in the motor must be taken into account when calculating the flux in a single coil.

Setting up the mesh equations for both the rotor as stator circuits the following set of equations are obtained.

$$\begin{aligned} \mathbf{v}_{sabc} &= \mathbf{r}_s \mathbf{i}_{sabc} + \frac{d\boldsymbol{\psi}_{sabc}}{dt} \\ \mathbf{0} &= \mathbf{r}_r \mathbf{i}_{rabc} + \frac{d\boldsymbol{\psi}_{rabc}}{dt} \ . \end{aligned} \tag{3.1}$$

The signal vectors in this model are given by

$$\begin{gathered} \mathbf{v}_{sabc} = \begin{bmatrix} v_{sa} & v_{sb} & v_{sc} \end{bmatrix}^T \quad \mathbf{i}_{sabc} = \begin{bmatrix} i_{sa} & i_{sb} & i_{sc} \end{bmatrix}^T \quad \mathbf{i}_{rabc} = \begin{bmatrix} i_{ra} & i_{rb} & i_{rc} \end{bmatrix}^T \\ \boldsymbol{\psi}_{sabc} = \begin{bmatrix} \psi_{sa} & \psi_{sb} & \psi_{sc} \end{bmatrix}^T \quad \boldsymbol{\psi}_{rabc} = \begin{bmatrix} \psi_{ra} & \psi_{rb} & \psi_{rc} \end{bmatrix}^T \ , \end{gathered}$$

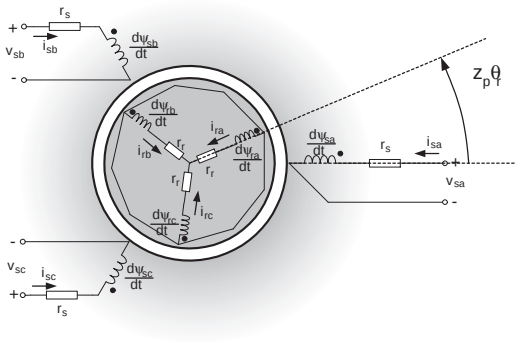

Figure 3.3: The electrical circuit diagram of the induction motor, placed in the mechanical structure of the induction motor. The three outer circuits are the circuits of the three phases of the stator and the inner circuit is the rotor circuit.

and the parameter matrices are

$$\mathbf{r}_s = r_s\mathbf{I} \qquad\qquad \mathbf{r}_r = r_r\mathbf{I}\ ,$$

where r_s and r_r are the electrical resistances in respectively the stator and rotor coils, see Fig. 3.3.

The flux linkages $\boldsymbol{\psi}_{sabc}$ and $\boldsymbol{\psi}_{rabc}$ in (3.1) are given by the following expression. Here the assumption concerning saturation, described in the start of this section, is used.

$$\begin{aligned}\boldsymbol{\psi}_{sabc} &= \mathbf{l}_s\mathbf{i}_{sabc} + \mathbf{l}_m(z_p\theta_r)\mathbf{i}_{rabc}\\ \boldsymbol{\psi}_{rabc} &= \mathbf{l}_r\mathbf{i}_{rabc} + \mathbf{l}_m(z_p\theta_r)^T\mathbf{i}_{sabc}\ .\end{aligned} \tag{3.2}$$

The parameter matrices $\mathbf{l}_s$ and $\mathbf{l}_r$ are defined by

$$\mathbf{l}_s = l_{ls}\mathbf{I} + \mathbf{l}_m(0) \qquad\qquad \mathbf{l}_r = l_{lr}\mathbf{I} + \mathbf{l}_m(0)\ ,$$

where l_{ls} and l_{lr} are the leakage inductances in the stator and rotor windings respectively, and $\mathbf{l}_m$ is the mutual inductance and is given by

$$\mathbf{l}_m(\theta_e) = l_m\begin{bmatrix}\cos(\theta_e) & \cos(\theta_e+\frac{2\pi}{3}) & \cos(\theta_e+\frac{4\pi}{3})\\ \cos(\theta_e+\frac{4\pi}{3}) & \cos(\theta_e) & \cos(\theta_e+\frac{2\pi}{3})\\ \cos(\theta_e+\frac{2\pi}{3}) & \cos(\theta_e+\frac{4\pi}{3}) & \cos(\theta_e)\end{bmatrix}\ , \tag{3.3}$$

where l_m is a constant and $\theta_e = z_p\theta_r$ is the electrical angle between the stator and rotor phases, see Fig. 3.3.

3.2.2 Transformation to Stator Fixed $dq0$-coordinates

From the model described in the abc-coordinates it is seen that the mutual inductance matrix (3.3) is a function of $z_p\theta_r$. This dependency can be removed using a variable transformation from the abc-coordinates of the stator and rotor variables respectively to stator fixed $dq0$-coordinates. This variable transformation is given by

$$\mathbf{x}_{sdq0} = \mathbf{T}_{dq0}(0)\mathbf{x}_{sabc} \qquad \mathbf{x}_{rdq0} = \mathbf{T}_{dq0}(-z_p\theta_r)\mathbf{x}_{rabc} \ , \tag{3.4}$$

where subscript s and r denote the stator variables and rotor variables respectively, and $z_p\theta_r$ is the electrical angle between the stator and rotor circuit, see Fig. 3.3. In this transformations $\mathbf{T}_{dq0}$ is given by

$$\mathbf{T}_{dq0}(\theta) = \frac{2}{3}\begin{bmatrix} \cos(\theta) & \cos(\theta+\frac{2\pi}{3}) & \cos(\theta+\frac{4\pi}{3}) \\ \sin(\theta) & \sin(\theta+\frac{2\pi}{3}) & \sin(\theta+\frac{4\pi}{3}) \\ \frac{1}{2} & \frac{1}{2} & \frac{1}{2} \end{bmatrix} \ .$$

Equations (3.1) and (3.2), describing the electrical and magnetic system of the induction motor respectively, are transformed using the transformation (3.4). Hereby the following description of the induction motor is obtained,

$$\begin{aligned} \mathbf{v}_{sdq} &= \mathbf{R}_s\mathbf{i}_{sdq} + \tfrac{d\boldsymbol{\psi}_{sdq}}{dt} \\ \mathbf{v}_{s0} &= r_s i_{s0} + \tfrac{d\psi_{s0}}{dt} \\ \mathbf{0} &= \mathbf{R}_r\mathbf{i}_{rdq} + \tfrac{d\boldsymbol{\psi}_{rdq}}{dt} - z_p\omega_r\mathbf{J}\boldsymbol{\psi}_{rdq} \\ 0 &= r_r i_{r0} + \tfrac{d\psi_{r0}}{dt} \ , \end{aligned} \tag{3.5}$$

where $z_p\omega_r = \frac{dz_p\theta_r}{dt}$, as θ_r is a function of time. The flux linkages in these equations are given by

$$\begin{aligned} \boldsymbol{\psi}_{sdq} &= \mathbf{L}_s\mathbf{i}_{sdq} + \mathbf{L}_m\mathbf{i}_{rdq} \\ \psi_{s0} &= l_{ls}i_{s0} \\ \boldsymbol{\psi}_{rdq} &= \mathbf{L}_r\mathbf{i}_{rdq} + \mathbf{L}_m\mathbf{i}_{sdq} \\ \psi_{r0} &= l_{lr}i_{r0} \ . \end{aligned} \tag{3.6}$$

In (3.5) and (3.6) the $dq0$-space is split into dq-coordinates and 0-coordinates of reasons, which will become obvious in the following. The parameter matrices $\mathbf{R}_s$, $\mathbf{R}_r$, $\mathbf{L}_s$ $\mathbf{L}_r$, and $\mathbf{L}_m$ do all have a diagonal structure, and are given by,

$$\begin{aligned} \mathbf{R}_s = \text{diag}\{r_s,\ r_s\} \qquad \mathbf{R}_r &= \text{diag}\{r_r,\ r_r\} \\ \mathbf{L}_s &= \text{diag}\{\tfrac{3}{2}l_m + l_{ls},\ \tfrac{3}{2}l_m + l_{ls}\} \\ \mathbf{L}_r &= \text{diag}\{\tfrac{3}{2}l_m + l_{lr},\ \tfrac{3}{2}l_m + l_{lr}\} \\ \mathbf{L}_m &= \text{diag}\{\tfrac{3}{2}l_m,\ \tfrac{3}{2}l_m\} \\ \mathbf{J} &= \begin{bmatrix} 0 & -1 \\ 1 & 0 \end{bmatrix} \ . \end{aligned}$$

Rewriting (3.5) and (3.6), and using the magnetizing current $\mathbf{i}_{mdq}$ defined such that it fulfils the equation $\boldsymbol{\psi}_{rdq} = \mathbf{L}_m \mathbf{i}_{mdq}$, the induction motor model becomes

$$\mathbf{L}'_s \frac{d\mathbf{i}_{sdq}}{dt} = -\left(\mathbf{R}_s + \mathbf{R}'_r\right)\mathbf{i}_{sdq} + \left(\mathbf{R}'_r - z_p\omega_r \mathbf{J}\mathbf{L}'_m\right)\mathbf{i}_{mdq} + \mathbf{v}_{sdq} \tag{3.7a}$$

$$l_{ls}\frac{di_{s0}}{dt} = -r_s i_{s0} + v_{s0} \tag{3.7b}$$

$$\mathbf{L}'_m \frac{d\mathbf{i}_{mdq}}{dt} = \mathbf{R}'_r \mathbf{i}_{sdq} - \left(\mathbf{R}'_r - z_p\omega_r \mathbf{J}\mathbf{L}'_m\right)\mathbf{i}_{mdq} \tag{3.7c}$$

$$l_{lr}\frac{d\psi_{r0}}{dt} = -r_r\psi_{r0}\ , \tag{3.7d}$$

where

$$\mathbf{R}'_r = \mathbf{L}_m\mathbf{L}_r^{-1}\mathbf{R}_r\mathbf{L}_r^{-1}\mathbf{L}_m \qquad \mathbf{L}'_s = \mathbf{L}_s - \mathbf{L}_m\mathbf{L}_r^{-1}\mathbf{L}_m \qquad \mathbf{L}'_m = \mathbf{L}_m\mathbf{L}_r^{-1}\mathbf{L}_m\ ,$$

meaning that the new matrices retain the diagonal structure.

Equation (3.7d) shows that $\lim_{t\to\infty}\psi_{r0} = 0$ for every possible operating conditions. Moreover ψ_{r0} is not influencing the rest of the model equations. Therefore, (3.7d) can be excluded from the final induction motor model.

3.2.3 Grid Connections

The stator windings described in (3.1) can either be connected in a $\mathbf{Y}$- or Δ-connection as shown in Fig. 3.4. In this figure only the terminal voltages $\mathbf{v}_{tabc} = \begin{bmatrix} v_{ta} & v_{tb} & v_{tc} \end{bmatrix}^T$

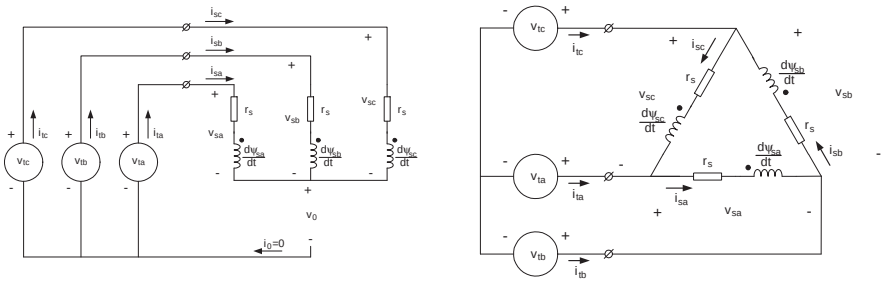

(a) $\mathbf{Y}$-connection.

(b) Δ-connection.

Figure 3.4: Example of the stator windings connected in a $\mathbf{Y}$- and Δ-connection respectively. The stator circuit in this figure is the same as the one shown in figure 3.3.

and the terminal currents $\mathbf{i}_{tabc} = \begin{bmatrix} i_{ta} & i_{tb} & i_{tc} \end{bmatrix}^T$ are measurable. Therefore a relationship between the voltages and currents at the terminals of the motor, and the voltages and currents in (3.1) must be defined. This relationship is, in the following, established for a $\mathbf{Y}$- and Δ-connected motor respectively.

The Y-connected induction motor

In the case of a **Y**-connected stator, the mappings between the stator variables and the terminal variables are given by,

$$\mathbf{v}_{tabc} = \mathbf{v}_{sabc} + \mathbf{1}v_0 \qquad \mathbf{i}_{tabc} = \mathbf{I}\mathbf{i}_{sabc} \ ,$$

where $\mathbf{1} = \begin{bmatrix} 1 & 1 & 1 \end{bmatrix}^T$, and v_0 is the voltage between the star point of the supply and the star point of the stator circuit, see Fig. 3.4(a). Transforming these equations to $dq0$-coordinates the description becomes,

$$\begin{aligned} \mathbf{v}_{sdq} &= \mathbf{v}_{tdq} & \mathbf{i}_{tdq} &= \mathbf{i}_{sdq} \\ v_{s0} &= v_{t0} - v_0 & i_{t0} &= i_{s0} \ . \end{aligned}$$

Moreover it is seen from Fig. 3.4(a) that the relationsship $0 = i_{sa} + i_{sb} + i_{sc}$ must hold for this circuit, therefore the currents $i_{s0} = i_{t0} = 0$.

Using the expression $v_{s0} = v_{t0} - v_0$, obtained above, and the fact the $i_{s0} = 0$, the expression of the zero sequence quantities described by (3.7b) becomes,

$$0 = v_{t0} - v_0 \ . \tag{3.8}$$

This shows that (3.7b) has no impact on the motor performance, therefore it can be excluded from the final model of a **Y**-connected induction motor.

From the above argumentation the **Y**-connected induction motor is modelled by the following set of equations,

$$\mathbf{L}'_s \frac{d\mathbf{i}_{sdq}}{dt} = -\left(\mathbf{R}_s + \mathbf{R}'_r\right)\mathbf{i}_{sdq} + \left(\mathbf{R}'_r - z_p\omega_r\mathbf{J}\mathbf{L}'_m\right)\mathbf{i}_{mdq} + \mathbf{v}_{tdq} \tag{3.9a}$$

$$\mathbf{L}'_m \frac{d\mathbf{i}_{mdq}}{dt} = \mathbf{R}'_r\mathbf{i}_{sdq} - \left(\mathbf{R}'_r - z_p\omega_r\mathbf{J}\mathbf{L}'_m\right)\mathbf{i}_{mdq} \ , \tag{3.9b}$$

where the measurable terminal current $\mathbf{i}_{tdq}$ is given by,

$$\mathbf{i}_{tdq} = \mathbf{i}_{sdq} \ . \tag{3.9c}$$

Remark 3.2.1 *From the expression of the star point voltage (3.8) it is seen that the start point voltage of the induction motor v_0 equals the star point voltage of the supply v_{t0} in the no-fault case. This can be used for fault detection in* **Y***-connected induction motors, whenever the star point voltage of the motor is measured. This scheme uses that $\int_T (v_{s0} - v_{t0})^2 dt \neq 0$ when a fault has happend in the motor, and in the no-fault case $\int_T (v_{s0} - v_{t0})^2 dt = 0$ (Tallam et al., 2002).*

The Δ-connected induction motor

In the case of a Δ-connected stator the mappings between the stator variables and the terminal variables are given by,

$$\mathbf{v}_{sabc} = \mathbf{K}_\Delta \mathbf{v}_{tabc} \qquad \mathbf{i}_{tabc} = \mathbf{K}_\Delta^T \mathbf{i}_{sabc} \ ,$$

where the linear mapping $\mathbf{K}_\Delta$ is given by,

$$\mathbf{K}_\Delta = \begin{bmatrix} 1 & -1 & 0 \\ 0 & 1 & -1 \\ -1 & 0 & 1 \end{bmatrix} \ .$$

Transforming these equations to $dq0$-coordinates the description becomes,

$$\mathbf{v}_{sdq0} = \mathbf{T}_{dq0} \mathbf{K}_\Delta \mathbf{T}_{dq0}^{-1} \mathbf{v}_{tdq0} \qquad \mathbf{i}_{tdq0} = \mathbf{T}_{dq0} \mathbf{K}_\Delta^T \mathbf{T}_{dq0}^{-1} \mathbf{i}_{sdq0} \ .$$

The structures of these linear mappings are,

$$\begin{bmatrix} \mathbf{v}_{sdq} \\ v_{s0} \end{bmatrix} = \begin{bmatrix} \mathbf{B}_v & \mathbf{0} \\ \mathbf{0} & 0 \end{bmatrix} \begin{bmatrix} \mathbf{v}_{tdq} \\ v_{t0} \end{bmatrix} \qquad \begin{bmatrix} \mathbf{i}_{tdq} \\ i_{t0} \end{bmatrix} = \begin{bmatrix} \mathbf{C}_i & \mathbf{0} \\ \mathbf{0} & 0 \end{bmatrix} \begin{bmatrix} \mathbf{i}_{sdq} \\ i_{s0} \end{bmatrix} \ .$$

This shows that $v_{s0} = 0$ despite of the value of $\mathbf{v}_{tdq0}$, and i_{t0} despite of the value of $\mathbf{i}_{sdq0}$.

Using the fact $v_{s0} = 0$ in (3.7b) it becomes,

$$l_{ls} \frac{di_{s0}}{dt} = - r_s i_{s0} \ .$$

This shows that $\lim_{t\to\infty} i_{s0} = 0$ for every possible operating conditions. Moreover i_{s0} is not affecting the rest of the model equations. Therefore (3.7b) can be excluded from the final model of a Δ-connected induction motor.

From the above argumentation the Δ-connected induction motor is modelled by the following set of equations,

$$\mathbf{L}_s' \frac{d\mathbf{i}_{sdq}}{dt} = - \left(\mathbf{R}_s + \mathbf{R}_r'\right) \mathbf{i}_{sdq} + \left(\mathbf{R}_r' - z_p \omega_r \mathbf{J} \mathbf{L}_m'\right) \mathbf{i}_{mdq} + \mathbf{B}_v \mathbf{v}_{tdq} \tag{3.10a}$$

$$\mathbf{L}_m' \frac{d\mathbf{i}_{mdq}}{dt} = \mathbf{R}_r' \mathbf{i}_{sdq} - \left(\mathbf{R}_r' - z_p \omega_r \mathbf{J} \mathbf{L}_m'\right) \mathbf{i}_{mdq} \ , \tag{3.10b}$$

where the measurable terminal current $\mathbf{i}_{tdq}$ is given by,

$$\mathbf{i}_{tdq} = \mathbf{C}_i \mathbf{i}_{sdq} \ . \tag{3.10c}$$

3.2.4 The Torque Expression

From energy consideration it is shown, in (Krause et al., 1994), that the torque produced by the induction motor is given by,

$$T_e = \mathbf{i}_{sabc}^T \frac{\partial \mathbf{l}_m(z_p\theta_r)}{\partial \theta_r} \mathbf{i}_{rabc} \ ,$$

where $\mathbf{i}_{sabc}$ is the current of the stator windings and $\mathbf{i}_{rabc}$ is the current in the rotor. Including the transformations (3.4) into this expression it becomes,

$$T_e = (\mathbf{T}_{dq0}(0)^{-1}\mathbf{i}_{sdq0})^T \frac{\partial \mathbf{l}_m(z_p\theta_r)}{\partial \theta_r} (\mathbf{T}_{dq0}(-z_p\theta_r)^{-1}\mathbf{i}_{rdq0}) \ .$$

Simplifying the expression and using $\mathbf{L}_m\mathbf{i}_{mdq} = \mathbf{L}_r\mathbf{i}_{rdq} + \mathbf{L}_m\mathbf{i}_{sdq}$ the following torque expression is obtained,

$$T_e = \frac{3}{2} z_p L'_m \left(i_{md}i_{sq} - i_{mq}i_{sd}\right) \ , \tag{3.11}$$

where $L'_m = L_m^2/L_r$, meaning that L'_m is the diagonal element of $\mathbf{L}'_m$.

3.3 The Hydraulic Part of the Centrifugal Pump

This section is concerned with modelling the hydraulic part of the centrifugal pump. The hydraulic part of the centrifugal pump consists of the inlet and outlet of the pump, and the impeller and the diffuser inside the pump. These components are all shown in Fig. 3.5. The impeller is the rotating part of the pump, which induces a rotational speed into the liquid. This speed is transformed into a static pressure in the diffuser and volute. Hereby a pressure difference between the impeller eye and the outlet of the volute is obtained. This will be formulized in this section.

The model, presented in this section, describes the pressure and torque of the pump as functions of the flow and speed respectively. This means that the obtained model has a structure as shown in Fig. 3.6. In this figure ω_r is the angular speed of the impeller, Q_p is the volume flow, and H_p and T_p are the pressure and torque produced by the pump respectively.

In the literature a polynomial model of the centrifugal pump can be found (Sayers, 1990; Stepanoff, 1957). This model describes the torque load of the centrifugal pump under steady state operation. Here, the aim is to derive a dynamic model of the pump. Such a model is needed in the design of FDI observers. Fortunately, it is well know from the literature that a control volume approach can be used in the derivation of the dynamics of a hydraulic system (Roberson and Crowe, 1993). This approach is used in this section to obtain a model describing the dynamics as well as the steady state operation of the centrifugal pump. The obtained model has a nonlinear but simple structure, which is usable in model based FDI algorithms.

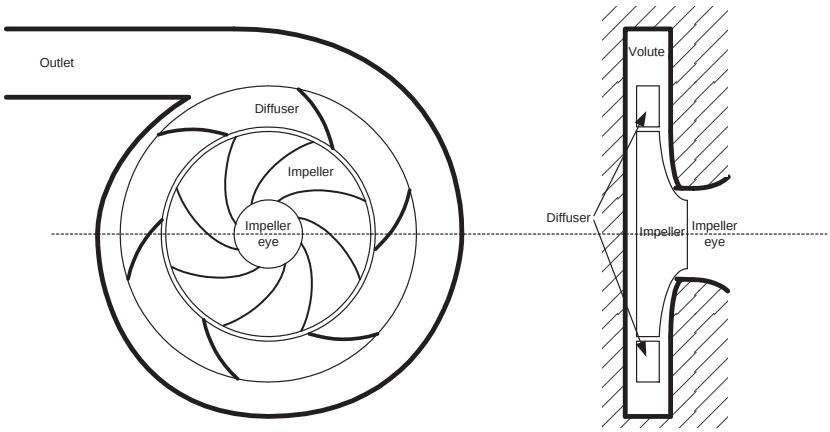

Figure 3.5: The mechanical construction of a single stage in a centrifugal pump. To the left-hand side a top view is shown and to the right-hand side a side view is shown.

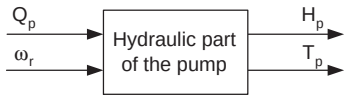

Figure 3.6: Definition of the flows and pressures used in the definition of the losses in the pump.

It is possible to obtain more accurate models of the centrifugal pump using finite volume solutions of Navier-Stokes equations. With these solutions it is not only possible to calculate the pressure between the inlet and outlet of the pump, but also possible to calculate the pressure distributions inside the pump. However, these solutions include heavy calculations and are therefore not usable in the design of FDI algorithms.

3.3.1 The Principle of the Centrifugal Pump Dynamics

Before the derivation of the mathematical model of the centrifugal pump is presented, the operation of the pump is described in informal terms. This includes a description of the expected dynamic performance of the impeller. In Sections 3.3.2 and 3.3.3 the impeller performance is treated formally and mathematical expressions of the performance is obtained.

In Fig. 3.7 the velocity triangle of the fluid at a given radius inside the impeller is shown (Sayers, 1990). In this figure $\mathbf{U}$ is the tangential speed of the impeller, i.e.

$|\mathbf{U}| = r\omega_r$, $\mathbf{C}$ is the liquid speed, and $\mathbf{W}$ is the liquid speed in proportion to the impeller, all defined at the same radius r. Moreover the liquid speed $\mathbf{C}$ is divided into a tangential and radial component named $\mathbf{C}_x$ and $\mathbf{C}_r$ respectively.

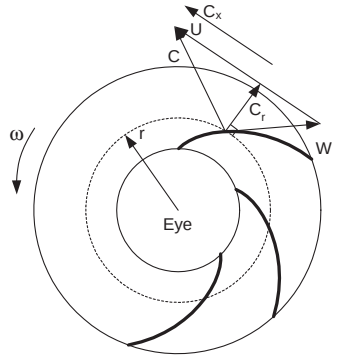

Figure 3.7: The impeller of a centrifugal pump. At a given radius r the liquid speed $\mathbf{C}$, the impeller speed $\mathbf{U}$, and the liquid speed in proportion to the impeller $\mathbf{W}$ are shown. Moreover the liquid speed $\mathbf{C}$ is divided into a tangential and radial component named $\mathbf{C}_x$ and $\mathbf{C}_r$ respectively.

The torque acting on the impeller due to the liquid inside the impeller must be equal to the change of momentum of the liquid inside the impeller. As the liquid at all time is flowing through the impeller there must be a change of momentum from the liquid flowing into the impeller to the liquid flowing out of the impeller. This change of momentum is due to the increase in the liquid speed $\mathbf{C}_2 - \mathbf{C}_1$, where $\mathbf{C}_1$ and $\mathbf{C}_2$ are the liquid speed at inlet and outlet of the impeller respectively. $\mathbf{C}_1$ and $\mathbf{C}_2$ are both functions of the impeller angular speed ω_r and the volume flow Q_i, meaning that the mathematical expression describing this part must be on the form

$$T = f_t(Q_i, \omega_r) \ ,$$

where T is the torque component, Q_i is the volume flow and ω_r is the angular speed of the impeller. The energy added to the liquid due to this torque component is converted into static pressure in the diffuser and volute. Therefore the expression of the pressure produced by the pump must be on the form

$$H_i = f_h(Q_i, \omega_r) \ ,$$

here H_i is the pressure produced by the impeller.

This is not the only phenomenon changing the momentum of the liquid inside the impeller, as transients in the tangential speed of the liquid $\frac{d\mathbf{C}_x}{dt}$ also will change the

momentum. Now recognizing that the velocity triangle in Fig. 3.7 will be fulfilled at all time, and that the direction of the liquid speed in proportion to the impeller $\mathbf{W}$ is fixed due to the impeller blades. This means that changes of the tangential speed of the impeller $\mathbf{U}$ will induce changes in $\mathbf{C}_x$, and therefore the momentum of the liquid inside the impeller is changed. Moreover, $\mathbf{C}_x$ will also change if the radial speed of the liquid $\mathbf{C}_r$ is changed. This change is explained by the velocity triangle, which has to be fulfilled all the time. This means that a change in the volume flow Q_i will change the momentum of the liquid inside the impeller, as $\mathbf{C}_r$ is proportional to Q_i.

From the above consideration the model describing the torque acting on the impeller due to the liquid, must be on the form,

$$T_i = f_t(Q_i, \omega_r) + f_t'(Q_i, \omega_r, \tfrac{d\omega_r}{dt}) + f_t''(Q_i, \omega_r, \tfrac{dQ_i}{dt}) \quad ,$$

where T_i is the impeller torque, Q_i is the volume flow, ω_r is the angular speed of the impeller and f_h, f_h' and f_h'' are functions to be decided. In fact in Section 3.3.2 the control volume approach is used to derived an expression of the torque. Here it is shown that the torque is described by,

$$T_i = \left(-a_{t2}Q_i^2 + a_{t1}\omega_r Q_i + a_{t0}\omega_r^2\right) + J_{M_v}\frac{d\omega_r}{dt} - K_Q\frac{dQ_i}{dt} \ ,$$

where a_{t2}, a_{t1}, a_{t0}, J_{M_v} and K_Q are constants described in Section 3.3.2. An expression of the pressure produced by the pump is derived in Section 3.3.3. Here it is shown that the pressure expression becomes,

$$H_i = \rho g(-a_{h2}Q_i^2 + a_{h1}\omega_r Q_i + a_{h0}\omega_r^2) \ ,$$

where a_{h2}, a_{h1} and a_{h0} are constants described in Section 3.3.3.

3.3.2 The Torque Expression

In this section an expression of the torque acting on the impeller is derived using control volume considerations. In (Roberson and Crowe, 1993, p. 242) a control volume equation is derived, describing the torque properties of the given control volume. The obtained equation is (Roberson and Crowe, 1993, p. 243),

$$\sum_j T_j = \int_{cs} (\mathbf{r} \times \mathbf{c})\rho\mathbf{C} \bullet d\mathbf{A} + \frac{d}{dt}\int_{cv} (\mathbf{r} \times \mathbf{c})\rho dV \ , \tag{3.12}$$

where all T_j are external torques on the control volume, $\mathbf{r}$ is a radius vector, and $\mathbf{c}$ is the fluid speed at the radius vector $\mathbf{r}$. $\mathbf{C}$ is the fluid speed in proportion to a infinitesimal control surface dA and $d\mathbf{A}$ is an infinitesimal area vector describing the direction and size of the infinitesimal control surface dA. Finally ρ is the mass density of the liquid and dV is an infinitesimal volume. The subscribes cs and cv on the intergrals denote the control surface and the control volume respectively. The first term on the right-hand

side of (3.12) describes the momentum change due to the liquid flow and the second term describes the dymanics.

To be able to utilize (3.12) for calculating the torque acting on the impeller, a control volume must be defined. As only the overall performance of the impeller is of interest in this work the control volume is chosen as the inside of the impeller, see Fig. 3.8(a). The control V is represented by the hatched area with a uniform hight h and the control

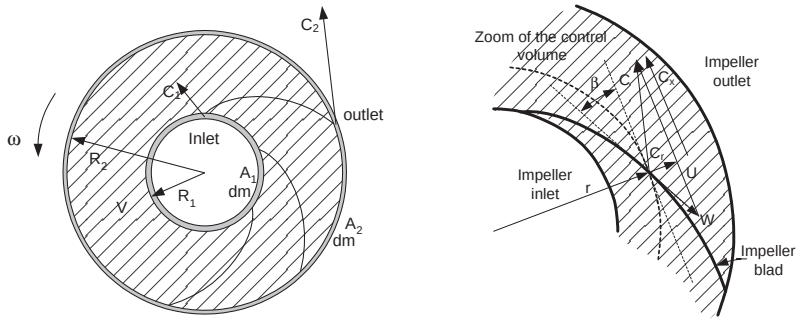

(a) The control volume defined on the impeller. The hatched area defines the control volume V with a uniform hight h, and dm is a small mass entering and leaving the impeller in time dt through the areas A_1 and A_2 respectively.

(b) The speed triangle at a given point of the impeller blad. c is the fluid speed, w is the fluid speed in proportion to the impeller, and u is the tangential speed of the impeller.

Figure 3.8: Definition of the control volume and fluid speed inside the control volume.

areas A_1 and A_2 are the inlet and outlet surface of the impeller respectively.

At a given radius $r = |\mathbf{r}|$ the velocity triangle in Fig. 3.8(b) can be assumed equally positioned proportional to the radius vector $\mathbf{r}$ for all angles of $\mathbf{r}$. Therefore the cross product $\mathbf{r} \times \mathbf{c}$ is constant for all angles of $\mathbf{r}$ and can be expressed by,

$$\mathbf{r} \times \mathbf{c} = r c_x \ , \tag{3.13}$$

where $r = |\mathbf{r}|$ and c_x is defined in Fig. 3.8(b). c_x is in general a function of the radius r.

As the liquid is assumed incompressible the inlet mass flow must equal the outlet mass flow. This means that,

$$\int_{A_2} \rho \mathbf{C}_2 \bullet d\mathbf{A} = \int_{A_1} \rho \mathbf{C}_1 \bullet d\mathbf{A} = \frac{dm}{dt} \ , \tag{3.14}$$

where $\frac{dm}{dt}$ is the mass flow, $\mathbf{C}_i$ is the speed of the fluid at the infinitesimal surface dA and $d\mathbf{A}$ is an infinitesimal area vector describing the direction and size of the infinitesimal surface dA.

From Fig. 3.8(a) it is seen that the infinitesimal volume dV equals,

$$dV = 2\pi r h dr \ , \tag{3.15}$$

where r is the radius at a given slice of the disc forming the impeller with hight h.

Using (3.13), (3.14), and (3.15) in (3.12), the torque expression is reduced to,

$$T_i = \frac{dm}{dt}\left(r_2 c_{x2} - r_1 c_{x1}\right) + \frac{d}{dt} 2\pi h \rho \int_{R_1}^{R_2} r^2 c_x(r) dr \ , \tag{3.16}$$

where T_i is the component of the shaft torque created by the fluid inside the impeller. In (3.16) the first term on the right-hand side describes the time derivative of the change of momentum between the liquid entering and leaving the impeller. This term is the pressure or head producing part and is in the following denoted the steady state torque term. The second term on the right-hand side describes the torque necessary to change the speed of the impeller when the mass of the impeller itself is not taken into account. This term is in the following denoted the transient torque term.

The steady state torque expression

From Fig. 3.8(b) it is seen that the speed $c_x = u - c_r \cot(\beta)$, where u is the tangential speed of the impeller and is given by $u = r\omega_r$. Moreover, if the area of a slice of the impeller with radius r is defined as $A_r = 2\pi r h$, then the volume flow inside the impeller is given by $Q_i = c_r A_r$. Using these considerations the following expressions of c_x are obtained,

$$c_x = u - c_r \cot(\beta) = r\omega_r - \frac{Q_i}{A_r}\cot(\beta) = r\omega_r - \frac{Q_i}{2\pi r h}\cot(\beta) \ . \tag{3.17}$$

Using (3.17) at the inlet and outlet of the impeller to obtain an expression of c_{x1} and c_{x2}. Then used these expressions in the first term on the right-hand side of (3.16) to obtain the following expression for the steady state torque,

$$T_i = \rho\left(r_2^2 - r_1^2\right) Q_i \omega_r - \rho\left(\frac{r_2\cot(\beta_2)}{A_2} - \frac{r_1\cot(\beta_1)}{A_1}\right) Q_i^2 \ , \tag{3.18}$$

where the mass flow $\frac{dm}{dt}$ is replaced by ρQ_i. Equation (3.18) models the steady state torque load of the impeller.

Beside the torque described by (3.18) and extra torque term $T_f = K_n \omega_r^2$ (Sayers, 1990) is added. This term models the hydraulic friction due to liquid between the volute and the impeller, see Fig. 3.5. Adding this term the final steady state expression of the torque becomes,

$$T_p = -\, a_{t2} Q_i^2 + a_{t1}\omega_r Q_i + a_{t0}\omega_r^2 \ , \tag{3.19}$$

where,

$$a_{t2} = \rho\left(\frac{r_2\cot(\beta_2)}{A_2} - \frac{r_1\cot(\beta_1)}{A_1}\right) \qquad a_{t1} = \rho\left(r_2^2 - r_1^2\right) \qquad a_{t0} = K_n \ .$$

The transient torque expression

The transient torque component is given by the second term on the right-hand side of (3.16). Using (3.17) to describe c_x in this expression the following expression is obtained,

$$T_t = J_{M_v} \frac{d\omega_r}{dt} - K_Q \frac{dQ_i}{dt} \ , \tag{3.20}$$

where J_{M_v} and K_Q are constants and represent the moment of inertia of the water inside the impeller, and the effects of flow changes on the impeller torque respectively. These constants are given by,

$$J_{M_v} = 2\pi h\rho \int_{R_1}^{R_2} r^3 dr \qquad K_Q = \rho \int_{R_1}^{R_2} r \cot(\beta(r)) dr \ .$$

The first term on the right-hand side of (3.20) describes the change of momentum of the liquid inside the impeller due to changes in the impeller speed. The second term on the right-hand side describes the tangential change of liquid speed due to flow changes. As it is a change of speed in the tangential direction it will affect the transient component of the shaft torque, as it is shown in (3.20).

The combined torque expression

From (3.19) and (3.20) the final expression of the external torque on the impeller is found,

$$T_p = -a_{t2} Q_i^2 + a_{t1} \omega_r Q_i + a_{t0} \omega_r^2 + J_{M_v} \frac{d\omega_r}{dt} - K_Q \frac{dQ_i}{dt} \ , \tag{3.21}$$

where T_p is the external torque on the impeller.

3.3.3 The Head Expression

In this section an expression of the head is derived from the torque expression (3.18), presented in the previous section. Head is defined by,

$$H_p = \rho g H \ ,$$

where H is the head and H_p is the pressure. The theoretical head H_e is given by $H_e = P/(Q_i \rho g)$, where g is the gravity and $P = T_i \omega_r$ is the power. Including this in (3.18) the following expression is obtained,

$$H_e = \left(\frac{r_2^2}{g} - \frac{r_1^2}{g} \right) \omega_r^2 - \left(\frac{r_2}{g A_2} cot(\beta_2) - \frac{r_1}{g A_1} cot(\beta_1) \right) \omega_r Q_i \ . \tag{3.22}$$

The head described by (3.22) is the theoretical obtainable head of the impeller. This head is not equal to the head between the inlet and outlet of the pump due to head losses. The following types of head losses are expected to influence the theoretical head (Sayers, 1990),

- Slip factor, here named σ_s.
- Shock losses, here named h_s.
- Friction losses, here named h_f.

The slip factor is an empirical factor used to account for re-circulating flow inside the impeller. The two last head losses are due to friction and shock losses inside the impeller and at the inlet of the impeller respectively. The head losses affect the theoretical head as shown in the following equation,

$$H + h_s + h_f = \sigma_s H_e \ , \tag{3.23}$$

where H is the head between the inlet and outlet of the pump. The shock and friction losses are given by,

$$h_s = K_s(Q_i - Q_d)^2 \qquad h_f = K_f Q_i^2 \ ,$$

where Q_d is the design flow, which is a linear expression of the angular velocity e.i. $Q_d = K_d\omega_r$. K_s, K_f and K_d are all constants. When including these expressions in (3.23) the model describing the head becomes,

$$H = -a_{h2}Q_i^2 + a_{h1}\omega_r Q_i + a_{h0}\omega_r^2 \ , \tag{3.24}$$

where H is the head produced by the pump, ω_r is the impeller speed, and Q_i is the volume flow through the impeller. The parameters in the expression are given by,

$$a_{h2} = K_s + K_f \qquad a_{h1} = 2K_sK_d - \sigma_s\left(\frac{r_2}{gA_2}cot(\beta_2) - \frac{r_1}{gA_1}cot(\beta_1)\right)$$
$$a_{h0} = \sigma_s\left(\frac{r_2^2}{g} - \frac{r_1^2}{g}\right) - K_sK_d^2 \ .$$

The slip factor σ_s in the expression above is, as explained before, an empirical scaling factor and is in general a non-linear function of the flow and the angular velocity, (Sayers, 1990). However, if this factor is assumed constant the parameters a_{h2}, a_{h1} and a_{h0} are also constants.

3.3.4 Leakage Flow and Pressure Losses in the Inlet and Outlet

The model equations derived in the previous part of this section describe the relations between the speed and flow of the impeller, and the pressure generated by the impeller.

The impeller is not the only component affecting the hydraulic performance of the pump, as the fluid also passes through the inlet, the diffuser, the volute and the outlet on its way through the pump, see Fig. 3.6. To have a complete model of the hydraulic performance of the pump, leakage flow and pressure losses caused by these components must be considered.

In Fig. 3.9 the leakage flow q, the inlet and outlet flow Q_p, and the impeller flow Q_i are presented.

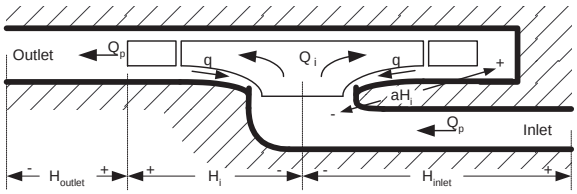

Figure 3.9: Sketch of the flows inside the centrifugal pump. Q_p is the main flow component and q is the leakage flow between the pressure and suction side of the impeller.

The leakage flow q in this figure is calculated using,

$$K_J \frac{d}{dt} q = a\rho g H_i - K_l q^2 \ ,$$

where K_J is a constant depending on the mass of the fluid involved in the leakage, a is a scaling constant taking into account that the pressure acting on leakage flow is not the same as the pressure delivered by the impeller, and finally K_l models pressure losses in the loop of the leakage flow q.

The pressure losses H_{inlet} and H_{outlet} in Fig. 3.9, at the inlet and outlet of the pump respectively, are modelled by adding an extra pressure loss term K_c in the flow Q_p. These pressure losses are called casing losses, as the pressure losses are caused by the casing of the pump.

If each of the pressure losses are symbolized as valves, and the theoretical pressure $\rho g H_e$ is symbolized as a pump without losses, the diagram in Fig. 3.10 describes the operation of the centrifugal pump.

Pump model including leakage flow

Including the description of the lekage flow q in the expressions of the impeller head and torque in (3.24) and (3.21) respectively, the following model of the centrifugal pump is

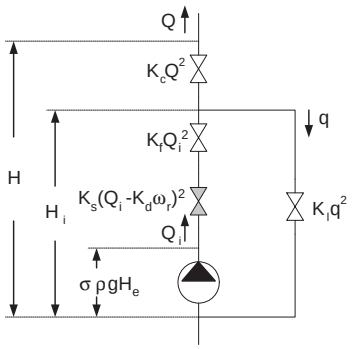

Figure 3.10: Diagram of the centrifugal pump. The valves describe the losses inside the centrifugal pump, and the pump symbol symbolizes generated pressure without losses.

obtained,

$$\begin{aligned} K_J \tfrac{dq}{dt} &= \rho g(-a_{h2}(Q_p+q)^2 + a_{h1}(Q_p+q)\omega_r + a_{h0}\omega_r^2) - K_l q^2 \\ H_p &= \rho g(-a_{h2}(Q_p+q)^2 + a_{h1}(Q_p+q)\omega_r + a_{h0}\omega_r^2) - K_c Q_p^2 \\ T_p &= -a_{t2}(Q_p+q)^2 + a_{t1}(Q_p+q)\omega_r + a_{t0}\omega_r^2 + J_{M_v}\tfrac{d\omega_r}{dt} - K_Q\left(\tfrac{dQ_p}{dt} + \tfrac{dq}{dt}\right), \end{aligned} \tag{3.25}$$

where H_p is the pressure generated by the pump, T_p is the impeller torque and $Q_p = Q_i - q$ is the inlet flow of the pump.

Simplified pump model

When the leakage flow q in Fig. 3.10 can be neglected a simplified model of the pump can be used. The leakage flow can be neglected when Assumption 3.3.1 holds.

Assumption 3.3.1 *For most centrifugal pumps the following assumptions hold in the no fault case,*

1. *The dynamics of the leakage flow q is at least a decade faster than the main dynamics of the system, i.e. $\frac{dq}{dt} \approx 0$ almost all the time.*
2. *$|q| << |Q_p|$ meaning that $Q_p \approx Q_i$.*
3. *When 2 does not hold $T_p \approx a_{t0}\omega_r^2$ in (3.25).*

When these assumptions hold the effect of the leakage flow on the pump performance is neglible.

When Assumption 3.3.1 holds the model (3.25) can be simplified to become,

$$\begin{aligned} H_p &= \rho g(-(a_{h2}+K_c)Q_p^2 + a_{h1}\omega_r Q_p + a_{h0}\omega_r^2) \\ T_p &= -a_{t2}Q_p^2 + a_{t1}\omega_r Q_p + a_{t0}\omega_r^2 + J_{M_v}\frac{d\omega_r}{dt} - K_Q\frac{dQ_p}{dt} \ . \end{aligned} \tag{3.26}$$

3.3.5 Multi Stage Pumps

To be able to increase the pressure generated by the pump without increasing the diameter of the pump, normally a set of pump stages are connected in series. Hereby the pressure across the pump becomes,

$$H = H_1 + H_2 + \cdots + H_n \tag{3.27}$$

where n is the number of pump stages. If these n pump stages are identical, meaning that $H_i = H_{i1} = \cdots = H_{in}$ and $q = q_1 = \cdots = q_n$ the model of a multi stage centrifugal pump is given by the sum of each stage,

$$\begin{aligned} nK_J\frac{dq}{dt} &= n\rho g\left(-a_{h2}(Q_p+q)^2 + a_{h1}(Q_p+q)\omega_r + a_{h0}\omega_r^2\right) - nK_l q^2 \\ H_p &= n\rho g\left(-a_{h2}(Q_p+q)^2 + a_{h1}(Q_p+q)\omega_r + a_{h0}\omega_r^2\right) - nK_c Q_p^2 - K_c' Q_p^2 \\ T_p &= n\left(-a_{t2}(Q_p+q)^2 + a_{t1}(Q_p+q)\omega_r + a_{t0}\omega_r^2\right) + \\ &\quad nJ_{M_v}\frac{d\omega_r}{dt} - nK_Q\left(\frac{dQ_p}{dt} + \frac{dq}{dt}\right) \ . \end{aligned}$$

In this model nK_c expresses the pressure losses due to the guidens of the flow from one stage to the next. Therefore, an extra casing loss term K_c' is added to model losses at the inlet and outlet of the pump.

If Assumption 3.3.1 still holds, which is normally the case, this model can be reduced to,

$$\begin{aligned} H_p &= \rho g\left(-\left(n(a_{h2}+K_c)+K_c'\right)Q_p^2 + na_{h1}\omega_r Q_p + na_{h0}\omega_r^2\right) \\ T_p &= -na_{t2}Q_p^2 + na_{t1}\omega_r Q_p + na_{t0}\omega_r^2 + nJ_{M_v}\frac{d\omega_r}{dt} - nK_Q\frac{dQ_p}{dt} \ . \end{aligned}$$

From this it is seen that the structure of the model is the same for a serie connected set of identical stages, as for a single stage centrifugal pump.

Pump curves

Normally centrifugal pumps are described by two so-called pump curves. This is through for both multi stage and single stage pumps. The two curves depict the volume flow versus the pressure and the power of the pump respectively. Normally the curves are only depitch for one particular speed value, which is denoted the norminal speed. An example of these pump curves is shown in Fig. 3.11.

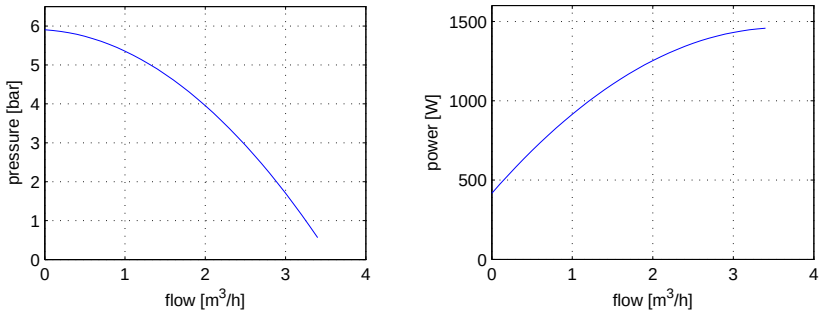

(a) Volume flow versus pressure difference. (b) Volume flow versus power consumption.

Figure 3.11: Pump curves describing the performance of a centrifugal pump at nominal speed.

3.4 The Mechanical Part of the Centrifugal Pump

In this section the mechanical part of the pump is treated, meaning that a model describing the moment of inertia and the friction losses in the mechanical parts of the pump is derived. The mechanical parts of interest when modelling the dynamics are:

- The rotor of the motor.
- The bearings in the motor and pump.
- The impeller.
- The shaft Seals.

Using Newton's second law the dynamics of the mechanical parts can be described by,

$$J_m \frac{d\omega}{dt} = T_e - T_l \ ,$$

where T_e is the torque produced by the motor (3.11), T_l is the load torque created by the impeller (3.26) and mechanical friction losses respectively, and finally J_m is the moment of inertia of the mechanical system.

The moment of inertia of the mechanical parts J_m is given by the sum of the moment of inertia of all rotating parts of the pump, i.e. it is given by,

$$J_m = J_r + J_s + J_i \ .$$

Here J_r is the moment of inertia of the induction motor rotor, J_s is the moment of inertia of the shaft, and J_i is the moment of inertia of the impeller.

If the friction losses T_f of the bearings and shaft seals are assumed linear, i.e. $T_f = B\omega_r$, the load torque is given by,

$$T_l = B\omega_r + \left(-a_{t2}Q_p^2 + a_{t1}\omega_r Q_p + a_{t0}\omega_r^2\right) + J_{M_v}\frac{d\omega_r}{dt} - K_Q\frac{dQ_p}{dt} \ .$$

In this equation the first term on the right-hand side models the mechanical friction losses, and the last term models the load torque of the impeller (3.21).

Including the load torque expression in the mechanical equations the model of the mechanical system is obtained,

$$J\frac{d\omega_r}{dt} = T_e - B\omega_r - \left(-a_{t2}Q_p^2 + a_{t1}\omega_r Q_p + a_{t0}\omega_r^2\right) + K_Q\frac{dQ_p}{dt} \ ,$$

where $J = J_m + J_{M_v}$. The term $\frac{dQ_p}{dt}$ in the above expression means that the mechanical system depends upon the dynamics of the hydraulic application. This dependency is in almost all applications very small, meaning that the following assumption holds for almost all applications.

Assumption 3.4.1 *It is assumed that the dynamics of the hydraulic application, in which the pump is placed, is such that,*

$$\left|K_Q\frac{dQ_p}{dt}\right| << \left|-a_{t2}Q_p^2 + a_{t1}\omega_r Q_p + a_{t0}\omega_r^2\right| \ ,$$

at all time. When this assumption holds it means that the application dynamics is so slow that its effect on the pump dynamics is negliable.

Using this assumption the mechanical expression becomes,

$$J\frac{d\omega_r}{dt} = T_e - B\omega_r - \left(-a_{t2}Q_p^2 + a_{t1}\omega_r Q_p + a_{t0}\omega_r^2\right) \ .$$

3.5 Final Model of the Centrifugal Pump

The model derived in the previous sections is described on state space form by the following system,

$$\begin{aligned} \dot{\mathbf{x}} &= \mathbf{f}(\mathbf{x}) + \mathbf{G}\mathbf{u} + \mathbf{m}(\mathbf{x}, \mathbf{w}) \\ \mathbf{y} &= \mathbf{h}(\mathbf{x}, \mathbf{w}) \ . \end{aligned} \tag{3.28}$$

In this system the state vector is,

$$\mathbf{x} = \begin{bmatrix} i_{sd} & i_{sq} & i_{md} & i_{mq} & \omega_r \end{bmatrix}^T \ ,$$

where i_{sd} and i_{sq} are the motor currents in a dq-frame fixed on the stator, i_{md} and i_{mq} are the magintizing currents described in the same frame, and finally ω_r is the mechanical speed of the pump.

The inputs of the system consist of the known input vector $\mathbf{u}$ and the unknown input vector $\mathbf{w}$, given by,

$$\mathbf{u} = \begin{bmatrix} v_{sd} & v_{sq} \end{bmatrix}^T \qquad \mathbf{w} = \begin{bmatrix} Q_p \end{bmatrix}^T \ ,$$

where v_{sd} and v_{sq} are the supply voltages of the motor described in the same dq-frame as the motor currents, and the unknown input is the volume flow Q_p through the pump.

Except for the known inputs it is assumed that three variables are measured. These are the motor currents and the pump pressure respectively. Therefore, the measurement vector $\mathbf{y}$ in (3.28) is given by,

$$\mathbf{y} = \begin{bmatrix} i_{sd} & i_{sq} & H_p \end{bmatrix}^T \ .$$

The matrix $\mathbf{G}$, the vector fields $\mathbf{f}(\mathbf{x})$ and $\mathbf{m}(\mathbf{x}, \mathbf{w})$ and the mapping $\mathbf{h}(\mathbf{x}, \mathbf{w})$ in (3.28) are presented below,

$$\mathbf{f}(\mathbf{x}) = \begin{pmatrix} -\frac{R_s+R'_r}{L'_s} i_{sd} + \frac{R'_r}{L'_s} i_{md} - z_p \omega_r \frac{L'_m}{L'_s} i_{mq} \\ -\frac{R_s+R'_r}{L'_s} i_{sq} + z_p \omega_r \frac{L'_m}{L'_s} i_{md} + \frac{R'_r}{L'_s} i_{mq} \\ \frac{R'_r}{L'_m} i_{sd} - \frac{R'_r}{L'_m} i_{md} + z_p \omega_r i_{mq} \\ \frac{R'_r}{L'_m} i_{sq} - z_p \omega_r i_{md} - \frac{R'_r}{L'_m} i_{mq} \\ \frac{1}{J} \frac{3}{2} z_p L_m \left(i_{md} i_{sq} - i_{mq} i_{sd} \right) - \frac{B}{J} \omega_r \end{pmatrix}$$

$$\mathbf{G} = \begin{pmatrix} \frac{1}{L'_s} & 0 \\ 0 & \frac{1}{L'_s} \\ 0 & 0 \\ 0 & 0 \\ 0 & 0 \end{pmatrix} \qquad \mathbf{m}(\mathbf{x}, \mathbf{w}) = \begin{pmatrix} 0 \\ 0 \\ 0 \\ 0 \\ -\frac{1}{J} f_T(Q_p, \omega_r) \end{pmatrix}$$

$$\mathbf{h}(\mathbf{x}, \mathbf{w}) = \begin{pmatrix} i_{sd} \\ i_{sq} \\ f_H(Q_p, \omega_r) \end{pmatrix} \ ,$$

where the first four rows in the model represent the electrical part of the induction motor and the fifth row describes the mechanical part of the pump.

In this model the expression $f_H(Q_p, \omega_r)$ describes the pressure produced by the pump, and the expression $f_T(Q_p, \omega_r)$ describes the load torque of the pump. These expressions are derived in Section 3.3, and are given by,

$$\begin{aligned} f_H(Q_p, \omega_r) &= \rho g \left(-a_{h2} Q_p^2 + a_{h1} Q_p \omega_r + a_{h0} \omega_r^2 \right) \\ f_T(Q_p, \omega_r) &= -a_{t2} Q_p^2 + a_{t1} Q_p \omega_r + a_{t0} \omega_r^2 \ , \end{aligned} \tag{3.29}$$

where a_{h2}, a_{h1}, a_{h0} and a_{t2}, a_{t1}, a_{t0} are constant parameters found from the physical properties of the pump, see Section 3.3.

The model presented above is not valid in the whole state space since the functions $f_H(Q_p, \omega_r)$ and $f_T(Q_p, \omega_r)$ are only valid for positive flow and speed. Therefore, the state space of interest for this system is given by $\mathcal{D} = \{(\mathbf{x}, \mathbf{w}) | (x_1, \cdots, x_4) \in R^4, x_5 \in R_+, w \in R_+\}$, where $x_1, \cdots, x_5$ are states in the state vector and $\mathbf{w}$ is the unknown input signal.

3.6 Discussion

In this chapter a model of the centrifugal pump including an induction motor drive is derived. The obtained model is a fifth-order lumped parameter system, making Fault Detection and Identification designs, based on this model, possible. However, the model is very nonlinear, therefore a linearized version of the model is only expected to work in a small neighborhood around the point of linearization. The model is composed of three sub-models describing the electrical part of the motor, the mechanical parts of the system and the hydraulic parts of the system respectively.

In the derivation of the model the dynamics is taking into account. It is shown that under two assumptions given in the chapter, and if the mass of the liquid inside the impeller is added to the mass of the impeller itself, the model of the hydraulics becomes purely algebraic. This means that the liquid inside the impeller affects the moment of inertial in the mechanical description of the pump, and that no additional dynamics are added to the model due to the hydraulics of the pump.

The obtained model or sub-models will in the following be used in the derivation of FDI-algorithms. Moreover, the understanding of the system obtained through the model, is used in the design of a test setup, where a number of hydraulic, mechanical and electrical faults can be simulated.

Chapter 4

System Analysis and Fault Modelling

In (Jørgensen, 1995), (Bøgh, 1997) and (Izadi-Zamanabadi, 1999) systematic methods for developing fault detection, isolation and accommodation algorithms are presented. These systematic methods include analysis tools aimed to identify faults and their causes in physical systems. Failure Mode and Effect Analysis (FMEA) and Fault Propagation Analysis (FPA) are proposed, as a way to start the development of these fault detection, isolation and accommodation algorithms. These analysis tools will in this chapter be used to analyse the centrifugal pump, resulting in a list of faults, which are expected to happend in centrifugal pumps. A subset of these faults are chosen for futher investigation.

In Chapter 2 two basically different approaches to the fault detection and isolation (FDI) problem were introduced. The first of these approaches is the signal-based approach, where a set of events are extracted from the set of measurements on the system. The second approach is the model-based approach, where a model of the system is used to extract knowledge of abnormal operation of the system. In Chapter 2 it is argued that robustness is treated extensively in the second approach, but is hardly considered in the first approach.

The model obtained using the FMEA and FPA is a logical model connecting faults in the system with a set of effects chosen by the user. In this chapter a method for using this model to analyse the robustness of signal based fault detection schemes is proposed. This is done by defining a set of disturbing events, which are treated in the same way as the faults in the FEMA and FPA. Hereby a model connecting both the faults and disturbing events to the chosen set of end effects is obtained. The robustness of the signal-based fault detection scheme is then obtained by analysing the connection among faults, disturbing events and end-effects, where the end-effects are chosen as a subset of the measurable events in the system. To help doing this a set of definitions and theorems

are developed.

By including the notation of disturbing events in the FPA, the use of the approach is extended to handle robustness of signal-based fault detection schemes. However, it does not solve the problem with the manual steps in the analysis. One of these manual steps is the cutting of loops inherent in the system under investagation (Bøgh, 1997). In this chapter an automated way of handling these loops is proposed, meaning that the remaining manual step is to setup the event model.

The chapter starts by presenting some preliminaries on the FMEA and FPA and their use in connection with fault detection, isolation and accommodation in Section 4.1. The remaining parts of the chapter are devoted to the presentation of the contributions on the FMEA and FPA obtained in this work. First, the theoretical contributions are presented, followed by the FMEA and FPA results on the centrifugal pump. In Section 4.2 the theoretical results are presented. They are obtained using FMEA and FPA for robustness analysis of signal-based fault detection schemes. In Section 4.3 the results obtained by using the ideas, developed in Section 4.2, on the centrifugal pump are presented. This includes a list of faults expected in the system, a FMEA and FPA model of the system, and an analysis of the signal based detection possibilities. Finally, the chapter ends with a presentation of test results obtained on a test setup particular developed for this propose, and some concluding remarks. This is in Section 4.4 and 4.5 respectively.

4.1 Method for Fault Analysis

In (Izadi-Zamanabadi, 1999) a structured method for developing fault detection, isolation and accommondation algorithms is described. The method includes 8 steps where step numbers 1, 2 and 6 are interesting from a fault detection and isolation point of view. These steps are shortly described here:

Fault modeling - step 1: In this step a qualitative model of the faults in each componet of the system is made. This is done by dividing the system into suitable components. In each of these components the faults and their effects are identified and described. This is done using the Failure Mode and Effect Analysis (FMEA).

Fault propagation analysis (FPA)- step 2: In this step the propagation of the identified faults through the component of the systems is analysed. The result of this analysis is a description of the connection between the faults in the system and a set of interesting effects. This analysis is called Fault Propagation Analysis (FPA), and is performed by first identifing the functional connection between the components of the system, ending with a functional diagram (Bøgh, 1997). After that this diagram is used for the fault propagation analysis.

Detector design - step 6: In this step detectors for detecting the fault in the system are developed. Different approaches have be used in this step. The state of the art on the area of fault detection and isolation in pumps is presented in Chapter 2.

In (Izadi-Zamanabadi, 1999) an extension to this step is proposed using structural analysis. Structural analysis will also be used in this thesis as a tool for analysing the model structure of the system before designing residual generators.

In this chapter the two first steps are performed on the centrifugal pump, while the rest of the thesis is devoted to the last step.

From the above list it is seen that FMEA and FPA are used in steps 1 and 2. These analysis tools form a systematic way of creating a high level qualitative model of the system under consideration. The model needs only to be descriptive for the behaviour under faulty conditions, which allow the model to be simple compared to dynamical models.

Traditionally the FMEA and FPA have been used for analysing the fault behaviour of a system, and to identify reconfiguration possiblities. Hereby the conditions for fault robust control of the given system are obtained (Blanke et al., 2003). However, in this work the purpose of introducing the FMEA and FPA is different. Here these analysis tools are used as a first step in developing FDI algorithms. The purpose of using FMEA and FPA is two folded, as it is used for both identifing the set of most important faults in the system, and analysing different combinations of sensors for detection possiblities. These sensor combinations are in this thesis denoted sensor configurations. The first of these purposes is the normal outcome of a FMEA analysis when used in the design of fault robust control algorithms (Blanke et al., 2003) and qualitative analysis of products.

4.1.1 Preliminaries: The FMEA and FPA

This section contains a short presentation of the FMEA and FPA, and their utilizations in developing Fault Robust Control algorithms. This presentation is included for readers not familiar with these analysis tools, and their use in the area of fault detection and accommodation.

FMEA is a tool originally developed by reliability engineers to analyse components of a system for possible failures, and their causes and effects (Blanke et al., 2003). This tool is for analysing single components of a system, therefore the first step in a FMEA is to identify these components in the system. Each of the components is then analysed resulting in a set of tables including information about the failure modes, failure causes, failure effects and risk assessment for each component. An example of such a table is shown in Table 4.1.1, where a pressure sensor is considered. The table can also include risk code and actions required. But this information is not used, when the FMEA is utilized for designing fault detection and accommodation algorithms, therefore it is omitted here.

This FMEA table includes information of the importance of each of the faults in the *risk assessment* column, and the connection between the failure modes and the failure effects can be deduced from the *Failure mode* and *Failure Effect* column. Mathematrically this connection can be expressed via the fault propagation matrix defined in Definition 4.1.1.

Table 4.1: An example of a typical FMEA worksheet (Blanke et al., 2003, Chap. 4). In this example the result of analysing a pressure sensor is shown.

Item ident.	*Failure mode*	*Failure cause*	*Failure effect*	*Risk assessment*
Pressure sensor	Clogging	Dirt	Zero output	High
	Broken supply wire	Mechanical vibration	Undefined output	Low

Definition 4.1.1 (Fault propagation matrix) *(Blanke et al., 2003, p. 78) For a given boolean mapping* $\mathbf{M}$*,*

$$\mathbf{M} : \mathcal{F} \times \mathcal{E} \rightarrow \{0, 1\}$$

of the finite set of component faults $\mathcal{F}$ *onto the finite set of effects* $\mathcal{E}$*. The fault propagation matrix is defined as follows*

$$m_{i,j} = \begin{cases} 1 & \text{if } f_{cj} = 1 \rightarrow e_{ci} = 1 \\ 0 & \text{otherwise} \end{cases},$$

where f_{cj} *is the* j^{th} *component in* $\mathbf{f}_c \in \mathcal{F}$*, and* e_{ci} *is the* i^{th} *component in* $\mathbf{e}_c \in \mathcal{E}$*.*

As described in the beginning of this section the FMEA is a component-based analysis. Therefore only knowledge on each component is gained through this analysis. A system will, in most cases, contain several components, and faults in one component can affect other components in the system. Therefore a given fault in one component can cause total failure in the system due to propagation of the fault effects through other components in the system. To analyse the propagation of the identified faults, the fault propagation analysis (FPA) is used. The aim of the FPA is to identify the connection from the set of all failure modes in the system to a decided set end-effects $\mathbf{e}_{end}$. These end-effects are normally the set of effects causing mailfunction of the system.

The result of the FPA is a fault propagation model or diagram. The first step in the derivation of this model is to describe the physical connections of the components analysed using the FMEA. The model describing these connections is called the functional model. Using the functional model the propagation of the effects of one part to the effects on another part is described, and depicted in a FPA diagram. An example of such a diagram is shown in Fig. 4.1. The propagation of the faults is also described mathematically using propagation matrices defined as in Definition 4.1.1, where parts of the propagation matrix propagate one set of effects onto another set of effects. In this case the set $\mathcal{F}$ contains the possible input effect vectors and $\mathcal{E}$ contains the possible output effect vectors.

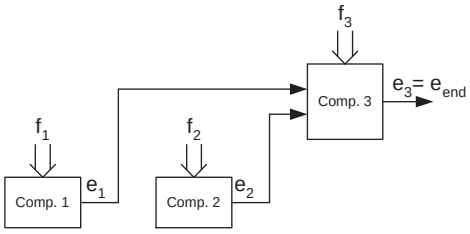

Figure 4.1: The propagation of failures in a system. The failures $\mathbf{f}_1$ and $\mathbf{f}_2$ are propergated through component 3, thereby their end effects are identified in $\mathbf{e}_3 = \mathbf{e}_{end}$.

The result of the FPA is a connection between faults in the system and a decided set of end-effects. The understanding of the propagation can be used to identify where in the system faults can be stopped in order to prevent total failure of the system. This knowledge can then be used in the development of reconfiguration logic for fault accommodation.

In Fig. 4.1 it is emphasized that the connections between the faults in the system and the end-effects are given by simple propagation through the components of the diagram. Unfortunately this is not always the case, as loops can occure in the FPA diagram (Blanke et al., 2003, Chap. 4). An example of a FPA diagram with a loop is shown in Fig. 4.2. Such loops arise due to the physical structure of the system, and can therefore

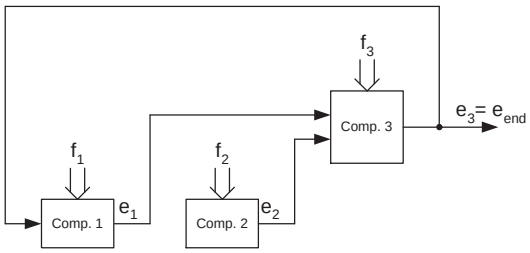

Figure 4.2: Loop example in a fault propagation diagram of a system contaning three components.

not be avoided in the model. Instead the loops are treated by cutting the connection somewhere in the loop, and then extend the set of faults with the cutted effects. Afterwards each of the cutted effects are analysed to decide if they could be removed from the FPA or should be treated as an extra fault.

In the above text it is mentioned that the FMEA and FPA traditionally are used for designing Fault Tolerant Control systems. But if the end-effects are chosen as a subset

of the measurable effects in the system, the FPA can be used in the development of FDI algorithms. An example of this is shown in (Thomsen, 2000). Here the FPA is used for analysing sensor configurations, revealing the connection between the faults in the system and the set of measurable signals. Hereby the usability of different sensor configuration can be analysed. In the following this approach is further developed to handle robustness with respect to events in the system, which should not be considered as faults. Finally, the developed approach is used in the analysis of the centrifugal pump.

4.2 Automated FPA

This section is concerned with the theoretical contributions to the FMEA and FPA, when used in connection with FDI design. Firstly, an algorithm is proposed, which automates the cutting of loops in the FPA diagram. Secondly, robustness of the chosen signal events is considered.

4.2.1 The Automated FPA Algorithm

From the FPA diagram in Fig. 4.1 it is seen that a general component of this diagram has a structure as shown in Fig. 4.3. Here $\mathbf{f}_i$ is a vector containing the possible faults

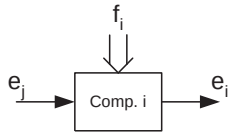

Figure 4.3: A single component in a FMEA. $\mathbf{f}_i$ is the possible failures of the component, $\mathbf{e}_j$ is effects affecting the component and $\mathbf{e}_i$ is the effects on the component performance due to $\mathbf{f}_i$ and $\mathbf{e}_j$ respectively.

in the component, $\mathbf{e}_j$ contains the effects affecting the component, and $\mathbf{e}_i$ contains the effects on the component due to $\mathbf{f}_i$ and $\mathbf{e}_j$ respectively. The component shown in Fig. 4.3 implies that a component in the FPA diagram can be described as defined in definition 4.2.1.

Definition 4.2.1 (Component description) *The i^{th} component c_i in the system $\mathcal{S}$ contaning n components, i.e. $\mathcal{S} = \bigcup_{i=1}^{n} c_i$, is described by,*

$$\mathbf{e}_i \leftarrow \mathbf{A}^i_{f_i} \cdot \mathbf{f}_i + \sum_{j=1}^{i-1} \mathbf{A}^i_j \cdot \mathbf{e}_j + \sum_{j=i+1}^{n} \mathbf{A}^i_j \cdot \mathbf{e}_j \ , \tag{4.1}$$

where

- $\mathbf{A}^i_{f_i} : \mathcal{F}_i \times \mathcal{E}_i \rightarrow \{0,1\}$ *and* $\mathbf{A}^i_j : \mathcal{E}_j \times \mathcal{E}_i \rightarrow \{0,1\}$ *are propagation matrices on form described in Definition 4.1.1.*
- $\mathbf{f}_i \in \mathcal{F}_i = \{0,1\}^{n_i}$ *is the set of faults associated with* i^{th} *component.*
- $\mathbf{e}_j \in \mathcal{E}_j = \{0,1\}^{m_j}$ *is the set of effects associated with* j^{th} *component.*
- $+$ *is the boolean disjunction operator* $\vee$ *and* $\cdot$ *is the boolean conjunction operator* $\wedge$*. Both defined as vector operators.*

Remark 4.2.1 *In Definition 4.2.1* $\mathbf{A}^i_j = 0$ *means that there does not exist a connection from component* j *to component* i *in the FPA diagram. And* $\mathbf{A}^i_{f_i} = 0$ *means that no faults affect the* i^{th} *component.*

Remark 4.2.2 *This description is similar to the one used in (Jørgensen, 1995; Blanke et al., 2003) except for opertator and matrix notation. In (Blanke et al., 2003, Chap. 4) all the matrices* $\mathbf{A}^i_{f_i}$ *and* $\mathbf{A}^j_i$ *are lumped into one matrix* $\mathbf{M}^f_i$*. An example of such a matrix is shown below,*

$$\mathbf{e}_i \leftarrow \mathbf{M}^f_i \otimes \begin{pmatrix} \mathbf{f}_i \\ \mathbf{e}_1 \\ \mathbf{e}_2 \\ \vdots \\ \mathbf{e}_n \end{pmatrix} = \begin{pmatrix} \mathbf{M}^f_{i,f} & \mathbf{M}^f_{i,e_1} & \mathbf{M}^f_{i,e_2} & \dots & \mathbf{M}^f_{i,e_n} \end{pmatrix} \otimes \begin{pmatrix} \mathbf{f}_i \\ \mathbf{e}_1 \\ \mathbf{e}_2 \\ \vdots \\ \mathbf{e}_n \end{pmatrix} ,$$

where $\mathbf{A}^i_f = \mathbf{M}^f_i$ *and* $\mathbf{A}^i_j = \mathbf{M}^f_{i,e_j}$ *in Definition 4.2.1.*

The component description in Definition 4.2.1 is slightly different from the conventional one as seen in Remark 4.2.2. The reason for this will be obvious later in this section.

In Definition 4.2.1 a description of each component in the FPA diagram is defined. Moreover the structure of the diagram is implicit given by the set of propagation matrices, which equals 0. An example of a FPA diagram is shown in Fig. 4.1. The structure of this diagram can be described by a graph G_e and a graph G_f, where G_e contains the structure of the propagation of the effects in the system, and G_f contains the structure of the propagation from the fault vectors $\mathbf{f}_i$ to the effect vectors $\mathbf{e}_i$ $\forall i \in \{1, 2, \cdots, n\}$. The graphs G_e and G_f are defined as in Definition 4.2.2.

Definition 4.2.2 (Graph representation) *A graph representation of a FPA diagram is defined by two graphs, namely a directed graph (digraph)* G_e *and a bi-partite graph* G_f*. The digraph* G_e *is a graph with* n *vertices* $\mathcal{Y}$*. Where the vertex* $y_i \in \mathcal{Y}$ *is associated with the effect vectors* $\mathbf{e}_i$*. The edges of* G_e *are defined by the following rule,*

- *A directed edge exists from* y_i *to* y_j *if the matrix* $\mathbf{A}^j_i \neq 0$*, where the matrix* $\mathbf{A}^j_i$ *is defined in Definition 4.2.1.*

The bi-partite graph G_f is a graph with m vertices $\mathcal{U}$ and n vertices $\mathcal{Y}$. Where the vertex $u_i \in \mathcal{U}$ is associated with the fault vector $\mathbf{f}_i$ and the vertex $y_j \in \mathcal{Y}$ is associated with the effect vector $\mathbf{e}_j$. The edges of G_f are defined by the following rule,

- *An edge exists between u_i and y_j if the matrix $\mathbf{A}_{f_j}^i \neq 0$, where the matrix $\mathbf{A}_{f_j}^i$ is defined in Definition 4.2.1.*

A example of the graphs defined in Definition 4.2.2 are shown in Figs. 4.4 and 4.5. The above definition defines a general graph representation of the FPA diagram. The adjacency matrix D_e associeated with G_e includes the structure of the FPA diagram, meaning that loops in the FPA diagram are seen in this matrix. Using this graph representation it is possible to define the properties for the system to be on calculable form. This is formulated in Defintion 4.2.3. Here the calculability is defined from the structure of the adjacency matrix D_e of G_e.

Definition 4.2.3 (Calculable graph reprecentation) *The system described by the graph representation in Definition 4.2.2 is on calculable form if the n vertices in $\mathcal{Y}$ are ordered, e.i. $\mathcal{Y} = \{y_1, y_2, \cdots, y_n\}$, such that the adjacency matrix D_e associated with G_e has the following structure,*

$$D_e = \begin{bmatrix} 0 & 0 & \dots & 0 & 0 & 0 \\ d_{2,1} & 0 & \dots & 0 & 0 & 0 \\ d_{3,1} & d_{3,2} & \dots & 0 & 0 & 0 \\ \vdots & \vdots & \ddots & \vdots & \vdots & \vdots \\ d_{n-1,1} & d_{n-1,2} & \dots & d_{n-1,n-2} & 0 & 0 \\ d_{n,1} & d_{n,2} & \dots & d_{n,n-2} & d_{n,n-1} & 0 \end{bmatrix},$$

where $d_{i,j} \in \{0, 1\}$. Moreover the vertex representing the end-effect $\mathbf{e}_{end}$ must be the last vertex in $\mathcal{Y}$, i.e. the vertex y_n is associated with $\mathbf{e}_{end}$.

All FPA diagrams with a graph representation as defined in Defintion 4.2.2, which do not contain loops, can be transformed to this form by changing the order of the vertices in $\mathcal{Y}$ (Shih, 1999).

If the graph representation is on the form defined in Definition 4.2.3 the following theorem can be used for calculating the connection between faults and end-effects.

Theorem 4.2.1 *Let the graph representation of a system be on the form defined in Definition 4.2.3, with n vertrices in $\mathcal{Y}$ and m vertices in $\mathcal{U}$. Then by association of the edge $d_{i,j}$ in D_e with $\mathbf{A}_j^i$, the connection between the faults $\mathbf{f} = \begin{pmatrix} \mathbf{f}_1^T & \mathbf{f}_2^T & \cdots & \mathbf{f}_m^T \end{pmatrix}^T$ and the end-effect vector $\mathbf{e}_n$ is given by,*

$$\mathbf{e}_n \leftarrow \begin{bmatrix} \mathbf{T}_1 & \mathbf{T}_2 & \dots & \mathbf{T}_{n-1} & \mathbf{I} \end{bmatrix} \cdot \mathbf{A}_f \cdot \mathbf{f} \tag{4.2}$$

where,

$$\mathbf{T}_{n-1} = \mathbf{A}^n_{n-1}$$
$$\mathbf{T}_{n-k} = \mathbf{A}^n_{n-k} + \sum_{i=1}^{k-1} \mathbf{T}_{n-i} \cdot \mathbf{A}^{n-i}_{n-k}$$

and

$$\mathbf{A}_f = \begin{bmatrix} \mathbf{A}^1_{f_1} & \mathbf{A}^1_{f_2} & \cdots & \mathbf{A}^1_{f_m} \\ \mathbf{A}^2_{f_1} & \mathbf{A}^2_{f_2} & \cdots & \mathbf{A}^2_{f_m} \\ \vdots & \vdots & \ddots & \vdots \\ \mathbf{A}^n_{f_1} & \mathbf{A}^n_{f_2} & \cdots & \mathbf{A}^n_{f_m} \end{bmatrix}.$$

In $\mathbf{A}_f$ the submatrix $\mathbf{A}^i_{f_j} \neq 0$ if there is an edge from the vertex $u_j \in \mathcal{U}$ to the vertex $y_i \in \mathcal{Y}$ else $\mathbf{A}^i_{f_j} = 0$.

Proof: If the graph G_e of a system, defined as in Definition 4.2.2, is on the form defined in Definition 4.2.3 the logical structure of the system is given by,

$$\begin{aligned} \mathbf{e}_1 &= \mathbf{A}^1_f \cdot \mathbf{f} \\ \mathbf{e}_2 &= \mathbf{A}^2_1 \cdot \mathbf{e}_1 + \mathbf{A}^2_f \cdot \mathbf{f} \\ \mathbf{e}_3 &= \mathbf{A}^3_1 \cdot \mathbf{e}_1 + \mathbf{A}^3_2 \cdot \mathbf{e}_2 + \mathbf{A}^3_f \cdot \mathbf{f} \\ &\vdots \\ \mathbf{e}_{n-1} &= \mathbf{A}^n_1 \cdot \mathbf{e}_1 + \mathbf{A}^n_2 \cdot \mathbf{e}_2 + \cdots + \mathbf{A}^n_{n-2} \cdot \mathbf{e}_{n-2} + \mathbf{A}^{n-1}_f \cdot \mathbf{f} \\ \mathbf{e}_n &= \mathbf{A}^n_1 \cdot \mathbf{e}_1 + \mathbf{A}^n_2 \cdot \mathbf{e}_2 + \cdots + \mathbf{A}^n_{n-2} \cdot \mathbf{e}_{n-2} + \mathbf{A}^n_{n-1} \cdot \mathbf{e}_{n-1} + \mathbf{A}^n_f \cdot \mathbf{f} \end{aligned} \tag{4.3}$$

where each $\mathbf{A}^j_i$ corresponds to $d_{j,i}$ in the adjacency matrix D_e of the digraph G_e, and $\mathbf{f} = \begin{pmatrix} \mathbf{f}_1^T & \mathbf{f}_2^T & \cdots & \mathbf{f}_m^T \end{pmatrix}^T$, where m is the number of components affected by faults.

We search for a solution of $\mathbf{e}_n$ on the form,

$$\mathbf{e}_n = \begin{bmatrix} \mathbf{T}_1 & \mathbf{T}_2 & \cdots & \mathbf{T}_{n-1} & \mathbf{T}_n \end{bmatrix} \cdot \mathbf{A}_f \cdot \mathbf{f} \tag{4.4}$$

where $\mathbf{A}_f$ is given by,

$$\mathbf{A}_f = \begin{bmatrix} {\mathbf{A}^1_f}^T & {\mathbf{A}^2_f}^T & \cdots & {\mathbf{A}^n_f}^T \end{bmatrix}^T.$$

The structure of $\mathbf{A}_f$ corresponds to the structure of the adjacency matrix $D_f : \mathcal{F} \to \mathcal{E}$ of the bigraph G_f.

From (4.3) and (4.4) it is seen that $\mathbf{T}_n$ propagates the effects from $\mathbf{A}^n_f \cdot \mathbf{f}$ to $\mathbf{e}_n$, therefore $\mathbf{T}_n$ can be found by setting $\mathbf{A}^i_f = 0$ for all $i \neq n$. From (4.3) it is seen that all $\mathbf{e}_j$ for $j < n$ are equal to zeros in this case. This implies that,

$$\mathbf{e}_n = \mathbf{T}_n \cdot \mathbf{A}^n_f \cdot \mathbf{f} = \mathbf{I} \cdot \mathbf{A}^n_f \cdot \mathbf{f}$$

meaning that,

$$\mathbf{T}_n = \mathbf{I} \tag{4.5}$$

$\mathbf{T}_{n-1}$ is found by setting $\mathbf{A}_f^i = 0$ for all $i \neq n-1$. From (4.3) and (4.4) it is seen that all $\mathbf{e}_j$ for $j < n-1$ are equal to zeros in this case, and $\mathbf{e}_{n-1} = \mathbf{A}_f^{n-1} \cdot \mathbf{f}$. This implies that,

$$\mathbf{e}_n = \mathbf{T}_{n-1} \cdot \mathbf{A}_f^{n-1} \cdot \mathbf{f} = \mathbf{A}_{n-1}^n \cdot \mathbf{e}_{n-1}$$

meaning that,

$$\mathbf{T}_{n-1} = \mathbf{A}_{n-1}^n \tag{4.6}$$

where $\mathbf{T}_{n-1}$ propagates the effect vector $\mathbf{e}_{n-1}$ to $\mathbf{e}_n$.

Choose $k \in \{2, 3, \cdots, n-1\}$ and assuming that all $\mathbf{T}_{n-i}$ are known for $i < n-k$, then $\mathbf{T}_{n-k}$ is found by setting $\mathbf{A}_f^i = 0$ for all $i \neq n-k$. From (4.3) and (4.4) it is seen that all $\mathbf{e}_j$ for $j < n-k$ are equal to zeros in this case, and $\mathbf{e}_{n-k} = \mathbf{A}_f^{n-k} \cdot \mathbf{f}$. This means that,

$$\mathbf{e}_n = \mathbf{T}_{n-k} \cdot \mathbf{A}_f^{n-k} \cdot \mathbf{f} = \left(\mathbf{A}_{n-k}^n + \mathbf{T}_{n-(k-1)} \cdot \mathbf{A}_{n-k}^{n-(k-1)} + \cdots + \mathbf{T}_{n-1} \cdot \mathbf{A}_{n-k}^{n-1} \right) \cdot \mathbf{e}_{n-k}$$

where $\mathbf{T}_{n-i}$ propagates the effect vector $\mathbf{e}_{n-i}$ to $\mathbf{e}_n$. From this equations it is seen that,

$$\begin{aligned} \mathbf{T}_{n-k} &= \mathbf{A}_{n-k}^n + \mathbf{T}_{n-(k-1)} \cdot \mathbf{A}_{n-k}^{n-(k-1)} + \cdots + \mathbf{T}_{n-1} \cdot \mathbf{A}_{n-k}^{n-1} \\ \mathbf{T}_{n-k} &= \mathbf{A}_{n-k}^n + \sum_{i=1}^{k-1} \mathbf{T}_{n-i} \cdot \mathbf{A}_{n-k}^{n-i} \end{aligned} \tag{4.7}$$

which complets the proof. □

The above theorem represents a simple solution for finding the connection between fault and end-effects in the system. The theorem uses Definition 4.2.3, which is the same as assuming that no loops exist in the FPA diagram. Therefore, loops must be cutted before the theorem can be used. This is a well known problem and is described in (Blanke, 1996; Blanke et al., 2003; Bøgh, 1997). In these references it is suggested that a solution to the loop problem is to cut loops at places, which are sensible in a physical sense.

However, it can be argued that optimal cuts would be the set of cuts, which maximizes the number of faults seen in the chosen end-effects. By intuition these cuts would be placed such that the backward walk from the end-effect to the cut is as long as possible. As an example see Fig. 4.4, where y_4 is chosen as the vertex associated with the end-effect vector.

In this figure the edges d_2, d_3 and d_4 form a loop. This loop can be cutted at each of these edges. But by cutting d_4 all faults associated with the vertises y_2 and y_3 can be seen in the effects associated with the vertex y_4. This is not the case if the loop is cutted at either d_2 or d_3. By doing this either all effects associated with y_2 and y_3, or the effects associated with y_2 can not be seen in the effects of y_4. When d_4 is cutted it is possible to do the backward walk $y_4 \rightarrow y_3 \rightarrow y_2$, whereas in the other two cases the

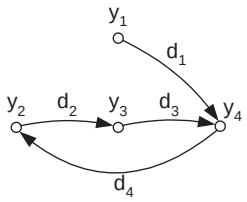

Figure 4.4: An example of the graph G_e from Definition 4.2.2. This graph represents the structure of the FPA diagram.

backward walk would be $y_4 \rightarrow y_3$ and y_4 respectively. This confirms the connection between faults seen in the end-effect and the possible steps in the backward walk.

In the following an algorithm is presented. This algorithm is designed to sort out the set of vertrices $\mathcal{Y}$ and cut edges in G_e such that the possible backward walks in G_e are maximized and D_e is on the form defined in Definition 4.2.3. When an edge is cutted it means that the propagation of an effect vector is removed from the analysis. In (Blanke et al., 2003) it is argued that the cutted effects should be added to the fault vector, and thereby treated as additional faults. In the following algorithm this is done by adding vertices to the set $\mathcal{U}$ and edges to G_f corresponding to each cutted effect. As the set of vertices $\mathcal{U}$ corresponds to the faults in the system, the set of cutted effects are hereby added to the set of faults as argued in (Blanke et al., 2003). The algorithm is given below, and an example of using this algorithm is shown in the example ending this section.

Algorithm 4.2.1 (The cutting algorithm) *Assuming that a system is described by two graphs, as defined in Definition 4.2.2, with n vertices $y_i \in \mathcal{Y}$ and m vertices $u_i \in \mathcal{U}$, where $\mathcal{Y}$ and $\mathcal{U}$ are ordered sets. Let $D_f : \mathcal{U} \rightarrow \mathcal{Y}$ be the adjacency matrix associated with the graph G_f and $D_e : \mathcal{Y} \rightarrow \mathcal{Y}$ be the adjacency matrix associated with the graph G_e. Then the algorithm is as follows:*

Initialization: *Transform D_f and D_e such that the vertex in $\mathcal{Y}$ associated with the end-effect $\mathbf{e}_{end}$ is the last vertex $\mathcal{Y}$, and for all vertices at position 1 to $n-1$ in $\mathcal{Y}$; remove all vertices with zero colomns in D_e recusively, and set $i = n'$ such that the vertex y_i is associated with $\mathbf{e}_{end}$, where n' is the number of vertices after removing zero colomns.*

Step 1: *If there are non-zero elements above the diagonal element in the i^{th} colomn of D_e then, set these equal to zero and add the vertex y_i to the set of vertices $\mathcal{U}$ and add a colomn in D_f corresponding to this new vertex $y_i \in \mathcal{U}$. This new colomn must have zero elements at position i to n' and a structure corresponding to the i^{th} colomn of D_e at position 1 to $i-1$.*

Step 2: *Sort out the vertices at possition* 1 *to* $i-1$ *in* $\mathcal{Y}$ *such that the vertex at position* $i-1$ *is the vertex with edges incident to one or more of the vertices at position* i *to* n' *and with fewest edges incident to the vetices at position* 1 *to* $i-1$.

Step 3: *Set* $i := i-1$ *and go to step 1.*

Using this algorithm on a given graph representation, the graphs G_f and G_e are forced to have a structure as defined in Definition 4.2.3. Therefore Theorem 4.2.1 states the connection between fault and end-effects. The obtained logical expression is on the form,

$$\mathbf{e}_{end} \leftarrow \mathbf{A} \cdot \mathbf{f} \ . \tag{4.8}$$

In this expression $\mathbf{f}$ contains both the faults in the system, and the effects cutted using the cutting Algorithm 4.2.1. As it is argued in (Blanke et al., 2003; Bøgh, 1997), each of the cutted effects should be analysed to check if they can be omitted in the analysis, or should be treated as an additional fault.

Remark 4.2.3 *It would be possible to define the two graphs in Definition 4.2.3 such that each vertex in* $\mathcal{U}$ *is associated with a single fault* f_i *and not a fault vector* $\mathbf{f}_i$*, and likewise each vertex* $\mathcal{Y}$ *is associated with a single effect* e_i *and not a vector of effects* $\mathbf{e}_i$*. This approach is not chosen here as the physical meaning is somewhat lost by doing that.*

In the following example the result of using this algorithm on a small system containing only four components is shown.

Example

Using Definition 4.2.1 a system containing 4 components is shown in Table 4.2.1. Here

Table 4.2: An example of a system containing 4 components. $\mathbf{f}_i$ contains failure modes and $\mathbf{e}_i$ contains failure effects in the i'th component, and $\mathbf{A}^i_{f_i}$ and $\mathbf{A}^i_j$ are fault propagation matrices.

Part	Name	Failures	Effects	Transformations
c_1	Comp. 1	$\mathbf{f}_1$	$\mathbf{e}_1$	$\mathbf{A}^1_{f_1}, \mathbf{A}^1_4$
c_2	Comp. 2	0	$\mathbf{e}_2$	$\mathbf{A}^2_3$
c_3	Comp. 3	$\mathbf{f}_3$	$\mathbf{e}_3$	$\mathbf{A}^3_{f_3}, \mathbf{A}^3_1, \mathbf{A}^3_2$
c_4	Comp. 4	$\mathbf{f}_4$	$\mathbf{e}_4$	$\mathbf{A}^4_{f_4}, \mathbf{A}^4_1, \mathbf{A}^4_3$

it is seen that each component c_i is described by the propagation matrices $\mathbf{A}^i_{f_i}$ and $\mathbf{A}^i_j$. The $\mathbf{A}^i_j = 0$ is omitted in the system representation.

The graph representation of the system in Table 4.2.1 is, according to Definition 4.2.2, given by the following two graphs,

$$D_f = \begin{bmatrix} 1_{1,f1} & 0 & 0 \\ 0 & 0 & 0 \\ 0 & 1_{3,f3} & 0 \\ 0 & 0 & 1_{4,f4} \end{bmatrix} \qquad D_e = \begin{bmatrix} 0 & 0 & 0 & 1_{1,4} \\ 0 & 0 & 1_{2,3} & 0 \\ 1_{3,1} & 1_{3,2} & 0 & 0 \\ 1_{4,1} & 0 & 1_{4,3} & 0 \end{bmatrix}$$

where the set of vertices $\mathcal{U} = \{u_{f_1}, u_{f_3}, u_{f_4}\}$ and $\mathcal{Y} = \{y_{e_1}, y_{e_2}, y_{e_3}, y_{e_4}\}$. In these adjacency matrices the symbol $1_{j,i}$ corresponds to a 1 in the matrix, and the subscript i, j denotes the position of vertices joint by the edge before the transformation. Here the edge is incident from the j^{th} vertex and incident to i^{th} vertex.

In these sets the vertex u_{f_i} is assosiated with the fault vector $\mathbf{f}_i$ and likewise the vertex y_{e_j} is assosiated with the effect vector $\mathbf{e}_j$. The graphs are shown in Fig. 4.5.

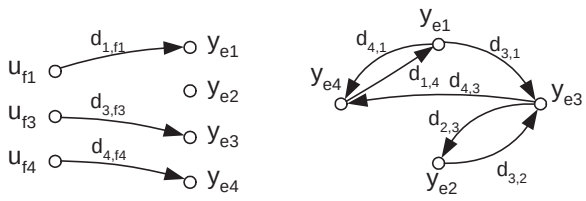

Figure 4.5: The graphs G_f (Fig. (a)) and G_e (Fig. (b)) before edges are cutted.

Now choose $\mathbf{e}_3$, e.i. $y_{e_3} \in \mathcal{Y}$, as the end-effect in the analysis. With this end-effect the adjacency matrix D_e of the graph representation is not on the form defined in Definition 4.2.3. Therefore the cutting Algorithm 4.2.1 is used to cut and sort edges in G_e to obtain the form defined in Definition 4.2.3. The first run through Algorithm 4.2.1 is shown below.

Initialization: Transforming D_f and D_e leads to the following matrix representation. Hereby the last vertex in $\mathcal{Y}$ becomes the vertex associated with the end-effect $\mathbf{e}_3$.

$$D_f = \begin{bmatrix} 1_{1,f1} & 0 & 0 \\ 0 & 0 & 0 \\ 0 & 0 & 1_{4,f4} \\ 0 & 1_{3,f3} & 0 \end{bmatrix} \qquad D_e = \begin{bmatrix} 0 & 0 & 1_{1,4} & 0 \\ 0 & 0 & 0 & 1_{2,3} \\ 1_{4,1} & 0 & 0 & 1_{4,3} \\ 1_{3,1} & 1_{3,2} & 0 & 0 \end{bmatrix}$$

with $\mathcal{U} = \{u_{f_1}, u_{f_3}, u_{f_4}\}$ and $\mathcal{Y} = \{y_{e_1}, y_{e_2}, y_{e_4}, y_{e_3}\}$. Set $i = n = 4$ meaning that the last vertex in $\mathcal{Y}$, y_{e_3}, is treated in the algorithm.

Step 1: Cut the edges above the i^{th} diagonal element, add the i^{th} vertex of $\mathcal{Y}$ to $\mathcal{U}$, and the cutted edges to G_f, e.i. D_f. This results in,

$$D_f = \begin{bmatrix} 1_{1,f1} & 0 & 0 & 0 \\ 0 & 0 & 0 & 1_{2,3} \\ 0 & 0 & 1_{4,f4} & 1_{4,3} \\ 0 & 1_{3,f3} & 0 & 0 \end{bmatrix} \quad D_e = \begin{bmatrix} 0 & 0 & 1_{1,4} & 0 \\ 0 & 0 & 0 & 0 \\ 1_{4,1} & 0 & 0 & 0 \\ 1_{3,1} & 1_{3,2} & 0 & 0 \end{bmatrix}$$

with $\mathcal{U} = \{u_{f_1}, u_{f_3}, u_{f_4}, u_{e_3}\}$ and $\mathcal{Y} = \{y_{e_1}, y_{e_2}, y_{e_4}, y_{e_3}\}$.

Step 2: Sorting out D_e such that the vertex at position $i-1$ is a vertex with edges incident to the i^{th} vertex, and as few as possible no zero elements above the diagonal in D_e. This results in,

$$D_f = \begin{bmatrix} 1_{f1,1} & 0 & 0 & 0 \\ 0 & 0 & 1_{f4,4} & 1_{3,4} \\ 0 & 0 & 0 & 1_{3,2} \\ 0 & 1_{f3,3} & 0 & 0 \end{bmatrix} \quad D_e = \begin{bmatrix} 0 & 1_{1,4} & 0 & 0 \\ 1_{4,1} & 0 & 0 & 0 \\ 0 & 0 & 0 & 0 \\ 1_{3,1} & 0 & 1_{3,2} & 0 \end{bmatrix}$$

with $\mathcal{U} = \{u_{f_1}, u_{f_3}, u_{f_4}, u_{e_3}\}$ and $\mathcal{Y} = \{y_{e_1}, y_{e_4}, y_{e_2}, y_{e_3}\}$.

Step 3: Set $i := i - 1$ and return to step 1. This means that the vertex y_{e_2} is treated in the next run through the algorithm.

After 5 cycils of the algorithm the following two adjact matrices are obtained,

$$D_f = \begin{bmatrix} 0 & 1_{4,f4} & 0 & 1_{4,3} & 1_{4,1} \\ 1_{1,f1} & 0 & 0 & 0 & 0 \\ 0 & 0 & 0 & 1_{2,3} & 0 \\ 0 & 0 & 1_{3,f3} & 0 & 0 \end{bmatrix} \quad D_e = \begin{bmatrix} 0 & 0 & 0 & 0 \\ 1_{1,4} & 0 & 0 & 0 \\ 0 & 0 & 0 & 0 \\ 0 & 1_{3,1} & 1_{3,2} & 0 \end{bmatrix}$$

where $\mathcal{U} = \{u_{f_1}, u_{f_3}, u_{f_4}, u_{e_3}, u_{e_1}\}$ and $\mathcal{Y} = \{y_{e_4}, y_{e_1}, y_{e_2}, y_{e_3}\}$. The resulting graphs are depicted in Fig. 4.6.

These are on the form defined in Definition 4.2.3, hence Theorem 4.2.1 can be used to obtain relations between the faults and the end-effects. In this example the following connection between the extended fault vector and the end-effects is obtained,

$$\mathbf{e}_3 \leftarrow \begin{bmatrix} \mathbf{A}_1^3\mathbf{A}_{f_1}^1 & \mathbf{A}_{f_3}^3 & \mathbf{A}_1^3\mathbf{A}_4^1\mathbf{A}_{f_4}^4 & (\mathbf{A}_2^3\mathbf{A}_3^2 + \mathbf{A}_1^3\mathbf{A}_4^1\mathbf{A}_3^4) & \mathbf{A}_1^3\mathbf{A}_4^1\mathbf{A}_1^4 \end{bmatrix} \cdot \begin{bmatrix} \mathbf{f}_1 \\ \mathbf{f}_3 \\ \mathbf{f}_4 \\ \mathbf{e}_3 \\ \mathbf{e}_1 \end{bmatrix} .$$

The remaining task is to analyse each cut to validate the results against the physical proporties of the system.

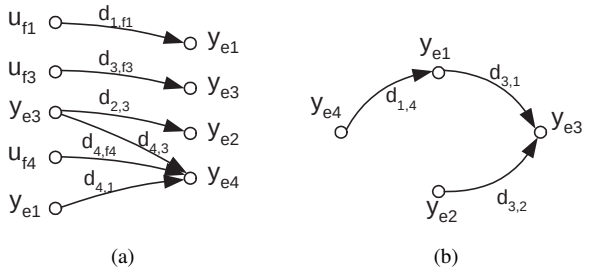

Figure 4.6: The graphs G_f (Fig (a)) and G_e (Fig. (b)) after edges are cutted.

4.2.2 Sensor Configuration and Disturbing Events

In the previous section analysis tools was derived, which can establish an expression between faults and end-effects in a system. Using these analysis tools it is possible to obtain knowledge about the effects of faults in any component of the system. This is normally used to identify the effects of the faults on the overall performance of the system. However, the analysis tools could also be used to identify the connection between faults and the measurable effects in a given system. If the identification of these connections is the goal of the analysis, the end-effect should be chosen as a subset of the measurable effects in the system. This subset should be interpreted as a given sensor configuration, which hereby is analysed. The result of the analysis can in this case be used to develop a logical detection scheme based on events extracted from measurements.

If the analysis tools are used for evaluating detection capabilities of different sensor configurations, it is important to take disturbing events in the system into account. Here disturbing events are defined as events, which affect the system, but should not be detected. This means that the only difference between faults and disturbing events is that the faults should be detected and the disturbing events should not. As the only difference between faults and disturbing events is their interpretation, it is possible to use the analysis tools presented in the previous section, for analysing system with disturbing events. This is done by extending the faults vector with the set of disturbing events. Duing this, the end-effects are given by the following expression,

$$\mathbf{e}_{end} \leftarrow \begin{pmatrix} \mathbf{A}_f & \mathbf{A}_d \end{pmatrix} \cdot \begin{pmatrix} \mathbf{f} \\ \mathbf{d} \end{pmatrix} , \tag{4.9}$$

where $\mathbf{f}$ is the set of faults in the system, $\mathbf{d}$ is the set of disturbing events, and $\mathbf{A}_f$, $\mathbf{A}_d$ are logical matrices defined as in Definition 4.1.1. This means that (4.9) is only a factorization of (4.8). The factorization into $\mathbf{f}$ and $\mathbf{d}$ of the fault vector is formilized in the following definition.

Definition 4.2.4 (Faults and Disturbing Events) *Define the set of all possible events in (4.8) as $\mathcal{F} = \bigcup_{i=1}^{n} \mathcal{F}_i$ where each $\mathcal{F}_i$ is the set of events associated with the i^{th} component and n is the number of components in the system. This set can be split into a set which should be detected $\mathcal{F}_f \subseteq \mathcal{F}$ and a set which should not $\mathcal{F}_d \subseteq \mathcal{F}$, where $\mathcal{F}_f \cap \mathcal{F}_d = \emptyset$. $\mathcal{F}_d$ and $\mathcal{F}_f$ denote the set of disturbing events and faults repectively.*

From (4.9) it is seen that the end-effects are given by $\mathbf{e}_{di} \leftarrow \mathbf{A}_d \cdot \mathbf{d}_i$ in the no fault case, i.e. $\mathbf{f} = 0$. Here $\mathbf{e}_{di}$ is the effect vector generated by the i^{th} disturbing event vector $\mathbf{d}_i \in \mathcal{F}_d$. Likewise, it is seen that the end-effects are given by $\mathbf{e}_{fj} \leftarrow \mathbf{A}_f \cdot \mathbf{f}_k + \mathbf{A}_d \cdot \mathbf{d}_j$ in the case of the fault vector $\mathbf{f}_k \in \mathcal{F}_f$ and the j^{th} disturbing event vector $\mathbf{d}_j \in \mathcal{F}_d$. For a fault vector $\mathbf{f}_k$ to distinguishable from the no fault case all possible effect vectors in the faulty case $\mathbf{e}_{fj}$ must be different from all possible effect vectors in the no fault case $\mathbf{e}_{di}$, i.e.

$$\mathbf{e}_{fj} \neq \mathbf{e}_{di} \qquad \forall \mathbf{d}_i, \mathbf{d}_j \in \mathcal{F}_d \tag{4.10}$$

where $\mathbf{e}_{fj} \leftarrow \mathbf{A}_f \cdot \mathbf{f}_k + \mathbf{A}_d \cdot \mathbf{d}_j$ and $\mathbf{e}_{di} \leftarrow \mathbf{A}_d \cdot \mathbf{d}_i$. If this expression is true for all $\mathbf{d}_i, \mathbf{d}_j \in \mathcal{F}_d$ the given fault $\mathbf{f}_k$ is said to be detectable in a logical sense. This is formalized in the following definition.

Definition 4.2.5 *(***Logical Robust Fault Detectability)** *The fault vector $\mathbf{f}_k \in \mathcal{F}_f$ is logical detectable if the effect vector $\mathbf{e}_{end}$ in the case of the fault vector $\mathbf{f}_k$ is different from the effect vector $\mathbf{e}_{end}$ in the no fault case. This must be true for all possible combinations of disturbing events in both the fault and in the no fault case.*

From (4.10) it is seen that for a fault to be logical detectable in a robust manner, it is necessary that at least one of the effects of the fault cannot be corrupted by any disturbing events. The following theorem states the conditions for this to be possible.

Theorem 4.2.2 (Logical Robust Fault Detectability) *Let $\mathcal{I}_f$ be the set of vectors with only 1 element different from zero. Let $\mathbf{f}_k \in \mathcal{I}_f$ be a vector with only the k^{th} element different from zero, and let $\mathbf{A}_f$ and $\mathbf{A}_d$ be defined as in (4.9). Let $(\mathbf{A}_f)_{j,k}$ be the j,k^{th} element in $\mathbf{A}_f$ and likewise for $(\mathbf{A}_d)_{j,k}$, then the fault described by $\mathbf{f}_k$ is logically detectable iff,*

$$\exists\, j \in \{1, 2, \cdots, n_e\} \;:\; (\mathbf{A}_f)_{j,k} = 1 \text{ and } \sum_{i=1}^{n_d} (\mathbf{A}_d)_{j,i} = 0 \tag{4.11}$$

where n_e is the number of end-effects and n_d is the number of disturbing events. This is the same as saying that $\mathbf{f}_k$ can be distinguished from all possible combinations of disturbing events.

Proof: $(\mathbf{A}_f)_{j,k} = 1$ implies that the j^{th} element of $\mathbf{e}_{f_k} \leftarrow \mathbf{A}_f \mathbf{f}_k$ is equal to 1 for $\mathbf{f}_k \in \mathcal{F}_f$. Moreover, $\sum_{i=1}^{n_d} (\mathbf{A}_d)_{j,i} = 0$ implies that the j^{th} element in $\mathbf{e}_d \leftarrow \mathbf{A}_d \mathbf{d}$ is equal to zero for

all $\mathbf{d} \in \mathcal{F}_d$, i.e. the j^{th} element of $\mathbf{e}$ will always be equal to zero in the no fault case. This again implies that, only faults can affect the j^{th} element in $\mathbf{e}$. Therefore, if the j^{th} element of $\mathbf{e} \leftarrow \mathbf{A}_f\mathbf{f} + \mathbf{A}_d\mathbf{d}$ is different from zero it must be due to $\mathbf{f}$. $\mathbf{f}_k$ will cause the j^{th} element in $\mathbf{e}$ to be different from zero, therefore (4.11) implies that $\mathbf{f}_k$ is robust detectable.

Now assume that $\mathbf{e}_{f_k} \neq \mathbf{e}_d$, where

$$\mathbf{e}_{f_k} \leftarrow \mathbf{A}_f \cdot \mathbf{f}_k + \mathbf{A}_d \cdot \mathbf{d} \tag{4.12a}$$

$$\mathbf{e}_d \leftarrow \mathbf{A}_d \cdot \mathbf{d} \; . \tag{4.12b}$$

This implies that there exists an element j in $\mathbf{e}_{f_k}$ and $\mathbf{e}_d$, such that the j^{th} element in $\mathbf{e}_{f_k}$ is different from the j^{th} element in $\mathbf{e}_d$. For this to be true the j^{th} element in $\mathbf{e}_d$ must be equal to zero, as the term $\mathbf{A}_d \cdot \mathbf{d}$ is part of both (4.12a) and (4.12b). For $\mathbf{e}_d$ to be zero for all $\mathbf{d} \in \mathcal{F}_d$ the j^{th} row of $\mathbf{A}_d$ must equal zero, i.e. $\sum_{i=1}^{n_d}(\mathbf{A}_d)_{j,i} = 0$. Therefore, for the j^{th} element of $\mathbf{e}_{f_k}$ to be different from the j^{th} element of $\mathbf{e}_d$, the j^{th} element of $\mathbf{e}_{f_k}$ must be different from zero. This implies that $(\mathbf{A}_f)_{j,k} = 1$ for the fault $\mathbf{f}_k$ to be detectable. □

Remark 4.2.4 *From Theorem 4.2.2 it is seen that if $\mathcal{F}_d = \emptyset$, meaning that no disturbing events exist in the system, then the demand for detectability of $\mathbf{f}_k$ reduces to $(\mathbf{A}_f)_{j,k} = 1$ for some $j \in \{1, 2, \cdots, n_e\}$.*

If Theorem 4.2.2 is fulfilled for a given fault in a system, then this fault is detectable despite of the disturbing events affecting the system.

In some cases not all disturbing events are independent. As an example there could exist two disturbing events d_1 and d_2; d_1 saying that an input to a given component is increasing and d_2 saying that the same input is decreasing. In this case d_1 and d_2 are mutually excluded or $d_1 = 1 \rightarrow d_2 = 0$ and $d_2 = 1 \rightarrow d_1 = 0$. When this is the case Theorem 4.2.2 is too restrictive.

In general such dependencies between disturbing events can be described by,

$$d_{i_1} = 1, d_{i_2} = 1, \cdots, d_{i_\alpha} = 1 \; \rightarrow \; d_{j_1} = 0, d_{j_2} = 0, \cdots, d_{j_\beta} = 0 \tag{4.13}$$

where there are α disturbing events d_{i_1} to d_{i_α}, which exclude β disturbing events d_{j_1} to d_{j_β}. The following Corollary relaxes the demands for logical robust fault detection, when h dependencies on the form (4.13) are assumed.

Corollary 4.2.1 (Logical Robust Fault Detectability) *For the c^{th} dependency expression on the form (4.13), define $\alpha + 1$ fault propagation matrices, where α matrices are formed by setting the i_l^{th} column equal 0, $l \in \{1, 2, \cdots, \alpha\}$, and one matrix is formed by setting the $j_1^{th}, j_2^{th}, \cdots, j_\beta^{th}$ columns equal 0. These matrices form the set,*

$$\mathcal{A}_c = \{\mathbf{A}_{d,i_1}, \mathbf{A}_{d,i_2}, \cdots, \mathbf{A}_{d,i_\alpha}, \mathbf{A}_{d,j}\} \; . \tag{4.14}$$

If there are h dependency expression there exist $\mathcal{A}_1$ to $\mathcal{A}_h$ of this sets each corresponding to one dependency expression. This means that there exists $h' = \prod_{x=1}^{h}(\alpha_c + 1)$ different

combinations given by the set,

$$\mathcal{A}_h = \left\{ \mathbf{A}_h \mid \mathbf{A}_h = \bigwedge_{c=1}^{h} \mathbf{A}_c,\ \mathbf{A}_c \in \mathcal{A}_c \right\} .$$

Iff Theorem 4.2.2 holds for a fault $\mathbf{f}_k \in \mathcal{I}_f$ for all $\mathbf{A}_h \in \mathcal{A}_h$, then the fault is logical detectable.

Proof: Before stating the proof a set of disturbing event vectors is defined. From Theorem 4.2.2 it is obvious that all end-effects, which can be affected by disturbing events, will be affected if all elements in $\mathbf{d}$ is equal to 1. Let this worst case vector be given by $\mathbf{1}_d$. When there are mutual excluded disturbing events, as given in (4.13), the vector $\mathbf{1}_d$ becomes too restictive. In this case the vectors with the maximal possible number of elements equal to one, must form the set of worst case vectors. Let this set be given by,

$$\mathcal{D}_c = \{\mathbf{d}_1, \mathbf{d}_2, \cdots, \mathbf{d}_m\}$$

Examining (4.13) the first $m-1$ vectors must be formed by setting one of the elements i_1 to i_α equal to zero. The m^{th} vector is formed by setting the elements $j_1, \cdots, j_\beta$ equal to zero. From this it is deduced that there exist $m = \alpha + 1$ independent vectors in $\mathcal{D}_c$ describing the possible worst case disturbing event vectors, when the mutual exclusion (4.13) exists. If there exist h of these mutual exclusions, forming h sets of vectors $\mathcal{D}_1, \mathcal{D}_2, \cdots, \mathcal{D}_h$ all possible worst case vectors can be defined as,

$$\mathcal{D} = \{\mathbf{d} \mid \mathbf{d} = \mathbf{d}_1 \wedge \mathbf{d_2} \wedge \cdots \wedge \mathbf{d}_h,\ \text{where } \mathbf{d}_1 \in \mathcal{D}_1,\ \mathbf{d}_2 \in \mathcal{D}_2, \cdots, \mathbf{d}_h \in \mathcal{D}_h\}$$

where $\wedge$ is the logical "and" operator. Each of the elements in $\mathcal{D}$ is formed by $\alpha_c + 1$ vectors, meaning that the total number of vectors becomes $\Pi_{c=1}^{h}(\alpha_c + 1)$.

To prove Corollary 4.2.1 recognise that Theorem 4.2.2 holds for all $\mathbf{A}_h \in \mathcal{A}_h$. This implies that $\mathbf{f}_k$ is logical robust detectable with respect to each $\mathbf{A}_h \in \mathcal{A}_h$, which again implies that $\mathbf{e}_f \neq \mathbf{e}_d$ where $\mathbf{e}_f \leftarrow \mathbf{A}_f\mathbf{f}_k + \mathbf{A}_h\mathbf{d}$ and $\mathbf{e}_d \leftarrow \mathbf{A}_h\mathbf{d}$. $\mathbf{A}_h = \bigwedge_{c=1}^{h} \mathbf{A}_c$, where $\mathbf{A}_c \in \mathcal{A}_c$ is on the form described in the corollary. From the definition of $\mathbf{A}_c$ it is seen that for each $\mathbf{A}_c \in \mathcal{A}_c$ there corresponds exactly one $\mathbf{d}_c \in \mathcal{D}_c$ such that $\mathbf{A}_c\mathbf{1}_d = \mathbf{A}_d\mathbf{d}_c$. Using this the following is true for each $\mathbf{A}_h \in \mathcal{A}_h$,

$$\mathbf{A}_h\mathbf{1}_d = \left(\bigwedge_{c=1}^{h} \mathbf{A}_c\right)\mathbf{1}_d = \left(\bigwedge_{c=1}^{h} \mathbf{A}_c\mathbf{1}_d\right) = \left(\bigwedge_{c=1}^{h} \mathbf{A}_d\mathbf{d}_c\right) = \mathbf{A}_d\left(\bigwedge_{c=1}^{h} \mathbf{d}_c\right) = \mathbf{A}_d\mathbf{d}$$

where $\mathbf{d} \in \mathcal{D}$. Due to the one to one correspondency between $\mathbf{d}_c \in \mathcal{D}_c$ and $\mathbf{A}_c \in \mathcal{A}_c$ the above equation implies that if Theorem 4.2.2 hold for each $\mathbf{A}_h \in \mathcal{A}_h$, then $\mathbf{f}_k$ is logical robust detectable for every disturbing event vector $\mathbf{d} \in \mathcal{D}$. In the start of the proof it was argued that all worst case disturbing event vectors are contained in $\mathcal{D}$. Therefore, $\mathbf{f}_k$ is detectable for all possible disturbing event vectors.

To show sufficiency just reverse the proof. □

Theorem 4.2.2 and alternatively Corollay 4.2.1 states the demands for a fault to be robust detectable in a logical sense. If this is the case for a set of faults in a system, it

is interesting to know if the faults in this set can be distinguished from each other i.e. $\mathbf{e}_{f_k} \neq \mathbf{e}_{f_i}$ whenever $f_k \neq f_i$ where $f_k, f_i \in \mathcal{I}_f$. The following theorem states the demands for this to be possible,

Theorem 4.2.3 (Logical Fault Identification) *Let $\mathcal{I}_f$ be the set of vectors with only 1 element different from zero. Let $\mathbf{f}_k \in \mathcal{I}_f$ be the vector describing the k^{th} fault and let $(\mathbf{A}_f)_k$ denote the k^{th} column in $\mathbf{A}_f$ then the fault described by $\mathbf{f}_k$ can be distinguished from all other $\mathbf{f} \in \mathcal{I}_f$ in a logical sense iff,*

$$(\mathbf{A}_f)_k \neq (\mathbf{A}_f)_i \;\; \forall i \neq k, i \in \{1, 2, \cdots, n\} \; . \tag{4.15}$$

Proof: Two faults $\mathbf{f}_k$ and $\mathbf{f}_i$ ($\mathbf{f}_k \neq \mathbf{f}_i$, $\mathbf{f}_k, \mathbf{f}_i \in \mathcal{I}_f$) are distinguishable if $\mathbf{e}_{f_k} \neq \mathbf{e}_{f_i}$, where $\mathbf{e}_{f_k} \leftarrow \mathbf{A}_f \mathbf{f}_k$ and $\mathbf{e}_{f_i} \leftarrow \mathbf{A}_f \mathbf{f}_i$. Let $\mathbf{f}_k$ be a vector with only the k^{th} element different from zero. Then $\mathbf{e}_{f_k}$ equals the k^{th} column in $\mathbf{A}_f$, i.e. $(\mathbf{A}_f)_k$. Likewise, let $\mathbf{f}_i$ be a vector with only the i^{th} element different from zero. Then $\mathbf{e}_{f_i}$ equals the i^{th} column in $\mathbf{A}_f$, i.e. $(\mathbf{A}_f)_i$. From this it is immediately seen that (4.15) implies that $\mathbf{e}_{f_k} \neq \mathbf{e}_{f_i}$ whenever $f_k \neq f_i$, where $f_k, f_i \in \mathcal{I}_f$. This completes the proof. □

Remark 4.2.5 *It should be noted that the effects used for fault identification must not be corrupted by disturbing events. Therefore if there are disturbing events in the system only the end-effects e_j associated with $\sum_{i=1}^{n_d} (\mathbf{A}_d)_{j,i} = 0$ should be used in Theorem 4.2.3.*

Remark 4.2.6 *In (Blanke et al., 2003) a methods for defining the logical connection from the effects to the faults is given, i.e. $\mathbf{f} \leftarrow \mathbf{B} \odot \mathbf{e}$ where $\odot$ is a special operator defined in (Blanke et al., 2003). Using this expression it is possible to identify a given fault from the measurable effects, whenever Theorem 4.2.3 is fulfilled for the system.*

If both Theorems 4.2.2 and 4.2.3 are fulfilled for a set of faults in a system, then this set of faults are said to be robust identifiable in a logical sense. Whenever this is the case it is possible to measure a set of effect in the system, and from these measurements detect and isolate the faults.

Unfortunately for many systems it is not possible to find a set of measurable effects where both Theorems 4.2.2 and 4.2.3 are fulfilled. However, in many cases Theorem 4.2.3 is fulfilled but not Theorem 4.2.2. In these cases the problem is that the disturbing events cannot be distinguished from the faults in a logical sense. However, it might still be possible to quantitatively decouple the disturbing events from the faults using model-based techniques.

4.3 Pump Applications

In this section first the FMEA technique will be used for analysing the centrifugal pump, and second the algorithm presented in the previous section will be utilized for analysing

sensor configuration on the centrifugal pump. In the first subsection the division of the system into useful components is described. In the second subsection each of these components are then analysed for their faults and fault effects. This is done by using the FMEA. The result of this analysis is a set of possible faults in the system. 7 of these faults are chosen for further investigation. Using this subset, different sensor configurations are analysed, showing their capability in fault detection and isolation, when signal-based fault detection methods are used.

The centrifugal pump under investigation in this section should be seen as a general centrifugal pump, meaning that the faults identified are general centrifugal pump faults. Therefore in real application only a subset of these faults will occur in practice. Even though no particular type of pump is chosen in the investigation, a CR5-10 Grundfos pump is used as an example, whenever it can illustrate the presented ideas.

4.3.1 Component Identification in the Centrifugal Pump

The FMEA and FPA are component based analysis tools, therefore the first step is to divide the system, in this case the centrifugal pump, into suitable components. In (Bøgh, 1997) three approaches are proposed for this division. These are the component hierarchy model, the physical structure model, and the functional structure model. In the first approach, the system is divided into components based on the functionality of the components, and in the physical structure model, physical components are identified. In the last approach the functionality of the components is identified, meaning that a model of the functional connection between the components is obtained.

In this work the physical structure model is used to identify components for the FMEA, whereas the functional structure model is used for the FPA. In Fig. 4.7 a component diagram of the pump is shown. In this diagram 7 physical components are identified. In Fig. 4.8 each of these components are identified on a CR 5-10 Grundfos pump.

In the middle of Fig. 4.8 the centrifugal pump is shown, and each component, identified in Fig. 4.7, is shown in separate subfigures. On the top left corner the induction motor, driving the pump, is shown. In the physical structure diagram this motor is again divided into an electrical and a mechanical component.

Below the motor, the centrifugal pump is shown. The centrifugal pump is also divided into two components in the physical structure diagram, namely a hydraulic and a mechanical component. The hydraulic component covers the parts directly involved in the energy transfer from mechanical to hydraulic energy, and the mechanical component covers the remeaning parts. The middel figure to the left is a zoom of the hydraulic parts. Here the impeller and the guide vanes are seen.

On the top to the right the shaft is shown. The CR5-10 Grundfos pump has a short shaft connection. In other pumps this can be longer and often positioned horisontal and not vertical as in the CR5-10 case. The two last figures show the inlet and outlet part of the pump. In some pump applications the inlet part can be equiped with a filter to avoid

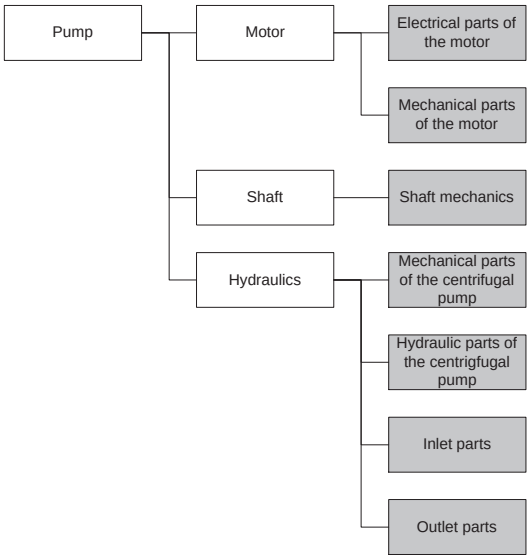

Figure 4.7: Physical structure diagram of the centrifugal pump. First the pump is divided into three components; the motor, the shaft, and the hydraulics. These components are again divided into 7 components.

large impurities to enter the pump.

The functional connection between the identified components, shown in Fig. 4.7, is presented in Fig. 4.9. To cover the functionality of the pump two extra non physical components are added. These are, a component covering the dynamics of the mechanical parts of the pump, and a component deriving the pressure difference produced by the pump. Each component is named in Table 4.3.

Each of the components in Table 4.3 will in the next subsection be analysed using the FMEA.

4.3.2 FMEA on the System Components

Each of the components identified in the previous section, see Table 4.3, is in this section described with respect to the functionality of the components, the faults in the components, and the disturbing events affecting the components. Here a fault denotes an event causing malfunction of a given component, and therefore should be detected. Whereas a disturbing event is an event affecting the component, but should not be detected. The faults and disturbing events, and their effects on each component are analysed using the FMEA. The full result of this analysis is presented in Appendix A, whereas only the faults and disturbing events are presented in this section. Beside the faults, disturbing

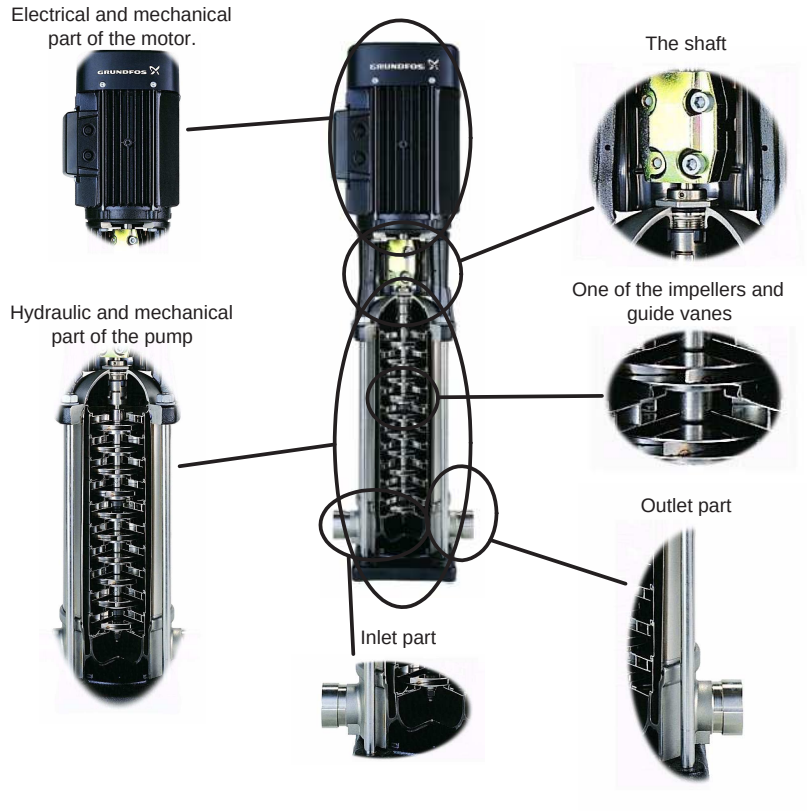

Figure 4.8: A real pump example of the component chosen for the FMEA. The pump is a CR5-10 Grundfos pump drived by a 1.5 [KW] induction motor.

events, and their effects on the components, the propagation matrices are presented in Appendix A.

c_1: Electrical part of the induction motor

This component contains the electrical parts of the induction motor driving the centrifugal pump. This includes the grid connections, the stator windings, and the rotor bars. This component converts electrical energy from the grid to mechanical energy on the shaft of the pump. The faults identified in the component are,

f_{em1} Loss of one or more phases of the supply voltage.

f_{em3} Short circuit between windings in the motor.

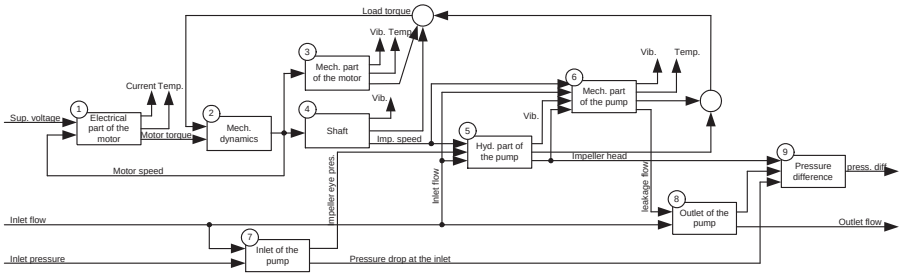

Figure 4.9: The functional connection between the components used in the FMEA of the pump system.

Table 4.3: Description if the components in the centrifugal pump.

Comp.	Name
c_1	Electrical part of the induction motor
c_2	Mechanical dynamics
c_3	Mechanical part of the induction motor
c_4	Shaft
c_5	Hydraulic part of the centrifugal pump
c_6	Mechanical part of the centrifugal pump
c_7	Inlet part of the pump
c_8	Outlet part of the pump
c_9	Pressure difference

f_{em4} Short circuit to ground.

f_{em5} Broken rotor bar.

f_{em6} Eccentric air gab due to bend or misaligned motor shaft.

The main effects of all these faults are higher harminics oscillations in the motor current and torque respectively.

Beside the faults described above the following set of disturbing events can affect the component.

d_{em1} Unbalanced supply voltage.

d_{em2} Increased supply voltage.

d_{em3} Decreased supply voltage.

d_{em4} Increased supply frequency with constant V/f relationship.

d_{em5} Decreased supply frequency with constant V/f relationship.

c_2: Mechanical dynamics

This component contains the mass of all rotating parts in the pump. It is introduced in the functional model to cover the convertion from torque to speed. As it is not a physical component, but a functional signal transformation, no faults are identified in the component.

c_3: Mechanical part of the induction motor

This component contains the ball bearings and the shaft of the motor. The functionality of the component is to transfer torque produced by the electrical part of the motor to the shaft connecting the centrifugal pump and the motor. The faults identified on the component are:

f_{mm1} Ware of the bearings in the motor.

f_{mm2} Rub impact between the stator and the rotor due to a bend or misaligned motor shaft.

The main effect of these faults is vibrations in the mechanical structure of the motor, beside that small torque oscillation can occur.

c_4: Shaft mechanics

This component contains the shaft and the shaft connection attaching the motor and pump shaft. The functionality of the component is to transfer the torque on the motor shaft to torque on the pump shaft. The faults identified on the component are,

f_{sh1} Broken shaft.

f_{sh2} Misalignment between the motor and pump.

f_{sh3} Bend shaft.

The main effect of these faults are mechanical vibrations and, in the case of the last two faults, torque oscillations.

c_5: Hydraulics of the centrifugal pump

This component contains the impeller, the diffuser, the volute, and the guide vanes of the centrifugal pump. The component converts mechanical energy from the shaft to hydraulic energy induced into the liquid pumped by the pump. The faults identified in the component are the following,

f_{i1} Dry running.

f_{i2} Impurities fixed on the impeller, causing inbalance.

f_{i3} Wear of the impeller.

f_{i4} Blocked or partial blocked flow field inside the impeller.

f_{i5} Blocked impeller rotation.

f_{i6} Wear of the sealing ring.

f_{i7} Missing sealing ring.

f_{i8} Loss of the impeller.

The main effects of these faults are changes in the value of pressure and the load torque generated by the impeller at a given flow. Moreover some of the faults can induce pressure oscillations. These pressure oscillations can be either harmonics of the rotational frequency, or noise like signals covering a larger frequency span.

Beside the faults described above the following set of disturbing events can affect the component.

d_{i1} Decreased flow through the pump.

d_{i2} Increased flow through the pump.

c_6: Mechanical part of the pump

This component contains those mechanical parts of the pump not directly involved in the energy transformation from mechanical to hydraulic energy (the parts involved in the energy transformation are contained in component c_5, *hydraulics of the centrifugal pump*). This means that parts such as the shaft of the pump, bearings inside the pump, and the casing are included in this component. The functionality of the component is to secure the hydraulic parts in the right possition, and to lead the liquid to and from the hydraulic part of the pump. The faults identified in the component are the following:

f_{mp1} Dry running.

f_{mp2} Inlet flow equal to zero.

f_{mp3} Ware of the bearings in the pump.

f_{mp4} Ware of seals.

f_{mp5} Rub impact between the impeller and the cassing.

The first two of these faults are connected to the cooling of the pump, and therefore the main effect of these faults is an increased temperature of the pump. The main effects of the last four faults are mechanical vibrations and leakages from the pump casing.

Beside the faults described above the following set of disturbing events can affect the component.

d_{mp1} Decreased flow through the pump.

d_{mp2} Increased flow through the pump.

c_7: Inlet of the pump

This component includes the inlet parts of the pump, which can contain a suction pipe and/or a filter. The functionality of the component is to lead the liquid to the impeller. The faults identified in the part are the following,

f_{ip2} Low pressure at the inlet of the pump.

f_{ip3} Opstruction of the inlet of the pump.

The main effect of these faults is that the inlet pressure to the impeller becomes too low.

Beside the faults described above the following set of disturbing events can affect the component.

d_{ip1} Decreased flow through the pump.

d_{ip2} Increased flow through the pump.

d_{ip3} High frequency pressure oscillations.

c_8: Outlet of the pump

This component includes the outlet part of the pump, which can contain an outlet pipe or a riser pipe. The length of this pipe is defined by the two points where the pressure difference generated by the pump is measured. The component is leading the liquid from the pump to a given distination. The faults identified in this component are:

f_{op2} Leakage on the outlet pipe.

f_{op3} Opstruction of the outlet pipe.

The main effects of these faults are leakages from the system and decreased pressure produced by the pump.

Beside the faults described above the following set of disturbing events can affect the component.

d_{ip1} Decreased flow through the pump.

d_{ip2} Increased flow through the pump.

c_9: Generated differential pressure

This component is not a physical component, but a collection of the pressure effects affecting the pressure difference across the pump. The component is necessary in the functional model as the effects on the pressure difference is a function of head losses in the inlet and the outlet components and the hydraulics of the centrifugal pump.

Sensor components

This work is not concerned with sensor faults, even though it is an important field. Instead sensors are seen as components, which are able to measure special effects on the system. Hence, they collect the end-effects used in the sensor analysis.

The list of possible sensors is long, some of the most important, with respect to the centrifugal pump applications, are the following,

- Current sensors.
- Voltage sensors.
- Vibration sensors on the stator and/or the pump mechanics.
- Pressure difference sensor (between outlet and inlet).
- Absolute pressure sensor at the inlet and/or the outlet of the pump.
- Flow sensor at the inlet and/or the outlet of the pump.
- Temperature sensors inside the stator, bearings and/or seals.
- Speed sensors, on the motor and/or the pump shaft.

Of these especially the pressure difference sensor is often used for control purposes. Likewise, if the speed of the motor is controlable normally expressions of the currents and the voltages of the motor are also available. If the system is equipped with a surveillance system, a subset of all the sensor information can be available. Unfortunately, this is only the case in very few centrifugal pump applications.

4.3.3 Identifying Interesting Faults

Normally, in the FMEA it is common to include risk assessments and frequencies for the faults expected in the given component. These risk assessments and frequencies are attached to a given product. In this work no specific centrifugal pump is chosen, instead the general components forming a centrifugal pump is analysed. Therefore, it has not been possible to make a risk assessment and even less possible to include frequencies of the faults. Instead the FMEA has be used to identify a set of common faults in centrifugal pumps, and their effects on the component under investagation. The obtained set can then be used as a gross set when analysing a specific centrifugal pump.

As neither risk assessments nor frequencies are identified for the faults on the centrifugal pump these cannot be used as guidelines for choosing faults for further investagation. Instead a set of fault is chosen using the following criteria:

- The fault must be expected to happen in real life applications.
- It must be possible to simulate the fault on a test-bench without changing components in the pump.

The first of these criteria is included to insure the relavance of the faults from an industrial point of view. The second criterion is included to make it possible to simulate the fault behaviour in real time on a test-bench.

Using these criteria the following set of faults is chosen for futher investagation,

Fault Group	Faults	Fault Description
f_{e1}	f_{em3}	Short circuit between stator windings.
f_{h1}	f_{i4}	Inc. hydraulic resistance inside the pump.
f_{h2}	f_{ip3}	Inc. hydraulic resistance at inlet.
f_{h3}	f_{i6} f_{i7}	Wear of or missing sealing ring
f_{m1}	f_{mp5}	Rub impact between impeller and casing
f_{in1}	f_{i1} f_{mp1} f_{ip1} f_{op1}	Dry running.
f_{in2}	f_{ip2}	Too low inlet pressure. Can cause cavitation.

Of these faults f_{i1} , f_{mp1} , f_{ip1} , f_{op1} , and f_{ip2} are input faults meaning that they are caused by unsuitable operation of the application in which the pump is placed. These type of faults are also called external faults. Even though these faults are not dirrectly connected to the components of the pump, they are very important to detect. The reason is that dry running will destroy the bearings of the pump in a few seconds, and too low inlet pressure will cause cavitation inside the pump, which again will destroy the impeller over time.

Beside these faults of course all disturbing events affecting the system must be taken into account in the following analysis. The disturbing events are,

Dist. Group	Dist.	Dist. description
d_{e1}	d_{em1}	Unbalanced supply voltage.
d_{e2}	d_{em2}	Increased supply voltage.
d_{e3}	d_{em3}	Decreased supply voltage.
d_{e4}	d_{em4}	Increased supply freq. with const. V/f.
d_{e5}	d_{em5}	Decreased supply freq. with const. V/f.
d_{h1}	d_{i1} d_{mp1} d_{ip1} d_{ip1}	Decreased flow through the pump.
d_{h2}	d_{i2} d_{mp2} d_{ip2} d_{ip2}	Increased flow through the pump.
d_{h3}	d_{ip3}	High frequency pressure oscillations.

Collecting the chosen fault and disturbing events the following logical fault vector is obtained,

$$\mathbf{f}_e = \begin{pmatrix} \mathbf{f}^T & \mathbf{d}^T \end{pmatrix}^T \tag{4.16}$$

where,

$$\begin{aligned} \mathbf{f} &= \begin{pmatrix} f_{e1} & f_{h1} & f_{h2} & f_{h3} & f_{m1} & f_{in1} & f_{in2} \end{pmatrix} \\ \mathbf{d} &= \begin{pmatrix} d_{e1} & d_{e2} & d_{e3} & d_{e4} & d_{e5} & d_{h1} & d_{h2} & d_{h3} \end{pmatrix} . \end{aligned} \tag{4.17}$$

In the next section the effects of this fault vector on different measureable signals are analysed.

4.3.4 FPA on the General Pump System

In Section 4.2.1 it is argued that logical models of the components forming the system can be described as defined in Definition 4.2.1. Using this definition the component model of the centrifugal pump, presented in Section 4.3.1, is given in Table 4.4.

Table 4.4: The component description of the centrifugal pump. The structure of each of the logical matrices is given in Appendix A.

Comp.	Faults	Effects	Transformations
c_1	$\mathbf{f}_{em}$	$\mathbf{e}_{em}$	$\mathbf{A}_f^{em}, \mathbf{A}_{dy}^{em}$
c_2	0	$\mathbf{e}_{dy}$	$\mathbf{A}_{em}^{dy}, \mathbf{A}_{mm}^{dy}, \mathbf{A}_{sh}^{dy}, \mathbf{A}_{mp}^{dy}, \mathbf{A}_i^{dy}$
c_3	$\mathbf{f}_{mm}$	$\mathbf{e}_{mm}$	$\mathbf{A}_f^{mm}, \mathbf{A}_{dy}^{mm}$
c_4	$\mathbf{f}_{sh}$	$\mathbf{e}_{sh}$	$\mathbf{A}_f^{sh}, \mathbf{A}_{dy}^{sh}$
c_5	$\mathbf{f}_i$	$\mathbf{e}_i$	$\mathbf{A}_f^i, \mathbf{A}_{sh}^i, \mathbf{A}_{ip}^i$
c_6	$\mathbf{f}_{mp}$	$\mathbf{e}_{mp}$	$\mathbf{A}_f^{mp}, \mathbf{A}_{sh}^{mp}, \mathbf{A}_i^{mp}$
c_7	$\mathbf{f}_{ip}$	$\mathbf{e}_{ip}$	$\mathbf{A}_f^{ip}$
c_8	$\mathbf{f}_{op}$	$\mathbf{e}_{op}$	$\mathbf{A}_f^{op}, \mathbf{A}_{mp}^{op}$
c_9	0	$\mathbf{e}_{dh}$	$\mathbf{A}_i^{dh}, \mathbf{A}_{op}^{dh}, \mathbf{A}_{ip}^{dh}$

Having a model on this form Algorithm 4.2.1 and Theorem 4.2.1 can be used to derived the connection from the faults and disturbing events, to any effect vector $\mathbf{e}$ in the system. Therefore, by identifing all measureable effects of interest it is possible to establish a connection between faults and disturbing events, and a subset of the measurable effects. This connection can then be used to evaluate the usability of the given sensor configuration, when the design of signal-based fault detection schemes is considered.

In the previous section a list of sensors used on centrifugal pumps is presented. Moreover, it is argued that some of these sensors are only used in special applications. The most frequently used sensors are the electrical sensors and the pressure difference

sensor. Therefore these should attend special attention when developing intelligent FDI algorithms. The electrical and pressure sensors are often used for control purposes in hydraulic applications, and are therefore often available for other purposes too. This means that the cost of implementing a supervision system is reduced considerably by using only these sensors as input to the FDI algorithms.

Beside the sensors just mentioned, the flow sensor is considered. Flow sensors are normally expensive, but by using the newest micro technology it is possible to reduce the cost considerably. This means that this sensor will become interesting in even small centrifugal pump applications. Also a sensor measuring the impeller eye pressure is considered. The flow sensor and the impeller eye pressure sensor are considered to be additional sensors and are therefore increasing the cost of implementing the supervision system.

To summarize; the effects seen in the following sensors are analysed using the FPA,

- Current sensors.
- Voltage sensors.
- pressure difference sensor (between outlet and inlet).
- Flow sensor.
- Impeller eye pressure sensor.

The results of the FPA using these sensors are presented in the following, where each of the logical matrices are obtained by using Algorithm 4.2.1.

Effects on the electrical part of the motor

The effects measurable using the current and voltage sensors are all found in component c_1 *Electrical Part of the Motor*. The measurable effects on this component are,

$e_{em,i1}$	$\sim$	Increased current.
$e_{em,i2}$	$\sim$	Decreased current.
$e_{em,i3}$	$\sim$	Oscillations in the length of the pack transform current.
$e_{em,i4}$	$\sim$	Unbalanced stator current.
$e_{em,v1}$	$\sim$	Zero voltage in one or more of the phases.
$e_{em,v2}$	$\sim$	Oscillations in the length of the pack transform voltage.

The connection between these effects and the faults and disturbing events in the system is given by the following logical equation,

$$\begin{pmatrix} e_{em,i1} \\ e_{em,i2} \\ e_{em,i3} \\ e_{em,i4} \\ e_{em,v1} \\ e_{em,v2} \end{pmatrix} \leftarrow \left(\begin{array}{cccccccc|cccccccc} 1 & 0 & 0 & 1 & 1 & 0 & 0 & 0 & 1 & 0 & 0 & 1 & 0 & 1 & 0 \\ 0 & 1 & 1 & 0 & 0 & 1 & 1 & 0 & 0 & 1 & 1 & 0 & 0 & 0 & 1 \\ 1 & 1 & 0 & 0 & 1 & 0 & 0 & 1 & 0 & 0 & 0 & 0 & 0 & 0 & 0 \\ 0 & 0 & 0 & 0 & 0 & 0 & 0 & 0 & 0 & 0 & 0 & 0 & 0 & 0 & 0 \\ 0 & 0 & 0 & 0 & 0 & 0 & 0 & 0 & 0 & 0 & 0 & 0 & 0 & 0 & 0 \\ 0 & 0 & 0 & 0 & 0 & 0 & 0 & 1 & 0 & 0 & 0 & 0 & 0 & 0 & 0 \end{array}\right) \begin{pmatrix} \mathbf{f} \\ \mathbf{d} \end{pmatrix} \tag{4.18}$$

where $\mathbf{f}$ is the fault vector and $\mathbf{d}$ is disturbing event vector, both defined in (4.17).

Effects on the pressure difference generated by the pump

The effects measuable using the pressure difference sensor are all found in component c_9 *Pressure Difference*. The measurable effects on this component are,

$e_{op,h1}$	$\sim$	Increased pressure difference across the pump.
$e_{op,h2}$	$\sim$	Decreased pressure difference across the pump.
$e_{op,h3}$	$\sim$	Zero pressure difference across the pump.
$e_{op,h4}$	$\sim$	Harmonic oscillations in the pressure difference signal.
$e_{op,h5}$	$\sim$	High frequence oscillations in the pressure difference signal.
$e_{op,h6}$	$\sim$	Pressure difference across the pump is not defined.

The connection between these effects and the faults and disturbing events in the system is given by the following logical equation,

$$\begin{pmatrix} e_{dh1} \\ e_{dh2} \\ e_{dh3} \\ e_{dh4} \\ e_{dh5} \\ e_{dh6} \end{pmatrix} \leftarrow \left(\begin{array}{ccccccc|cccccccc} 0 & 0 & 0 & 0 & 0 & 0 & 0 & 0 & 0 & 0 & 1 & 0 & 0 & 1 & 0 \\ 0 & 1 & 1 & 1 & 1 & 0 & 1 & 0 & 0 & 0 & 0 & 1 & 0 & 0 & 1 \\ 0 & 0 & 0 & 0 & 0 & 1 & 0 & 0 & 0 & 0 & 0 & 0 & 0 & 0 & 0 \\ 0 & 1 & 0 & 0 & 1 & 0 & 0 & 0 & 0 & 0 & 0 & 0 & 0 & 0 & 0 \\ 0 & 0 & 1 & 0 & 1 & 0 & 1 & 0 & 0 & 0 & 0 & 0 & 1 & 0 & 0 \\ 0 & 0 & 0 & 0 & 0 & 1 & 0 & 0 & 0 & 0 & 0 & 0 & 0 & 0 & 0 \end{array}\right) \begin{pmatrix} \mathbf{f} \\ \mathbf{d} \end{pmatrix} \tag{4.19}$$

where $\mathbf{f}$ is the fault vector and $\mathbf{d}$ is disturbing event vector, both defined in (4.17).

Effects on the flow measurement

Using a flow sensor it is possible to measure effects on the flow input, meaning that the effects of the input faults and disturbing events, which are associated with the flow, are measurable with this sensor. The measurable effects on this component are,

$$\begin{array}{lcl} e_{q1} & \sim & \text{Increased flow} \\ e_{q2} & \sim & \text{Decreased flow} \\ e_{q3} & \sim & \text{Not defined} \end{array}$$

The connection between these effects, and the faults and disturbing events in the system is given by the following logical equation,

$$\begin{pmatrix} e_{q1} \\ e_{q2} \\ e_{q3} \end{pmatrix} \leftarrow \left(\begin{array}{ccccccc|cccccccc} 0 & 0 & 0 & 0 & 0 & 0 & 0 & 0 & 0 & 0 & 0 & 0 & 0 & 1 & 0 \\ 0 & 0 & 0 & 0 & 0 & 0 & 0 & 0 & 0 & 0 & 0 & 0 & 1 & 0 & 0 \\ 0 & 0 & 0 & 0 & 0 & 1 & 0 & 0 & 0 & 0 & 0 & 0 & 0 & 0 & 0 \end{array} \right) \begin{pmatrix} \mathbf{f} \\ \mathbf{d} \end{pmatrix} \tag{4.20}$$

where $\mathbf{f}$ is the fault vector and $\mathbf{d}$ is disturbing event vector, both defined in (4.17).

Effects on the impeller eye pressure measurement

It is well known that the inlet pressure has large impact on the pump performance, as cavitation will occur if this pressure becomes too low. If cavitation does occure it will destroy the pump over time. Therefore, by measuring the pressure at the impeller eye it might be possible to detect decreases in this pressure and thereby detect the possibilities for cavitation. Moreover measuring the pressure at the impeller eye pressure noise due to cavitation might be measurable. The effects in the impeller eye pressure are found in component c_7 *Inlet of the Pump* and c_5 *Hydraulic part of the centrifugal pump*, where the mean pressure is coming from c_7 and the pressure noise due to cavitation is coming from c_5. The measurable effects are,

$$\begin{array}{lcl} e_{eh1} & \sim & \text{Noise like pressure oscillations} \\ e_{eh2} & \sim & \text{Impeller eye pressure not defined} \\ e_{eh3} & \sim & \text{Impeller eye pressure too low} \end{array}$$

The connection between these effects and the faults and disturbing events in the system is given by the following logical equation,

$$\begin{pmatrix} e_{eh1} \\ e_{eh2} \\ e_{eh3} \end{pmatrix} \leftarrow \left(\begin{array}{ccccccc|cccccccc} 0 & 0 & 1 & 0 & 1 & 0 & 1 & 0 & 0 & 0 & 0 & 0 & 1 & 0 & 0 \\ 0 & 0 & 0 & 0 & 0 & 1 & 0 & 0 & 0 & 0 & 0 & 0 & 0 & 0 & 0 \\ 0 & 0 & 1 & 0 & 0 & 0 & 1 & 0 & 0 & 0 & 0 & 0 & 0 & 0 & 0 \end{array} \right) \begin{pmatrix} \mathbf{f} \\ \mathbf{d} \end{pmatrix} \tag{4.21}$$

4.3.5 Sensor Configuration Analysis

In this section different combinations of the proposed sensors are analysed with repect to logical robustness and identification. This is done by analysing the logical connection between the measurable effects in each sensor and the faults in the system. In this analysis both logical robustness and identification possibilities are considered. The logical

connections between faults and effects were established for each of the sensors in the previous section.

The robustness of the different sensor configurations could be analysed using Theorem 4.2.2, but by looking at the description of the disturbing events in Section 4.3.3 the following mutually exclusive expressions of the disturbing events are recognized,

$$\begin{aligned} d_{e2} = 1 \ &\rightarrow \ d_{e3} = 0 \qquad & d_{e3} = 1 \ &\rightarrow \ d_{e2} = 0 \\ d_{e4} = 1 \ &\rightarrow \ d_{e5} = 0 \qquad & d_{e5} = 1 \ &\rightarrow \ d_{e4} = 0 \\ d_{h2} = 1 \ &\rightarrow \ d_{h1} = 0 \qquad & d_{h1} = 1 \rightarrow \ d_{h2} &= 0 \end{aligned}$$

as d_{e2}, d_{e4} and d_{h2} are increased voltage, frequency and flow respectively, and d_{e3}, d_{e5} and d_{h1} are decreased voltage, frequency and flow. These dependencies are taken into account using Corollary 4.2.1. When the robustness properties are estabilised the possibilities for fault identification of the detectable fault can be analysed, using Theorem 4.2.3.

The results are presented in two logical vectors $\mathcal{R}_r$ and $\mathcal{R}_i$, where $\mathcal{R}_r$ contains the results of the robustness analysis, and $\mathcal{R}_i$ contains the results of the identificability analysis. Such that,

$$\text{if the property holds for } f_j \text{ then } r_j := 1 \text{ ,else } r_j := 0$$

where f_j is the j^{th} component in the fault vector $\mathbf{f}$ and r_j is the j^{th} component in either $\mathcal{R}_r$ or $\mathcal{R}_i$ dependent on which property is analysed. The fault vector $\mathbf{f}$ is given by,

$$\mathbf{f} = \begin{pmatrix} f_{e1} & f_{h1} & f_{h2} & f_{h3} & f_{m1} & f_{in1} & f_{in2} \end{pmatrix}$$

where each f_j is described in Section 4.3.3. Three sensor configurations are considered in the following, these are,

1. Sensors measuring the electrical quantities, e.i. the voltage and current measurements.

2. Sensors measuring the electrical quantities and the pressure difference across the pump.

3. Sensors measuring the electrical quantities, the pressure difference and the volume flow.

4. Sensors measuring the electrical quantities, the pressure difference, the volume flow and the impeller eye pressure.

The results of the analysis of these different sensor configurations are presented in the following.

Electrical measurements

Firstly, only the effects in the electrical measurements are considered, e.i. the effects measurable using the current and voltage sensors. The connection from the faults and disturbing events, to their effect on the electrical quantities is given by (4.18). This equation is on the form,

$$\mathbf{e} \leftarrow \begin{bmatrix} \mathbf{A}_f & \mathbf{A}_d \end{bmatrix} \cdot \begin{bmatrix} \mathbf{f} \\ \mathbf{d} \end{bmatrix}$$

meaning that Theorem 4.2.2 and Corollary 4.2.1 can be used to establish the logical robust fault detection possibilities. The result of this analysis is shown below,

$$\mathcal{R}_r = \begin{pmatrix} 0 & 0 & 0 & 0 & 0 & 0 & 0 \end{pmatrix} . \tag{4.22}$$

From $\mathcal{R}_r$ it is seen that it is not possible to distinguish any of the faults from possible logical combinations of disturbing events. This means that non of these effects can be used in a robust signal-based fault detection scheme.

Electrical and pressure difference measurements

Secondly, consider the effects on the electrical measurements and the pressure difference measurement. These are given by (4.18) and (4.19). The result of this analysis is shown below,

$$\mathcal{R}_r = \begin{pmatrix} 0 & 1 & 0 & 0 & 1 & 1 & 0 \end{pmatrix} . \tag{4.23}$$

Here it is seen that 3 of the 6 faults are detectable using signal-based methods.

Normally it is impossible to measure the high frequency components in the pressure signal using standard pressure sensors. To analyse the detection properties under this assumption, the high frequency pressure component $e_{op,h5}$ is removed from the analysis. Moreover it is assumed that the pressure value is always available, meaning that the effect $e_{op,h6}$ is also removed. The result of this test is shown below,

$$\mathcal{R}_r = \begin{pmatrix} 0 & 1 & 0 & 0 & 1 & 1 & 0 \end{pmatrix} . \tag{4.24}$$

By comparing this result with the result from the analysis including the high frequency components, it is seen that all the fault information, not corrupted by disturbing events, is contained in the low frequency parts of the pressure signal.

Electrical, pressure difference and flow measurements

In the third analysis the electrical measurements are combined with both a pressure measurement containing high frequency components and a flow measurement. These are given by (4.18), (4.19) and (4.20) repectively. The result of this test is shown below,

$$\mathcal{R}_r = \begin{pmatrix} 0 & 1 & 0 & 0 & 1 & 1 & 0 \end{pmatrix} . \tag{4.25}$$

Comparing these results, with the results of the analysis where only the electrical measurements and the pressure sensor are considered, it is seen that no addition information is added using the flow sensor. This is in fact true when only logical combinations are considered. But, as it will be shown in Chapter 6, The flow sensor can be used for disturbance decoubling, when model-based methods are used. Hereby, it becomes possible to detect the fault f_{h3} corresponding to increased leakage flow inside the pump.

Electrical, pressure difference, flow and impeller eye pressure measurements

As the last analysis a pressure sensor measuring the impeller eye pressure is added. This means that effect in the electrical quantities, the pressure difference, the volume flow, and the impeller eye pressure are assumed known. These are given by (4.18), (4.19), (4.20) and (4.21) respectively. The result of this analysis is shown below,

$$\mathcal{R}_r = \begin{pmatrix} 0 & 1 & 1 & 0 & 1 & 1 & 1 \end{pmatrix} . \tag{4.26}$$

Here it is seen that only the faults f_{e1} and f_{h1} corresponding to inter-turn short circuit and leakage flow are undetectable. To check the possibilities for identification of the the 5 detectable faults, the effects not corrupted by disturbing events are analysed using Theorem 4.2.3. The logical expression of the faults is given by the following expression.

$$\begin{pmatrix} e_{em,i4} \\ e_{em,v1} \\ e_{dh3} \\ e_{dh4} \\ e_{dh6} \\ e_{q3} \\ e_{eh2} \\ e_{eh3} \end{pmatrix} \leftarrow \begin{pmatrix} 0 & 0 & 0 & 0 & 0 & 0 & 0 \\ 0 & 0 & 0 & 0 & 0 & 0 & 0 \\ 0 & 0 & 0 & 0 & 0 & 1 & 0 \\ 0 & 1 & 0 & 0 & 1 & 0 & 0 \\ 0 & 0 & 0 & 0 & 0 & 1 & 0 \\ 0 & 0 & 0 & 0 & 0 & 1 & 0 \\ 0 & 0 & 0 & 0 & 0 & 1 & 0 \\ 0 & 0 & 1 & 0 & 0 & 0 & 1 \end{pmatrix} \cdot \begin{pmatrix} \mathbf{f} \end{pmatrix} .$$

In this expression the effects, which can be corrupted by disturbing events, are removed. The result of the detectability analysis is shown below,

$$\mathcal{R}_i = \begin{pmatrix} x & 0 & 0 & x & 0 & 1 & 0 \end{pmatrix} \tag{4.27}$$

where x corresponds to the fault not robust detectable. Here it is seen that only one fault is distinguishable from the other faults, when all the effects corrupted by disturbing events are removed.

4.4 Detection Algorithm for the Centrifugal Pump

In this section an example of a robust signal-based detection scheme is developed. The obtained detection scheme is tested on a test-bench particular developed for this purpose.

4.4.1 Decision Logic

In the analysis presented in the previous section the system was assumed to be disturbed by 8 different disturbing events, see Section 4.3.3. If this assumption is relaxed by removing the disturbing event d_{e1} the robust detection properbilities are increased. Removing this disturbing event is the same as assuming that the supply voltage is balanced at all times. Now consider the sensor configuration including the following sensors,

- Current sensors.
- Voltage sensors.
- Low bandwide pressure difference sensor.

With this sensor configuration the result of the FPA is the following,

$$\mathcal{R}_r = \begin{pmatrix} 1 & 1 & 0 & 0 & 1 & 1 & 0 \end{pmatrix} \qquad \mathcal{R}_i = \begin{pmatrix} 1 & 0 & x & x & 0 & 1 & x \end{pmatrix}$$

where the x's in $\mathcal{R}_i$ indicates that the given fault is not robust detectable (the interpretation of $\mathcal{R}_r$ and $\mathcal{R}_i$ is described in Section 4.3.5). From $\mathcal{R}_r$ it is seen that four faults are logical robust detectable. This means that the following fault vector is detectable using the considered sensor configuration,

$$\mathbf{f} = \begin{pmatrix} f_{e1} & f_{h1} & f_{m1} & f_{in1} \end{pmatrix} .$$

The connection between the measurable effects, and the faults and disturbing events is in this particular case given by the following logical equation,

$$\begin{pmatrix} e_{em,i3} \\ e_{dh3} \\ e_{dh4} \end{pmatrix} \leftarrow \begin{pmatrix} 1 & 1 & 1 & 0 \\ 0 & 0 & 0 & 1 \\ 0 & 1 & 1 & 0 \end{pmatrix} \begin{pmatrix} f_{e1} \\ f_{h1} \\ f_{m1} \\ f_{in1} \end{pmatrix} , \tag{4.28}$$

where the measurable effects not in use are removed. From (4.28) it is easy to see that the faults f_{h1} and f_{m1} are indistinguishable as they affect the same measurable effect. This is also shown in $\mathcal{R}_i$. Likewise it is seen in $\mathcal{R}_i$ that the faults f_{e1} and f_{in1} can be distinguished from the remaining two faults. This is confirmed by examination of (4.28). The detection logic is very simple in this case, and is given by,

$$\begin{aligned} e_{em,i3} &\rightarrow f_{e1} \\ e_{em,i3} \vee e_{dh4} &\rightarrow f_{h1} \\ e_{em,i3} \vee e_{dh4} &\rightarrow f_{m1} \\ e_{dh3} &\rightarrow f_{in1} . \end{aligned} \tag{4.29}$$

In this expression $e_{em,i3}$ indicates frequency components of the length of the Park transformed motor currents, where the length of the Park current vector is given by,

$$\|\mathbf{i}_{sdq}\| = \|\mathbf{T}_{dq}\mathbf{i}_{sabc}\| .$$

In this expression the same notation as in Chapter 3 is used. The effect e_{dh3} corresponds to zero difference pressure, when the pump is running. Finally, the effect e_{dh4} corresponds to low freqency harmonic oscillations in the pressure measurements. Here low frequency components correspond to frequencies larger than 0 [Hz] and up to 2-4 times the supply voltage frequency.

4.4.2 Test Results

To test the validity of the decision logic, derived in the previous subsection, data sets obtained by simulating faults on a centrifugal pump is analysed. These data are obtained by running tests on a test-bench particular developed for testing fault detection algorithms in this project. A sketch of the test-bench is shown in Fig. 4.10. The pump used in the test-bench is a Grundfos 1.5 (KW) CR5-10 pump.

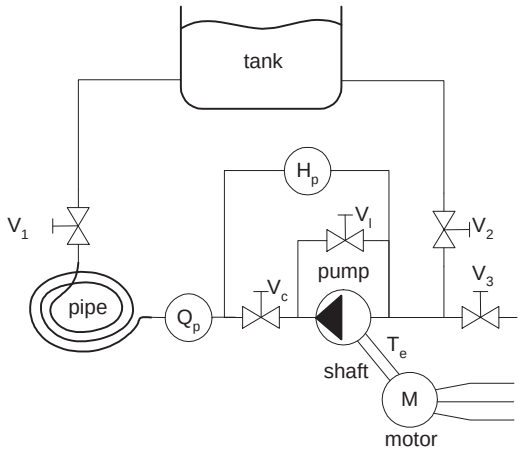

Figure 4.10: Sketch of the test-bench. The measurements are the electrical quantities, the pressure difference H_p delivered by the pump and the volume flow through the pump Q_p.

In the tank and pipe system, connected to this pump, the valve V_1 is used to model disturbances in the system. The inter-turn short circuit is simulated by shorting windings in phase a in the costimized designed stator particular developed for this purpose. Dry running is simulated by closing V_2 and opening V_3, and rub impact is simulated by adding an extra force on the shaft. During the test, presented here, this is done by mounting twist on the shaft, which rubs against the mechanical connection between the pump and motor. Hereby an oscilating force, similar to the one expected in a pump during fault f_{m1}, is added. Finally, clogging inside the pump can be simulated by the closing valve V_c. However, this valve simulates clogging of for example an inlet filter,

Table 4.5: Summing of the test results. Here, the faults denoted inter-turn, Dry-running, and rub-impact corresponds to f_{e1}, f_{m1}, and f_{in1} respectively. Likewise, and increase in σ_{is}, and σ_h corresponds to $e_{em,i3}$, and e_{dh4} respectively. Finally, when μ_h approximate zero it corresponds to e_{dh3}.

	Normal	Inter-turn	Rub-impact	Dry-running
μ_{is}	2.7366	5.2066	4.6263	2.0450
σ_{is}	0.0037	**0.4954**	**0.0141**	0.0041
μ_h	2.2178	2.2561	1.6402	**0.1054**
σ_h	0.0003	0.0006	**0.0067**	0.0010

and not clogging in one of the channels in the impeller, which was assumed in the logical analysis. Therefore, results from this test are not considered here.

The measurable effects considered in these tests are affecting the current and the pressure measurements, therefore only these will be analysed in the following test results. To evaluate the robustness of the approach, signals obtained on the pump at constant speed and at different positions of valve V_1 are analysed. The different valve positions simulates the no fault condition at different hydraulic loads. Results from this test are shown in Fig. 4.11. From these test results it is obvious that the DC-level of the considered signals are not usable for fault detection. This was also predicted by the FPA-analysis performed in Section 4.4.1.

Figs. 4.12, 4.13, and 4.14 depitch the current and pressure signals when the pump is exposed to the three faults f_{e1}, f_{m1}, and f_{in1} denoting inter-trun short circuit, rub impact, and dry running respectively. The results of these tests are summarized in Table 4.5. In the evaluation of the results σ_{is} and σ_h are used as measurements of the end-effects $e_{em,i1}$ and e_{h4} respectively. The end-effect e_{dh3} is assumed triggered when $\mu_h \approx 0$.

Considering the results presented in Table 4.5 it is seen that σ_{is} is increased considerably in the case of the inter-turn fault f_{e1} and the rub-impact fault f_{m1}. Comparing these results with the decision logic in (4.29), and rembering that σ_{is} is a measure of the end-effect $e_{em,i1}$ it fits perfectly. Likewise, by using σ_h as a measure of the e_{dh4} it is seen that the rub-impact faults f_{m1} is the only fault which increases σ_h. This also fits the results of (4.29) perfectly. Finally, the only fault forcing μ_h close to zero is the dry-running fault f_{in1}. As $\mu_h \approx 0$ is considered a measure of e_{dh1} this also fits the results of (4.29).

4.5 Discussion

In the literature it is described how Failure Mode and Effect Analysis (FMEA) and Fault Propagation Analysis (FPA) are used in the design of Fault Tolerant Control (FTC). However, these tools are general analysis tools, and could as well be used in the design

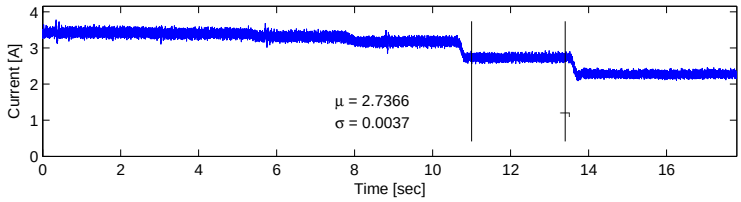

(a) Length of the Park current vector.

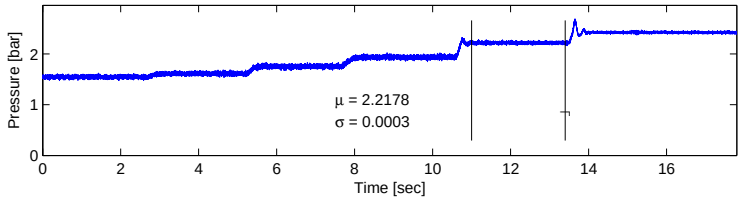

(b) Pressure difference across the pump.

Figure 4.11: Results obtained when running the pump at constant speed and different positions of valve V_1. The change in valve position simulates different load condition of the pump.

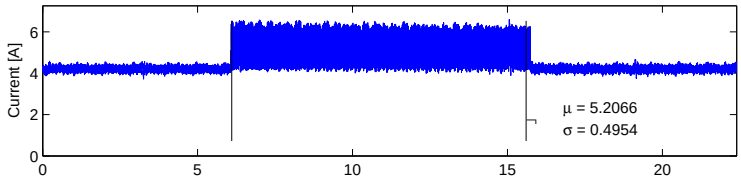

(a) Length of the Park current vector.

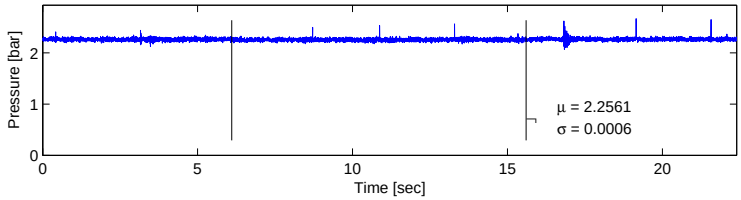

(b) Pressure difference across the pump.

Figure 4.12: Results obtained when introducing an inter-turn short circuit in phase a of the induction motor stator. The fault is introduced at time 6.05 [sec] and removed at time 5.75 [sec]. The mean and variance of the two presented signals are calculted from data between the two indicator lines. During the test the pump is running at constant speed and with valve V_1 fixed at a constant position.

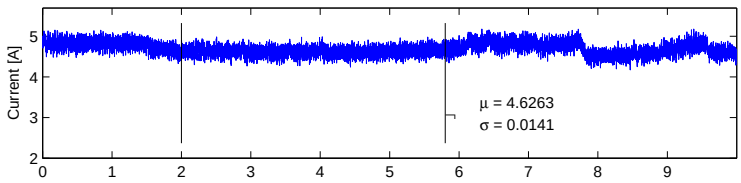

(a) Length of the Park current vector.

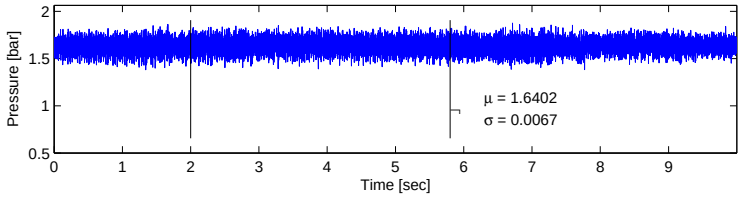

(b) Pressure difference across the pump.

Figure 4.13: Results obtained when introducing a rub-impact fault on the pump. Here, the pump is affected by the fault during the whole data series. The mean and variance of the two presented signals are calculated from data between the two indicator lines. During the test the pump is running at constant speed and with valve V_1 fixed at a constant position.

of Fault Detection and Identification (FDI) alogrithms. In this chapter these algorithms are used as analysis and design tools in the design of signal-based FDI algorithms.

In the first part of the chapter some theoretical considerations on using FPA in the design of signal-based FDI are considered. It is well known that some workarounds are necessary in the FPA when loops occur in the system model. Normally, this is handled by cutting the loops and then treat the cutted effects as additional faults in the system. In this chapter an algorithm for identifing the optimal cuts in the loops is developed. From the result obtained using this algorithm it is easy to find the connection between the faults in the system and any set of end-effects. This can be done by using a theorem also prestented in this chapter. Hereby the step of cutting loops in FPA is fully automated, meaning that the only manual work necessary in the FPA is to set up the event model of the system. The developed algorithm can be used in the design of FTC as well as FDI.

One of the main concerns in the design of FDI algorithms is how to handle disturbances in the system. This is necessary to avoid generating fault alarms. To treat this problem in the frame work of the FPA, it is proposed to define a set of disturbing events. These disturbing events are treated as faults in the FPA analysis, meaning that the connection between faults as well as disturbing events can be established using the automated FPA. When this connection is established the connection between disturbing events and end-effect is used to identify those of the end-effects, which will be corrupted by disturbing events. Hereby it is possible to find the end-effects, which can be used for

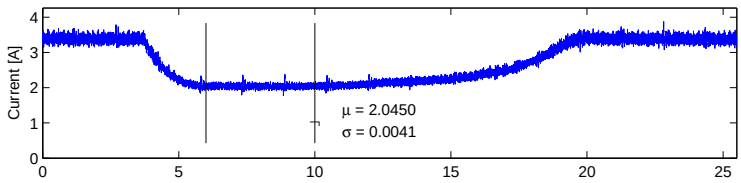

(a) Length of the Park current vector.

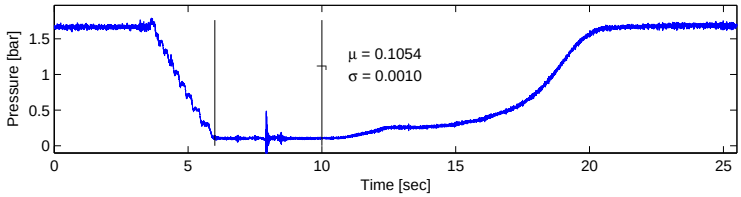

(b) Pressure difference across the pump.

Figure 4.14: Results obtained when introducing a dry running fault at the test setup. The fault is introduced at time 3.5 [sec] and removed at time 10 [sec]. The mean and variance of the two presented signals are calculated from data between the two indicator lines. During the test the pump is running at constant speed and with valve V_1 fixed at a constant position.

fault detection in a robust manner. A theorem for doing this is developed in the chapter.

In the second part of the chapter the FMEA and FPA are used in an analysis of a centrifugal pump. First the FMEA is used to identify all faults expected to happen in a centrifugal pump. This result can be used when a fault detection scheme should be developed, as it contains information about the faults, which should be expected in a centrifugal pump. In the presented analysis a list of possible disturbing events are also included. The results of the FMEA are used in the FPA to analyse different set of measurable end-effects for their fault detection capabilities. The analysed end-effects are all measurable by conventional sensors, meaning that only voltage, current, pressure, and flow sensors are considered. This analysis shows that the sensor configurations analysed have pure detection capabilities, when all identified disturbing events are taken into account. However, by relaxing the number of disturbing events a robust signal based detection algorithm is developed, using only current and pressure measurements. This algorithm is tested on a test-bench, where it is shown to work as expected.

Chapter 5

A New approach for Stator Fault Detection in Induction Motors

Stator faults are according to (Kliman et al., 1996) the most common electrical faults in electrical motors. Moreover according to (Bonnett and Soukup, 1992) most of these faults start as an inter-turn short circuit in one of the stator coils. The increased heat due to this short circuit will eventually cause turn to turn or turn to ground faults, and finally lead to a breakdown of the stator, (Wiedenbrug et al., 2003) and references included. The time, from an inter-turn short circuit has occurred to breakdown of the stator, can be very short. In (Gerada et al., 2004) it is argued that the time from an inter-turn short circuit has occured to the temperature in the short circuit exceed the breakdown temperature of the insulation can be as small as 1 to 2 [sec].

Inter-turn short circuits are caused by several different influences on the stator. For example mechanical stress during assembling or during operation can create scratches in the insulation, which again can cause short circuits. If the motor is placed in wet environment, moisture can cause flow of current from scratch to scratch, which can make a hot spot and thereby destroy the insulation. Moreover, if the motor is supplied with a PWM voltage source, partial discharges due to very high amplitude alternating voltage between the turns can degrade the insulation over time and cause a short circuits.

In the literature different approaches are proposed for detection of inter-turn short circuits. In (Cruz and Cardoso, 2001) the stator currents are transformed using the Park transformation. Second order harmonics in the length of the transformed current vector is then used for fault detection. In (Cash, M. A. et al., 1997; García et al., 2004) oscillations in the voltage between the line neutral and the star point of the motor are used as a fault indicators. This is also shown in (Tallam et al., 2002) using a model of a faulty motor. In (Lee et al., 2003) estimation of the negative impedance of the motor is used as a fault indicator, and in (Arkan et al., 2001) the negative sequence current is used for the same purpose. In (Briz et al., 2003) high frequency voltage injection in the supply

voltage is utilized to create a response on the motor current. This response contains information of the inter-turn short circuit fault.

In this chapter a model-based approach is proposed. The proposed approach is based on a model of the induction motor including an inter-turn fault in the stator. Different approaches for modelling inter-turn short circuits in the stator windings are found in the literature. In (Joksimovic and Penman, 2000) a higher order model is used. This model is an extension of the model presented in (Luo et al., 1995). This type of model is used for simulating higher order effects in the motor, but the obtained model is of high order. The inter-turn short circuit fault has its main harmonics in the lower frequency range. Therefore observers designed on the basis of this type of model will be of unnecessary high order for this kind of fault. In (Williamson and Mirzoian, 1985) a steady state model of both inter-turn and turn-turn faults in an induction motor is developed using a low order model. In (Tallam et al., 2002) a transient model of the same order as the one presented in (Williamson and Mirzoian, 1985) is developed. This model describes an $\mathbf{Y}$-connected induction motor with an inter-turn short circuit in phase a.

In this chapter an adaptive observer is proposed for estimation of the inter-turn short circuit fault. Theoretical considerations on adaptive observers can for example be found in (Besancon, 2000; Rajamani and Hedrick, 1995; Cho and Rajamani, 1997). Based on these contributions a new observer scheme is proposed, specially designed for handling bi-linear systems. The observer is formulated in general terms, hence is usable in other applications. The proposed observer is capable of simultaneously estimating the speed of the motor, the amount of turns involved in the short circuit, and an expression of the current in the short circuit. The observer is based on a model, developed particular for this purpose. This model is based on the same ideas as the model described in (Tallam et al., 2002). However, the model developed in this chapter is valid for both $\mathbf{Y}$- and Δ-connected induction motors, and does includes both inter-turn and turn-turn short circuits. Moreover, the model has a more useful structure compared to (Tallam et al., 2002). Using three copies of the designed adaptive observer the phase affected by the inter-turn short circuit is identified using an approach described in (Zhang, 2000).

As a model-based approach for fault estimation is proposed in this chapter, the chapter starts by deriving a model of the induction motor with an inter-turn short circuit in Section 5.1. This model is in Section 5.2 used in the design of the proposed adaptive observer. In Section 5.3 test results from tests on a customized designed motor are presented. Finally concluding remarks end the chapter.

5.1 Model of the Stator Short Circuit

As described in the introduction, this chapter is concerned with detection of inter-turn short circuit faults. In this work the model-based approach is used, meaning that a model of the motor is needed in the derivation of the FDI algorithm. The derivation of this model is considered in this section, meaning that a model of an induction motor including a stator fault is derived.

A turn-turn short circuit denotes a short circuit between windings in two different phases of the stator, see Fig. 5.1. Here a short circuit between phase a and b in a **Y**-connected and a Δ-connected stator is shown.

(a) Short circuit between turns in phase a and b in a **Y**-connected stator.

(b) Short circuit between turns in phase a and b in a Δ-connected stator.

Figure 5.1: Simplified electrical diagram of a three phase **Y**-connected and Δ-connected stator with a turn-turn short circuit between phase a and b.

An inter-turn fault is, in contrast with the turn-turn fault, a short circuit between windings in the same phase coil. However, an inter-turn fault can be treated as a special case of the turn-turn fault, as it can be modelled by assuming that no turns, of for example phase b, are involved in the short circuit. However, it can be argued that this is a rather limited model assumption for the inter-turn fault, because the short circuit always must be connected to the end point of the phase coil in this case. But, if the electrical circuit is assumed linear, all short circuits in a coil can be represented by a short circuit connected to the end point of the given coil. This new short circuit must of cause have the same amount of turns as the real short circuit.

In the following, a model of an induction motor, including a turn-turn short circuit between phase a and b, is developed. The model is developed under the assumption that the short circuit does not affect the overall angular position of the coil in the motor.

5.1.1 The Y-connected Motor in abc-coordinates

First the **Y**-connected motor is considered. Setting up the mesh equations for the **Y**-connected motor shown in Fig. 5.1(a) and rearranging these equations, a model describing a motor with a short circuit between phase a and b is found. Using the matrix

notation presented in Chapter 3 this model is given by the following set of equations,

$$\mathbf{v}_{sabc} = \mathbf{r}_s(\mathbf{i}_{sabc} - \boldsymbol{\gamma} i_f) + \frac{d\boldsymbol{\psi}_{sabc}}{dt} \tag{5.1a}$$

$$\boldsymbol{\gamma}^T \mathbf{v}_{sabc} = r_f i_f + l_f \frac{di_f}{dt} \tag{5.1b}$$

$$0 = \mathbf{r}_r \mathbf{i}_{rabc} + \frac{d\boldsymbol{\psi}_{rabc}}{dt} \tag{5.1c}$$

$$\boldsymbol{\psi}_{sabc} = \mathbf{l}_s(\mathbf{i}_{sabc} - \boldsymbol{\gamma} i_f) + \mathbf{l}_m(\theta)\mathbf{i}_{rabc} \tag{5.1d}$$

$$\boldsymbol{\psi}_{rabc} = \mathbf{l}_r \mathbf{i}_{rabc} + \mathbf{l}_m(\theta)(\mathbf{i}_{sabc} - \boldsymbol{\gamma} i_f)\ , \tag{5.1e}$$

where (5.1a) and (5.1d) describe the voltages and the flux linkages in each of the stator phases, (5.1c) and (5.1e) describe the voltages and the flux linkages in each of the rotor phases, and finally (5.1b) describes the current in the short circuit. In these equations $\mathbf{v}_{sabc}$ contains the voltages across each stator phase, $\mathbf{i}_{sabc}$ is the current running into each stator phase, and i_f is the current in the short circuit. The matrices $\mathbf{r}_s$, $\mathbf{r}_r$, $\mathbf{l}_s$, $\mathbf{l}_r$, and $\mathbf{l}_m(\theta)$ have the same form as in the case of a motor with no faults. These matrices are given in Section 3.2.1.

The vector $\boldsymbol{\gamma}$ in (5.1a) to (5.1e) represents the position and the amount of turns in the short circuit. The vector is, in the case of a short circuit between phase a and b, given by

$$\boldsymbol{\gamma} = \begin{bmatrix} \gamma_a & -\gamma_b & 0 \end{bmatrix}^T\ , \tag{5.2}$$

where γ_a is the amount of turns affected in phase a, and γ_b is the amount of turns affected in phase b by the short circuit. The inductor and the resistor in (5.1b) are given by

$$l_f = \left(\gamma_a(1-\gamma_a) + \gamma_b(1-\gamma_b)\right) l_{ls}, \quad r_f = \left(\gamma_a(1-\gamma_a) + \gamma_b(1-\gamma_b)\right) r_s + r_i \tag{5.3}$$

where r_s is the stator resistance, l_{ls} is the leakage inductance of the stator, and r_i is the resistance in the insulation break. $r_i = \infty$ means that no short circuit has occurred and $r_i \neq \infty$ means that a leakage current is flowing. The evolution from $r_i = \infty$ to $r_i = 0$ is very fast in most insulating materials, meaning that the value of r_i can be assumed to equal either ∞ or 0 in most cases.

5.1.2 The Δ-connected Motor in abc-coordinates

To set up the model of the Δ-connected induction motor the same procedure as used in the case of a $\mathbf{Y}$-connected motor is used.

Setting up the mesh equations for the Δ-connected motor depicted in Fig. 5.1(b) and rearranging these equations, a model describing the Δ-connected motor with a short circuit between phase a and b is obtained. Using the same matrix notation as used in the

previous section the following set of equations is obtained,

$$\mathbf{v}_{sabc} = \mathbf{r}_s(\mathbf{i}_{sabc} - \boldsymbol{\gamma} i_f) + \frac{d\boldsymbol{\psi}_{sabc}}{dt} \tag{5.4a}$$

$$\boldsymbol{\gamma}^T \mathbf{v}_{sabc} = r_f i_f + l_f \frac{di_f}{dt} \tag{5.4b}$$

$$0 = \mathbf{r}_r \mathbf{i}_{rabc} + \frac{d\boldsymbol{\psi}_{rabc}}{dt} \tag{5.4c}$$

$$\boldsymbol{\psi}_{sabc} = \mathbf{l}_s(\mathbf{i}_{sabc} - \boldsymbol{\gamma} i_f) + \mathbf{l}_m(\theta)\mathbf{i}_{rabc} \tag{5.4d}$$

$$\boldsymbol{\psi}_{rabc} = \mathbf{l}_r \mathbf{i}_{rabc} + \mathbf{l}_m(\theta)(\mathbf{i}_{sabc} - \boldsymbol{\gamma} i_f)\ . \tag{5.4e}$$

This model has the same structure as the one modelling the $\mathbf{Y}$-connected motor. Moreover the parameters $\mathbf{r}_s$, $\mathbf{r}_r$, r_f, $\mathbf{l}_s$, $\mathbf{l}_r$, $\mathbf{l}_m$ and l_f in this model have the same values as in the model of the $\mathbf{Y}$-connected motor. The only difference is the vector $\boldsymbol{\gamma}$ modelling the amount of turns involved in the short circuit, which in this case is given by

$$\boldsymbol{\gamma} = \begin{bmatrix} \gamma_a & \gamma_b & 0 \end{bmatrix}^T\ . \tag{5.5}$$

5.1.3 Transformation to a Stator fixed $dq0$-frame

Comparing the models developed in the two previous sections it is seen that the model of the $\mathbf{Y}$-connected and Δ-connected motor has the same structure. This model structure will in this section be transformed to a stator fixed $dq0$-frame.

Using the $dq0$-transformation $\mathbf{T}_{dq0}(\theta)$ presented in Section 3.2.2 the models presented in (5.1) and (5.4) are transformed into the following,

$$\begin{aligned}
\mathbf{v}_{sdq} &= \mathbf{R}_s(\mathbf{i}_{sdq} - \mathbf{T}_{dq}\boldsymbol{\gamma} i_f) + \tfrac{d\boldsymbol{\psi}_{sdq}}{dt} \\
v_{s0} &= r_s(i_{s0} - \mathbf{T}_0^T \boldsymbol{\gamma} i_f) + \tfrac{d\psi_{s0}}{dt} \\
0 &= \mathbf{R}_r \mathbf{i}_{rdq} + \tfrac{d\boldsymbol{\psi}_{rdq}}{dt} - z_p\omega_r \mathbf{J}\boldsymbol{\psi}_{rdq} \\
0 &= r_r i_{r0} + \tfrac{d\psi_{r0}}{dt} \\
l_f \tfrac{di_f}{dt} &= -r_f i_f + \boldsymbol{\gamma}^T \mathbf{T}_{dq0}^{-1} \mathbf{v}_{sdq0}\ ,
\end{aligned} \tag{5.6}$$

where the flux linkages are given by

$$\begin{aligned}
\boldsymbol{\psi}_{sdq} &= \mathbf{L}_s(\mathbf{i}_{sdq} - \mathbf{T}_{dq}\boldsymbol{\gamma} i_f) + \mathbf{L}_m \mathbf{i}_{rdq} \\
\psi_{s0} &= l_{ls}(i_{s0} - \mathbf{T}_0^T \boldsymbol{\gamma} i_f) \\
\boldsymbol{\psi}_{rdq} &= \mathbf{L}_r \mathbf{i}_{rdq} + \mathbf{L}_m(\mathbf{i}_{sdq} - \mathbf{T}_{dq}\boldsymbol{\gamma} i_f) \\
\psi_{r0} &= l_{lr} i_{r0}\ .
\end{aligned} \tag{5.7}$$

In these expressions $\mathbf{T}_{dq}$ contains the two first rows and $\mathbf{T}_0$ contains the last row of $\mathbf{T}_{dq0}$. The parameter matrices in this model $\mathbf{R}_s$, $\mathbf{R}_r$, $\mathbf{L}_s$ $\mathbf{L}_r$, and $\mathbf{L}_m$ do all have diagonal structures, and are given in Section 3.2.2.

From (5.6) and (5.7) it is seen that it is convenient to define a new current vector $\mathbf{i}'_{sdq0} = \mathbf{i}_{sdq0} - \mathbf{T}_{dq0}\boldsymbol{\gamma} i_f$. This current equals the amount of the stator current, which

generates air gab flux. Rewriting (5.6) and (5.7) using the same procedure as described in Section 3.2, and introducing the current $\mathbf{i}'_{sdq0}$ the induction motor model becomes,

$$\begin{aligned}
\mathbf{L}'_s \tfrac{d\mathbf{i}'_{sdq}}{dt} &= -(\mathbf{R}_s + \mathbf{R}'_r)\mathbf{i}'_{sdq} + (\mathbf{R}'_r - z_p\omega_r \mathbf{J}\mathbf{L}'_m)\mathbf{i}_{mdq} + \mathbf{v}_{sdq} \\
l_{ls} \tfrac{di'_{s0}}{dt} &= -r_s i'_{s0} + v_{s0} \\
\mathbf{L}'_m \tfrac{d\mathbf{i}_{mdq}}{dt} &= \mathbf{R}'_r \mathbf{i}'_{sdq} - (\mathbf{R}'_r - z_p\omega_r \mathbf{J}\mathbf{L}'_m)\mathbf{i}_{mdq} \\
l_f \tfrac{di_f}{dt} &= -r_f i_f + \boldsymbol{\gamma}^T \mathbf{T}_{dq0}^{-1} \mathbf{v}_{sdq0} \ ,
\end{aligned} \tag{5.8}$$

where

$$\mathbf{R}'_r = \mathbf{L}_m \mathbf{L}_r^{-1} \mathbf{R}_r \mathbf{L}_r^{-1} \mathbf{L}_m \qquad \mathbf{L}'_s = \mathbf{L}_s - \mathbf{L}_m \mathbf{L}_r^{-1} \mathbf{L}_m \qquad \mathbf{L}'_m = \mathbf{L}_m \mathbf{L}_r^{-1} \mathbf{L}_m \ ,$$

meaning that the new matrices retain the diagonal structure.

5.1.4 Grid Connections

In the model presented in (5.8) the voltages $\mathbf{v}_{sdq0}$ and the currents $\mathbf{i}_{sdq0}$ are defined as the quantities related to each phase in the motor. These are in general not measurable, therefore the connection between these quantities and the quantities of the terminal of the motor must be establised. This is done in Section 3.2.3 in Chapter 3 for an induction motor without stator faults. In the following the connection established in Section 3.2.3 is used to obtain the final model of the $\mathbf{Y}$- and Δ-connected induction motors with an inter-turn short circuit in the stator.

The Y-connected Case

From Section 3.2.3 the relationships between the phase quantities and the measurable quantities are given by

$$\begin{aligned}
\mathbf{v}_{sdq} &= \mathbf{v}_{tdq} & \mathbf{i}_{tdq} &= \mathbf{i}_{sdq} \\
v_{s0} &= v_{t0} - v_0 & i_{t0} &= i_{s0} \ ,
\end{aligned}$$

where quantities with subscript s are related to the phases of the motor, and quantities with subscript t are related to the terminals of the motor, and are therefore measurable. Moreover in the $\mathbf{Y}$-connected case $i_{s0} = i_{t0} = 0$. Introducing these relationships in (5.8) the model of the $\mathbf{Y}$-connected induction motor with a stator short circuit becomes

$$\mathbf{L}'_s \frac{d\mathbf{i}'_{sdq}}{dt} = -(\mathbf{R}_s + \mathbf{R}'_r)\mathbf{i}'_{sdq} + (\mathbf{R}'_r - z_p\omega_r \mathbf{J}\mathbf{L}'_m)\mathbf{i}_{mdq} + \mathbf{v}_{tdq} \tag{5.9a}$$

$$l_{ls} \frac{di'_{s0}}{dt} = -r_s i'_{s0} + (v_{t0} - v_0) \tag{5.9b}$$

$$\mathbf{L}'_m \frac{d\mathbf{i}_{mdq}}{dt} = \mathbf{R}'_r \mathbf{i}'_{sdq} - (\mathbf{R}'_r - z_p\omega_r \mathbf{J}\mathbf{L}'_m)\mathbf{i}_{mdq} \tag{5.9c}$$

$$l_f \frac{di_f}{dt} = -r_f i_f + \boldsymbol{\gamma}^T \mathbf{T}_{dq0}^{-1} (\mathbf{v}_{tdq0} - \mathbf{v}_0) \ , \tag{5.9d}$$

and the measurable currents are given by

$$\mathbf{i}_{tdq0} = \mathbf{i}'_{sdq0} + \mathbf{T}_{dq0}\boldsymbol{\gamma} i_f \ . \tag{5.9e}$$

From (5.9e) it is seen that $i'_{s0} = -\frac{1}{3}(\gamma_a - \gamma_b)i_f$ as $i_{t0} = 0$ in the **Y**-connected case. Using this expression in (5.9b), and using the obtained expression to eliminate $v_{t0} - v_0$ in (5.9d) a new expression of the short circuit current i_f is found. This expression is given by

$$L_f \tfrac{di_f}{dt} = -R_f i_f + \boldsymbol{\gamma}^T \mathbf{T}_{dq}^{-1} \mathbf{v}_{tdq} \ , \tag{5.10}$$

where $\mathbf{T}_{dq}^{-1}$ is a matrix consisting of the two first columns of $\mathbf{T}_{dq0}^{-1}$, and L_f and R_f are scalars and are given by

$$L_f = l_f + \tfrac{1}{3}(\gamma_a - \gamma_b)^2 l_{ls} \qquad\qquad R_f = r_f + \tfrac{1}{3}(\gamma_a - \gamma_b)^2 r_s \ .$$

The final model of the **Y**-connected induction motor then becomes

$$\begin{aligned}
\mathbf{L}'_s \tfrac{d\mathbf{i}'_{sdq}}{dt} &= -(\mathbf{R}_s + \mathbf{R}'_r)\mathbf{i}'_{sdq} + (\mathbf{R}'_r - z_p\omega_r \mathbf{J}\mathbf{L}'_m)\mathbf{i}_{mdq} + \mathbf{v}_{tdq} \\
\mathbf{L}'_m \tfrac{d\mathbf{i}_{mdq}}{dt} &= \mathbf{R}'_r \mathbf{i}'_{sdq} - (\mathbf{R}'_r - z_p\omega_r \mathbf{J}\mathbf{L}'_m)\mathbf{i}_{mdq} \\
L_f \tfrac{di_f}{dt} &= -R_f i_f + \boldsymbol{\gamma}^T \mathbf{T}_{dq}^{-1} \mathbf{v}_{tdq} \\
\mathbf{i}_{tdq} &= \mathbf{i}'_{sdq} + \mathbf{T}_{dq}\boldsymbol{\gamma} i_f \ ,
\end{aligned} \tag{5.11}$$

where $\boldsymbol{\gamma} = \begin{pmatrix} \gamma_a & -\gamma_b & 0 \end{pmatrix}^T$.

The Δ-connected Case

From Section 3.2.3 the relationships between the phase quantities and the measurable quantities in the Δ-connected case are given by,

$$\begin{bmatrix} \mathbf{v}_{sdq} \\ v_{s0} \end{bmatrix} = \begin{bmatrix} \mathbf{B}_v & \mathbf{0} \\ \mathbf{0} & 0 \end{bmatrix} \begin{bmatrix} \mathbf{v}_{tdq} \\ v_{t0} \end{bmatrix} \qquad \begin{bmatrix} \mathbf{i}_{tdq} \\ i_{t0} \end{bmatrix} = \begin{bmatrix} \mathbf{C}_i & \mathbf{0} \\ \mathbf{0} & 0 \end{bmatrix} \begin{bmatrix} \mathbf{i}_{sdq} \\ i_{s0} \end{bmatrix} \ ,$$

here again quantities with subscript s are related to the phases of the motor, and quantities with subscript t are related to the terminals of the motor, and are therefore measurable. Introducing these relationships in (5.8) the model of the Δ-connected induction motor with a stator short circuit becomes

$$\mathbf{L}'_s \frac{d\mathbf{i}'_{sdq}}{dt} = -(\mathbf{R}_s + \mathbf{R}'_r)\mathbf{i}'_{sdq} + (\mathbf{R}'_r - z_p\omega_r \mathbf{J}\mathbf{L}'_m)\mathbf{i}_{mdq} + \mathbf{B}_v \mathbf{v}_{tdq} \tag{5.12a}$$

$$l_{ls} \frac{di'_{s0}}{dt} = -r_s i'_{s0} \tag{5.12b}$$

$$\mathbf{L}'_m \frac{d\mathbf{i}_{mdq}}{dt} = \mathbf{R}'_r \mathbf{i}'_{sdq} - (\mathbf{R}'_r - z_p\omega_r \mathbf{J}\mathbf{L}'_m)\mathbf{i}_{mdq} \tag{5.12c}$$

$$l_f \frac{di_f}{dt} = -r_f i_f + \boldsymbol{\gamma}^T \mathbf{T}_{dq0}^{-1} \begin{bmatrix} \mathbf{B}_v \\ \mathbf{0} \end{bmatrix} \mathbf{v}_{tdq} \ , \tag{5.12d}$$

and the measurable currents are given by

$$\mathbf{i}_{tdq} = \begin{bmatrix}\mathbf{C}_i & \mathbf{0}\end{bmatrix}\left(\mathbf{i}'_{sdq0} + \mathbf{T}_{dq0}\boldsymbol{\gamma} i_f\right) \ . \tag{5.12e}$$

In the Δ-connected case the current $i'_{s0} = i_{s0} - \frac{1}{3}(\gamma_a - \gamma_b)i_f$. From (5.12b) it is seen that $i'_{s0} \to 0$ as $t \to \infty$, meaning that $i_{s0} \to \frac{1}{3}(\gamma_a - \gamma_b)i_f$ as $t \to \infty$. This shows that the circulating current in the Δ-connected motor will be proportional to the current in the short circuit i_f.

The final model of the Δ-connected induction motor with a short circuit fault becomes

$$\begin{aligned}
\mathbf{L}'_s \tfrac{d\mathbf{i}'_{sdq}}{dt} &= -(\mathbf{R}_s + \mathbf{R}'_r)\mathbf{i}'_{sdq} + (\mathbf{R}'_r - z_p\omega_r\mathbf{J}\mathbf{L}'_m)\mathbf{i}_{mdq} + \mathbf{B}_v\mathbf{v}_{tdq} \\
\mathbf{L}'_m \tfrac{d\mathbf{i}_{mdq}}{dt} &= \mathbf{R}'_r\mathbf{i}'_{sdq} - (\mathbf{R}'_r - z_p\omega_r\mathbf{J}\mathbf{L}'_m)\mathbf{i}_{mdq} \\
l_f \tfrac{di_f}{dt} &= -r_f i_f + \boldsymbol{\gamma}^T\mathbf{T}_{dq}^{-1}\mathbf{B}_v\mathbf{v}_{tdq} \\
\mathbf{i}_{tdq} &= \mathbf{C}_i\mathbf{i}'_{sdq} + \mathbf{C}_i\mathbf{T}_{dq}\boldsymbol{\gamma} i_f \ ,
\end{aligned} \tag{5.13}$$

where $\boldsymbol{\gamma} = \begin{pmatrix}\gamma_a & \gamma_b & 0\end{pmatrix}^T$ in the Δ-connected case, and $\mathbf{T}_{dq}^{-1}$ consists of the two first columns of $\mathbf{T}_{dq0}^{-1}$ as in the $\mathbf{Y}$-connected case.

5.1.5 Torque Expression

An expression of the torque developed by an induction motor, not affected by faults, is derived in Section 3.2.4. In the following the same approach is used to derive an expression of the torque developed by an induction motor affected by a turn-turn short curcuit fault in the stator. This torque expression is based on the same idea as used in (Tallam et al., 2002). From (Krause et al., 1994) the torque produced by the induction motor is given by

$$T_e = z_p\mathbf{i}_s^T\frac{\partial\mathbf{l}_{fm}(\theta)}{\partial\theta}\mathbf{i}_r \ , \tag{5.14}$$

where $\mathbf{i}_s$ is the current in the stator windings and $\mathbf{i}_r$ is the current in the rotor. In the case of a stator with faults, the current in each part of the faulty windings must be defined. In the case of a stator with a single turn-turn short circuit between phase a and b, the currents $\mathbf{i}_s$ and $\mathbf{i}_r$ are given by

$$\begin{gathered}
\mathbf{i}_s = \begin{bmatrix} i_{sa} & i_{sa} - \text{sign}(\boldsymbol{\gamma}_1)i_f & i_{sb} & i_{sb} - \text{sign}(\boldsymbol{\gamma}_2)i_f & i_{sc}\end{bmatrix}^T \\
\mathbf{i}_r = \begin{bmatrix} i_{ra} & i_{rb} & i_{rc}\end{bmatrix}^T \ ,
\end{gathered}$$

where $\boldsymbol{\gamma}_1$ and $\boldsymbol{\gamma}_2$ are the first and second elements in $\boldsymbol{\gamma}$ respectively. The matrix $\mathbf{l}_{fm}(z_p\theta_r)$ is the mutual inductance matrix between the stator and rotor. $\mathbf{l}_{fm}(z_p\theta_r)$

is in the case of a turn-turn fault between phase a and b given by,

$$\mathbf{l}_{fm}(\theta) = l_m \begin{bmatrix} (1-\gamma_a)\cos(\theta) & (1-\gamma_a)\cos(\theta+\frac{2\pi}{3}) & (1-\gamma_a)\cos(\theta-\frac{2\pi}{3}) \\ \gamma_a\cos(\theta) & \gamma_a\cos(\theta+\frac{2\pi}{3}) & \gamma_a\cos(\theta-\frac{2\pi}{3}) \\ (1-\gamma_b)\cos(\theta-\frac{2\pi}{3}) & (1-\gamma_b)\cos(\theta) & (1-\gamma_b)\cos(\theta+\frac{2\pi}{3}) \\ \gamma_b\cos(\theta-\frac{2\pi}{3}) & \gamma_b\cos(\theta) & \gamma_b\cos(\theta+\frac{2\pi}{3}) \\ \cos(\theta+\frac{2\pi}{3}) & \cos(\theta-\frac{2\pi}{3}) & \cos(\theta) \end{bmatrix} .$$

The torque expression in (5.14) can be rearranged to become

$$T_e = z_p \left(\mathbf{i}_{sabc} - \boldsymbol{\gamma} i_f\right)^T \frac{\partial \mathbf{l}_m(z_p\theta_r)}{\partial\theta} \mathbf{i}_{rabc} \,, \tag{5.15}$$

where $\boldsymbol{\gamma}$ is given by (5.2) and (5.5) in the $\mathbf{Y}$- and Δ-connected cases respectively. $\mathbf{l}_m(\theta)$ has the same structure as in the no fault case, and is given in Section 3.2.1.

Transforming the torque expression in (5.15) using the transformation $\mathbf{T}_{dq0}$ and using that $\mathbf{L}_m\mathbf{i}_{mdq} = \mathbf{L}_r\mathbf{i}_{rdq} + \mathbf{L}_m\mathbf{i}_{sdq}$, the following torque expression is obtained,

$$T_e = \frac{3}{2} z_p L'_m \left(i_{md} i'_{sq} - i_{mq} i'_{sd}\right)$$

where $L'_m = L_m^2/L_r$, meaning that L'_m is the diagonal element of $\mathbf{L}'_m$.

Remark 5.1.1 *By examining the electrical model of an induction motor with an inter-turn short circuit (5.11) or (5.13) and the torque expression given above, it can be seen that no torque ripples should be expected, if the load is constant at a given speed and the motor is supplied with a balanced three phase sinusoidal voltage.*

5.2 An Adaptive Observer for Inter-turn Fault Detection

According to (Bonnett and Soukup, 1992) most stator burnouts start as an inter-turn short circuit in one of the stator coils. The increased heat due to this short circuit will eventually cause turn to turn and turn to ground faults and finally lead to a burnout of the stator. In (Gerada et al., 2004) the time, from an inter-turn short circuit has occured to an insulation breakdown due to heat, is investagated on a 15 [KW] motor. Here it is shown that this time slot can be as short as 2 [sec]. This means that a fast and reliable detection scheme is necessary, but also that the most important of the inter-turn and the turn-turn faults are the inter-turn faults. Therefore, a detection scheme, which can detect inter-turn short circuits in the stator of an induction motor, is considered in this section.

The considered detection scheme is based on the model developed in the previous section. This model is used in the derivation of an observer which can estimate the inter-turn short circuit faults. Only inter-turn short circuits in phase a are considered, as three

identical observers, which can detect faults in phase a, b and c respectively, can be used for identification. The approach used for this is described at the end of this section and is based on (Zhang, 2000).

In the model developed in the previous section an inter-turn short circuit in phase a is modelled by setting $\gamma_b = 0$ in the vector $\boldsymbol{\gamma}$. Doing this the parameters R_f and L_f in both the **Y**- and Δ-connected motors can be expressed by

$$R_f = f(\gamma_a)r_s + r_i \qquad\qquad L_f = f(\gamma_a)l_{ls} \ ,$$

where $f(\gamma_a)$ equals $\gamma_a(1 - \frac{2}{3}\gamma_a)$ and $\gamma_a(1 - \gamma_a)$ in the **Y**- and Δ-connected cases respectively. In section 5.1.1 it is argued that the resistor r_i in the expression of R_f is almost always either equal to ∞ or 0. Therefore the assumption that $r_i = 0$ is almost always true if a short circuit has occurred. Using this and considering γ_a as a state in the system the model of both the **Y**- and Δ-connected motors with an inter-turn short circuit can be expressed as

$$\begin{aligned}
\mathbf{L}'_s \tfrac{d\mathbf{i}'_{sdq}}{dt} &= -(\mathbf{R}_s + \mathbf{R}'_r)\mathbf{i}'_{sdq} + (\mathbf{R}'_r - z_p\omega_r\mathbf{J}\mathbf{L}'_m)\mathbf{i}_{mdq} + \mathbf{B}_v\mathbf{v}_{tdq} \\
\mathbf{L}'_m \tfrac{d\mathbf{i}_{mdq}}{dt} &= \mathbf{R}'_r\mathbf{i}'_{sdq} - (\mathbf{R}'_r - z_p\omega_r\mathbf{J}\mathbf{L}'_m)\mathbf{i}_{mdq} \\
\tfrac{di_f}{dt} &= -\tfrac{r_s}{l_{ls}}i_f + \tfrac{1}{l_{ls}}\begin{bmatrix}\frac{\gamma_a}{f(\gamma_a)} & 0\end{bmatrix}\mathbf{B}_v\mathbf{v}_{tdq} \\
\tfrac{d\gamma_a}{dt} &= 0 \ ,
\end{aligned} \tag{5.16a}$$

where the measurable outputs are given by

$$\mathbf{i}_{tdq} = \mathbf{C}_i\left(\mathbf{i}'_{sdq} + \begin{bmatrix}\frac{2}{3}\gamma_a \\ 0\end{bmatrix} i_f\right) \ . \tag{5.16b}$$

The only differences between the model of the **Y**- and Δ-connected induction motors are the structures of $\mathbf{B}_v$, $\mathbf{C}_i$, and $f(\gamma_a)$. In the **Y**-connected case $\mathbf{B}_v = \mathbf{C}_i = \mathbf{I}$ and in the Δ-connected case $\mathbf{B}_v$ and $\mathbf{C}_i$ are given in Section 3.2.3 of Chapter 3.

The model in (5.16) represents an induction motor with an inter-turn short circuit in the stator. However, by setting $\gamma_a = 0$ a motor not affected by a fault can be modelled. This is true because setting $\gamma_a = 0$ represents a short circuit involving 0 turns, which have the same effect on the motor performance as when no short cicuits have occured. To ensure the validity of this model the term $\frac{\gamma_a}{f(\gamma_a)}$ must be bounded when $\gamma_a \to 0$. The term is given by

$$\frac{\gamma_a}{f(\gamma_a)} = \frac{\gamma_a}{\gamma_a(1 - a\gamma_a)} \ ,$$

where a equals $\frac{2}{3}$ and 1 in the **Y**- and Δ-connected cases respectively. From this expression it is seen that $\frac{\gamma_a}{f(\gamma_a)}$ is bounded on the set $\{\gamma_a : 0 \leq \gamma_a < 1\}$, which contains all possible values of γ_a.

A surprising fact when modelling the no fault case by setting $\gamma_a = 0$ is that the fault current i_f is not equal to zero in the no fault case. This is because the model expresses

the limit of the fault current when $\gamma_a \rightarrow 0$, when the no fault case is modelled in this way. The model is still correct in the no fault case, as the fault current only affects the remaining model in the output expression (5.16b), and here the fault current is multiplied with γ_a which is equal to zero.

From (5.16) it is seen that the model of the induction motor contains one unknown variable ω_r, which represents the speed of the rotor. If this variable is modelled as an unknown but constant parameter, an adaptive observer approach can be used for state estimations, and thereby estimation of the fault. The design of this adaptive observer is considered in Section 5.2.1. The design of the feedback gain in the adaptive observer is considered in Section 5.2.2, and finally the identification of the phase affected by a given inter-turn short circuit fault is considered in Section 5.2.3.

5.2.1 The Adaptive Observer

An adaptive observer exists for the system in (5.16) if it can be transformed into the adaptive observer form defined in Definition 5.2.1. This definition is a bilinear version of the general nonlinear definition given in (Besancon, 2000).

Definition 5.2.1 *Consider a system on the form*

$$\begin{array}{l} \frac{d\mathbf{z}}{dt} = \mathbf{A}(\mathbf{u},\boldsymbol{\theta})\mathbf{z} + \mathbf{B}\mathbf{u} \\ \mathbf{y} = \mathbf{C}\mathbf{z} \ , \end{array} \tag{5.17}$$

where $\mathbf{z}(t) \in R^n$ *contains the states of the system,* $\mathbf{y}(t) \in R^d$ *contains the meassurable outputs,* $\boldsymbol{\theta} \in R^k$ *contains unknown but constant parameters and* $\mathbf{C} = \begin{bmatrix} \mathbf{I} & \mathbf{0} \end{bmatrix}$. *This system is said to be on bilinear adaptive form if,*

1. $\mathbf{A}(\mathbf{u},\boldsymbol{\theta})$ *is bounded for all* $\boldsymbol{\theta} \in \mathcal{D}_\theta \subseteq R^k$ *and* $\mathbf{u}(t) \in \mathcal{U} \subseteq R^m$, *where* $\mathcal{D}_\theta$ *is the parameter space and* $\mathcal{U}$ *is the input space,*
2. *the set* $(\mathbf{A}(\mathbf{u},\boldsymbol{\theta}), \mathbf{C})$ *is an observable pair for every* $\boldsymbol{\theta} \in \mathcal{D}_\theta$ *and* $\mathbf{u}(t) \in \mathcal{U}$,
3. $\mathbf{A}_{\theta_1}(\mathbf{u})$ *to* $\mathbf{A}_{\theta_k}(\mathbf{u})$ *are linear independent matrices for every* $\mathbf{u}(t) \in \mathcal{U}$,
4. *Ker* $\{\mathbf{C}\} \bigcap \left(\bigcup_{i=1}^{k} \mathit{Im}\, \{\mathbf{A}_{\theta_i}(\mathbf{u})\} \right)$.

where

$$\mathbf{A}(\mathbf{u},\boldsymbol{\theta}) = \mathbf{A}_0(\mathbf{u}) + \sum_{i=1}^{k} \theta_i \mathbf{A}_{\theta_i}(\mathbf{u}) \ .$$

Remark 5.2.1 *Item Number 4 in Definition 5.2.1 means that* $\mathbf{A}_{\theta_i}(\mathbf{u})$ *and* $\mathbf{C}$ *can be put on the following form using a state transformation*

$$\mathbf{A}_{\theta_i}(\mathbf{u}) = \begin{bmatrix} \mathbf{A}'_{\theta_i}(\mathbf{u}) \\ \mathbf{0} \end{bmatrix} \qquad \mathbf{C} = \begin{bmatrix} \mathbf{I} & \mathbf{0} \end{bmatrix}$$

After this state transformation the only states, which are directly affected by θ_i, are the measurable states.

For systems on the form defined by Definition 5.2.1 an adaptive observer exists according to the following proposition.

Proposition 5.2.1 *For a system of the form defined in Definition 5.2.1 an adaptive observer exists and has the following structure,*

$$\begin{aligned} \tfrac{d\hat{\mathbf{z}}}{dt} &= \mathbf{A}(v_{sd}, \hat{\omega}_r)\hat{\mathbf{z}} + \mathbf{B}\mathbf{u} + \mathbf{K}(v_{sd})(\mathbf{y} - \mathbf{C}\hat{\mathbf{z}}) \\ \tfrac{d\hat{\omega}_r}{dt} &= \kappa \hat{\mathbf{z}}^T \mathbf{A}'^T_{\omega_r}(\mathbf{y} - \mathbf{C}\hat{\mathbf{z}}) \ , \end{aligned} \tag{5.18}$$

where $\kappa > 0$ is a design constant, $\mathbf{A}(v_{sd}, \hat{\omega}_r)$ is a copy of the system matrix and $\mathbf{A}'_{\omega_r}$ is the upper submatrix of $\mathbf{A}_{\omega_r}$, as defined in Definition 5.2.1.

System (5.18) is an adaptive observer if there exists a $\mathbf{K}(v_{sd})$ stabilizing the system, i.e. there exists a $\mathbf{P}(\omega_r)$ fulfilling the following Matrix Inequality (MI),

$$\begin{aligned} \left(\mathbf{A}(v_{sd}, \omega_r) - \mathbf{K}(v_{sd})\mathbf{C}\right)^T \mathbf{P}(\omega_r) + \\ \mathbf{P}(\omega_r)\left(\mathbf{A}(v_{sd}, \omega_r) - \mathbf{K}(v_{sd})\mathbf{C}\right) \prec 0 \\ -\mathbf{P}(\omega_r) \prec 0 \ . \end{aligned} \tag{5.19}$$

where $\mathbf{P}(\omega_r)$ is Hermitian and is resticted to be on the form

$$\mathbf{P}(\omega_r) = \begin{bmatrix} \mathbf{I} & \mathbf{0} \\ \mathbf{0} & \mathbf{Q}(\omega_r) \end{bmatrix} \ .$$

Proof: Defining the state estimation error as $\mathbf{e}_z = \mathbf{z} - \hat{\mathbf{z}}$, and the parameter estimation errors as $e_{\omega_r} = \omega_r - \hat{\omega}_r$, the dynamics of the errors become

$$\frac{d\mathbf{e}_z}{dt} = \left(\mathbf{A}(v_{sd}, \omega_r) - \mathbf{K}(v_{sd})\mathbf{C}\right)\mathbf{e}_z + \mathbf{A}_{\omega_r}\hat{\mathbf{z}}e_{\omega_r} \tag{5.20a}$$

$$\frac{de_{\omega_r}}{dt} = -\kappa \hat{\mathbf{z}}^T \mathbf{A}^T_{\omega_r}\mathbf{e}_z \ , \tag{5.20b}$$

where it is used that $\dot{e}_{\omega_r} = -\dot{\hat{\omega}}_r$ as $\dot{\omega}_r = 0$. A candidate for a Lyapunov function for the system is given by

$$V = \mathbf{e}_z^T \mathbf{P}(\omega_r)\mathbf{e}_z + \frac{2}{\kappa}e^2_{\omega_r} \ .$$

Taking the derivative along the trajectory of (5.20) we obtain

$$\begin{aligned} \dot{V} = \mathbf{e}_z^T \big(\left(\mathbf{A}(v_{sd}, \omega_r) - \mathbf{K}(v_{sd})\mathbf{C}\right)^T \mathbf{P}(\omega_r) + \\ \mathbf{P}(\omega_r)\left(\mathbf{A}(v_{sd}, \omega_r) - \mathbf{K}(v_{sd})\mathbf{C}\right)\big)\mathbf{e}_z \ . \end{aligned} \tag{5.21}$$

Here the structure of $\mathbf{P}(\omega_r)$ guarantees that the adaptation term (5.20b) cancel out the second term on the right of (5.20a). Equation (5.21) shows that $\mathbf{e}_z \to 0$ as $t \to \infty$ if (5.19) is fulfilled for every $\underline{\omega}_r \leq \omega_r \leq \overline{\omega}_r$ and $\underline{v}_{sd} \leq v_{sd} \leq \overline{v}_{sd}$.

To show that the error of the parameter estimate also tends to zero the La-Salle's theorem is used (Khalil, 2002). This theorem can be used to state that an error system as (5.20) is asymptotically stable if the only positive invariant space with respect to (5.20) in $E \subset R^{n+1}$ is $\mathbf{e}_z = 0$ and $e_{\omega_r} = 0$, where E is the space of all error vectors $\mathbf{e} = \begin{bmatrix}\mathbf{e}_z & e_{\omega_r}\end{bmatrix}^T$, which make $\dot{V} = 0$. Now by considering (5.20), when $\dot{V} = 0$, we obtain

$$\begin{aligned} 0 &= \mathbf{A}_{\omega_r}\hat{\mathbf{z}}e_{\omega_r} \\ \dot{e}_{\omega_r} &= 0 \ . \end{aligned}$$

This shows that the positive invariant space E is given by $\mathbf{e}_z = 0$ and $e_{\omega_r}\mathbf{A}_{\omega_r}\hat{\mathbf{z}} = 0$. Moreover, it shown that the error e_{ω_r} is constant. This implies that the system is stable.

However, to show that $e_{\omega_r} \to 0$ demands of persistent of excitation need to be defined. The persistent of excitation demand can in this case by formulated as:
There must exist a time series $\hat{\mathbf{z}}(t)$, $t \in [t_0, t_0 + T]$, which guarantees that $e_{\omega_r}\mathbf{A}'_{\omega_r}\hat{\mathbf{z}} = 0$ implies that $e_{\omega_r} = 0$. This leads to

$$\exists \alpha_1, \alpha_2, T > 0 \quad : \quad \alpha_1 \leq \int_{t_0}^{t_0+T} \hat{\mathbf{z}}^T \mathbf{A}'^T_{\omega_r}\mathbf{A}'_{\omega_r}\hat{\mathbf{z}}\, dt \leq \alpha_2 \ ,$$

which in the case of the induction motor is fulfilled whenever either i_{sd} or i_{sq} is different from zero and T is chosen different from the period of the oscillating currents. □

Using a nonlinear transformation $\mathbf{\Phi}$ on (5.16), this system is transformed into a form, which fulfills Definition 5.2.1. The transformation $\mathbf{\Phi} : \mathbf{x} \to \mathbf{z}$ maps the original states

$$\mathbf{x} = \begin{bmatrix}\mathbf{i}'^T_{sdq} & \mathbf{i}^T_{mdq} & i_f & \gamma_a\end{bmatrix}^T \tag{5.22}$$

into the new states $\mathbf{z} \in R^6$, and is given by

$$\mathbf{\Phi}(\mathbf{x}) = \begin{pmatrix} \mathbf{i}'_{sdq} + \begin{bmatrix}\frac{2}{3}\gamma_a \\ 0\end{bmatrix} i_f \\ \mathbf{L}'^{-1}_m \mathbf{L}'_s \mathbf{i}'_{sdq} + \mathbf{i}_{mdq} + \mathbf{L}'^{-1}_m \mathbf{L}'_s \begin{bmatrix}\frac{2}{3}\gamma_a \\ 0\end{bmatrix} i_f \\ \frac{2}{3}\gamma_a i_f \\ \frac{\gamma_a^2}{l_{ls} f(\gamma_a)} \end{pmatrix} \ . \tag{5.23}$$

When this transformation is used on system (5.16) it is transformed into a bilinear system on the form,

$$\begin{aligned} \tfrac{d\mathbf{z}}{dt} &= (\mathbf{A}_0 + \omega_r \mathbf{A}_{\omega_r} + v_{sd}\mathbf{A}_{v_{sd}})\mathbf{z} + \mathbf{B}\mathbf{u} \\ \mathbf{y} &= \mathbf{C}\mathbf{z} \ , \end{aligned} \tag{5.24}$$

where the input vector $\mathbf{u} = \mathbf{v}_{tdq}$, the output vector $\mathbf{y} = \mathbf{i}_{tdq}$, and the matrices in (5.24) are given by

$$\mathbf{A}_0 = \begin{bmatrix} -\mathbf{L}_s'^{-1}(\mathbf{R}_s + \mathbf{R}_r') - \mathbf{L}_m'^{-1}\mathbf{R}_r' & \mathbf{L}_s'^{-1}\mathbf{R}_r' & \begin{bmatrix} \frac{R_s+R_r'}{L_s'} - \frac{r_s}{l_{ls}} \\ 0 \end{bmatrix} & 0 \\ -\mathbf{L}_m'^{-1}\mathbf{R}_s & 0 & \begin{bmatrix} \frac{R_s}{L_m'} - \frac{r_s}{l_{ls}} \\ 0 \end{bmatrix} & 0 \\ 0 & 0 & -\frac{r_s}{l_{ls}} & 0 \\ 0 & 0 & 0 & 0 \end{bmatrix}$$

$$\mathbf{A}_{\omega_r} = \begin{bmatrix} z_p\mathbf{J} & -z_p\mathbf{J}\mathbf{L}_s'^{-1}\mathbf{L}_m' & 0 & 0 \\ 0 & 0 & 0 & 0 \\ 0 & 0 & 0 & 0 \\ 0 & 0 & 0 & 0 \end{bmatrix} \qquad \mathbf{A}_{v_{sd}} = \begin{bmatrix} 0 & 0 & 0 & \begin{bmatrix} \frac{2}{3l_{ls}} \\ 0 \end{bmatrix} \\ 0 & 0 & 0 & \begin{bmatrix} \frac{2(l_m+l_{ls})}{3L_m l_{ls}} \\ 0 \end{bmatrix} \\ 0 & 0 & 0 & \frac{2}{3l_{ls}} \\ 0 & 0 & 0 & 0 \end{bmatrix}$$

$$\mathbf{B} = \begin{bmatrix} \mathbf{L}_s'^{-1} \\ \mathbf{L}_m'^{-1} \\ 0 \\ 0 \end{bmatrix} \mathbf{B}_v \qquad \mathbf{C} = \mathbf{C}_i \begin{bmatrix} \mathbf{I} & 0 & 0 & 0 \end{bmatrix} .$$

If ω_r is treated as an unknown but constant parameter, system (5.24) fulfills Definition 5.2.1 except for the observability condition when $v_{sd} = 0$. However, it can be argued that, when the induction motor is running, the fraction of time where $v_{sd} = 0$ tends to zero. This is so because v_{sd} passes zero but does never stay there during normal operation. Therefore the system described by (5.24) is observable at all the times, meaning that Definition 5.2.1 is fulfilled.

As (5.24) fulfills Definition 5.2.1 an adaptive observer is given by Proposition 5.2.1. This observer becomes

$$\mathcal{O}_a : \begin{cases} \frac{d\hat{\mathbf{z}}}{dt} = (\mathbf{A}_0 + \hat{\omega}_r\mathbf{A}_{\omega_r} + v_{sd}\mathbf{A}_{v_{sd}})\hat{\mathbf{z}} + \mathbf{B}\mathbf{u} + \mathbf{K}(\mathbf{u})(\mathbf{y} - \mathbf{C}\hat{\mathbf{z}}) \\ \frac{d\hat{\omega}_r}{dt} = \kappa(\mathbf{y} - \mathbf{C}\hat{\mathbf{z}})^T\mathbf{A}_{\omega_r}\hat{\mathbf{z}} \\ \hat{\mathbf{x}} = \mathbf{\Phi}^{-1}(\hat{\mathbf{z}}) \ . \end{cases} \tag{5.25}$$

In this design $\mathbf{K}(\mathbf{u})$ is the stabilizing feedback gain and $0 < \kappa$ is the adaptation gain. κ should be chosen such that the adaptation speed is suitable. $\mathbf{K}(\mathbf{u})$ should be chosen according to Proposition 5.2.1. The calculation of $\mathbf{K}(\mathbf{u})$ is considered in the following section.

5.2.2 Calculation of the Observer Gain

Proposition 5.2.1 states that a $\mathbf{K}(\mathbf{u})$ must exist, which guarantees that the following Matrix Inequality (MI) is fulfilled,

$$\begin{aligned}\left(\mathbf{A}(\mathbf{u},\boldsymbol{\theta})-\mathbf{K}(\mathbf{u})\mathbf{C}\right)^T\mathbf{P}(\boldsymbol{\theta})+\mathbf{P}(\boldsymbol{\theta})\left(\mathbf{A}(\mathbf{u},\boldsymbol{\theta})-\mathbf{K}(\mathbf{u})\mathbf{C}\right)&\prec 0\\ -\mathbf{P}(\boldsymbol{\theta})&\prec 0\end{aligned} \tag{5.26}$$

for all $\mathbf{u}\in\mathcal{U}$ and $\boldsymbol{\theta}\in\mathcal{D}_\theta$. In the induction motor case this is the same as saying that the MI must be fulfilled for all possible values of v_{sd} and ω_r.

Before the design of the induction motor case is considered a general approach for analysis and synthesis of the observer gain is given. This analysis and synthesis approach is restricted to the subset of systems defined in Definition 5.2.1, and where $\mathbf{A}(\mathbf{u},\boldsymbol{\theta})$ is given by

$$\mathbf{A}(\mathbf{u},\boldsymbol{\theta})=\mathbf{A}_0+\sum_{i=1}^{k}\theta_i\mathbf{A}_i+\sum_{j=1}^{m}u_j\mathbf{A}_{k+j}\ , \tag{5.27}$$

meaning that $\mathbf{A}(\mathbf{u},\boldsymbol{\theta})$ is affine with respect to $\mathbf{u}$ and $\boldsymbol{\theta}$. Here $\mathrm{Im}\{\mathbf{A}_i\}\bigcap\mathrm{Ker}\{\mathbf{C}\}=0$ for all $i\in\{1,\cdots,k\}$ must be true for Definition 5.2.1 to be fulfilled. Moreover, $\mathbf{A}(\mathbf{u},\boldsymbol{\theta})$ must be bounded, which is the case for (5.27) whenever $\mathcal{D}_\theta$ and $\mathcal{U}$ are bounded sets.

Analysis

First the analysis of stability is considered when a candidate for $\mathbf{K}(\mathbf{u})$ is given. Assume that $\mathbf{K}(\mathbf{u})$ has a structure such that it can be written as $\mathbf{K}(\mathbf{u})=\mathbf{K}_0+\sum_{j=1}^{m}u_j\mathbf{K}_j$, i.e. it is affine with respect to $\mathbf{u}$. If this is the case the MI in (5.26) is affine with respect to $\mathbf{u}$. Moreover, assume that the sets $\mathcal{U}$ and $\mathcal{D}_\theta$ are on a form such that the set of unknown $\mathbf{u},\boldsymbol{\theta}$ in (5.26) can be descibed by a convex hull (Scherer and Weiland, 1999), see Appendix B.2. Let this convex hull be given by

$$\boldsymbol{\Delta}=\mathrm{co}\left\{\boldsymbol{\Delta}_0\right\}\qquad,\ \boldsymbol{\Delta}_0=\left\{(\mathbf{u},\boldsymbol{\theta})\mid u_j\in\{\underline{u}_j,\overline{u}_j\},\theta_i\in\{\underline{\theta}_i,\overline{\theta}_i\}\right\}\ ,$$

where $\underline{u}_j$ and $\overline{u}_j$ $j\in\{1,\cdots,m\}$ are elements in $\mathcal{U}$, forming a convex hull on $\mathcal{U}$. Likewise, $\underline{\theta}_i$ and $\overline{\theta}_i$ $i\in\{1,\cdots,k\}$ are elements in $\mathcal{D}_\theta$ forming a convex hull on $\mathcal{D}_\theta$.

With this choise of $\mathbf{K}(\mathbf{u})$ and $\boldsymbol{\Delta}_0$, (5.26) can be reformulated as a Linear Matrix Inequality (LMI). This means that feasibility of this LMI on the set $\boldsymbol{\Delta}_0$ is a proof of stability of the adaptive observer (5.18), with the chosen $\mathbf{K}(\mathbf{u})$. The LMI is given by the following expression (Scherer and Weiland, 1999, Prop. 2.40), see Appendix B.2,

$$\begin{aligned}\left(\mathbf{A}(\mathbf{u},\boldsymbol{\theta})-\mathbf{K}(\mathbf{u})\mathbf{C}\right)^T\mathbf{P}(\boldsymbol{\theta})+\mathbf{P}(\boldsymbol{\theta})\left(\mathbf{A}(\mathbf{u},\boldsymbol{\theta})-\mathbf{K}(\mathbf{u})\mathbf{C}\right)&\prec 0\\ -\mathbf{P}(\boldsymbol{\theta})&\prec 0\\ \mathbf{A}_i^T\mathbf{P}_i+\mathbf{P}_i\mathbf{A}_i&\succeq 0\ ,\end{aligned} \tag{5.28}$$

which must be fulfilled for all $(\mathbf{u}, \boldsymbol{\theta}) \in \boldsymbol{\Delta}_0$ and all $i \in \{1, \cdots, k\}$. In this LMI $\mathbf{P}(\boldsymbol{\theta})$ is on the form $\mathbf{P}(\boldsymbol{\theta}) = \mathbf{P}_0 + \sum_{i=1}^{k} \theta_i \mathbf{P}_i$.

The feasability of this LMI states that the adaptive observer in Proposition 5.2.1 is stable for the given $\mathbf{K}(\mathbf{u})$. However, if there are limits on the change rate of the supply signals $\mathbf{u}$, this rate limit can be incorporated in the stability analysis, relaxing the condition. To see this, let $\dot{\mathbf{u}}$ be contained in the set $\boldsymbol{\Lambda}$ given by

$$\boldsymbol{\Lambda} = \text{co}\left\{\boldsymbol{\Lambda}_0\right\} \qquad , \; \boldsymbol{\Lambda}_0 = \text{co}\left\{\dot{\mathbf{u}} \mid \dot{u}_j \in \{\underline{\lambda}_j, \overline{\lambda}_j\}\right\} \; ,$$

and let $\mathbf{P}$ in (5.28) be an affine function of both $\boldsymbol{\theta}$ and $\mathbf{u}$. Then the stability condition can be formulated by the following LMI (Scherer and Weiland, 1999, Prop. 2.43), see Appendix B.2,

$$\begin{aligned} \left(\mathbf{A}(\mathbf{u}, \boldsymbol{\theta}) - \mathbf{K}(\mathbf{u})\mathbf{C}\right)^T \mathbf{P}(\boldsymbol{\theta}, \mathbf{u}) + \mathbf{P}(\boldsymbol{\theta}, \mathbf{u}) \left(\, * \,\right) + \mathbf{P}(0, \boldsymbol{\lambda}) &\prec \mathbf{P}_0 \\ -\mathbf{P}(\boldsymbol{\theta}, \mathbf{u}) &\prec 0 \\ \mathbf{A}_i^T \mathbf{P}_i + \mathbf{P}_i \mathbf{A}_i &\succeq 0 \; , \end{aligned} \tag{5.29}$$

where $*$ denotes a copy of the contents of the previous bracket and $\mathbf{P}(\boldsymbol{\theta}, \mathbf{u})$ is on the form $\mathbf{P}(\boldsymbol{\theta}, \mathbf{u}) = \mathbf{P}_0 + \sum_{i=1}^{k} \theta_i \mathbf{P}_i + \sum_{j=1}^{m} u_j \mathbf{P}_{j+k}$. The LMI must be fulfilled for all $(\mathbf{u}, \boldsymbol{\theta}) \in \boldsymbol{\Delta}_0$, $\boldsymbol{\lambda} \in \boldsymbol{\Lambda}_0$ and all $i \in \{1, \cdots, k+m\}$.

Remark 5.2.2 *The LMI's presented in (5.28) or (5.29) are not the only LMI formulation for stability analysis of (5.18). The problem can also be transformed to the standard formulation used in the robust control community. Doing this performance demands defined in the frequency domaín can be included in the analysis. However, this approach is not prestented here, as it is the author oppinion that (5.28) and (5.29) are easier to follow, due to the straightforward connection to Lyapunov stability.*

Synthesis

The LMI presented in (5.28) and (5.29) can only be used for analysis, because $\mathbf{P}$ is a function of $\boldsymbol{\theta} \in \mathcal{D}_\theta$ and $\mathbf{u} \in \mathcal{U}$. However, introducing the restriction that $\mathbf{P}$ is constant over $\mathcal{D}_\theta$ and $\mathcal{U}$, the LMI is made solvable for $\mathbf{K}(\mathbf{u}) = \mathbf{K}_0 + \sum_{j=1}^{m} u_j \mathbf{K}_j$. Introducing this restriction in (5.26) it becomes

$$\begin{aligned} \left(\mathbf{A}(\mathbf{u}, \boldsymbol{\theta}) - \mathbf{K}(\mathbf{u})\mathbf{C}\right)^T \mathbf{P} + \mathbf{P} \left(\mathbf{A}(\mathbf{u}, \boldsymbol{\theta}) - \mathbf{K}(\mathbf{u})\mathbf{C}\right) &\prec 0 \\ -\mathbf{P} &\prec 0 \; , \end{aligned} \tag{5.30}$$

which must be fulfilled for all $(\mathbf{u}, \boldsymbol{\theta}) \in \boldsymbol{\Delta}_0$. Using the transformations $\mathbf{L}_j = \mathbf{K}_j \mathbf{P}$ $j \in \{0, 1, \cdots, m\}$, (5.30) can be rewritten to become

$$\begin{aligned} \left(\mathbf{P}\left(\mathbf{A}_0 + \textstyle\sum_{i=1}^{k} \theta_k \mathbf{A}_i\right) - \mathbf{L}_0 \mathbf{C}\right)^T + \left(\, * \,\right) + & \\ \sum_{j=1}^{m} u_j \left[\left(\mathbf{P}\mathbf{A}_{k+j} - \mathbf{L}_j \mathbf{C}\right)^T + \left(\, * \,\right)\right] &\prec 0 \\ -\mathbf{P} &\prec 0 \; , \end{aligned} \tag{5.31}$$

where $*$ denotes a repetition of the contents of the previous bracket. This expression is affine in $\mathbf{P}$ and $\mathbf{L}_j$ $j \in \{1, \cdots, m\}$, meaning that if a solution exists for $\mathbf{P}$ and $\mathbf{L}_j$ it can be found using the LMI (5.31). $\mathbf{P}$ has full rank, meaning that the transformation $\mathbf{L}_j = \mathbf{K}_j\mathbf{P}$ is solvable for all $\mathbf{K}_j$ $j \in \{1, \cdots, m\}$.

The assumption that $\mathbf{P}(\boldsymbol{\theta})$ is constant for all $\boldsymbol{\theta}$, is the same as saying that the parameters in $\boldsymbol{\theta}$ can change arbitrary fast. However, the parameters $\boldsymbol{\theta}$ are assumed constant in the design of the adaptation part of the observer, meaning that conservatism is introduced by this calculation of $\mathbf{K}(\mathbf{u})$.

Observer Gain in the Induction Motor Case

The only unknown parameter in the induction motor case is the speed ω_r, meaning that $\boldsymbol{\theta} = \omega_r$. Likewise, there is only one input making the system bilinear, namely v_{sd}, i.e. $\mathbf{u} = v_{sd}$. Based on this the convex hull for this system is given by

$$\boldsymbol{\Delta} = \text{co}\{\boldsymbol{\Delta}_0\} \qquad , \ \boldsymbol{\Delta}_0 = \{(v_{sd}, \omega_r) \mid v_{sd} \in \{\underline{v}_{sd}, \overline{v}_{sd}\}, \omega_r \in \{\underline{\omega}_r, \overline{\omega}_r\}\} \ ,$$

where $\underline{v}_{sd} < 0 < \overline{v}_{sd}$ and $\underline{\omega}_r < 0 < \overline{\omega}_r$. In Section 5.2.1 it is argued that the induction motor system is not observable when $v_{sd} = 0$. Therefore, the MI (5.26) can never have a solution on $\boldsymbol{\Delta}_0$. It is also argued that v_{sd} only goes through zero and never stays there. Therefore, the fraction of time where $v_{sd} = 0$ tends to zero. Using this argument it is only necessary to check stability in the set $\{v_{sd} \mid \underline{v}_{sd} \leq v_{sd} \leq \overline{v}_{sd}\} \backslash \ 0$. This can be done by reformulating the MI (5.26) obtaining the following LMI,

$$\begin{aligned} \left(\mathbf{A}(v_{sd}, \omega_r) - \mathbf{K}(v_{sd})\mathbf{C}\right)^T \mathbf{P}(\omega_r) + \mathbf{P}(\omega_r)\,(\,*\,) &\prec 0 \\ \left(\mathbf{A}(-v_{sd}, \omega_r) - \mathbf{K}(-v_{sd})\mathbf{C}\right)^T \mathbf{P}(\omega_r) + \mathbf{P}(\omega_r)\,(\,*\,) &\prec 0 \\ -\mathbf{P}(\omega_r) &\prec 0 \ , \end{aligned} \tag{5.32}$$

where $*$ denotes a copy of the contents of the previous bracket, and $\mathbf{A}(v_{sd}, \omega_r) = \mathbf{A}_0 + \omega_r\mathbf{A}_{\omega_r} + v_{sd}\mathbf{A}_{v_{sd}}$. The matrices $\mathbf{A}_0$, $\mathbf{A}_{\omega_r}$, $\mathbf{A}_{v_s d}$, $\mathbf{B}$, and $\mathbf{C}$ in the above LMI are all defined in Section 5.2.1. This LMI should be feasible on the set given by

$$\boldsymbol{\Delta}_0 = \{(v_{sd}, \omega_r) \mid v_{sd} \in \{\epsilon, \overline{v}_{sd}\}, \omega_r \in \{\overline{\omega}_r, \underline{\omega}_r\}\} \qquad \epsilon > 0$$

for the adaptive observer to exist. For the induction motor used in the tests presented at the end of this chapter the conservatism imposed in the synthesis is too restrictive, i.e. no solution can be found. However, it is still possible to check stability for a given $\mathbf{K}(v_{sd})$ without introducing conservatism in the analysis. This is done by using the analysis approach presented by the LMI (5.29), taking limits on the change rate of the supply signal v_{sd} into account. Utilizing this approach the stability of the observer with a given

feedback gain $\mathbf{K}(v_{sd})$ is checked by the LMI,

$$\begin{aligned}
\left(\mathbf{A}(v_{sd},\omega_r)-\mathbf{K}(v_{sd})\mathbf{C}\right)^T\mathbf{P}(\omega_r,v_{sd})+\mathbf{P}(\omega_r,v_{sd})\,(\,*\,)& \\
+\mathbf{P}(0,\dot{v}_{sd}) \prec \mathbf{P}_0 & \quad (5.33a)\\
-\mathbf{P}(\omega_r,v_{sd}) \prec 0 & \quad (5.33b)\\
\left(\mathbf{A}(-v_{sd},\omega_r)-\mathbf{K}(-v_{sd})\mathbf{C}\right)^T\mathbf{P}(\omega_r,-v_{sd})+\mathbf{P}(\omega_r,-v_{sd})\,(\,*\,)& \\
+\mathbf{P}(0,\dot{v}_{sd}) \prec \mathbf{P}_0 & \quad (5.33c)\\
-\mathbf{P}(\omega_r,-v_{sd}) \prec 0 & \quad (5.33d)\\
\mathbf{A}_{w_r}^T\mathbf{P}_{w_r}+\mathbf{P}_{w_r}\mathbf{A}_{w_r} \succeq 0 & \quad (5.33e)\\
\mathbf{A}_{v_{sd}}^T\mathbf{P}_{v_{sd}}+\mathbf{P}_{v_{sd}}\mathbf{A}_{v_{sd}} \succeq 0\,, & \quad (5.33f)
\end{aligned}$$

where $*$ denotes a copy of the contents of the previous bracket, and $\mathbf{A}(v_{sd},\omega_r)=\mathbf{A}_0+\omega_r\mathbf{A}_{\omega_r}+v_{sd}\mathbf{A}_{v_{sd}}$. The matrices $\mathbf{A}_0$, $\mathbf{A}_{\omega_r}$, $\mathbf{A}_{v_sd}$, $\mathbf{B}$, and $\mathbf{C}$ in the above LMI are all defined in Section 5.2.1. This LMI should be feasible on the set given by,

$$\left\{(v_{sd},\dot{v}_{sd},\omega_r)\mid v_{sd}\in\{\epsilon,\overline{v}_{sd}\},\dot{v}_{sd}\in\{\underline{\lambda},\overline{\lambda}\},\omega_r\in\{\underline{\omega}_r,\overline{\omega}_r\}\right\}\qquad \epsilon>0$$

for the adaptive observer to exist. In the LMI the inequalities (5.33a) to (5.33d) are introduced to check stability of the two regions defined by $0 < v_{sd}$ and $v_{sd} < 0$ respectively. The inequalities (5.33e) and (5.33f) are introduced to guarantee convexity of (5.33a) and (5.33c) with respect to the parameter ω_r and the input v_{sd}. The analysis approach presented by the LMI (5.33) is utilized in the design of the observer, used in the tests prestented in Section 5.3.

Remark 5.2.3 *In the above text it is argued that the observer is stable for all values of the voltage v_{sd} between $-\overline{v}_{sd}$ and $\overline{v}_{sd}$ [V] except for $v_{sd}=0$, and all speeds between $\underline{\omega}_r$ and $\overline{\omega}_r$ [rad/sec], if the LMI (5.33) is feasiable. This is not the same as saying that it is possible to estimate the fault and speed at zero speed, due to demands for persistence of excitation, see the proof of Proposition 5.2.1.*

Remark 5.2.4 *Fault tolerant control can be obtained using the current vector $\mathbf{i}'_{sdq}$, estimated by the proposed observer, as input to the current controllers in a traditional motor control system. This current is the part of the stator current producing air gab flux. Therefore, by using this current the control is not affected by the short circuit.*

This current vector is given by the two first terms of the state vector $\mathbf{x}$ in (5.22), which is calculated using $\mathbf{x}=\mathbf{\Phi}^{-1}(\mathbf{z})$, where $\mathbf{\Phi}$ is defined in (5.23).

5.2.3 Identification of the Faulty Phase

According to (Zhang, 2000) isolation between different faults can be obtained using a set of adaptive observers. Here it is shown that the estimator fault $\mathbf{e}_y=\mathbf{y}-\hat{\mathbf{y}}$ is an

indicator of the correctness of the model used in the observer design. This means that when only one of the observer faults approximate zero it indicates that the fault modelled by this particular observer has happened in the system. This approach can, in the case of the induction motor, be used if three identical observers are designed, each detecting a stator winding fault in one of the three phases. This is considered in the following.

The adaptive observer $\mathcal{O}_a$ in (5.25), is capable of estimating an inter-turn fault in phase a. However, the same observer can be used to estimate a fault in phase b and c by using another phase sequence as argument in the transformation $\mathbf{T}_{dq0}$. To estimate a fault in phase b the following transformation must be used,

$$\mathbf{v}_{sdq0} = \mathbf{T}_{dq0}\mathbf{v}_{sbca} \qquad \mathbf{i}_{sdq0} = \mathbf{T}_{dq0}\mathbf{i}_{sbca} \ ,$$

where $x_{sbca} = \begin{bmatrix} x_{sb} & x_{sc} & x_{sa} \end{bmatrix}^T$ and $x \in \{v, i\}$. When these signal vectors are used as input to the observer in (5.25), the observer can estimate faults in phase b, and is therefore called $\mathcal{O}_b$. Likewise, an observer $\mathcal{O}_c$ for estimating inter-turn faults in phase c is found by using yet another phase sequence resulting in the following transformations,

$$\mathbf{v}_{sdq0} = \mathbf{T}_{dq0}\mathbf{v}_{scab} \qquad \mathbf{i}_{sdq0} = \mathbf{T}_{dq0}\mathbf{i}_{scab} \ .$$

Using these transformations in the approach presented in (Zhang, 2000) the overall structure of the fault identification and estimation algorithm becomes as depitched in Fig. 5.2. Here the error signals $\mathbf{e}_{ya}$, $\mathbf{e}_{yb}$ and $\mathbf{e}_{yc}$ are used for identification of the phase affected by a inter-turn fault, and $\hat{\mathbf{x}}_a$, $\hat{\mathbf{x}}_b$ and $\hat{\mathbf{x}}_c$ are the estimates of the states including the estimates of the fault current i_f and the fault size γ.

The affected phase is in this work identified by comparing the square error, of each error signal $\mathbf{e}_{ya}$, $\mathbf{e}_{yb}$ and $\mathbf{e}_{yc}$, with a predefined threshold value. The square error is calculated using $\mathbf{e}_i^T\mathbf{e}_i$.

Remark 5.2.5 *The approach used here is based on a predefined threshold value. This threshold must be chosen as a trade-off between how small a fault can be detected and robustness in the system. However, the problem of choosing this threshold can be overcome by comparing the square error of the three error signals $\mathbf{e}_{ya}$, $\mathbf{e}_{yb}$, and $\mathbf{e}_{yc}$. If the levels of these error signals are alike no fault has occurred, and if a fault has occured it is identified by the signal with the smallest square error. However, using these approaches you cannot be sure to identify the correct fault, you will just identify the fault most likely to have occured among the modelled faults.*

5.3 Test Results

In this section the identification and estimation approaches described in the previous section are tested on an induction motor setup, where inter-turn stator faults can be simulated. The electrical circuit of the stator is shown in Fig. 5.3. The motor used in the

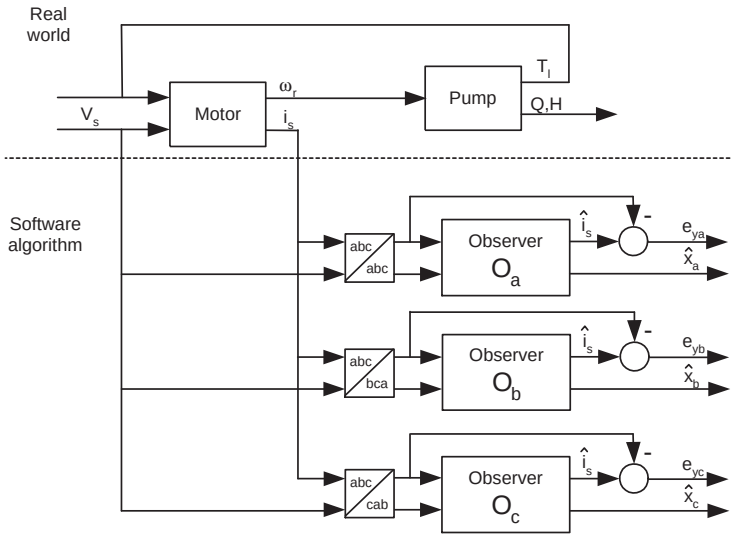

Figure 5.2: The structure of the identification algorithm for identification and estimation of inter-turn short circuits. Here $\mathbf{e}_{ya}$, $\mathbf{e}_{yb}$ and $\mathbf{e}_{yc}$ are used for identification of the affected phase, and $\hat{\mathbf{x}}_a$, $\hat{\mathbf{x}}_b$ and $\hat{\mathbf{x}}_c$ are the estimates of the states including the estimates of the fault current i_f and the fault size γ.

tests is a 1.5 [KW] customized Grundfos motor, supplied with a Danfoss frequency converter. The speed, the three phase currents, and the three phase voltages are available at the test setup. The voltage to the motor is controlled using a linear voltage to frequency relation, with a voltage boost at low frequencies. All tests are preformed at supply frequencies around 30 $[Hz]$ to avoid too large short circuit currents and thereby burnout of the motor during the tests. The tests are performed with the induction motor connected in a Δ-connection as it is shown Fig. 5.3. However, similar results can be found for a $\mathbf{Y}$-connected motor in (Kallesøe et al., 2004c).

In the first, of the two following subsections, the identification capabilities of the proposed algorithm are tested. In the second subsection the estimation capabilities of the adaptive observer are tested. In these tests the algorithm is tested against three different operating conditions. These are,

- Constant speed at 25 $[Hz]$ supply frequency and balanced supply voltage.
- Speed changes at every 1 second between 25 and 40 $[Hz]$ and balanced supply voltage.
- Constant speed at 25 $[Hz]$ supply frequency and a 5 % voltage decrease in phase

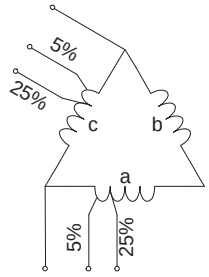

Figure 5.3: The electrical circuit of the stator in the test setup. Two points of phases a and b and their end points are available at the terminal box.

a, meaning that the supply voltage is unbalanced.

5.3.1 Test of Identification Capabilities

In this subsection the identification capability of the identification algorithm, presented in Section 5.2.3, is tested. Three tests are performed, each testing one of the three operating conditions described above. In each of the tests a short circuit of 5% of the windings is introduced in phase a and c respectively. The results of the test with constant speed and balanced supply are shown in Fig. 5.4, the results of the test with speed changes and balanced supply are shown in Fig. 5.5, and finally the results of the test with constant speed and unbalanced supply are shown in Fig. 5.6.

All the tests show that the phase, in which the fault is introduced, can be recognised by the level of the observer error signal. From all three tests it is seen that this error signal is considerable lower for the observer modelling the particular fault. However, it is also seen that the level of the observer error signal is changing in the case of a fault, even in the observer modelling the particular fault. This is especially a problem in the case of a fault in phase a, see Figs. 5.4 and 5.5. This unexpected behaviour is due to an inherent imbalance between the phases in the costumer-designed motor used in the tests. The phenomenon is not so dominant in Fig. 5.6, where the supply voltage is unbalanced. This is because the unbalance in the voltage does account for some of the imbalance of the phases.

From Fig. 5.5, presenting the results of the test with the speed changes, it is seen that the error signal is in average larger and is oscillating compared to the two other tests. This is due to the violation of the constant speed assumption in the design of the adaptive fault observers. However, it is still possible to recognize the phase, in which the fault is introduced, using the observer error signal.

Comparing the results of Figs. 5.4 and 5.6 it is seen that, beside of the problem with

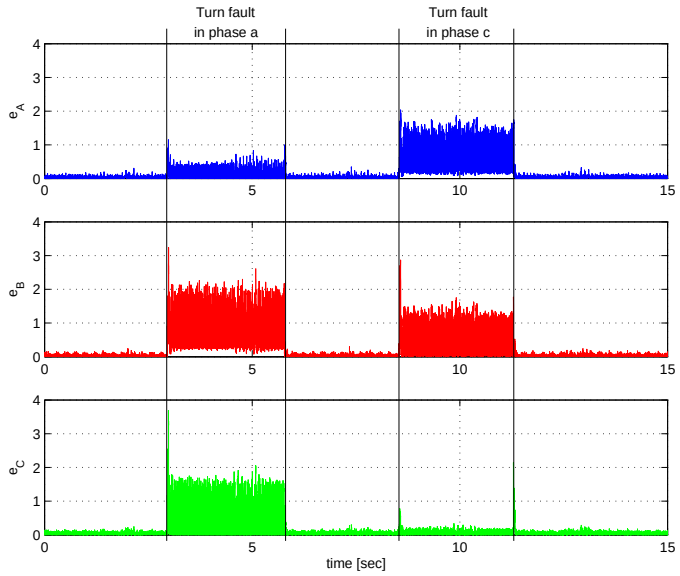

Figure 5.4: The mean square error of the observers $\mathcal{O}_a$, $\mathcal{O}_b$, and $\mathcal{O}_c$ respectively. In this test the speed is constant and the supply voltage is balanced, and faults are imposed seperately in phase a and c.

the inherent imbalance in the phases, the results are comparable. This shows that the algorithm is able to handle unbalanced supply conditions, which also was expected as no assumption were put on the supply voltage in the design. This means that the observer can manage any distortion of the supply voltage as long as it does not introduce too large oscillations in the speed.

5.3.2 Test of Estimation Capabilities

In this subsection the estimation capability of the adaptive observer, derived in the previous section, is tested. The observer is tested under the three different operating conditions described in the start of this section. In each of the tests the algorithm is tested with no short circuit, 5% of the windings short circuited, and 25% of the windings short circuited in phase a. The results of the test with constant speed and balanced supply are shown in Fig. 5.7(a) and 5.7(b). The results of the test with speed changes and balanced supply are shown in Fig. 5.8(a) and 5.8(b), and finally the results of the test with constant speed and unbalanced supply are shown in Fig. 5.9(a) and 5.9(b).

All the tests have shown that the observer is stable. From the first test, presented in Fig. 5.7(a) and 5.7(b), it is seen that the speed is estimated without any bias. It is also seen that there is a bias on the estimated fraction of turns in the short circuit. This bias is

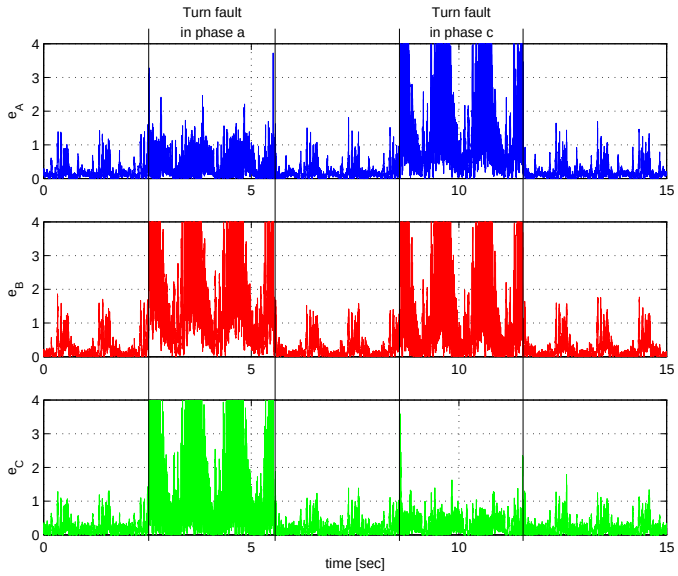

Figure 5.5: The mean square error of the observers $\mathcal{O}_a$, $\mathcal{O}_b$, and $\mathcal{O}_c$ respectively. In this test the speed is variating and the supply voltage is balanced, and faults are imposed seperately in phase a and c.

partly due to noise on the measurements, partly due to mismatch between the real motor parameters and the motor parameters used in the observer, and partly due to the initial imbalance between the three stator phases. This bias is repeated in each of the three tests.

Results from the second test, presented in 5.8(a) and 5.8(b), show that the observer is capable of estimating the wanted quantities despite of speed changes. Still it is seen that the speed changes affect the estimated amount of turns in the short circuit. This is because of the constant speed assumption used in the design. It is, however, still possible to use the estimate of the fault.

From the results of the last test, presented in 5.9(a) and 5.9(b), it is seen that an unbalanced supply of 5% is not affecting the performance of the observer.

5.4 Conclusion

An adaptive observer for simultaneous estimation of the motor states, the speed, and the amount of turns in an inter-turn short circuit is proposed. The observer is tested on a customized designed induction motor. The tests have shown that the observer can estimate an inter-turn fault despite of speed changes and unbalanced supply conditions.

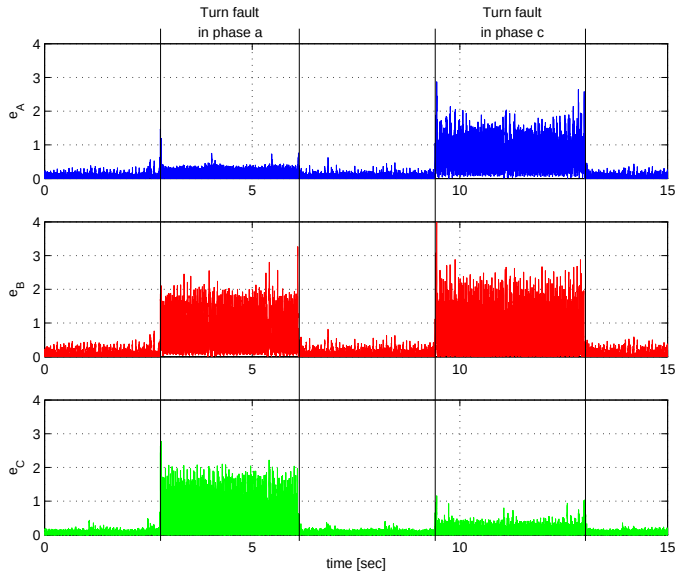

Figure 5.6: The mean square error of the observers $\mathcal{O}_a$, $\mathcal{O}_b$, and $\mathcal{O}_c$ respectively. In this test the speed is constant and the supply voltage is unbalanced, and faults are imposed seperately in phase a and c.

This makes the estimation scheme usable in inverter feed induction motor drives, or in motor applications supplied by a bad grid. Using three of these observers it is shown that it is possible to identify the phase affected by a given inter-turn short circuit.

The adaptive observer is based on a model of an induction motor including an inter-turn short circuit. This model is a simplification of the model presented in the start of this chapter, as the derived model describes the motor behaviour in both the inter-turn and the turn-turn short circuit cases. Moreover, the model describes the motor when it is connected in a $\mathbf{Y}$-connection as well as a Δ-connection.

Comparing the approach presented here with traditional approaches, the main advance is that the obtained observer is based on a dynamic model of the system. This means that the detection capabilities are not affected by dynamic changes in the electrical system. The main drawback of the proposed approach is the need for the motor parameters. However, in the cases where the approach is used in a frequency converter application, this problem can be solved by parameter identification methods at start up (Rasmussen, 1995).

The proposed adaptive observer can be used for fault-tolerant control of the induction motor, as the impact of the inter-turn short circuit is estimated. This is so because it is possible to obtain control in the case of an inter-turn short circuit, meaning that it is possible to control the process, driven by the motor, to a fail-safe mode, or to reduce the

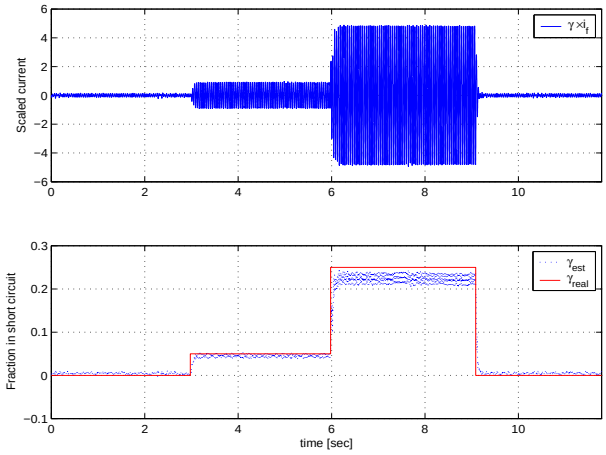

(a) The top figure shows the estimation of the scaled current $\gamma_a i_f$ and the bottom figure shows the estimated and real amount of windings affected by the short circuit.

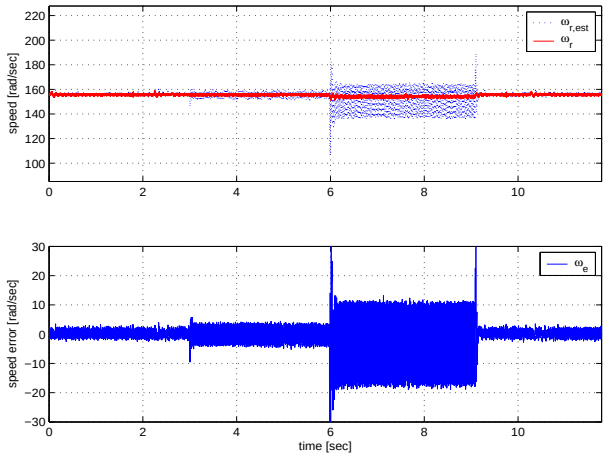

(b) The top figure shows the estimated and the measured speed and the bottom figure shows the error between the estimated and measured speed ω_e.

Figure 5.7: The results from tests of estimation capabilities of the adaptive observer. In this test the speed is constant and the supply voltage is balanced.

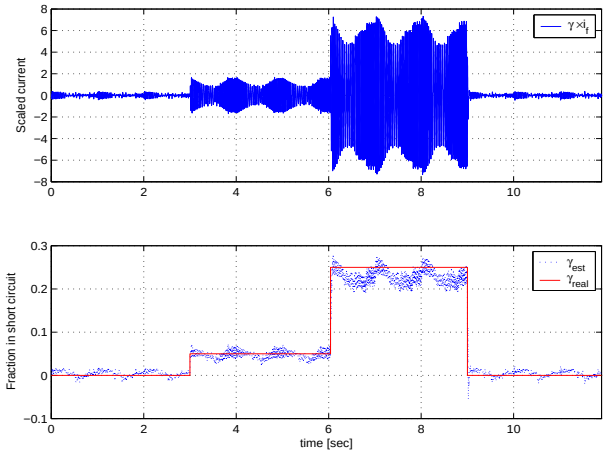

(a) The top figure shows the estimation of the scaled current $\gamma_a i_f$ and the bottom figure shows the estimated and real amount of windings affected by the short circuit.

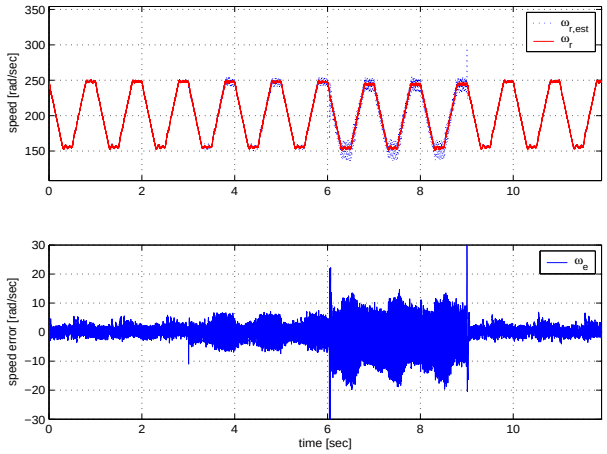

(b) The top figure shows the estimated and the measured speed and the bottom figure shows the error between the estimated and measured speed ω_e.

Figure 5.8: The results from tests of estimation capabilities of the adaptive observer. In this test the speed is variating and the supply is balanced.

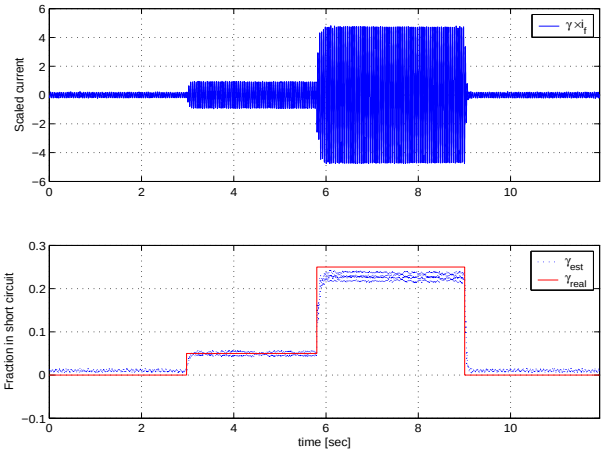

(a) The top figure shows the estimation of the scaled current $\gamma_a i_f$ and the bottom figure shows the estimated and real amount of windings affected by the short circuit.

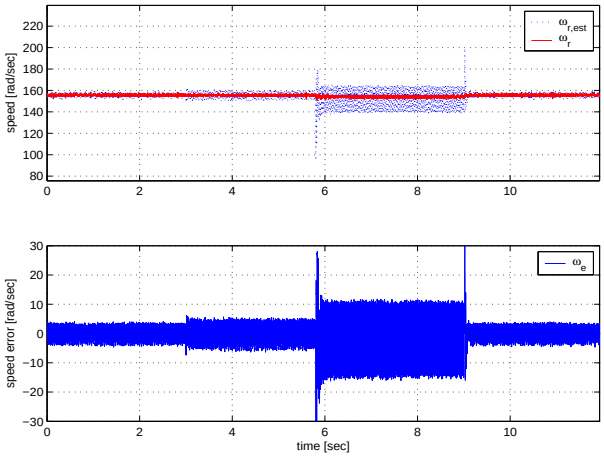

(b) The top figure shows the estimated and the measured speed and the bottom figure shows the error between the estimated and measured speed ω_e.

Figure 5.9: The results from tests of estimation capabilities of the adaptive observer. In this test the speed is constant and the supply voltage is unbalanced.

level of the current in the short circuit, and thereby increase the time from the occurrence of the inter-turn short circuit to a stator burnout.

Chapter 6

A New Approach for FDI in Centrifugal Pumps

The topic of this chapter is FDI on the hydraulic and mechanical part of the centrifugal pump. The model-based approach is used for this purpose, meaning that a set of residual generator are developed, each based on the centrifugal pump model presented in Chapter 3. The centrifugal pump model is highly nonlinear, which is why methods based on a linearization of the model will, in general, fail to work on a larger area around the operating point of the linearization. Therefore nonlinear methods should be considered, when the operating point is changed frequently or is unknown. In a lot of applications this is infact the case.

Beside robustness with respect to the operating point, it is important that the algorithms do not depend on knowledge of the application of the pump. This means that the developed algorithms should work in spite of the hydraulic system in which the pump is placed. The Structural Analysis (SA) (Blanke et al., 2003; Izadi-Zamanabadi, 2001; Izadi-Zamanabadi and Staroswiecki, 2000) is a tool designed to identify subsystems, which are independent of the rest of the system. Therefore this tool will be chosen for identification of subsystems, which can be used for FDI on the centrifugal pump in a robust manner.

The common way to obtain residual generators from subsystem identified using SA is to derive Analytical Redundance Relations (ARR) (Blanke et al., 2003). Unfortunately, in general the derived ARR's are functions of the derivatives of the measurements in the system. These are normally not known and are difficult to calculate. To overcome this problem a novel method to derived state space realizations of the subsystems identified using SA is developed in this chapter. Using this method the obtained state space realizations are decoupled from any unknown algebraic variables or inputs. Therefore, the decoupling problem is solved and the only remaining problem is to design a stable residual observer.

The chapter starts by presenting some preliminaries on SA in Section 6.1. Then the state space realization, developed in this work, is described in Section 6.2. After that FDI on the centrifugal pump is considered. This is done by presenting the model of the pump in Section 6.3, followed by the results obtained using SA in Section 6.4. One of the results of the SA is that the system can be splitted into two cascade connected subsystems, of which only the second is affected by the mechanical and hydraulic faults considered in this chapter. Therefore only an observer has to be considered for the first subsystem. This observer must observe the connecting variables between the two subsystems. The design of this observer is described in Section 6.5. In Section 6.6 the design of the residual observers are considered. These observers are based on results obtained using SA on the second subsystem, and the realization theory developed in Section 6.2 of the chapter. Test results obtained on an industrial test-bench, which has been particularly developed for this purpose, are presented in Section 6.7. Finally, concluding remarks end the chapter.

6.1 Preliminaries: Structural Analysis

Structural Analysis (SA) is the study of the system properties, which are independent of the actual values of the parameters. Only links between the variables and parameters are represented in this analysis. These links result from the operating model and are called relations or constraints. They are independent of the operating model and are thus independent of the form under which this operating model is expressed (qualitative or quantitative data, analytical or non-analytical relations). The links are represented by a graph, on which a structural analysis is performed (Blanke et al., 2003; Izadi-Zamanabadi, 2001; Izadi-Zamanabadi and Staroswiecki, 2000). In this section some of the most important definitions and theorems of SA are presented. The presentation is based on (Blanke et al., 2003).

In SA a system is described by a set of variables $\mathcal{Z}$ and a set of constraints $\mathcal{C}$. Each constraint in $\mathcal{C}$ describes the connection between a subset of the variables in $\mathcal{Z}$, meaning that the equations and differential equations describing the system form the set of constraints. The definition of a system of this form is given below.

Definition 6.1.1 (System structure) *(Blanke et al., 2003) A system $\mathcal{S}$ is defined by two sets $\mathcal{C}$ and $\mathcal{Z}$, where,*

- *$\mathcal{Z}$ is the set of variables in the system.*
- *$\mathcal{C}$ is the set of constains in the system connecting the variables of the system.*

The following three assumptions must hold on the constraints $\mathcal{C}$ in $\mathcal{S}$ for the SA algorithms to work. Before these assumptions are presented, let $\mathcal{Z}_c = Q(c)$ denote the varibles constrained by c and let $n_c = |Q(c)|$ be the number of variables in c.

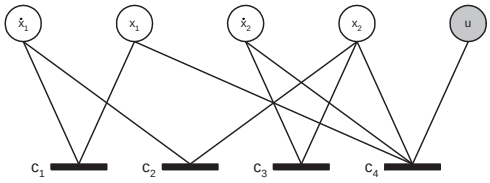

(a) Graph representation.

	$\mathcal{K}$	$\mathcal{X}$			
	u	x_1	$\dot{x}_1$	x_2	$\dot{x}_2$
c_1		1	1		
c_2			1	1	
c_3				1	1
c_4	1	1		1	1

(b) Table representation.

Figure 6.1: Structural representation of the connection between set of equations denoted constraint c_1 to c_4, and the set of variables $\mathcal{Z} = \{u, x_1, \dot{x}_1, x_2, \dot{x}_2\}$. Here $\mathcal{K} = \{u\}$ is the known variable, and $\mathcal{X} = \{x_1, \dot{x}_1, x_2, \dot{x}_2\}$ is the set of unknown variables.

Assumption 6.1.1 *(Blanke et al., 2003, Ass. 5.1) Any algebraic constraint $c \in \mathcal{C}$ defines a manifold of dimension $n_c - 1$ in the space of the variables $Q(c)$.*

Assumption 6.1.2 *(Blanke et al., 2003, Ass. 5.2) All the constraints in $\mathcal{C}$ are compatible.*

Assumption 6.1.3 *(Blanke et al., 2003, Ass. 5.3) All the constraints in $\mathcal{C}$ are independent.*

The structural model of $\mathcal{S}$, defined in Definition 6.1.1, is a model describing the connection between the variables $\mathcal{Z}$ and the constraints in $\mathcal{C}$ by a bi-partite graph. This graph is defined in the following definition.

Definition 6.1.2 (Structural model) *(Blanke et al., 2003, Sec. 5.2) The structural model (or the structure) of the system $(\mathcal{C}, \mathcal{Z})$ is a bi-partite graph $(\mathcal{C}, \mathcal{Z}, \mathcal{E})$ where $\mathcal{E} \subseteq \mathcal{C} \times \mathcal{Z}$ is the set of edges defined by:*

$$(c_i, z_j) \in \mathcal{E} \text{ if the variable } z_j \in \mathcal{Z} \text{ appears in the constaint } c_i \in \mathcal{C}.$$

An example of such a bi-partite graph is shown in Fig. 6.1. Both a graphical and a table representation of the the graph are shown here. Using the bi-partite graphs defined in Definition 6.1.2 the structure of the model equations forming the set of constraints $\mathcal{C}$ can be analysed. Two important properties in this analysis are *Reachability* and *Matching*. These are defined in the following definitions.

Definition 6.1.3 (Reachability) *(Blanke et al., 2003, Def. 5.8) A variable z_2 is reachable from a variable z_1 if there exists an alternated chain from z_1 to z_2 in the graph $(\mathcal{C}, \mathcal{Z}, \mathcal{E})$. A variable z_2 is reachable from a subset $\mathcal{X} \subseteq \mathcal{Z} \backslash \{z_2\}$ if the exists $z_1 \in \mathcal{X}$ such that z_2 is reachable from z_1. A subset of variables $\mathcal{Z}_2$ is reachable from a subset of variables $\mathcal{Z}_1$ if any variable of $\mathcal{Z}_2$ is reachable from $\mathcal{Z}_1$.*

Definition 6.1.4 (Matching) *(Blanke et al., 2003) A matching $\mathcal{M}$ is a subset of the edges $\mathcal{E}$ such that the endpoints of the edges have no common vertices, i.e.*

$$\forall e_i, e_j \in \mathcal{M} \; : \; e_i = (a, b), \; e_j = (\alpha, \beta), \; \textit{then } a \neq \alpha, \; b \neq \beta.$$

Definition 6.1.5 (Complete matching) *(Blanke et al., 2003) A matching is called complete with respect to $\mathcal{C}$ if $|\mathcal{M}| = |\mathcal{C}|$ holds. A matching is called complete with respect to $\mathcal{Z}$ if $|\mathcal{M}| = |\mathcal{Z}|$.*

When there exist a complete matching with respect to the unknown variables $\mathcal{X} \subset \mathcal{Z}$ in the system, it means that, in almost all cases, these variables can be eliminated by rewriting the system equations. To ensure this property the notation of calculability is used. Calculability is defined in the following definition.

Definition 6.1.6 (Calculability) *(Izadi-Zamanabadi and Staroswiecki, 2000) Let z_i, $i = 1, \cdots, p, \cdots, n$ be variables, which are related through a constraint c_i, e.g. $c_i(z_1, \cdots, z_n)$. The variable z_p is calculable if its value can be determined through the constraint c_i under the condition that the values of the other variables z_j, $j = 1, \cdots, n$, $j \neq p$ are known.*

When a matching of an unknown variable is done under the calculability constraint it is possible to calculate the given unknown variable in the space where the calculability condition is fulfilled. Unfortunately, this is not enough to state that a matching, where all the unknown variables are calculable, implies that all unknown variables can be eliminated. This fact will be considered later when the notation of causal matches is considered.

To connect the definitions given above to a system description as known from system theory, let a dynamic system $\mathcal{S}$ be described by the following set of equations,

$$\mathcal{S}: \quad \left\{ \begin{array}{lcl} \mathcal{C}_f & : & \dot{\mathbf{x}}_d = \mathbf{f}_x(\mathbf{x}_d, \mathbf{x}_a, \mathbf{u}) \\ \mathcal{C}_m & : & 0 = \mathbf{m}_x(\mathbf{x}_d, \mathbf{x}_a, \mathbf{u}) \\ \mathcal{C}_h & : & \mathbf{y} = \mathbf{h}_x(\mathbf{x}_d, \mathbf{x}_a, \mathbf{u}) \\ \mathcal{C}_d & : & \frac{d\mathbf{x}_d}{dt} = \dot{\mathbf{x}}_d \end{array} \right. , \tag{6.1}$$

where the set of variables $\mathcal{Z} = \mathbf{x}_d \cup \dot{\mathbf{x}}_d \cup \mathbf{x}_a \cup \mathbf{u} \cup \mathbf{y}$. $\mathcal{Z}$ can be decomposed into a set of unknown variables $\mathcal{X} = \mathbf{x}_d \cup \dot{\mathbf{x}}_d \cup \mathbf{x}_a$ and a set of known variables $\mathcal{K} = \mathbf{u} \cup \mathbf{y}$. The constaints $\mathcal{C}$ of system (6.1) are given by the set $\mathcal{C} = \mathcal{C}_f \cup \mathcal{C}_m \cup \mathcal{C}_h \cup \mathcal{C}_d$. The structural model of this system is shown in Table 6.1. Here G, F_i, M_i, H_i are boolean matrices describing the connections between the variables $\mathcal{Z}$ and the constaints $\mathcal{C}$. I is the identity matrix and X is a diagonal matrix denoting that $\mathbf{x}_d$ can only be calculated form $\dot{\mathbf{x}}_d$ up to an unknown but constant offset.

The structural model presented in Table 6.1 of the system $\mathcal{S}$ can have, but does not always have, one of following three properties,

Table 6.1: Incident matrix of a structural graph. This structural graph is a graph of a minimal over-constrained system, which can be a subsystem of a larger system.

	$\mathbf{y}^T$	$\mathbf{u}^T$	$\dot{\mathbf{x}}_d^T$	$\mathbf{x}_d^T$	$\mathbf{x}_a^T$
$\mathbf{f}_x$	0	G	I	F_1	F_2
$\mathbf{m}_x$	0	M_3	0	M_1	M_2
$\mathbf{h}_x$	I	H_3	0	H_1	H_2
$\mathbf{d}_x$	0	0	I	X	0

Definition 6.1.7 (Over-constrained graph)*(Blanke et al., 2003, Def. 5.9) A graph* $(\mathcal{C}, \mathcal{Z}, \mathcal{E})$ *is called over-constained if there is a complete matching on the variables* $\mathcal{Z}$ *but not on the constaints* $\mathcal{C}$*.*

Definition 6.1.8 (Just-constrained graph)*(Blanke et al., 2003, Def. 5.10) A graph* $(\mathcal{C}, \mathcal{Z}, \mathcal{E})$ *is called just-constained if there is a complete matching on the variables* $\mathcal{Z}$ *and on the constaints* $\mathcal{C}$*.*

Definition 6.1.9 (Under-constrained graph)*(Blanke et al., 2003, Def. 5.11) A graph* $(\mathcal{C}, \mathcal{Z}, \mathcal{E})$ *is called under-constained if there is a complete matching on the constaints* $\mathcal{C}$ *but not on the variables* $\mathcal{Z}$*.*

In the cases where the system $\mathcal{S}$ fails to conform to any of the three above properties, it can be proven that there exists a unique decomposition of $\mathcal{S}$ into three subsystems (Blanke et al., 2003),

$$\begin{aligned}\mathcal{S}^+ &= (\mathcal{C}^+, \mathcal{Z}^+)\\ \mathcal{S}^0 &= (\mathcal{C}^0, \mathcal{Z}^+ \cup \mathcal{Z}^0)\\ \mathcal{S}^- &= (\mathcal{C}^-, \mathcal{Z}^+ \cup \mathcal{Z}^0 \cup \mathcal{Z}^-),\end{aligned}$$

where $\mathcal{C} = \mathcal{C}^- \cup \mathcal{C}^0 \cup \mathcal{C}^+$ and $\mathcal{Z} = \mathcal{Z}^- \cup \mathcal{Z}^0 \cup \mathcal{Z}^+$. For this decomposition the subsystems $(\mathcal{C}^+, \mathcal{Z}^+)$, $(\mathcal{C}^0, \mathcal{Z}^0)$, and $(\mathcal{C}^-, \mathcal{Z}^-)$ are over-constrained, just-constrained, and under-constrained respectively. On the over-constrained and just-constrained subsystems the notion of causality is important, as it is used to state the conditions for structural observability. Causality is defined in the following definition.

Definition 6.1.10 (Causality) *(Blanke et al., 2003) A subsystem is called causal if there exists an alternating chain from* $k_i \in \mathcal{K}$ *to* $x_j \in \mathcal{X}$ *for all reachable* $x_j \in \mathcal{X}$ *and this chain is composed of only calculable matchings.*

A special and very important over-constrained subsystem is defined in the following definition.

Definition 6.1.11 (Minimal over-constrained subsystem) *(Izadi-Zamanabadi, 2001, Def. 4) A minimal over-constrained subsystem, $\mathcal{S}_{min} = (\mathcal{C}_{min}, \mathcal{Z}_{min})$ is an over-constrained subsystem with the following property:*

$$|\mathcal{C}_{min}| = 1 + |\mathcal{X}_{min}| \tag{6.2}$$

where $\mathcal{X}_{min} \subseteq \mathcal{Z}_{min}$ are the unknown variables contained in the set of constraints $\mathcal{C}_{min}$. Additionally, $\mathcal{C}_{min} \subseteq \mathcal{C}$ and $\mathcal{Z}_{min} \subseteq \mathcal{Z}$.

Such a minimal over-constrained subsystem contains information enough to derived exactly one residual. Therefore, if a set of minimal over-constrained subsystems is identified in a system, and the matchings, which define each of these subsystems, are causal, a set of residual generators can be derived. When the residual generators are derived by eliminating all unknown variables in the subsystem they are called Analytical Redundant Relations (ARR). If each of these residual generators are sensitive to different subsets of the faults affecting the system this can be used for fault identification. This is formalized in the following two theorems.

Theorem 6.1.1 (Structural observability) *(Blanke et al., 2003, The. 5.2) A necessary and sufficient condition for system (6.1) to be structural observable is that, under derivative causality*

1. *all the unknown variables $\mathcal{X}$ are reachable from the known ones,*
2. *the over-constrained and the just-constrained subsystems are causal,*
3. *the under-constrained subsystem is empty.*

For systems which are structural observable as stated in Theorem 6.1.1, and where the over-constraint subsystem is non empty, it is always possible to identify a number of minimal over-constraint subsystems, as defined in Definition 6.1.11.

Let one of the constraints $\varphi \in \mathcal{C}$ be corrupted by a fault. Let the unknown variables containted in the constraint be given by $\mathcal{X}_\varphi = Q(\varphi)$. Then the following theorem states the conditions for the fault corrupting the constraint φ to be monitorable or detectable.

Theorem 6.1.2 (Monitorability) *(Blanke et al., 2003, The. 5.3) Two equivalent necessary conditions for a fault φ to be monitorable are:*

(i) *$\mathcal{X}_\varphi$ is structural observable - according to Theorem 6.1.1 - in the system $(\mathcal{C}\backslash\{\varphi\}, \mathcal{Z})$,*

(ii) *φ belongs to the structurally observable over-constrained part of the system $(\mathcal{C}, \mathcal{Z})$.*

Algorithms exist, which can decompose a system $\mathcal{S}$ into all possible minimal over-constraint subsystems. For each of these minimal over-constraint subsystems the connection $n_c = n_x + 1$ holds, where $n_c = |\mathcal{C}|$ is the number of constraints and $n_x = |\mathcal{X}|$ is the number of unknown variables in these constraints (Izadi-Zamanabadi, 2001; Izadi-Zamanabadi and Staroswiecki, 2000). It is possible to derive an Analytical Redundant Relation (ARR) for each of these subsystems. Each of these ARR can be used to generate one residual, which is sensitive to a subset of the faults in the system $\mathcal{S}$ (Blanke et al., 2003). The connection between the subsystem used in the derivation of a given ARR and the faults is described by Theorem 6.1.2.

6.2 Realization

Realization denotes the task of finding a description of an over-constrained subsystem, identified using SA, which can be used for residual generation. A straightforward way to find such a residual generator, is to solve the set of constraints $\mathcal{C}$, forming the subsystem, for the unknown variables $\mathcal{X}$ in this set of constraints. The solution obtained using this approach is an Analytical Redundant Relation (ARR) (Blanke et al., 2003). Unfortunately in general the obtained ARR's are functions of the derivatives of the measurements, which are in general not calculable due to measurement noise.

To overcome the problem with the derivatives in the ARR's, a new approach is developed here. The main idea is to find a state space description of the subsystem identified using SA, meaning that the subsystem can be described on the form,

$$\begin{array}{c} \frac{d\mathbf{z}}{dt} = \mathbf{f}_z(\mathbf{z}, \mathbf{y}, \mathbf{u}) \\ \mathbf{g}_z(\mathbf{y}, \mathbf{u}) = \mathbf{h}_z(\mathbf{z}, \mathbf{y}, \mathbf{u}) \end{array} , \tag{6.3}$$

where $\mathbf{z}$ contains the states of the system, and $\mathbf{u}$ and $\mathbf{y}$ contain the known signals in the system. If a state space description (6.3) exists it can be used in the development of an observer, which enables residual generation. The decoupling of unknown inputs has not to be considered in this observer design, as this problem is already solved using SA and the realization techniques presented here.

Assuming that an over-constrained subsystem identified using SA is described by the following set of equations,

$$\mathcal{S}_x : \quad \left\{ \begin{array}{r} \dot{\mathbf{x}}_d = \mathbf{f}_x(\mathbf{x}_d, \mathbf{x}_a, \mathbf{u}) \\ 0 = \mathbf{m}_x(\mathbf{x}_d, \mathbf{x}_a, \mathbf{u}) \\ \mathbf{y} = \mathbf{h}_x(\mathbf{x}_d, \mathbf{x}_a, \mathbf{u}) \\ \frac{d\mathbf{x}_d}{dt} = \dot{\mathbf{x}}_d \end{array} \right. , \tag{6.4}$$

where $\mathbf{x}_d(t), \dot{\mathbf{x}}_d(t) \in R^n$, $\mathbf{x}_a(t) \in R^l$, $\mathbf{u}(t) \in R^p$ and $\mathbf{y}(t) \in R^d$. $\mathbf{f}_x$, $\mathbf{m}_x$, and $\mathbf{h}_x$ are sufficiently smooth maps. $\mathbf{f}_x$ is denoted a map, as the $\dot{\mathbf{x}}_d$ is considered a free variable constraint by the derivative constraint $\frac{d\mathbf{x}_d}{dt} = \dot{\mathbf{x}}_d$, in SA. Finally, $\mathbf{u}$ and $\mathbf{y}$ are the known input and output signals respectively, and $\mathbf{x}_d$, $\dot{\mathbf{x}}_d$, and $\mathbf{x}_a$ are unknown signals.

Let the subsystem, identified using SA, be given by $(\mathcal{C}, \mathcal{Z})$, then each equation in (6.4) is given by a constraint in $\mathcal{C}$. Likewise, the variables $\mathbf{u}, \mathbf{y} \subset \mathcal{K}$ and $\mathbf{x}_d, \dot{\mathbf{x}}_d, \mathbf{x}_a \subset \mathcal{X}$ are the known and unknown variables respectively. These variables form the set $\mathcal{Z}$, i.e. $\mathcal{Z} = \mathcal{K} \cup \mathcal{X}$. The graph representation of this system is shown in Table 6.2, where

Table 6.2: Incident matrix of a structural graph. This structural graph is a graph of a minimal over-constrained system, which can be a subsystem of a larger system.

	y	u	$\dot{x}_d$	x_d	x_c
$\mathbf{f}_x$	0	G	I	F_1	F_2
$\mathbf{m}_x$	0	M_3	0	M_1	M_2
$\mathbf{h}_x$	I	H_3	0	H_1	H_2
$\mathbf{d}_x$	0	0	I	X	0

G, F_i, M_i, H_i are boolean matrices describing the connection between the variables $\mathcal{Z}$ and the constaints $\mathcal{C}$. I is the identity matrix and X is a diagonal matrix denoting that $\mathbf{x}_d$ can only be calculated form $\dot{\mathbf{x}}_d$ up to a constant offset.

In the following a method is presented, which can be used to obtain the state space description (6.3) from the over-constraints subsystem (6.4). To obtain this state space description all the unknown algebraic variables $\mathbf{x}_a$ must be eliminated, or in other words a state and/or output transformation must be found such that the unknown signals $\mathbf{x}_a$ are decoupled from the residual output. When such a state space description exists a residual observer or residual filter of the following form can be obtained,

$$\begin{aligned} \tfrac{d\hat{\mathbf{z}}}{dt} &= \mathbf{f}_z(\hat{\mathbf{z}}, \mathbf{y}, \mathbf{u}) - \mathbf{k}(\mathbf{z}, \mathbf{y}, \mathbf{u})(\mathbf{g}_z(\mathbf{y}, \mathbf{u}) - \mathbf{h}_z(\hat{\mathbf{z}}, \mathbf{y}, \mathbf{u})) \\ \mathbf{r} &= \mathbf{q}(\mathbf{g}_z(\mathbf{y}, \mathbf{u}) - \mathbf{h}_z(\hat{\mathbf{z}}, \mathbf{y}, \mathbf{u})) \ . \end{aligned}$$

Here it is assumed that a stabilizing feedback $\mathbf{k}$ can be found. In the above equation $\mathbf{r}$ is the set of residual outputs, $\mathbf{u}$ is a set of known signals defined as input in the original system, $\mathbf{y}$ is the set of known signals defined as outputs in the original system, and $\hat{\mathbf{z}}$ contains the states of the residual filter. If the subsystem is a minimal over-constraint subsystem the residual $\mathbf{r}$ becomes a scalar r. This is infact normally the case.

In the following, first an output transformation is considered, eliminating a part of the algebraic variables $\mathbf{x}_a$. The remaining algebraic variables are eliminated using a state transformation. This is considered in Section 6.2.2. Finally, the two elimination approaches are composed into one algorithm in Section 6.2.3.

6.2.1 Output Transformation

In this subsection the eliminations of the algebraic variables $\mathbf{x}_a$, using only the algebraic constraints of system (6.4), is considered, i.e. the set of constraints formed by $\mathbf{m}_x$ and $\mathbf{h}_x$ are used. If the causal match, found using SA, shows that a subset of the variables in

$\mathbf{x}_a$ denoted $\mathbf{x}_{a1}$ and a subset of the variables $\mathbf{x}_d$ denoted $\mathbf{x}_{d1}$ are matched using $\mathbf{m}_x$ and $\mathbf{h}_x$. Then there must exist an explicite solution to these variables using $\mathbf{m}_x$ and $\mathbf{h}_x$. Let this solution be given by,

$$\begin{pmatrix} \mathbf{x}_{a1} \\ \mathbf{x}_{d1} \end{pmatrix} = \begin{pmatrix} \mathbf{g}_1(\mathbf{x}_{d2}, \mathbf{x}_{a2}, \mathbf{y}, \mathbf{u}) \\ \mathbf{g}_2(\mathbf{x}_{d2}, \mathbf{x}_{a2}, \mathbf{y}, \mathbf{u}) \end{pmatrix},$$

where $\mathbf{x}_a, \mathbf{x}_d$ are partitioned such that $\mathbf{x}_a = \begin{pmatrix} \mathbf{x}_{a1}^T & \mathbf{x}_{a2}^T \end{pmatrix}^T$, $\mathbf{x}_d = \begin{pmatrix} \mathbf{x}_{d1}^T & \mathbf{x}_{d2}^T \end{pmatrix}^T$. This proves the following lemma.

Lemma 6.2.1 *Let* $\mathbf{x}_a = \begin{pmatrix} \mathbf{x}_{a1}^T & \mathbf{x}_{a2}^T \end{pmatrix}^T$ *and* $\mathbf{x}_d = \begin{pmatrix} \mathbf{x}_{d1}^T & \mathbf{x}_{d2}^T \end{pmatrix}^T$ *be partitioned such that* $\mathbf{x}_{a1}$ *and* $\mathbf{x}_{d1}$ *are the unknown variables matched by the set of constraints* $\mathbf{m}_x \cup \mathbf{h}_x$*, then there must exist explicite solutions for* $\mathbf{x}_{a1}$ *and* $\mathbf{x}_{d1}$*. Let these solutions be denoted by,*

$$\begin{aligned} \mathbf{x}_{a1} &= \mathbf{g}_1(\mathbf{x}_{d2}, \mathbf{x}_{a2}, \mathbf{y}, \mathbf{u}) \\ \mathbf{x}_{d1} &= \mathbf{g}_2(\mathbf{x}_{d2}, \mathbf{x}_{a2}, \mathbf{y}, \mathbf{u}) \ , \end{aligned} \tag{6.5}$$

The above Lemma states that a solution exists for a subset of the algebraic variables $\mathbf{x}_a$ and a subset of the state variables $\mathbf{x}_d$ in the system, without introducing derivatives of any known variables, i.e. variables in $\mathcal{K}$. This solution can be used for elimination of these variables. Moveover under the following assumption an output transformation can be found, which has the property that the known and unknown variables in the output expression are separated.

Assumption 6.2.1 *It is assumed that the expression* $\mathbf{g}_2$ *in Lemma 6.2.1 exists and can be rewritten to become,*

$$\mathbf{h}_o(\mathbf{x}_d) = \mathbf{g}_o(\mathbf{y}, \mathbf{u}) \qquad , \ \mathbf{x}_d = \begin{pmatrix} \mathbf{x}_{d1}^T & \mathbf{x}_{d2}^T \end{pmatrix}^T \ . \tag{6.6}$$

Assumption 6.2.1 states that the algebraic variables matched by the algebraic constraints $\mathbf{m}_x$ and $\mathbf{h}_x$ can be eliminated using these. For linear systems, this is the same as assuming that disturbances in the output equation are decoupled using a transformation of the output, e.i. $\mathbf{Qy} = \mathbf{QCx} + \mathbf{QE}_d\mathbf{d}$ where $\mathbf{QE}_d = 0$.

Under Assumption 6.2.1 the following theorem can be used to derive a state space description where all unknown algebraic variables are contained in the differential equations.

Theorem 6.2.1 (Output Transformation) *If a causal match exists on an over-constrained subsystem on the form given in (6.4), then if Assumption 6.2.1 holds for this system, it can be rewritten to the following form,*

$$\mathcal{S}_o : \qquad \begin{cases} \frac{d\mathbf{x}_d}{dt} = \mathbf{f}_o(\mathbf{x}_d, \mathbf{x}_{a2}, \mathbf{y}, \mathbf{u}) \\ \mathbf{g}_o(\mathbf{y}, \mathbf{u}) = \mathbf{h}_o(\mathbf{x}_d) \ , \end{cases} \tag{6.7}$$

where $\mathbf{x}_{a2}$ *is a vector of algebraic variables.*

Proof: Using Lemma 6.2.1 and Assumption 6.2.1 the set of constraints $\mathbf{m}_x \cup \mathbf{h}_x$ can be rewritten to become,

$$\begin{aligned} \mathbf{x}_{a1} &= \mathbf{g}_1(\mathbf{x}_{d2}, \mathbf{x}_{a2}, \mathbf{y}, \mathbf{u}) \\ \mathbf{h}_o(\mathbf{x}_d) &= \mathbf{g}_o(\mathbf{y}, \mathbf{u}) \ , \end{aligned} \tag{6.8}$$

where $\mathbf{x}_a = \begin{pmatrix} \mathbf{x}_{a1}^T & \mathbf{x}_{a2}^T \end{pmatrix}^T$ and $\mathbf{x}_d = \begin{pmatrix} \mathbf{x}_{d1}^T & \mathbf{x}_{d2}^T \end{pmatrix}^T$. Using the first expression (6.8) to eliminate the variables $\mathbf{x}_{a1}$ in $\mathbf{f}_x$ in (6.4) it becomes,

$$\tfrac{d\mathbf{x}_d}{dt} = \mathbf{f}_o(\mathbf{x}_d, \mathbf{x}_{a2}, \mathbf{y}, \mathbf{u}).$$

Choose the second expression in (6.8) as the output equation, system (6.7) is obtained. □

In some cases all the algebraic variables in the vector $\mathbf{x}_a$ are match using the set of constraints $\mathbf{m}_x \cup \mathbf{h}_x$. When this is the case all the algebraic variables can be eliminated using the output transformation given in Theorem 6.2.1. This is stated in the following corollary.

Corollary 6.2.1 (Output Transformation) *If a causal match exists on an over-constrained subsystem on the form given in (6.4), then if Assumption 6.2.1 holds for this system and all algebraic varibles $\mathbf{x}_a$ are matched using $\mathbf{m}_x$ and $\mathbf{h}_x$, then the system can be rewritten to become,*

$$\mathcal{S}_o : \quad \begin{cases} \tfrac{d\mathbf{x}_d}{dt} = \mathbf{f}_o(\mathbf{x}_d, \mathbf{y}, \mathbf{u}) \\ \mathbf{g}_o(\mathbf{y}, \mathbf{u}) = \mathbf{h}_o(\mathbf{x}_d) \ . \end{cases} \tag{6.9}$$

6.2.2 State Transformation

The theorem and corollary, presented in the previous subsection, deal with the elimination of the algebraic variables, using the algebraic constraints $\mathbf{m}_x$ and the output maps $\mathbf{h}_x$. In general, it is not possible to eliminate all algebraic variables using these constraints. In order to eliminate the remaining algebraic variables a state space transformation is required, hence proposed. To be able to perform the state transformation it is required that system (6.7) admits a simpler form as specified by the following assumption.

Assumption 6.2.2 *The state space description of system (6.7) is of the following form*

$$\begin{aligned} \tfrac{d\mathbf{x}_d}{dt} &= \mathbf{f}_o'(\mathbf{x}_d, \mathbf{y}, \mathbf{u}) + \mathbf{G}_o(\mathbf{x}_d)\mathbf{x}_{a2} \\ \mathbf{g}_o(\mathbf{y}, \mathbf{u}) &= \mathbf{h}_o(\mathbf{x}_d) \ , \end{aligned} \tag{6.10}$$

where $\mathbf{G}_o(\mathbf{x}_d)$ is a $(n \times l_2)$ matrix with full column rank for all $\mathbf{x}_d \in \mathcal{D}_{\mathbf{x}_d}$. It is assumed that $n > l_2$ where l_2 is the number of elements in $\mathbf{x}_{a2}$.

Later, in the proof of the main theorem in this subsection, it will be shown that, for the over-constrained subsystems, $\mathbf{G}_o$ has full rank always.

The elimination of the algebraic variables $\mathbf{x}_{a2}$ in (6.10) are dealt with in the following Lemma.

Lemma 6.2.2 *Eliminating algebraic variables $\mathbf{x}_{a2}$ from the state space description of system (6.10) results in a new system on the form*

$$\tilde{\mathbf{D}}(\mathbf{x}_d)\tfrac{d\mathbf{x}_d}{dt} = \tilde{\mathbf{f}}'_o(\mathbf{x}_d, \mathbf{y}, \mathbf{u}) \ , \tag{6.11}$$

where $\tilde{\mathbf{D}}$ is an $(n - l_2) \times n$ matrix of function of $\mathbf{x}_d$ with full row rank.

Proof: Let the state space system (6.10) be scaled by an arbitrary $(n \times n)$ matrix $\mathbf{D}(\mathbf{x}_d)$, which is full rank for all $\mathbf{x}_d \in \mathcal{D}_{\mathbf{x}_d} \subseteq R^n$. Using $\mathbf{D}$ on (6.10) the system becomes,

$$\mathbf{D}(\mathbf{x}_d)\tfrac{d\mathbf{x}_d}{dt} = \mathbf{D}(\mathbf{x}_d)\mathbf{f}'_o(\mathbf{x}_d, \mathbf{y}, \mathbf{u}) + \mathbf{D}(\mathbf{x}_d)\mathbf{G}_o(\mathbf{x}_d)\mathbf{x}_{a2} \ .$$

Design the scaling matrix $\mathbf{D}$ such that the following condition is fulfilled,

$$\mathbf{D}(\mathbf{x}_d)\mathbf{G}_o(\mathbf{x}_d) = \begin{bmatrix} 0 \\ \mathbf{I}_{l_2 \times l_2} \end{bmatrix} \ . \tag{6.12}$$

The solution can easily be found using the Gauss-Jordan elimination method on the system,

$$\left[\ \mathbf{I}_{n\times n} \ \middle|\ \mathbf{G}_o(\mathbf{x}_d)\ \right] \qquad \rightarrow \qquad \left[\ \mathbf{D}(\mathbf{x}_d) \ \middle|\ \left[\ \begin{matrix} 0 \\ \mathbf{I}_{l_2\times l_2} \end{matrix}\ \right]\ \right].$$

When the scaling matrix $\mathbf{D}$ is used on the system, it becomes,

$$\mathbf{D}(\mathbf{x}_d)\tfrac{d\mathbf{x}_d}{dt} = \mathbf{D}(\mathbf{x}_d)\mathbf{f}'_o(\mathbf{x}_d, \mathbf{y}, \mathbf{u}) + \begin{bmatrix} 0_{(n-l_2)\times l_2} \\ \mathbf{I}_{l_2\times l_2} \end{bmatrix} \mathbf{x}_{a2} \ . \tag{6.13}$$

In this expression the first $(n - l_2)$ rows are independent of $\mathbf{x}_{a2}$. This means that $\mathbf{x}_{a2}$ has been eliminated in this part of the system. Using the first $(n - l_2)$ rows in (6.13) the final expression is obtained,

$$\tilde{\mathbf{D}}(\mathbf{x}_d)\tfrac{d\mathbf{x}_d}{dt} = \tilde{\mathbf{D}}(\mathbf{x}_d)\mathbf{f}'_o(\mathbf{x}_d, \mathbf{y}, \mathbf{u}) = \tilde{\mathbf{f}}'_o(\mathbf{x}_d, \mathbf{y}, \mathbf{u})$$

The matrix $\tilde{\mathbf{D}}(\mathbf{x}_d)$ is formed by the first $(n - k_2)$ rows of the matrix $\mathbf{D}(\mathbf{x}_d)$. □

The following additional assumption, that is required to prove the main theorem, is introduced.

Assumption 6.2.3 *The following condition for system (6.10) is fulfilled:*

$$\mathit{Span}\{\tfrac{\partial \mathbf{h}_o}{\partial \mathbf{x}_d}(\mathbf{x}_d)^T\} \ \bigcup \ \mathit{Ker}\left\{\mathbf{G}_o(\mathbf{x}_d)^T\right\} \tag{6.14}$$

must span R^n for all $\mathbf{x}_d \in \mathcal{D}_{\mathbf{x}_d}$.

Remark 6.2.1 *A linear version of (6.10) is given by the following state space model*

$$\begin{array}{r} \frac{d\mathbf{x}_d}{dt} = \mathbf{A}\mathbf{x}_d + \mathbf{B}\mathbf{u} + \mathbf{G}\mathbf{x}_{a2} \\ \mathbf{y} = \mathbf{C}\mathbf{x}_d \ . \end{array} \tag{6.15}$$

Comparing this expression with (6.10) it is seen that $\frac{\partial \mathbf{h}_o}{\partial \mathbf{x}_d}(\mathbf{x}_d)$ *and* $\mathbf{G}_o(\mathbf{x}_d)$ *in (6.10) corresponds to* $\mathbf{C}$ *and* $\mathbf{G}$ *in (6.15) respectively. Using these relations Assumtion 6.2.3 implies that rank*$\{\mathbf{CG}\}$ = *rank*$\{\mathbf{G}\}$*, which is exactly the demand for existence of an unknown input observer for linear systems (Chen and Patton, 1999, chap. 3).*

In the following the main theorem of this section is presented. Using this theorem it is possible to eliminate the remaining algebraic variables $\mathbf{x}_{a2}$ in system (6.10).

Theorem 6.2.2 (Realization) *By a state transformation, system (6.10) can, under assumption 6.2.3, be transformed into a new system of the following form*

$$\begin{array}{rl} \frac{d\mathbf{z}}{dt} = \mathbf{f}_z(\mathbf{z},\mathbf{y},\mathbf{u}) & = \boldsymbol{\mu}(\mathbf{x}_d)\tilde{\mathbf{f}}'_o(\mathbf{x}_d,\mathbf{y},\mathbf{u})|_{\mathbf{x}_d=\boldsymbol{\Psi}(\mathbf{z},\mathbf{y},\mathbf{u})} \\ \mathbf{g}_{o1}(\mathbf{y},\mathbf{u}) = \mathbf{h}_z(\mathbf{z},\mathbf{y},\mathbf{u}) & = \mathbf{h}_{o1}(\mathbf{x}_d)|_{\mathbf{x}_d=\boldsymbol{\Psi}(\mathbf{z},\mathbf{y},\mathbf{u})} \ . \end{array} \tag{6.16}$$

The inverse state transformation $\mathbf{x}_d = \boldsymbol{\Psi}(\mathbf{z},\mathbf{y},\mathbf{u})$ *is obtained as the local solution to*

$$\begin{pmatrix} \mathbf{g}_{o2}(\mathbf{y},\mathbf{u}) \\ \mathbf{z} \end{pmatrix} = \begin{pmatrix} \mathbf{h}_{o2}(\mathbf{x}_d) \\ \boldsymbol{\Phi}(\mathbf{x}_d) \end{pmatrix}, \tag{6.17}$$

with output map organized as

$$\mathbf{g}_o(\mathbf{y},\mathbf{u}) = \mathbf{h}_o(\mathbf{x}_d) \qquad \Leftrightarrow \qquad \begin{pmatrix} \mathbf{g}_{o1}(\mathbf{y},\mathbf{u}) \\ \mathbf{g}_{o2}(\mathbf{y},\mathbf{u}) \end{pmatrix} = \begin{pmatrix} \mathbf{h}_{o1}(\mathbf{x}_d) \\ \mathbf{h}_{o2}(\mathbf{x}_d) \end{pmatrix} \ .$$

The transformation $\mathbf{z} = \boldsymbol{\Phi}(\mathbf{x}_d)$ *is given by the partial differential equation (p.d.e.),*

$$\boldsymbol{\mu}(\mathbf{x}_d)\tilde{\mathbf{D}}(\mathbf{x}_d) = \frac{\partial \boldsymbol{\Phi}}{\partial \mathbf{x}_d} \ , \tag{6.18}$$

where $\tilde{\mathbf{D}}$ *is given by Lemma 6.2.2 and* $\boldsymbol{\mu}(\mathbf{x}_d)$ *is a* $l_2 \times l_2$ *scaling matrix with full rank for all* $\mathbf{x}_d \in \mathcal{D}_{\mathbf{x}_d} \subseteq R^n$.

Proof: The proof is done in two steps. In the first step it is shown that all $\mathbf{x}_{a2}$ can be eliminated in (6.10). In the second step it is shown that under Assumption 6.2.3 there exists a transformation transforming system (6.10) into (6.16).

Step 1: First it is shown that (6.10) is on a form such that Lemma 6.2.2 can be used in the elimination of the unknown algebraic variables $\mathbf{x}_{a2}$. To show this, it must be proven that $\mathbf{G}_o(\mathbf{x}_d)$ has full column rank and that the number of rows exceed the number of columns.

System (6.7) is by definition a over-constrained subsystem with the set of constraints $\mathcal{C}_{min} = \mathbf{d}_o \cup \mathbf{f}_o \cup \mathbf{h}_o$ and the set of unknown variables $\mathcal{X}_{min} = \dot{\mathbf{x}}_d \cup \mathbf{x}_d \cup \mathbf{x}_{a2}$. Using Definition 6.1.7 the following property must hold for (6.7)

$$|\mathbf{d}_o| + |\mathbf{f}_o| + |\mathbf{h}_o| = |\dot{\mathbf{x}}_d| + |\mathbf{x}_d| + |\mathbf{x}_{a2}| + k \ ,$$

where $|\cdot|$ is the number of elements in the given vector and $\mathbf{d}_o$ is the set of differential constraints (arranged in a vector) as described in Section 6.1. By definition $|\mathbf{d}_o| = |\dot{\mathbf{x}}_d|$. Moreover, some of the elements in $\mathbf{x}_d$ must be matched using $\mathbf{h}_o$. Let these elements be denoted $\mathbf{x}_{d1}$. Since all constraints in $\mathbf{h}_o$ are matched we have $|\mathbf{x}_{d1}| = |\mathbf{h}_o|$, and we get

$$|\mathbf{f}_o| = |\mathbf{x}_{d2}| + |\mathbf{x}_{a2}| + k \ , \tag{6.19}$$

where $\mathbf{x}_d = \begin{pmatrix} \mathbf{x}_{d1}^T & \mathbf{x}_{d2}^T \end{pmatrix}^T$. Under Assumption 6.2.2 (6.7) is restricted to be on the form (6.10). Here the number of columns in $\mathbf{G}_o$ are given by $l_2 = |\mathbf{x}_{a2}|$ and the number of rows are given by $|\mathbf{f}_o'| = |\mathbf{f}_o|$, which is strictly larger than $|\mathbf{x}_{a2}|$, see (6.19). Moreover from the match obtained from SA it is known that $\mathbf{x}_{a2}$ can be calculated using $\mathbf{f}_o$, which implies that $\mathbf{G}_o$ must have full column rank. Therefore, using Lemma 6.2.2 system (6.10) can be rewritten to,

$$\begin{aligned} \tilde{\mathbf{D}}(\mathbf{x}_d)\tfrac{d\mathbf{x}_d}{dt} &= \tilde{\mathbf{f}}_o'(\mathbf{x}_d, \mathbf{y}, \mathbf{u}) \\ \mathbf{g}(\mathbf{y}, \mathbf{u}) &= \mathbf{h}_o(\mathbf{x}_d) \ . \end{aligned} \tag{6.20}$$

A method for calculating $\tilde{\mathbf{D}}$ is given in the proof of Lemma 6.2.2. Multiplying the differential equation (6.20) with the scaling matrix $\boldsymbol{\mu}$, we obtain an expression for $\frac{d\mathbf{z}}{dt}$

$$\frac{d\mathbf{z}}{dt} = \boldsymbol{\mu}(\mathbf{x}_d)\tilde{\mathbf{D}}(\mathbf{x}_d)\frac{d\mathbf{x}_d}{dt} = \boldsymbol{\mu}(\mathbf{x}_d)\tilde{\mathbf{f}}_o'(\mathbf{x}_d, \mathbf{y}, \mathbf{u}) \ . \tag{6.21}$$

From this equation it is seen that $\boldsymbol{\Phi}$ is given by the p.d.e.

$$\frac{\partial \boldsymbol{\Phi}}{\partial \mathbf{x}_d} = \boldsymbol{\mu}(\mathbf{x}_d)\tilde{\mathbf{D}}(\mathbf{x}_d).$$

Step 2.: Next it is shown that there exists an expression on the form

$$\begin{pmatrix} \mathbf{g}_{o2}(\mathbf{y}, \mathbf{u}) \\ \mathbf{z} \end{pmatrix} = \begin{pmatrix} \mathbf{h}_{o2}(\mathbf{x}_d) \\ \boldsymbol{\Phi}(\mathbf{x}_d) \end{pmatrix} \ , \tag{6.22}$$

where $\mathbf{g}_{o2}(\mathbf{y}, \mathbf{u}) = \mathbf{h}_{o2}(\mathbf{x}_d)$ contains a subpart of the rows in $\mathbf{g}_o(\mathbf{y}, \mathbf{u}) = \mathbf{h}_o(\mathbf{x}_d)$. This expression must be solvable for all $\mathbf{x}_d$ in the system, i.e. a local solution must exists. For this to be true the inverse function theorem states that the Jacobian determinant of (6.22) must be different from zero, e.i.

$$\frac{\partial}{\partial \mathbf{x}_d}\begin{pmatrix} \mathbf{h}_{o2}(\mathbf{x}_d) \\ \boldsymbol{\Phi}(\mathbf{x}_d) \end{pmatrix} = \begin{pmatrix} \frac{\partial \mathbf{h}_{o2}(\mathbf{x}_d)}{\partial \mathbf{x}_d} \\ \boldsymbol{\mu}(\mathbf{x}_d)\tilde{\mathbf{D}}(\mathbf{x}_d) \end{pmatrix} \tag{6.23}$$

must have full rank for all $\mathbf{x}_d \in \mathcal{D}_{\mathbf{x}_d}$.

Using the proof of Lemma 6.2.2 it can be deduced that $\text{Span}\{(\boldsymbol{\mu}(\mathbf{x}_d)\tilde{\mathbf{D}}(\mathbf{x}_d))^T\} = \text{Span}\{\tilde{\mathbf{D}}(\mathbf{x}_d)^T\} = \text{Ker}\left\{\mathbf{G}_o(\mathbf{x}_d)^T\right\}$, and that $\tilde{\mathbf{D}}(\mathbf{x}_d)$ has full row rank for all $\mathbf{x}_d \in \mathcal{D}_{\mathbf{x}_d}$. Using Assumption 6.2.3 it is guaranteed that there exists a $\mathbf{h}_{o2} \subseteq \mathbf{h}_o$ such that $\frac{\partial \mathbf{h}_{o2}(\mathbf{x}_d)}{\partial \mathbf{x}_d}$ span the l_2 dimensional row space not spanned by $\tilde{\mathbf{D}}(\mathbf{x}_d)$. This implies that the matrix in (6.23) has full rank for all $\mathbf{x}_d \in \mathcal{D}_{\mathbf{x}_d}$, i.e. (6.22) can be solved for $\mathbf{x}_d$. Let the solution of $\mathbf{x}_d$ be given by

$$\mathbf{x}_d = \boldsymbol{\Psi}(\mathbf{z}, \mathbf{y}, \mathbf{u}).$$

Using this expression in (6.21) the final model becomes

$$\begin{aligned} \tfrac{d\mathbf{z}}{dt} &= \boldsymbol{\mu}(\mathbf{x}_d)\tilde{\mathbf{f}}'_o(\mathbf{x}_d,\mathbf{y},\mathbf{u})|_{\mathbf{x}_d=\boldsymbol{\Psi}(\mathbf{z},\mathbf{y},\mathbf{u})} \\ \mathbf{g}_{o1}(\mathbf{y},\mathbf{u}) &= \mathbf{h}_{o1}(\mathbf{x}_d,\mathbf{y},\mathbf{u})|_{\mathbf{x}=\boldsymbol{\Psi}(\mathbf{z},\mathbf{y},\mathbf{u})} \ . \end{aligned}$$

□

Remark 6.2.2 *The question arise about the existence of the solution* $\mathbf{z} = \boldsymbol{\Phi}(\mathbf{x})$ *that satisfies (6.18). In* R^2 *the problem can be formilized by*

$$\tfrac{\partial \boldsymbol{\Phi}}{\partial \mathbf{x}} = \boldsymbol{\mu}(\mathbf{x})\tilde{\mathbf{D}}(\mathbf{x}) \ \Leftrightarrow \ \begin{pmatrix} \frac{\partial \Phi}{\partial x_1} & \frac{\partial \Phi}{\partial x_2} \end{pmatrix} = \mu(\mathbf{x}) \begin{pmatrix} \tilde{d}_1(\mathbf{x}) & \tilde{d}_2(\mathbf{x}) \end{pmatrix}$$

which implies that,

$$\tfrac{\partial^2 \Phi}{\partial x_1 \partial x_2} - \tfrac{\partial^2 \Phi}{\partial x_1 \partial x_2} = \tfrac{\partial \mu \tilde{d}_1}{\partial x_2} - \tfrac{\partial \mu \tilde{d}_2}{\partial x_1} = 0$$

This expression can be solved for $\boldsymbol{\mu}$ *(in the* R^2 *case) using the intergrating factor approach (Nagle and Saff, 1996, chap. 2). When* $\boldsymbol{\mu}$ *is known* $\boldsymbol{\Phi}$ *can be found by simple intergration (this approach is used in the example in Section 6.2.4).*

The expression described above, can in R^3 *be described by*

$$\nabla \boldsymbol{\Phi}_i(\mathbf{x}) = [\boldsymbol{\mu}(\mathbf{x})\mathbf{f}(\mathbf{x})]_i$$

where i *denotes the* i^{th} *row in (6.18). Using the* ∇ *operator the following expression can be obtained*

$$\nabla \times \nabla \boldsymbol{\Phi}_i(\mathbf{x}) = \nabla \times [\boldsymbol{\mu}(\mathbf{x})\mathbf{f}(\mathbf{x})]_i = 0$$

Unfortunately, no procedure exists for finding $\boldsymbol{\mu}(\mathbf{x})$ *in* R^3.

Remark 6.2.3 *In general the existence of a solution to the p.d.e. (6.18) can be treated using Frobenius theorem (Isidori, 1995). A discussion on this approach is found in (Frisk and Åslund, 2003), which treats the solution to problems similar to (6.18).*

6.2.3 Elimination Algorithm

To summarize the results obtained in the previous two subsections, an algorithm is prestented below. This algorithm presents the steps necessary to obtain a state space description of (6.4).

1. First use Theorem 6.2.1 to eliminate a subset of the unknown algebraic variables $\mathbf{x}_a$. If all the algebraic variables can be eliminated using this approach Corollary 6.2.1 states the final solution. If this is not the case go to step 2.

2. Check if Assumptions 6.2.2 and 6.2.3 holds for the system. If it holds go to step 3, else it is not possible to transform the system into a state space description using the approach given here.

3. Use Theorem 6.2.2 to obtain the state transformation $\mathbf{\Psi}$, and derive the transformed system.

4. Finally, to design a residual observer, find a stabilizing feedback for the transformed system. This is not treated here.

In this section ideas for developing residual observers using over-constrainted subsystems found using SA are presented. Even though deriving residual observers were the aim of the section, it is possible to use the same ideas to identify subsystems which can be used in the development of reduced order observers. The following theorem can be used to formulate a necessary condition for this to be possible.

Theorem 6.2.3 (Observability and over-constraint subsystems) *If a linear system given by*

$$\begin{aligned} \frac{d\mathbf{x}}{dt} &= \mathbf{A}\mathbf{x} \\ \mathbf{y} &= \mathbf{C}\mathbf{x} \end{aligned} \tag{6.24}$$

is observable for all $\mathbf{x} \in R^n$, then there exists an over-constrained match of the unknown variables $\mathcal{X} = \dot{\mathbf{x}} \cup \mathbf{x}$ using the system constraints $\mathcal{C} = \mathbf{h} \cup \mathbf{f} \cup \mathbf{d}$.

The proof is given in (Blanke et al., 2003, Sec. 5.5.3).

Remark 6.2.4 *Theorem 6.2.3 states that if system (6.24) is observable, then there exist and over-constrained match on the system. Reversing this argument, it can be said that if there does not exist an over-constraints subsystem, then there does not exist an observable state space description of the system.*

Theorem 6.2.3 only holds for linear systems and does only states that a linear system must be over-constrained to be observerable. This is a rather weak statement. However, in most systems, found using SA, the statement holds in the nonlinear case as well as in the linear case. Moreover, it is most often the case that the parameters and the nonlinear structure of a given system is on a form, such that all identified over-constrained subsystems are also observable.

Remark 6.2.5 *The arguments presented in this section does not garantee the existence of a residual observer or a reduced order observer, as the stability of an observer implementation is not considered here.*

6.2.4 Ex: Satellite Case

According to (De Persis and Isidori, 2001) a point mass model of a satellite is described by the set of constraints given in (6.25),

$$\begin{array}{lcl} c_1 & : & \dot{\rho} = v \\ c_2 & : & \dot{v} = \rho\omega^2 - \theta_1 \frac{1}{\rho^2} + \theta_2 u_1 + d \\ c_3 & : & \dot{\phi} = \omega \\ c_4 & : & \dot{\omega} = -\frac{2v\omega}{\rho} + \theta_2 \frac{u_2}{\rho} + \theta_2 \frac{f}{\rho} \\ c_5 & : & y_1 = \rho \\ c_6 & : & y_2 = \phi \\ c_7 & : & y_3 = \omega \end{array} \tag{6.25}$$

and four derivative constraints of the form $\dot{x} = \frac{dx}{dt}$. In this model (ρ, ϕ) denotes the position of the satellite in polar coordinates on the plane, v is the radial velocity, ω is the angular velocity and u_1, u_2 are the radial and tangential thrust, respectively. f is the fault signal and d represents a disturbance signal. The parameters θ_1 and θ_2 are supposed to be known, constant and different from zero. The constraints c_1 to c_4 describe the dynamics of the satellite and the constraints c_5 to c_7 describe the measurement system on the satellite.

The structural graph of the satellite system (6.25) is shown in Table 6.3. From this

Table 6.3: The structure table of the satellite system. x means uni-directional relations and 1 means bi-directional relations, where uni-directional means that the given variable is not calculable from the relation, see definitions in (Izadi-Zamanabadi, 2001). The symbols ① show a matching for a part of the system.

	Known					Unknown									Faults
	y_1	y_2	y_3	u_1	u_2	d	$\dot{v}$	$\dot{\phi}$	ϕ	$\dot{\rho}$	v	$\dot{\omega}$	ρ	ω	f
c_2				1		1	1						1	1	
d_4								1	x						
d_2							1				x				
c_3								1						1	
c_6		1							1						
d_1										1			x		
c_1										①	1				
c_4					1						①	1	1	1	1
d_3												①		x	
c_5	1												①		
c_7			1											①	

table it is seen that a match exists, which includes the constraint affected by the fault f. Therefore the subsystem formed by this match can be used for fault detection. Moreover the subsystem does not contain the disturbance d, and is therefore robust with respect to

this disturbance. The match is given by the following set of constraints

$$\mathcal{C} = \{d_1, d_3, c_1, c_4, c_5, c_7\}.$$

Considering the theory developed in Section 6.2, the set of equations describing the identified subsystem must be described as in (6.4). The state, algebraic and output vectors are therefore given by

$$\mathbf{x}_d = \begin{pmatrix} \rho & \omega \end{pmatrix}^T \qquad \mathbf{x}_a = v \qquad \mathbf{y} = \begin{pmatrix} y_1 & y_3 \end{pmatrix}^T ,$$

and the vector field and vector functions are given by

$$\mathbf{f}_x = \begin{pmatrix} v \\ -\frac{2v\omega}{\rho} + \theta_2 \frac{u_2}{\rho} \end{pmatrix} \qquad \mathbf{m}_x = 0 \qquad \mathbf{h}_x = \begin{pmatrix} \rho \\ \omega \end{pmatrix}.$$

Form these expressions it is seen that the the vector field $\mathbf{f}_x$ must be used for the elimination of $\mathbf{x}_a$. $\mathbf{f}_x$ can be put on the form $\mathbf{f}'_o(\mathbf{x}_d, \mathbf{u}) + \mathbf{G}_o(\mathbf{x}_d)\mathbf{x}_a$, meaning that Assumption 6.2.2 is fulfilled. Duing this the expression becomes

$$\begin{pmatrix} \dot{\rho} \\ \dot{\omega} \end{pmatrix} = \begin{pmatrix} 0 \\ \theta_2 \frac{u_2}{\rho} \end{pmatrix} + \begin{pmatrix} 1 \\ -\frac{2\omega}{\rho} \end{pmatrix} v \, . \tag{6.26}$$

Hence, Lemma 6.2.2 can be used to obtain the matrix $\tilde{\mathbf{D}}$ as it is shown in the following by choosing

$$\mathbf{D}(\mathbf{x}_d) = \begin{pmatrix} d_{11}(\mathbf{x}_d) & d_{12}(\mathbf{x}_d) \\ d_{21}(\mathbf{x}_d) & d_{22}(\mathbf{x}_d) \end{pmatrix}, \tag{6.27}$$

we compute $\mathbf{D}(\mathbf{x}_d)\frac{d\mathbf{x}_d}{dt} = \mathbf{D}(\mathbf{x}_d)\mathbf{f}'_o(\mathbf{x}_d, \mathbf{u}) + \mathbf{D}(\mathbf{x}_d)\mathbf{G}_o(\mathbf{x}_d)\mathbf{x}_a$ and obtain

$$\mathbf{D}(\mathbf{x}_d)\frac{d\mathbf{x}_d}{dt} = \begin{pmatrix} d_{12}(\mathbf{x}_d)\theta_2 \frac{u_2}{\rho} \\ d_{22}(\mathbf{x}_d)\theta_2 \frac{u_2}{\rho} \end{pmatrix} + \begin{pmatrix} d_{11}(\mathbf{x}_d) - 2d_{12}(\mathbf{x}_d)\frac{\omega}{\rho} \\ d_{21}(\mathbf{x}_d) - 2d_{22}(\mathbf{x}_d)\frac{\omega}{\rho} \end{pmatrix}. \tag{6.28}$$

In order to fulfill condition (6.12) we choose:

$$d_{11}(\mathbf{x}_d) = 2\omega \qquad d_{12}(\mathbf{x}_d) = \rho \qquad d_{21}(\mathbf{x}_d) = 1 \qquad d_{22}(\mathbf{x}_d) = 0 \, .$$

According to (6.13) we get

$$\tilde{\mathbf{D}}(\mathbf{x}_d) = \begin{pmatrix} 2\omega & \rho \end{pmatrix},$$

and system (6.20) as:

$$\begin{pmatrix} 2\omega & \rho \end{pmatrix} \begin{pmatrix} \dot{\rho} \\ \dot{\omega} \end{pmatrix} = \begin{pmatrix} \theta_2 \frac{u_2}{\rho} \\ 0 \end{pmatrix}$$
$$\mathbf{y} = \begin{pmatrix} \rho \\ \omega \end{pmatrix} .$$

The transformation $\mathbf{\Phi}$ can therefore, according to Theorem 6.2.2, be found by solving the following p.d.e.

$$\frac{\partial \mathbf{\Phi}}{\partial \mathbf{x}_d} = \boldsymbol{\mu}(\mathbf{x}_d)\tilde{\mathbf{D}}(\mathbf{x}_d) = \boldsymbol{\mu}(\mathbf{x}_d)\begin{pmatrix} 2\omega & \rho \end{pmatrix}.$$

Choosing the integrating factor $\boldsymbol{\mu}(\mathbf{x}_d) = \rho$ the solution to the p.d.e. becomes

$$\mathbf{\Phi} = \omega\rho^2 \ .$$

When $\mathbf{\Phi}$ exists and Assumption 6.2.3 is fulfilled then the state transformation $\mathbf{\Psi}$ is, according to Theorem 6.2.2, given by the explicit solution to,

$$\begin{pmatrix} y_1 \\ z \end{pmatrix} = \begin{pmatrix} \rho \\ \omega\rho^2 \end{pmatrix},$$

where $y_1 = \rho$ is one of the output constraints, see (6.25). The solution to this equation becomes,

$$\begin{pmatrix} \omega \\ \rho \end{pmatrix} = \mathbf{\Psi} = \begin{pmatrix} z/(y_1^2) \\ y_1 \end{pmatrix}.$$

Using this transformation the state space representation of the identified subsystem becomes,

$$\mathcal{S}: \begin{cases} \dot{z} = \theta_2 y_1 u_2 \\ y_3 = z/(y_1^2) \ . \end{cases}$$

A residual observer for this system could be

$$\mathcal{O}: \begin{cases} \dot{z} = \theta_2 y_1 u_2 + k(y_1^2 y_3 - z) \\ r = q(y_1^2 y_3 - z) \ , \end{cases}$$

where k and q are design constants. The observer $\mathcal{O}$ is exactly the same observer as obtained in (De Persis and Isidori, 2001) using the geometric approach.

6.3 System Model

In this section the model of a general hydraulic application including a centrifugal pump is presented. Moreover, five faults, which are assumed to affect the centrifugal pump, are included in the model. Only quantities measurable at the pump site are assumed measured in this application. In the case, studied in this chapter, this means that the pressure H_p and the flow Q_p of the pump, and the supply voltage $\mathbf{v}_{sabc}$ and current $\mathbf{i}_{sabc}$ of the motor are assumed known.

In Chapter 3 a model describing a centrifugal pump driven by an induction motor was derived. From this model it is seen that the input to the pump is the supply voltage

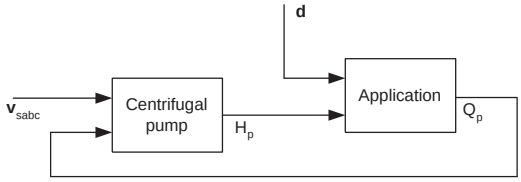

Figure 6.2: The centrifugal pump placed in a hydraulic application. The inputs to the centrifugal pump are the supply voltage $\mathbf{v}_{sabc}$ and the volume flow Q_p and the output is the pressure difference H_p. The inputs to the application are a set of unknown inputs $\mathbf{d}$ and the pressure difference of the pump H_p, and the output is the volume flow Q_p.

$\mathbf{v}_{sabc}$ and the volume flow Q_p, and the output is the pressure difference H_p delivered by the pump. This input/output structure is depicted in Fig. 6.2 where it is connected to a general hydraulic application. The inputs to this application are a set of unknown inputs $\mathbf{d}$ and the pressure difference H_p of the pump, and the output is the volume flow Q_p. The model of the system, depiced in Fig. 6.2, is formalized in the following subsections.

6.3.1 The Model of the Centrifugal Pump and its Application

It is assumed that the application is a dynamic system, which can be modelled by a set of first order ordinary differential equations. The structure of a model describing such a system is shown below,

$$\begin{aligned} \tfrac{d\mathbf{x}_Q}{dt} &= \mathbf{f}_A(\mathbf{x}_Q, H_p, \mathbf{d}) \\ Q_p &= h_A(\mathbf{x}_Q) \ , \end{aligned} \tag{6.29}$$

where $\mathbf{x}_Q$ is a vector containing the states of the hydraulic application and the vector $\mathbf{d}$ represents the unknown inputs to this application. H_p and Q_p are the pressure output and the volume flow of the centrifugal pump respectively.

The model of the centrifugal pump, presented in Chapter 3, is connected in a feedback loop with the application model, as it is depiced in Fig. 6.2. This results in the following model,

$$\begin{aligned} \tfrac{d\mathbf{x}_d}{dt} &= \mathbf{f}_x(\mathbf{x}_d, \mathbf{u}, \mathbf{d}) \\ \mathbf{y} &= \mathbf{h}_x(\mathbf{x}_d) \ , \end{aligned}$$

where the state vector $\mathbf{x}_d$ is given by,

$$\mathbf{x}_d = \begin{bmatrix} i_{sd} & i_{sq} & i_{md} & i_{mq} & \omega_r & \mathbf{x}_Q^T \end{bmatrix}^T ,$$

and the input vector $\mathbf{u}$ and the output vector $\mathbf{y}$ are given by,

$$\mathbf{u} = \begin{bmatrix} v_{sd} & v_{sq} \end{bmatrix}^T \qquad \mathbf{y} = \begin{bmatrix} i_{sd} & i_{sq} & H & Q \end{bmatrix}^T .$$

Finally, the unknown input vector $\mathbf{d}$ is the same vector as the unknown input vector prestented in (6.29). The vector field $\mathbf{f}_x$ of the system is described by the following set of equations,

$$\mathbf{f}_x(\mathbf{x}_d, \mathbf{u}, \mathbf{d}) = \begin{pmatrix} -\frac{R_s+R'_r}{L'_s} i_{sd} + \frac{R'_r}{L'_s} i_{md} - z_p \omega_r \frac{L'_m}{L'_s} i_{mq} + \frac{1}{L'_s} v_{sd} \\ -\frac{R_s+R'_r}{L'_s} i_{sq} + z_p \omega_r \frac{L'_m}{L'_s} i_{md} + \frac{R'_r}{L'_s} i_{mq} + \frac{1}{L'_s} v_{sq} \\ \frac{R'_r}{L'_m} i_{sd} - \frac{R'_r}{L'_m} i_{md} + z_p \omega_r i_{mq} \\ \frac{R'_r}{L'_m} i_{sq} - z_p \omega_r i_{md} - \frac{R'_r}{L'_m} i_{mq} \\ \frac{1}{J} \frac{3}{2} z_p L'_M \left(i_{md} i_{sq} - i_{mq} i_{sd} \right) - \frac{B}{J} \omega_r - f_T(h(\mathbf{x}_Q), \omega_r) \\ \mathbf{f}_A(\mathbf{x}_Q, H, \mathbf{d}) \end{pmatrix},$$

where $f_H(Q, \omega_r)$ and $f_T(Q, \omega_r)$ are given by,

$$\begin{array}{l} f_H(Q, \omega_r) = -a_{h2} Q^2 + a_{h1} Q \omega_r + a_{h0} \omega_r^2 \\ f_T(Q, \omega_r) = -a_{t2} Q^2 + a_{t1} Q \omega_r + a_{t0} \omega_r^2 \end{array} . \tag{6.30}$$

The output map of the system is given by,

$$\mathbf{h}_x(\mathbf{x}) = \begin{pmatrix} i_{sd} \\ i_{sq} \\ f_H(h_A(\mathbf{x}_Q), \omega_r) \end{pmatrix}.$$

This model represents the behaviour of the system when no fault has occured. In the following the effect of faults on the centrifugal pump is described.

6.3.2 Fault Models

Five faults are considered in this chapter, these are,

1. clogging inside the pump,
2. increased friction due to either rub impact or bearing faults,
3. increased leakage flow,
4. performance degradation due to cavitation,
5. dry running.

The first three faults are internal faults caused by impurities in the liquid and wear respectively. The fourth fault, cavitation, is caused by too low inlet pressure, meaning that the fault is external. Finally, the last fault, dry running, is a phenomenon caused by faults in the surrounding system, hence it is also an external fault. Even though it is not a fault in the pump, this fault is important to detect as sealing rings and bearings will be destroyed when the pump is running without water for only a few seconds.

The mentioned faults all affect the hydraulic part of the pump. The performance of the hydraulic part of the pump is modelled by f_H and f_T. These functions describe the pressure and the torque produced by the pump respectively. Moreover the flow measurement is part of the hydraulic description of the pump. Introducing the faults described above, the description of the hydraulics of the pump becomes,

$$\begin{aligned} H_p &= f_H(Q, \omega_r) - K_f Q^2 - C_{ch} f_c - C_{dh} f_d \\ T_p &= f_T(Q, \omega_r) + \Delta B \omega_r - C_{ct} f_c - C_{dt} f_d \\ y_3 &= Q - K_l \sqrt{H_p} \, . \end{aligned}$$

In this fault model $K_f \in R_+$ represents clogging, $\Delta B \in R_+$ represents rub impact, $K_l \in R_+$ represents increased leakage flow, $f_c \in R_+$ represents cavitation, and $f_d \in R_+$ represents dry runnning. The first three signals model the faults accurately, while the last two terms are linear approximations.

6.4 Structural Analysis

As stated in Section 6.1 the structural analysis is the study of the system properties, which are independent of the actual values of the parameters. Only links between the set of variables $\mathcal{X}$ and the set of constraints $\mathcal{C}$ are represented in the analysis. In this work the use of SA is two folded, as it is both used for identifying two cascade connected subsystems, and to identify subsystems which can be used for residual generations.

The system is splitted into two cascade connected subsystems to facilitate the derivation of residual generators. This is possible as the faults considered in this work only affect the second subsystem, meaning that only this subsystem must be considered when deriving residual generators.

As the SA is working on the two sets $\mathcal{C}$, $\mathcal{Z}$ these must be defined for the pump application before the results of the SA can be obtained. This is done in the Section 6.4.1. After that the splitting of the system is considered in Section 6.4.2. Finally this section ends with identifying subsystem for residual generation in Section 6.4.3.

6.4.1 Variables and Constraints of the System

The constraints $\mathcal{C}$ of the hydraulic system are identified from the model presented in Section 6.3. These constraints are given by

$$
\begin{array}{lcl}
c_1 & : & L'_s\dot{i}_{sd} = -(R_s + R'_r)i_{sd} + A_1 + v_{sd} \\
c_2 & : & L'_s\dot{i}_{sq} = -(R_s + R'_r)i_{sq} + A_2 + v_{sq} \\
c_3 & : & L'_m\dot{i}_{md} = -A_1 + R'_r i_{sd} \\
c_4 & : & L'_m\dot{i}_{mq} = -A_2 + R'_r i_{sq} \\
c_5 & : & J\dot{\omega}_r = T_e - B\omega_r - T_p \\
c_6 & : & \dot{\mathbf{x}}_Q = \mathbf{f}_A(\mathbf{x}_Q, H_p, \mathbf{u}_Q) \\
c_7 & : & A_1 = R'_r i_{md} + z_p\omega_r L'_m i_{mq} \\
c_8 & : & A_2 = R'_r i_{mq} - z_p\omega_r L'_m i_{md} \\
c_9 & : & T_e = \frac{3}{2} z_p L'_m \left(i_{md} i_{sq} - i_{mq} i_{sd}\right) \\
c_{10} & : & H_p = -a_{h2}Q_p^2 + a_{h1}Q_p\omega_r + a_{h0}\omega_r^2 \\
c_{11} & : & T_p = -a_{t2}Q_p^2 + a_{t1}Q_p\omega_r + a_{t0}\omega_r^2 \\
c_{12} & : & Q_p = h_A(\mathbf{x}_Q) \\
c_{13} & : & y_1 = i_{sd} \\
c_{14} & : & y_2 = i_{sq} \\
c_{15} & : & y_3 = H_p \\
c_{16} & : & y_4 = Q_p \ ,
\end{array}
\tag{6.31}
$$

where the constraints c_7 and c_8 are included to make the constraints c_1 to c_4 independent. Hereby Assumption 6.1.3 is fulfilled globally (Blanke et al., 2003).

In (6.31) the constraints c_1 to c_4 and c_7 to c_8 describe the electrical part of the induction motor, c_5 describes the mechanical dynamics of the pump, and c_6 describes the dynamics of the hydraulic applications. c_9, c_{10} and c_{11} describe the torque generated by the induction motor, the pressure difference generated by the centrifugal pump, and the load torque of the centrifugal pump respectively. c_{12} describes the volume flow through the pump and finally c_{13} to c_{16} describe the measurements on the system.

Two extra constraints can be deduced by differentating c_7 and c_8 with respect to time. Doing this the following additional constraints are obtained,

$$
\begin{array}{lcl}
c_{d7} & : & \dot{A}_1 = R'_r\dot{i}_{md} + z_p\dot{\omega}_r L'_m i_{mq} + z_p\omega_r L'_m\dot{i}_{mq} \\
c_{d8} & : & \dot{A}_2 = R'_r\dot{i}_{mq} - z_p\dot{\omega}_r L'_m i_{md} - z_p\omega_r L'_m\dot{i}_{md} \ .
\end{array}
\tag{6.32}
$$

Beside the constrains presented above, there is a differential constraint for each variable $\dot{x}_d$, meaning that a constraint on the form,

$$
d_i : \ \frac{dx_{di}}{dt} = \dot{x}_{di}, \tag{6.33}
$$

exists for each element in $\dot{\mathbf{x}}_d$. In this expression i denotes the i^{th} element in $\dot{\mathbf{x}}_d$.

From the constraints presented in (6.31) and (6.32) the set of variables are identified. These are given by,

$$
\mathcal{Z} = \dot{\mathbf{x}}_d \cup \mathbf{x}_d \cup \mathbf{x}_a \cup \mathbf{u} \cup \mathbf{y}
$$

where $\mathcal{X} = \dot{\mathbf{x}}_d \cup \mathbf{x}_d \cup \mathbf{x}_a$ are the unknown variables, which must be matched, and $\mathcal{K} = \mathbf{u} \cup \mathbf{y}$ are the known variables. $\mathbf{x}_d$, $\mathbf{x}_a$, $\mathbf{u}$, and $\mathbf{y}$ are given by,

$$\mathbf{x}_d = \begin{bmatrix} i_{sd} & i_{sq} & i_{md} & i_{mq} & \omega_r & A_1 & A_2 & \mathbf{x}_Q^T \end{bmatrix}^T$$
$$\mathbf{x}_c = \begin{bmatrix} H_p & Q_p & T_p & \mathbf{d}^T \end{bmatrix}^T \qquad \mathbf{u} = \begin{bmatrix} v_{sd} & v_{sq} \end{bmatrix}^T \qquad \mathbf{y} = \begin{bmatrix} y_1 & y_2 & y_3 & y_4 \end{bmatrix}^T .$$

6.4.2 Cascade Connected Systems

From the model of the system presented in Section 6.3 it is seen that the system is nonlinear. Therefore, traditionally a nonlinear transformation is required to enable a design of a residual observer (Garcia and Frank, 1997). This transformation is not easy to find due to the nonlinear nature of the system. Moreover, developing Analytical Redundancy Relations (ARR's), using for example Groebner basis (Cox et al., 1997) for variable eliminations, have not given any usable result. This is also due to the nonlinear nature of the system. Therefore, the system is divided into two cascade-connected subsystems by using structural consideration on the system (Blanke et al., 2003; Izadi-Zamanabadi and Staroswiecki, 2000).

Using SA it is shown that it is in fact possible to make this split. By analysing the relation describing the electrical part of the induction motor, it is seen from Table 6.4 that these constraints form an over-constraint system, see Definition 6.1.7. Therefore from Theorem 6.1.1 the system is structural observable, meaning that the set of constrains $\mathcal{C}_e$ form an observable subsystem for almost all parameters. This set is given by,

$$\mathcal{C}_e = \{d_1, d_2, d_{d7}, d_{d8}, c_1, c_2, c_3, c_4, c_7, c_8, c_9, c_{d7}, c_{d8}, c_{13}, c_{14}\} , \tag{6.34}$$

$\mathcal{C}_e$ is defined as the first subsystem. The remaining relations are defined as the second subsystem, meaning that the constrains of this subsystem are given by,

$$\mathcal{C}_m = \{d_5, d_6, c_5, c_6, c_{10}, c_{11}, c_{12}, c_{15}, c_{16}\}. \tag{6.35}$$

The connecting variables between the two subsystems are in this work defined as the estimates of ω_r and T_e, and will in the following be denoted $\hat{\omega}_r$ and $\hat{T}_e$ respectively.

It is also seen from the column at the right hand side of Table 6.4 that the faults treated in this chapter are not affecting the relations in the first subsystem. Therefore, it is only necessary to consider the second subsystem when designing residual generators for FDI on the system. Hence, the fault detection algorithm can be divided into two parts as shown in Fig. 6.3.

Using the relations describing the first part, an adaptive observer is designed. This observer observes the variables ω_r and T_e connecting the two parts. The design of this observer is considered in Section 6.5. But first SA is used to identify minimal over-constrained subsystems (see Definition 6.1.11) in the system formed by the constraints $\mathcal{C}_m$. The obtained results are presented in the following subsection,

Table 6.4: The structure table of the system. x implies that the given variable is not calculable using the constraint but does appear in the constraint (Izadi-Zamanabadi, 2001). The symbols ① show a matching for the first part of the system.

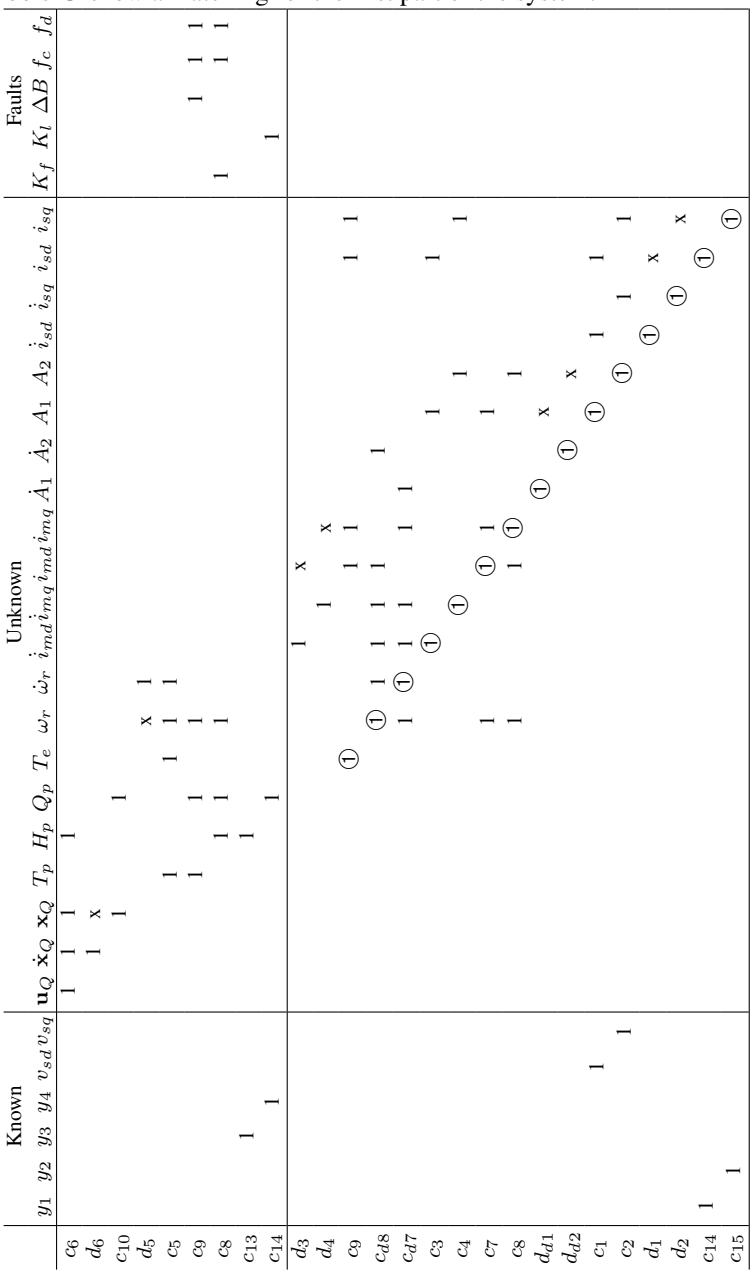

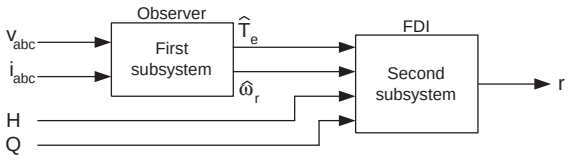

Figure 6.3: The division of the fault detection algorithm. In the first subpart the model of the electrical part of the motor is used, and in the second subpart the models of the mechanical and hydraulic parts of the system are used.

6.4.3 Structural Analysis on the Second Subsystem

The SA is in this section used for identification of four minimal over-constrained subsystems. Each of these subsystem can be utilized for detecting a subset of the faults in the centrifugal pump. The second subsystem is described by the set of constraints $\mathcal{C}_m$ in (6.35). Beside these constraints two extra constraints are defined to describe the connecting variables $\hat{\omega}_r$ and $\hat{T}_e$. These constraints are given by,

$$\begin{aligned} c_{15} &: \hat{\omega}_r = \omega_r \\ c_{16} &: \hat{T}_e = T_e \ . \end{aligned}$$

In Table 6.5 the graph of the second subsystem is shown. Here the two extra constraints are added.

Table 6.5: The structural model of the second subsystem $\mathcal{C}_m$ obtained in Section 6.4.2.

	Known				Unknown									Faults				
	y_3	y_4	$\hat{\omega}_r$	$\hat{T}_e$	$\mathbf{u}_Q$	$\dot{\mathbf{x}}_Q$	$\mathbf{x}_Q$	$\dot{\omega}_r$	T_p	ω_r	H_p	Q_p	T_e	K_f	K_l	ΔB	f_c	f_d
c_6					1	1	1				1							
d_6						1	x											
c_{10}							1					1						
d_5								1		x								
c_5								1	1	1			1					
c_9									1	1		1				1	1	1
c_8										1	1	1		1			1	1
c_{15}			1							1								
c_{13}	1										1							
c_{14}		1										1			1			
c_{16}				1									1					

Using the definitions and procedures described in (Blanke et al., 2003; Izadi-Zamanabadi, 2001), four minimal over-constrained subsystems are identified. The set

of constraints contained in each of these system are given by,

$$\begin{aligned} \mathcal{C}_{m1} &= \{d_5, c_5, c_9, c_{14}, c_{15}, c_{16}\} \\ \mathcal{C}_{m2} &= \{c_8, c_{13}, c_{14}, c_{15}\} \\ \mathcal{C}_{m3} &= \{d_5, c_5, c_8, c_9, c_{13}, c_{15}, c_{16}\} \\ \mathcal{C}_{m4} &= \{d_5, c_5, c_8, c_9, c_{13}, c_{14}, c_{16}\} \ . \end{aligned} \tag{6.36}$$

From these four minimal over-constrained subsystems, it is seen that the constraints d_6, c_6, and c_{10} are not contained in any of the matchings. These constraints describe the application in which the pump is placed. Therefore, when these are not used in a match it means that the matching is independent of the application model, and therefore no knowledge about the application is necessary for the algorithm to work.

Looking at the column to the right in table 6.5 the faults affecting each of the subsystems $\mathcal{C}_{mi}$ can be identified. The connections between the faults and the subsystems are shown below,

$$\begin{aligned} \mathcal{C}_{m1} &: \{K_l, \Delta B, f_c, f_d\} \\ \mathcal{C}_{m2} &: \{K_f, K_l, f_c, f_d\} \\ \mathcal{C}_{m3} &: \{K_f, \Delta B, f_c, f_d\} \\ \mathcal{C}_{m4} &: \{K_f, K_l, \Delta B, f_c, f_d\} \ . \end{aligned} \tag{6.37}$$

These connections show that the given faults are *Structurally monitorable* from the given set of constraints, see Theorem 6.1.2 (Blanke et al., 2003).

From the connection in (6.37) it is seen that the faults f_c and f_d are indistinguishable from a structural point of view, meaning that isolation of these faults is impossible using residual generator built on these sets of constraints. Moreover, it is seen that no additional information is added using $\mathcal{C}_{m4}$. Therefore the set,

$$\{\mathcal{C}_{m1},\ \mathcal{C}_{m2},\ \mathcal{C}_{m3}\} \ ,$$

contains the obtainable information about the faults in the system. The last relation $\mathcal{C}_{m4}$ could be used for validation in a robust fault detection scheme.

6.5 Observer for the Motor Part

In Section 6.4.2 it is shown, using SA, that the model of the centrifugal pump can be splitted into two subsystems, where the first system is *structurally observable*, see Theorem 6.1.1 (Blanke et al., 2003). When this is the case the behaviour model of the system is also observable for almost all parameters (Blanke et al., 2003). Therefore, it should be possible to derive an expression of the measurements and their derivatives for calculating the connecting variables.

Unfortunately, the derivatives of the measurements are not known. Therefore, an observer solution is investigated in this section. In the first part of the section a state space description of the system is derived from the constraints $\mathcal{C}_e$. In the last part an adaptive observer for observing the connecting variables is presented.

6.5.1 Realization of the set of Constraints $\mathcal{C}_e$

One approach for developing an observer to observe the speed and torque is to derive a dynamic description of the set of constraints using the theory presented in Section 6.2. The obtained dynamic description can then be used in the design of an observer.

In Section 6.4.2 the set of constraints $\mathcal{C}_e$ is identified. This set forms a match of the two connecting variables ω_r and T_e. From Table 6.4 it is seen that the constraint c_9 is used to match the variable T_e, which is not used in any other constraints in $\mathcal{C}_e$. Therefore, c_9 is not necessary in a match of the speed ω_r. However, it is seen that, when the speed is matched, c_9 can be used to calculate T_e, as all variables except T_e is matched in c_9. Therefore, when an expression for calculating ω_r is derived, then the derivation of an expression for calculating T_e is just a matter of form.

Based on the above argumentation only the calculation of ω_r is considered in the following. In Remark 6.2.4 it is argued that an observable state space description only exists if the given subsystem is over-constrained, which is not the case for the set $\mathcal{C}_e$. Therefore, by adding an extra constraint to $\mathcal{C}_e$ making the new set over-constraint and removing c_9, the following set is obtained

$$\mathcal{C}'_e = (\mathcal{C}_e \backslash c_9) \cup d_3 \ , \tag{6.38}$$

which fulfills the demand of existence given in Remark 6.2.4. The new set $\mathcal{C}'_e$ is formed by the following constraints,

$$\begin{aligned}
c_1 &: \quad L'_s \dot{i}_{sd} = -(R_s + R'_r) i_{sd} + A_1 + v_{sd} \\
c_2 &: \quad L'_s \dot{i}_{sq} = -(R_s + R'_r) i_{sq} + A_2 + v_{sq} \\
c_3 &: \quad L'_m \dot{i}_{md} = -A_1 + R'_r i_{sd} \\
c_4 &: \quad L'_m \dot{i}_{mq} = -A_2 + R'_r i_{sq} \\
c_7 &: \quad A_1 = R'_r i_{md} + z_p \omega_r L'_m i_{mq} \\
c_8 &: \quad A_2 = R'_r i_{mq} - z_p \omega_r L'_m i_{md} \\
c_{13} &: \quad y_1 = i_{sd} \\
c_{14} &: \quad y_2 = i_{sq} \\
c_{d7} &: \quad \dot{A}_1 = R'_r \dot{i}_{md} + z_p \dot{\omega}_r L'_m i_{mq} + z_p \omega_r L'_m \dot{i}_{mq} \\
c_{d8} &: \quad \dot{A}_2 = R'_r \dot{i}_{mq} - z_p \dot{\omega}_r L'_m i_{md} - z_p \omega_r L'_m \dot{i}_{md} \ .
\end{aligned}$$

In this set the unknown variables $\mathbf{x}_d \cup \mathbf{x}_a$ and the known variables $\mathbf{u} \cup \mathbf{y}$ are given by,

$$\mathbf{x}_d = \begin{bmatrix} i_{sd} & i_{sq} & i_{md} & A_1 & A_2 \end{bmatrix}^T \qquad \mathbf{x}_a = \begin{bmatrix} \dot{i}_{mq} & i_{mq} & \dot{\omega}_r & \omega_r \end{bmatrix}^T$$
$$\mathbf{u} = \begin{bmatrix} v_{sd} & v_{sq} \end{bmatrix}^T \qquad \mathbf{y} = \begin{bmatrix} y_1 & y_2 \end{bmatrix}^T \ .$$

Comparing the set (6.38) with the general system given by (6.4) the vector field $\mathbf{f}_x$, the algebraic maps $\mathbf{m}_x$ and the output maps $\mathbf{h}_x$ are constructed using the set of constraints $\{c_1, c_2, c_3, c_{d7}, c_{d8}\}$, $\{c_4, c_7, c_8\}$, and $\{c_{13}, c_{14}\}$ respectively. According to Theorem 6.2.1 and the match shown in Table 6.4, it is possible to eliminate a subset of the algebraic variables $\mathbf{x}_a$ in the system using the vector function $\mathbf{m}_x$. From the match presented

in Table 6.4 it is seen that the two algebraic variables $\dot{i}_{mq}$ and i_{mq} should be eliminated using $\mathbf{m}_x$. By eliminating these the following system is obtained,

$$\begin{array}{c} \frac{d\mathbf{x}_d}{dt} = \mathbf{f}'_o(\mathbf{x}_d, \mathbf{x}_{a2}, \mathbf{u}) \\ \mathbf{g}_o(\mathbf{y}) = \mathbf{h}_o(\mathbf{x}_d, \mathbf{x}_{a2}) \ , \end{array} \tag{6.39}$$

where $\mathbf{x}_{a2} = \begin{bmatrix} \omega_r & \dot{\omega}_r \end{bmatrix}^T$ and,

$$\mathbf{f}_o = \begin{pmatrix} -\frac{R_s+R'_r}{L'_s} i_{sd} + \frac{1}{L'_s} A_1 + \frac{1}{L'_s} v_{sd} \\ -\frac{R_s+R'_r}{L'_s} i_{sq} + \frac{1}{L'_s} A_2 + \frac{1}{L'_s} v_{sq} \\ -\frac{1}{L'_m} A_1 + \frac{R'_r}{L'_m} i_{sd} \\ \frac{R'_r}{L'_m}(R'_r i_{sd} - A_1) + z_p \dot{\omega}_r \left(\frac{L'_m}{R'_r} A_2 + z_p \omega_r \frac{{L'_m}^2}{R'_r} i_{md} \right) + z_p \omega_r (R'_r i_{sq} - A_2) \\ -\frac{R'_r}{L'_m} A_2 + \frac{{R'_r}^2}{L'_m} i_{sq} - z_p \dot{\omega}_r L'_m i_{md} - z_p \omega_r (R'_r i_{sd} - A_1) \end{pmatrix}$$

$$\mathbf{g}_o = \begin{pmatrix} 0 \\ y_1 \\ y_2 \end{pmatrix} \qquad \mathbf{h}_o = \begin{pmatrix} \left(R'_r + z_p^2 \omega_r^2 \frac{{L'_m}^2}{R'_r} \right) i_{md} + z_p \omega_r \frac{L'_m}{R'_r} A_2 - A_1 \\ i_{sd} \\ i_{sq} \end{pmatrix}.$$

The next step in the derivation of a state space description is to use the approach described in Theorem 6.2.2 to eliminate the algebraic variables $\mathbf{x}_{a2}$ in (6.39). Unfortunately, doing this the expression becomes huge, making it very difficult to find the state transformation $\mathbf{\Phi}$, see Theorem 6.2.2. This makes the obtained expression useless.

However, by eliminating the variables in $\mathbf{x}_{a2}$ in two steps an useful expression is obtained. To see this first $\dot{\omega}_r$ is eliminated in (6.39), and then the state transformation $\mathbf{T} : \mathbf{x}, \omega_r \rightarrow \mathbf{x}_d$ is used to transform the obtained system. Here $\mathbf{x} = \begin{bmatrix} i_{sd} & i_{sq} & i_{md} & i_{mq} \end{bmatrix}^T$ and $\mathbf{T}$ is given by

$$\mathbf{T}(\mathbf{x}, \omega_r) = \begin{pmatrix} i_{sd} \\ i_{sq} \\ i_{md} \\ R'_r i_{md} + z_p \omega_r L'_m i_{mq} \\ R'_r i_{mq} - z_p \omega_r L'_m i_{md} \end{pmatrix},$$

Doing this the traditional description of the electrical part of an induction motor is obtained, i.e. the transformed model has the following form

$$\begin{array}{c} \frac{d\mathbf{x}}{dt} = \mathbf{f}_x(\mathbf{x}, \omega_r, \mathbf{u}) \\ \mathbf{y} = \mathbf{h}_x(\mathbf{x}) \ , \end{array} \tag{6.40}$$

where

$$\mathbf{f}_x(\mathbf{x},\omega_r,\mathbf{u}) = \begin{pmatrix} -\frac{R_s+R'_r}{L'_s} i_{sd} + \frac{R'_r}{L'_s} i_{md} - z_p\omega_r \frac{L'_m}{L'_s} i_{mq} + \frac{1}{L'_s} v_{sd} \\ -\frac{R_s+R'_r}{L'_s} i_{sq} + z_p\omega_r \frac{L'_m}{L'_s} i_{md} + \frac{R'_r}{L'_s} i_{mq} + \frac{1}{L'_s} v_{sq} \\ \frac{R'_r}{L'_m} i_{sd} - \frac{R'_r}{L'_m} i_{md} + z_p\omega_r i_{mq} \\ \frac{R'_r}{L'_m} i_{sq} - z_p\omega_r i_{md} - \frac{R'_r}{L'_m} i_{mq} \end{pmatrix} \quad \mathbf{h}_x(\mathbf{x}) = \begin{pmatrix} i_{sd} \\ i_{sq} \end{pmatrix} .$$

As the second step the approach presented in Theorem 6.2.2 is used ones again. This time to eliminate ω_r in (6.40). Hereby the following state space description is obtained,

$$\begin{array}{c} \frac{d\mathbf{z}}{dt} = \mathbf{f}_z(\mathbf{z},\mathbf{u}') \\ y = h_z(\mathbf{z},\mathbf{u}') \ , \end{array} \tag{6.41}$$

where $\mathbf{z} \in \mathcal{D}_z \subset R^3$ and $\mathbf{u}' = \begin{bmatrix} v_{sd} & v_{sq} & y_2 \end{bmatrix}^T$. The vector field $\mathbf{f}_z$ and the nonlinear map h_z in this expression are given by,

$$\mathbf{f}_z(\mathbf{z},\mathbf{u}') = \begin{pmatrix} -\frac{R_s}{L'_s} z_1 + \frac{R_s\sqrt{2L'_m z_3 - z_2^2 + 2z_2 L'_s y_2 - {L'_s}^2 y_2^2}}{L'_s} + v_{sd} \\ -R_s y_2 + v_{sq} \\ -2\frac{R'_r L'_s + R'_r L'_m}{L'_s L'_m} z_3 + \frac{R'_r}{L'_m L'_s} z_2^2 - \frac{R'_r}{L'_m} z_2 y_2 + \frac{R'_r\sqrt{2L'_m z_3 - z_2^2 + 2z_2 L'_s y_2 - {L'_s}^2 y_2^2}\, z_1}{L'_m L'_s} \end{pmatrix}$$

$$h_z(\mathbf{z},\mathbf{u}') = \left(\frac{1}{L'_s} z_1 - \frac{\sqrt{2L'_m z_3 - z_2^2 + 2z_2 L'_s y_2 - {L'_s}^2 y_2^2}}{L'_s} \right) .$$

The system (6.41) is a state space realization of the set of constraints $\mathcal{C}'_e$, where all algebraic variables are eliminated. The speed of the motor can be calculated from the states of (6.41) using the following expression,

$$\omega_r = \frac{\frac{R'_r}{L'_m} z_2 + v_{sq} - L'_s \dot{y}_2 - \left(R_s + \frac{R'_r L'_s}{L'_m} + R'_r \right) y_2}{z_p\sqrt{2L'_m z_3 - z_2^2 + 2z_2 L'_s y_2 - {L'_s}^2 y_2^2}} ,$$

from which it is seen that ω_r is a function of $\dot{y}_2$, which in general is not known. Even though this expression is not usable for estimating the speed ω_r, the following remark on this system should be considered.

Remark 6.5.1 *If an observer can be found based on system (6.41), then this observer is a residual observer for the induction motor, which is independent of the speed ω_r.*

In this section it is argued that it is not possible to estimate the speed of the motor without knowing the derivative of at least one of the measurements. However, it is also shown that the subsystem identified using SA corresponds to the electrical part of an induction motor, see (6.40). Therefore, all the methods, described in the literature, for speed and torque estimation based on the electrical model can be used. In the following the adaptive observer, developed in Section 5.2.1, is utilized for estimating the connecting variables, i.e. motor speed and torque.

6.5.2 The Adaptive Observer

In most pump applications the speed is either constant most of the time or changing slowly over time. Therefore the speed can be assumed constant in the observer design, meaning that an adaptive observer can be used for estimating the states and speed of the motor simultaneously. This approach, of course, has the drawback that, when transient phases occurs, short time errors in the estimated signals must be expected.

Considering the motor description (6.40) obtained in the previous section, it is seen that this system can be rewritten to be on the following form

$$\begin{aligned} \tfrac{d\mathbf{x}}{dt} &= (\mathbf{A}_0 + \omega_r \mathbf{A}_{\omega_r})\mathbf{x} + \mathbf{B}\mathbf{u} \\ \mathbf{y} &= \mathbf{C}\mathbf{x}\ , \end{aligned} \tag{6.42}$$

where the state vector $\mathbf{x}$, the input vector $\mathbf{u}$ and the output vector $\mathbf{y}$ are given by

$$\mathbf{x} = \begin{bmatrix} i_{sd} & i_{sq} & i_{md} & i_{mq} \end{bmatrix}^T$$
$$\mathbf{u} = \begin{bmatrix} v_{sd} & v_{sq} \end{bmatrix}^T \qquad \mathbf{y} = \begin{bmatrix} i_{sd} & i_{sq} \end{bmatrix}^T\ ,$$

and the matrices in (6.42) are

$$\mathbf{A}_0 = \begin{bmatrix} -\frac{R_s+R_r'}{L_s'} & 0 & \frac{R_r'}{L_s'} & 0 \\ 0 & -\frac{R_s+R_r'}{L_s'} & 0 & \frac{R_r'}{L_s'} \\ \frac{R_r'}{L_m'} & 0 & -\frac{R_r'}{L_m'} & 0 \\ 0 & \frac{R_r'}{L_m'} & 0 & -\frac{R_r'}{L_m'} \end{bmatrix} \quad \mathbf{A}_{\omega_r} = \begin{bmatrix} 0 & 0 & 0 & -z_p\frac{L_m'}{L_s'} \\ 0 & 0 & z_p\frac{L_m'}{L_s'} & 0 \\ 0 & 0 & 0 & z_p \\ 0 & 0 & -z_p & 0 \end{bmatrix}$$

$$\mathbf{B} = \begin{bmatrix} \frac{1}{L_s'} & 0 \\ 0 & \frac{1}{L_s'} \\ 0 & 0 \\ 0 & 0 \end{bmatrix} \qquad \mathbf{C} = \begin{bmatrix} 1 & 0 & 0 & 0 \\ 0 & 1 & 0 & 0 \end{bmatrix}\ .$$

If the speed is assumed constant, this system is a linear system with one unknown but constant parameter. Using the transformation $\mathbf{x} = \mathbf{T}\mathbf{z}$ given by

$$\mathbf{T} = \begin{bmatrix} 1 & 0 & 0 & 0 \\ 0 & 1 & 0 & 0 \\ -\frac{L_s'}{L_m'} & 0 & 1 & 0 \\ 0 & -\frac{L_s'}{L_m'} & 0 & 1 \end{bmatrix}$$

the system (6.42) is tranformed to the adaptive observer form defined in Definition 5.2.1 in Section 5.2.1, where $\mathbf{A}(\mathbf{u}, \boldsymbol{\theta}) = \mathbf{A}(\boldsymbol{\theta})$ and $\boldsymbol{\theta} = \omega_r$. This means that an adaptive

observer is given by Proposition 5.2.1. Using this proposition the adaptive observer for the induction motor becomes

$$\mathcal{O}_e: \quad \begin{cases} \frac{d\hat{\mathbf{z}}}{dt} = (\mathbf{A}_0' + \hat{\omega}_r \mathbf{A}_{\omega_r}')\hat{\mathbf{z}} + \mathbf{B}'\mathbf{u} + \mathbf{K}(\mathbf{y} - \mathbf{C}'\hat{\mathbf{z}}) \\ \frac{d\hat{\omega}_r}{dt} = \kappa(\mathbf{y} - \mathbf{C}'\hat{\mathbf{z}})^T \mathbf{A}_{\omega_r}'' \hat{\mathbf{z}} \\ \hat{\mathbf{x}} = \mathbf{T}\hat{\mathbf{z}}\ , \end{cases} \tag{6.43}$$

where $\hat{\mathbf{z}} \in R^4$ contains the observer states, and $\hat{\omega}_r$ is the estimated speed. The matrices in the observer are

$$\begin{array}{ll} \mathbf{A}_0' = \mathbf{T}^{-1}\mathbf{A}_0\mathbf{T} & \mathbf{A}_{\omega_r}' = \mathbf{T}^{-1}\mathbf{A}_{\omega_r}\mathbf{T} \\ \mathbf{B}' = \mathbf{T}^{-1}\mathbf{B} & \mathbf{C}' = \mathbf{C}\mathbf{T}\ , \end{array}$$

and $\mathbf{A}_{\omega_r}''$ is a matrix composed by the two first rows of $\mathbf{A}_{\omega_r}'$. $\mathbf{K}$ and κ are design constants. $\mathbf{K}$ is chosen such that the LMI (5.28), described in Section 5.2.2, is feasible, and κ is chosen such that the convegence speed of $\hat{\omega}_r$ is suitable.

The connecting variables between the two subsystems are the speed and torque. Of these only the speed is directly available from the observer (6.43). However, using c_9 the torque can be calculated whenever the states of the motor are known. When the estimates of the states are used c_9 becomes,

$$c_9 \ : \ \hat{T}_e = 1.5 z_p L_m' \left(\hat{i}_{md}\hat{i}_{sq} - \hat{i}_{mq}\hat{i}_{sd} \right)\ ,$$

where $\hat{i}_{sd}$, $\hat{i}_{sq}$, $\hat{i}_{md}$ and $\hat{i}_{mq}$ are estimates of states in the original system presented in (6.42).

This observer is, as mentioned in the beginning of this subsection, developed under the assumption that the speed is constant i.e. $\frac{d\omega_r}{dt} = 0$. This assumption is not correct during transient phases, therefore it is expected that problems can arise when transients occur in the speed.

6.6 Observer Based Fault Detection and Isolation

In this section one ARR and three residual observers are designed. These are based on the four minimal over-constrained subsystems identified in Section 6.4.3. The design of the observers is partly based on the theory presented in Section 6.2, and partly based on a proposition presented in this section, which states the stability condition for the observers. Results obtained using the developed residual observers on the test setup are presented in Section 6.7.

6.6.1 The Residual Generators

Looking at the constraints forming the set $\mathcal{C}_{m2} = \{c_8, c_{13}, c_{14}, c_{15}\}$ it is seen that no differential constraints are included in this. Therefore an ARR obtained from this set

does not include derivatives. The ARR is given by,

$$r_2 = -a_{h2}y_4^2 + a_{h1}\hat{\omega}_r y_4 + a_{h0}\hat{\omega}_r^2 - y_3 \ . \tag{6.44}$$

It is also possible to obtain ARR's from the sets $\mathcal{C}_{m1}$, $\mathcal{C}_{m3}$ and $\mathcal{C}_{m4}$, but because a differential constraint is used in each of these sets, it is necessary to use derivatives of the output in these cases. To avoid this, three residual observers are developed in the following. The constraints contained in the sets $\mathcal{C}_{m1}$, $\mathcal{C}_{m3}$ and $\mathcal{C}_{m4}$ are given by (6.36), and are reproduced below for convenience,

$$\begin{aligned}
\mathcal{C}_{m1} &= \{d_5, c_5, c_9, c_{14}, c_{15}, c_{16}\} \\
\mathcal{C}_{m3} &= \{d_5, c_5, c_8, c_9, c_{13}, c_{15}, c_{16}\} \\
\mathcal{C}_{m4} &= \{d_5, c_5, c_8, c_9, c_{13}, c_{14}, c_{16}\} \ ,
\end{aligned}$$

where the constraints are given by,

$$\begin{aligned}
d_5 &: \quad \dot{\omega}_r = \tfrac{d\omega_r}{dt} \\
c_5 &: \quad J\dot{\omega}_r = T_e - B\omega_r - T_p \\
c_8 &: \quad H_p = -a_{h2}Q_p^2 + a_{h1}Q_p\omega_r + a_{h0}\omega_r^2 \\
c_9 &: \quad T_p = -a_{t2}Q_p^2 + a_{t1}Q_p\omega_r + a_{t0}\omega_r^2 \\
c_{13} &: \quad y_3 = H_p \\
c_{14} &: \quad y_4 = Q_p \\
c_{15} &: \quad \hat{\omega}_r = \omega_r \\
c_{16} &: \quad \hat{T}_e = T_e \ .
\end{aligned}$$

Comparing the sets $\mathcal{C}_{m1}$, $\mathcal{C}_{m3}$ and $\mathcal{C}_{m4}$ with the structure of (6.4), the vector field $\mathbf{f}_x$ is formed by the constraint c_5, the map $\mathbf{m}_x$ is formed by a subset of $\{c_8, c_9\}$, and the map $\mathbf{h}_x$ is formed by a subset of $\{c_{13}, c_{14}, c_{15}, c_{16}\}$. Using Corollary 6.2.1 on these sets it is shown that the sets $\mathcal{C}_{m1}$, $\mathcal{C}_{m3}$ and $\mathcal{C}_{m4}$ all can be transformed to systems with the following structure,

$$\begin{aligned}
\tfrac{dx_d}{dt} &= ax_d + f_x(x_d, v_1, u) + \mathbf{e}_1(x_d, v_1, u, \mathbf{f}) \\
g(v_1, v_2, u) &= h(x_d) + \mathbf{e}_2(x_d, v_1, v_2, u, \mathbf{f}) \ ,
\end{aligned} \tag{6.45}$$

where the state of the system $x_d = \omega_r$, the input $u = \hat{T}_e$, the outputs $v_1, v_2 \in \{\hat{\omega}_r, y_3, y_4\}$, and $\mathbf{f}$ is a vector containing the fault signals. This shows that the algebraic variables in system $\mathcal{C}_{m1}$, $\mathcal{C}_{m3}$ and $\mathcal{C}_{m4}$ can be decoupled using a transformation of the output equations only. For the three obtained systems the following assumption holds.

Assumption 6.6.1 *It is assumed that in the case where no faults have occurred, i.e.* $\mathbf{f} = 0$*, the output map* h *in (6.45) can be solved for* x_d *locally. Let this solution be given by,*

$$x_d = \tilde{g}(v_1, v_2, u) \ . \tag{6.46}$$

Using the above assumption the following proposition describes a residual observer for the system described by (6.45).

Proposition 6.6.1 *Under Assumption 6.6.1 the following observer is a residual observer for systems described by (6.45),*

$$\begin{array}{l} \frac{\hat{x}_d}{dt} = a\hat{x}_d + f_x(\tilde{g}(v_1, v_2, u), v_1, u) + k(\tilde{g}(v_1, v_2, u) - \hat{x}_d) \\ r = q(\tilde{g}(v_1, v_2, u) - \hat{x}_d) \end{array} . \tag{6.47}$$

The residual observer is asymptotical stable if $a-k < 0$. The fault input to this observer is given by,

$$f_f = (f_x(x_d, v_1, u) - f_x(x_d + \delta x_f, v_1, u)) + e_1(x_d, v_1, u, \mathbf{f}) - k\delta x_f \ ,$$

where f_f is a derived fault signal, which is strongly detectable. In the expression of f_f the signal δx_f is given by,

$$\delta x_f = h^{-1}(g(v_1, v_2, u) - \mathbf{e}_2(x_d, v_1, v_2, u, \mathbf{f})) - \tilde{g}(v_1, v_2, u) \ .$$

Proof: In the no fault case $\mathbf{f} = 0$ the observer error equation becomes,

$$\begin{aligned} \dot{e} &= (ax_d + f_x(x_d, v_1, u)) - (a\hat{x}_d + f_x(x_d, v_1, u) + k(x_d - \hat{x}_d)) \\ \dot{e} &= (a-k)e \end{aligned} \tag{6.48}$$

where (6.46) is used in the observer expression (6.47), meaning that $\tilde{g}(v_1, v_2, u) = x_d$. Equation (6.48) shows that the error dynamic of the observer is asymptotical stable if $a - k < 0$.

The expression of the derived fault signal f_f is obtained in the following by introducing the fault signals in the error equation of the observer. First, an expression of the fault when mapped through g is obtained. To this end define the function $\tilde{g}_f$ as,

$$g_f(v_1, v_2, u) = g(v_1, v_2, u) - \mathbf{e}_2(x_d, v_1, v_2, u, \mathbf{f}) = h(x_d)$$

From this expression it is seen that the function g_f must be used to obtain a map from the measurements v_1 and v_2 to the state x_d if a fault $\mathbf{f}$ has occured, i.e.

$$x_d = \tilde{g}_f(v_1, v_2, u) = h^{-1}(g(v_1, v_2, u) - \mathbf{e}_2(x_d, v_1, v_2, u, \mathbf{f}))$$

Define δx_f and x_f as $\delta x_f = x_d - x_f$ and $\delta x_f = \tilde{g}_f(y_1, y_2, u) - \tilde{g}(y_1, y_2, u)$ respectively. Using these signals the observer error equation, in the faulty case, i.e. $\mathbf{f} \neq 0$, becomes,

$$\begin{aligned} \dot{e} =& ae + f_x(x_d, y_1, u) - f_x(x_f, y_1, u) + \mathbf{e}_1(x, y_1, \mathbf{f}) - k(x_f - \hat{x}) \\ \dot{e} =& (a-k)e + (f_x(x_d, y_1, u) - f_x(x_d - \delta x_f, y_1, u)) + \mathbf{e}_1(x, y_1, \mathbf{f}) - k\delta x_f \end{aligned} \tag{6.49}$$

From this expression the following nonlinear expression of the fault can be identified,

$$f_f = (f_x(x_d, y_1, u) - f_x(x_d + \delta x_f, y_1, u)) + \mathbf{e}_1(x, y_1, \mathbf{f}) - k\delta x_f$$

Including this fault expression in the error equation (6.49) it becomes,

$$\dot{e} = (a-k)e + f_f$$
$$r = qe$$

From this expression it is seen that the derived fault signal f_f is strongly detectable. □

Remark 6.6.1 *The derived fault f_f is strongly detectable using this observer. This is not the case for the faults in* $\mathbf{f}$*, as the nonlinear expression of f_f can equal zero even though one of the entries in* $\mathbf{f}$ *is different from zero.*

Remark 6.6.2 *The observer described by Proposition 6.6.1 is designed under the assumption that a perfect model exists, and that the measurements are not affected by noise. This is, of course, not fulfilled in real life applications. To overcome this the gain k of the observer is chosen such that errors due to small model mismatchs and noise will be suppressed.*

Using Corollary 6.2.1 and Proposition 6.6.1 on the three over-constrained subsystems $\mathcal{C}_{m1}$, $\mathcal{C}_{m3}$, and $\mathcal{C}_{m4}$, the following three residual observers are obtained,

$$\mathcal{O}_{m1}: \begin{cases} J\frac{d\hat{x}_d}{dt} = -B\hat{x}_d - f_T(y_4, \hat{\omega}_r) + \hat{T}_e + k_1(\hat{\omega}_r - \hat{x}_d) \\ r_1 = q_1(\hat{\omega}_r - \hat{x}_d) \end{cases} \tag{6.50}$$

$$\mathcal{O}_{m3}: \begin{cases} J\frac{d\hat{x}_d}{dt} = -B\hat{x}_d - f_T(g_3(\hat{\omega}_r, y_3), \hat{\omega}_r) + \hat{T}_e + k_3(\hat{\omega}_r - \hat{x}_d) \\ r_3 = q_3(\hat{\omega}_r - \hat{x}_d) \end{cases} \tag{6.51}$$

$$\mathcal{O}_{m4}: \begin{cases} J\frac{d\hat{x}_d}{dt} = -B\hat{x}_d - f_T(y_4, g_4(y_3, y_4)) + \hat{T}_e + k_4(g_4(y_3, y_4) - \hat{x}_d) \\ r_4 = q_4(g_4(y_3, y_4) - \hat{x}_d) \end{cases} \tag{6.52}$$

where k_i is designed according to Proposition 6.6.1 and q_i is chosen such that the residuals have a reasonable value in the case of faults. The function f_T is given by

$$f_T(Q_p, \omega_r) = -a_{t2}Q_p^2 + a_{t1}Q_p\omega_r + a_{t0}\omega_r^2 \,,$$

and the functions g_3 and g_4 are derived from the output map h in (6.45), and are given by,

$$g_3(\hat{\omega}_r, y_3) = \frac{a_{h1}\hat{\omega}_r + \sqrt{a_{h1}^2\hat{\omega}_r^2 - 4a_{h2}(y_3 - a_{h0}\hat{\omega}_r^2)}}{2a_{h2}}$$
$$g_4(y_3, y_4) = \frac{-a_{h1}y_4 + \sqrt{a_{h1}^2y_4^2 + 4a_{h0}(y_3 + a_{h2}y_4^2)}}{2a_{h0}} \,.$$

These expressions are valid for $\hat{\omega}_r, y_4 \in R_+$ when the parameters of the pump used in the test are considered. Therefore the expressions are valid in the state space $\omega_r, Q \in R_+$, which is exactly the state space in which the model is valid, see Section 3.5.

6.7 Test Results

The final FDI algorithm is obtained by composing the adaptive observer developed in Section 6.5, and the residual generators developed in Section 6.6. The structure of the FDI algorithm is depitch in Fig. 6.4. In this algorithm the adaptive observer is used for

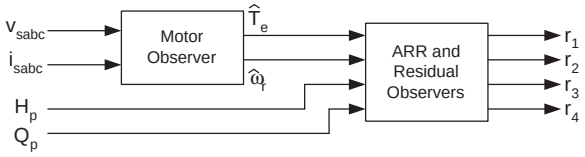

Figure 6.4: The final detection algorithm. The first part is the motor observer described in Section 6.5, and the second part is composed of the ARR and residual observers described in Section 6.6.

estimating the connection variables ω_r and T_e, based on the supply voltage $\mathbf{v}_{sabc}$ and the motor current $\mathbf{i}_{sabc}$. These connection variables are then, together with the flow and pressure measurement Q_p and H_p, used as input to the residual generators.

This detection algorithm is in the following tested on a Grundfos 1.5 (KW) CR5-10 pump. This pump is placed in a tank system as depicted in Fig. 6.5. In this tank system

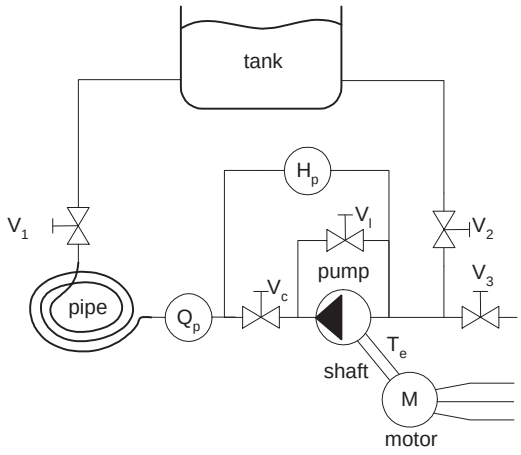

Figure 6.5: Sketch of the test setup. The measurements are the electrical quantitatives, the differential pressure H_p delivered by the pump and the volume flow through the pump Q_p.

the valve V_1 is used to model disturbances in the system. Clogging inside the pump is

modelled by the valve V_c and dry running is modelled by closing V_2 and opening V_3. Rub impact is modelled by adding an extra force to the shaft and cavitation is modelled by closing valve V_2 gradually. Leakage flow is modelled by opening V_l.

Test results have shown that the sensitivity to the faults f_c and f_d of the observer $\mathcal{O}_{m4}$ is very low. Infact it is so low that changes due to the faults are smaller than changes due to noise and parameter variations. Moreover in Section 6.4.3 it is shown that the obtainable fault information is included in the residuals r_1, r_2, and r_3. Therefore only these residuals are considered in the test presented in this section.

Since the tests are performed on a real system, noise is expected on the residuals. To overcome this problem a CUSUM algorithm (Basseville and Nikiforov, 1998) is used to detect changes in the mean of the residuals and thereby detect the faults. The CUSUM algorithm is shortly described in Appendix B.1. In the following, outputs of the CUSUM algorithms are denoted D_1 to D_3, where D_1 is the decision signal of r_1 and so forth.

All test results are shown in Fig. 6.6, Fig. 6.7 and Fig. 6.8. First robustness with respect to the operating point is tested. In this test both the position of the valve V_1 and the speed of the pump are changed during operation. During the test the valve is changed in three steps from medium to maximum opened. The speed of the pump is changed between 2380 and 2910 (rpm) each 2 (sec) during the test. The result of this test is shown in Fig. 6.6(a), where r_1 to r_3 are shown in the top figure and the decision signals D_1 to D_3 in the bottom figure. The test shows that the three residual generatores are robust with respect to the tested operating points, but also that there are some dependency to the operating point, see top figure of Fig. 6.6(a), This is partly due to problems with the flow sensor at zero flow and partly due to dependency between the parameters and the operating point.

Figures 6.6(b) to 6.8(b) show test results concerning isolability of the five faults considered in this chapter. All these tests are performed with V_1 half opened and an angular speed of approximately 2650 (rpm). Comparing D_1, D_2, and D_3 in the five figures it is seen that the faults are distinguishable except for cavitation and dry running shown in Fig.6.8(a) and Fig. 6.8(b) respectively. This was expected as the structural analysis in Section 6.4.3 already had predicted this.

6.8 Discussion

The first topic of the work presented in this chapter is realization of over-constrained subsystems identified using Structural Analysis (SA). It is well known that there is a straightforward connection between Analytical Redundant Relations (ARR's) and minimal over-constrained subsystem. Unfortunately, the obtained ARR's are in general functions of the derivatives of the measurements, which are difficult to calculate when the measurements are corrupted by noise.

To overcome this problem a new method for rewriting a subsystem identified using SA to a state space description is developed. The obtained state space description has the property, that the only unknown variables are the states of the system. The state space

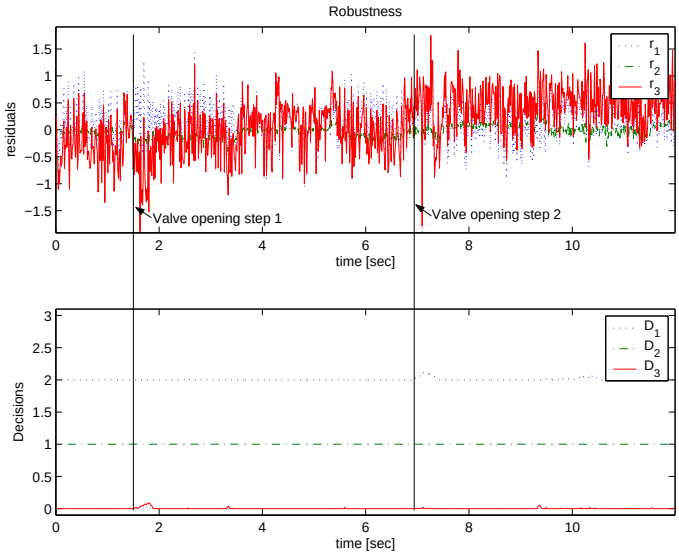

(a) Robustness test.

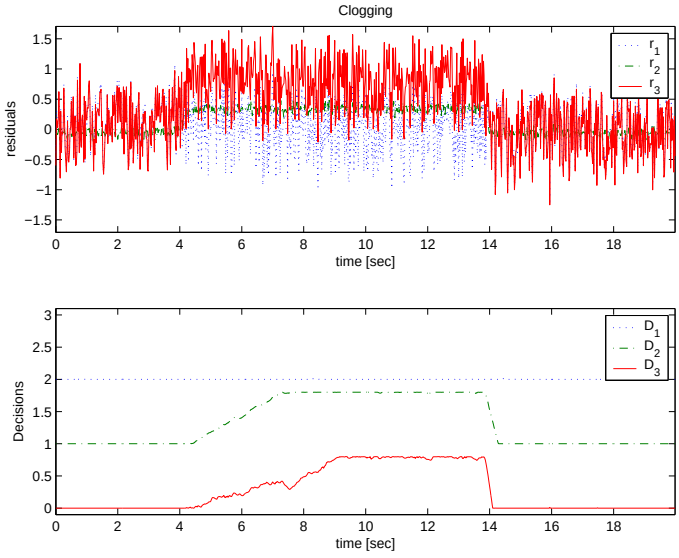

(b) Detection of the fault K_f clogging.

Figure 6.6: Test results from test of the developed algorithms on the test setup. The top figures shows the obtained residuals and the bottom figures shows decision signals obtained from CUSUM algorithms.

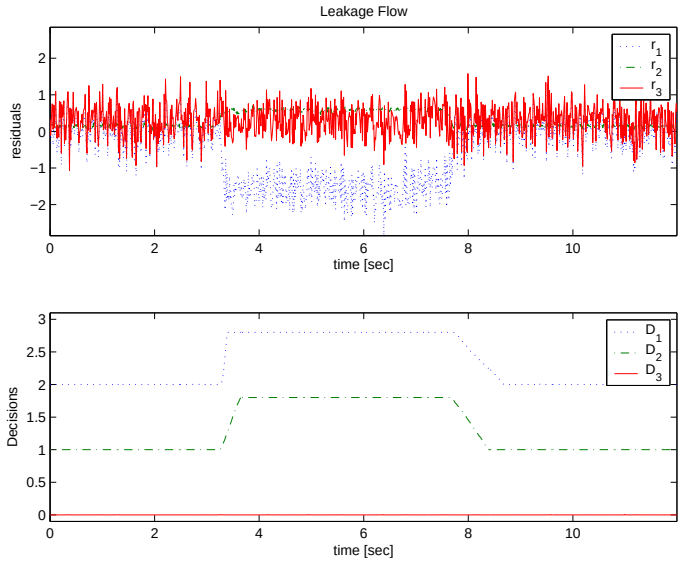

(a) Detection of the fault K_l leakage flow.

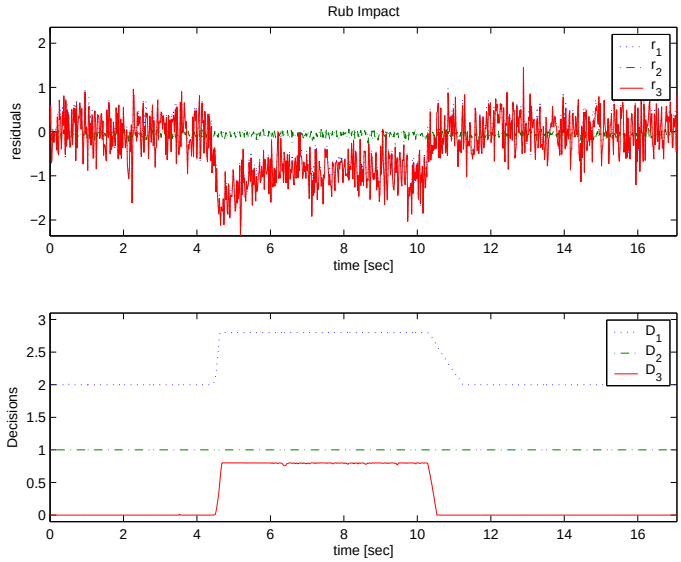

(b) Detection of the fault ΔB rub impact.

Figure 6.7: Test results from test of the developed algorithms on the test setup. The top figures shows the obtained residuals and the bottom figures shows decision signals obtained from CUSUM algorithms.

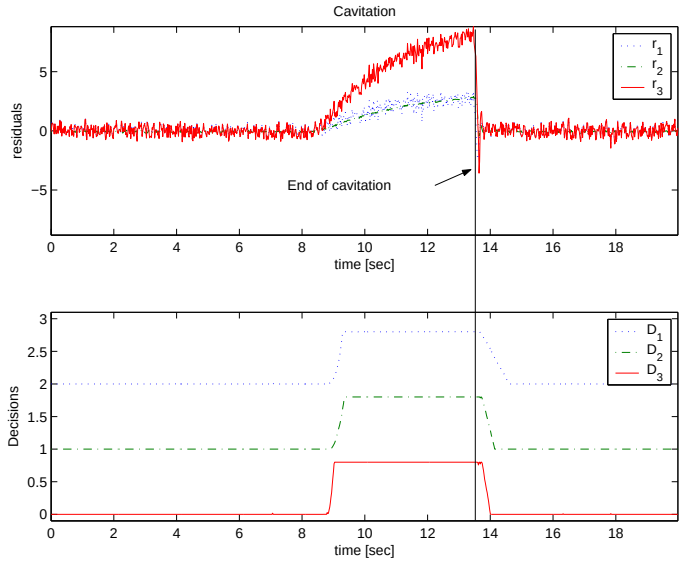

(a) Detection of the fault f_c cavitation.

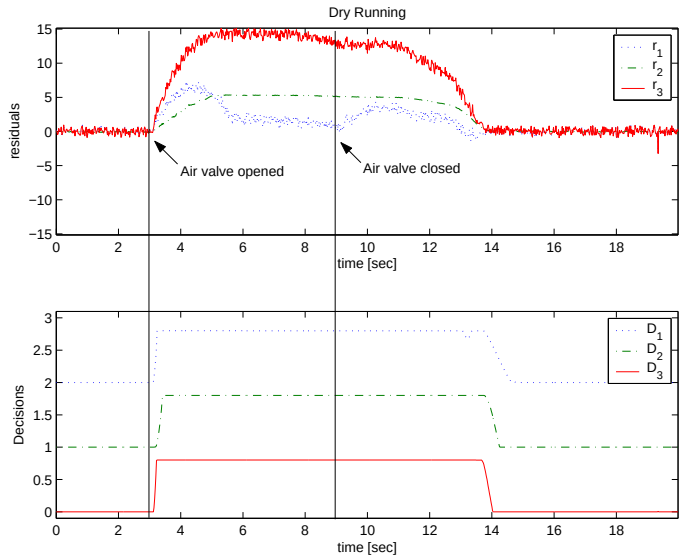

(b) Detection of the fault f_d dry running.

Figure 6.8: Test results from test of the developed algorithms on the test setup. The top figures shows the obtained residuals and the bottom figures shows decision signals obtained from CUSUM algorithms.

description can then be used for derivation of residual observers. In the design of these observers decoupling of unknown inputs has not to be considered, as the only unknown variables are the states of the system. The method is tested on a satellite model, showing that a residual observer can be obtained using this approach. Moreover the method is used to develop residual observer for the centrifugal pump application, which is the second topic of the chapter.

The second topic of the chapter is fault detection and isolation in a centrifugal pump placed in an arbitrary hydraulic application. An algorithm, which is capable of detection and isolation of five faults in a centrifugal pump, is developed. The proposed alogrithm is independent of the application in which the pump is placed. This makes the algorithm robust and usable in a wide range of applications, such as submersible application, waste water application, and heating application.

Tests have shown that it is possible to distinguish between four of the five faults under consideration, using three chosen residuals. But it is also shown that the algorithm is sensitive to the operating point. This is partly due to dependency between the operating point and the parameters in the model and partly due to flow sensor problems at zero flow. Even though the algorithm has a small inherent dependency of the operating point, it still performs considerably better than algorithms built on a linearized model, when the operating point is changed.

Chapter 7

FDI on the Centrifugal Pump: A Steady State Solution

In this chapter Structural Analysis (SA) is utilized to derive Analytical Redundant Relations (ARR's), which can be used for fault detection. The concept of SA is described in Section 6.1 in the previous chapter. The obtained ARR's are based on a steady state model of the pump. Here a steady state model denotes a model describing the pump under constant speed, pressure and flow conditions. The developed detection algorithm is only using electrical measurements on the motor, and the pressure and flow measurements on the centrifugal pump. The electrical measurements are in this case Root Mean Square (RMS) measurements of the voltage and current, the voltage frequency, and the electrical angle between the voltage and current. These measurements become constant when the system is running under steady state conditions, and can therefore be sampled at any given sample rate, provided the steady state conditions. Therefore, by using only these measurements the microprocessor load of the derived algorithm can be chosen freely. Moreover, the steady state measurements of the electrical signals are sometimes made available by modern motor protection units. All in all this makes the algorithm suitable for implementation in cost sensitive products.

The obtained algorithm is robust with respect to parameter variations and the operating point of the pump respectively, making it usable in real life applications. In the development of the FDI algorithm, the approach, presented in Section 6.4, of dividing the system into two cascade-connected subsystems is used. This is done to avoid two large residual expressions. The first of these subsystems consists of the electrical part of the induction motor driving the pump, and the second subsystem consists of the mechanical and hydraulic part of the pump. Theoretical considerations regarding to Structural Analysis (SA) are, among others, found in (Blanke et al., 2003; Izadi-Zamanabadi, 2001).

The faults, which only affect the second subsystem, are detected using Analytical

Redundancy Relations (ARR's). These relations are obtained through the utilization of structural analysis (Blanke et al., 2003) and the Groebner basis algorithm (Cox et al., 1997). Using this approach the obtained ARR's are polynomial. This is utilized in the development of a detection algorithm, which is robust with respect to parameter variations. Theoretical results on using the Groebner basis are given in (Staroswiecki and Comtet-Varga, 2001). Moreover, an overview of model-based methods using ARR's is given in (Staroswiecki, 2000).

This chapter starts by presenting the steady state model of a centrifugal pump placed in an arbitrarily hydraulic application. This is done in Section 7.1. Structural analysis on the derived steady state model is considered in Section 7.2, which includes; the division of the system into two suitable subsystems, derivation of an expression for calculating the connecting variables, and ARR expressions for fault detection. In Section 7.3 a method for robust fault detection using ARR's is considered. Section 7.4 presents some test results obtained on the industrial test bench, which also was used to obtain the test results presented in Chapter 6. Finally concluding remarks end the chapter.

7.1 Steady State Model of the System

In this section, the model of the centrifugal pump derived in Chapter 3, is reformulated to describe the pump under steady state conditions, only. The section is divided into three subsections, where the first one is concerned with the steady state model of the motor. The second one is concerned with the steady state model of the mechanical and hydraulic parts of the pump, and finally the last one is concerned with fault modelling. The obtained model will in the following be used in the derivation of a FDI algorithm based on low bandwidth measurements, such as Root Mean Square (RMS) measurement of the electrical quantities.

7.1.1 Steady State Motor Model

The model of the induction motor is described in Section 3.2. In this section both a model of a $\mathbf{Y}$-connected and a Δ-connected motor is derived. The obtained models are prestented in (3.9) and (3.10) respectively. Comparing these models it is seen that the following equations describe the motor in both cases,

$$\begin{aligned} \mathbf{L}'_s \tfrac{d\mathbf{i}_{sdq}}{dt} =& -(\mathbf{R}_s + \mathbf{R}'_r)\,\mathbf{i}_{sdq} + (\mathbf{R}'_r - z_p\omega_r \mathbf{J}\mathbf{L}'_m)\,\mathbf{i}_{mdq} + \mathbf{v}_{sdq} \\ \mathbf{L}'_m \tfrac{d\mathbf{i}_{mdq}}{dt} =& \mathbf{R}'_r \mathbf{i}_{sdq} - (\mathbf{R}'_r - z_p\omega_r \mathbf{J}\mathbf{L}'_m)\,\mathbf{i}_{mdq}\ . \end{aligned} \tag{7.1}$$

The variables $\mathbf{v}_{sdq}$, $\mathbf{i}_{sdq}$, and $\mathbf{i}_{mdq}$ are in general unknown. However, in the $\mathbf{Y}$-connected case the measurable electrical quantities at the terminals of the motor $\mathbf{i}_{tdq}$ and $\mathbf{v}_{tdq}$ equals $\mathbf{i}_{sdq}$ and $\mathbf{v}_{sdq}$ respectively. In the Δ-connected case these currents and voltages are given by the transformations $\mathbf{i}_{tdq} = \mathbf{C}_i\mathbf{i}_{sdq}$ and $\mathbf{v}_{sdq} = \mathbf{B}_v\mathbf{v}_{tdq}$ respectively, see Section 3.2.3.

To obtain a steady state model of the motor, a transformation of the motor states is used. This transformation takes the states described in the stator fixed reference frame $\mathbf{x}_{dq}$ and transform these to an arbitrary frame. In this case the arbitrary frame rotates with the frequency of the supply voltage ω_e. The new states are denoted $\mathbf{x}^e_{dq}$. The transformation is given by $\mathbf{x}_{dq} = \mathbf{T}(\theta_e)\mathbf{x}^e_{dq}$, where θ_e is the angle between the stator fixed frame and the arbitrary rotating frame. $\mathbf{T}$ is given by

$$\mathbf{T}(\theta_e) = \begin{bmatrix} \cos(\theta_e) & -\sin(\theta_e) \\ \sin(\theta_e) & \cos(\theta_e) \end{bmatrix} , \tag{7.2}$$

where θ_e is a function of time. Using this transformation to transform $\mathbf{v}_{sdq}$, $\mathbf{i}_{sdq}$, and $\mathbf{i}_{mdq}$, a new model is obtained with the property that all states are constant during steady state operation. Setting the derivatives of the states equal to zero, the following steady state model of the motor is obtained,

$$\begin{aligned} -\omega_e L'_s I^e_{sq} &= -(R_s + R'_r)I^e_{sd} + (R'_r I^e_{md} - z_p\omega_r L'_m I^e_{mq}) + V^e_{sd} \\ \omega_e L'_s I^e_{sd} &= -(R_s + R'_r)I^e_{sq} + (R'_r I^e_{mq} + z_p\omega_r L'_m I^e_{md}) + V^e_{sq} \\ -\omega_e L'_m I^e_{mq} &= -(R'_r I^e_{md} - z_p\omega_r L'_m I^e_{mq}) + R'_r I^e_{sd} \\ \omega_e L'_m I^e_{md} &= -(R'_r I^e_{mq} + z_p\omega_r L'_m I^e_{md}) + R'_r I^e_{sq} \ . \end{aligned}$$

Defining $I^e_{sd} = 0$ in the above model, meaning that the rotating reference frame is aligned with the current I^e_{sq}, the final steady state model of the motor is obtained,

$$\begin{aligned} -\omega_e L'_s I^e_{sq} &= (R'_r I^e_{md} - z_p\omega_r L'_m I^e_{mq}) + V^e_{sd} \\ 0 &= -(R_s + R'_r)I^e_{sq} + (R'_r I^e_{mq} + z_p\omega_r L'_m I^e_{md}) + V^e_{sq} \\ -\omega_e L'_m I^e_{mq} &= -(R'_r I^e_{md} - z_p\omega_r L'_m I^e_{mq}) \\ \omega_e L'_m I^e_{md} &= -(R'_r I^e_{mq} + z_p\omega_r L'_m I^e_{md}) + R'_r I^e_{sq} \ . \end{aligned} \tag{7.3}$$

The torque expression of the motor is given in (3.11) and repeated here for the sake of convenience,

$$T_e = \frac{3}{2} z_p L'_m \left(i_{md} i_{sq} - i_{mq} i_{sd}\right) \ .$$

Using the transformation $\mathbf{T}$, given in (7.2), a torque expression of the new variables is obtained. The expression becomes

$$T_e = \frac{3}{2} z_p L'_m \left(I^e_{md} I^e_{sq}\right) \ . \tag{7.4}$$

Equations (7.3) and (7.4) form the model of the induction motor during steady state operations. However, the electrical quantities V^e_{sd}, V^e_{sq}, and I^e_{sq} are not directly measurable. Therefore, a connection between these quantities and the measurable quantities must be established. The measurable quantities are the RMS values of the supply voltage V_{rms} and current I_{rms}, the supply frequency ω_e and the electrical angle between the voltage

and current ϕ. The angle ϕ is in this case defined as the angle between the voltage vector $\mathbf{V}^e_{tdq} = \begin{bmatrix} V^e_{td} & V^e_{tq} \end{bmatrix}^T$, and the current vector $\mathbf{I}^e_{tdq} = \begin{bmatrix} 0 & I^e_{tq} \end{bmatrix}^T$, where subscript t denotes quantities available at the terminals of the motor. The Euclidean length of the vectors $\mathbf{V}^e_{tdq}$ and $\mathbf{I}^e_{tdq}$ is connected to the RMS values of the measurable electrical quantities by $|\mathbf{V}^e_{tdq}| = \sqrt{2}V_{rms}$ and $|\mathbf{I}^e_{tdq}| = \sqrt{2}I_{rms}$. Using the RMS values V_{rms} and I_{rms} and the angle ϕ the voltages V^e_{td} and V^e_{tq}, and the current I^e_{tq} can be calculated using

$$V^e_{td} = -\sqrt{2}V_{rms}\sin(\phi) \qquad V^e_{tq} = \sqrt{2}V_{rms}\cos(\phi) \qquad I^e_{tq} = \sqrt{2}I_{rms}\ . \tag{7.5}$$

In the case of a $\mathbf{Y}$-connected motor the electrical quantities at the motor terminals V^e_{td}, V^e_{tq}, and I^e_{tq} and the quantities V^e_{sd}, V^e_{sq}, and I^e_{sq} in (7.3) are equivalent. However, in the case of a Δ-connected motor the transformation matrices $\mathbf{B}_v$ and $\mathbf{C}_i$ have to be considered. These matrices are defined in Section 3.2.3. It can be shown that

$$\mathbf{B}_v = \sqrt{3}T_\Delta \qquad\qquad \mathbf{C}_i^{-1} = \frac{1}{\sqrt{3}}T_\Delta\ ,$$

where T_Δ is a rotation matrix. Using these expressions in (7.1) to obtain the steady state model, it is seen that (7.3) can be used to model the steady state operation of the motor when it is connected in a Δ-connection if the following scalings of the electrical quantities are used,

$$V^e_{td} = \sqrt{3}V^e_{td} \qquad V^e_{tq} = \sqrt{3}V^e_{tq} \qquad I^e_{sq} = \frac{1}{\sqrt{3}}I^e_{tq}\ . \tag{7.6}$$

7.1.2 Steady State Pump Model

The hydraulic and the mechanical parts of the pump are derived in Section 3.4 and Section 3.3 respectively. Moreover, a model of a general hydraulic application is given in Section 6.3.2. In Section 3.4 it is shown that the mechanical part is described by the following differential equation,

$$J\frac{d\omega_r}{dt} = T_e - B\omega_r - T_p$$

where T_e is the torque produced by the motor, ω_r is the speed of the shaft, and T_p the load torque produced by the pump. Under steady state operation the speed is constant, i.e. $\frac{d\omega_r}{dt} = 0$, meaning that the steady state model of the mechanical part becomes,

$$0 = T_e - B\omega_r - f_T(Q_p, \omega_r)\ . \tag{7.7}$$

The hydraulic parts of the pump is considered as the parts involved with the energy transformation from mechanical to hydraulic energy. In the model derived in Section 3.3 this energy transformation is described by two maps given by

$$T_p = f_T(Q_p, \omega_r) \qquad\qquad H_p = f_H(Q_p, \omega_r)\ , \tag{7.8}$$

where T_p and H_p are the load torque and pressure produced by the pump respectively. The arguments of the maps f_T and f_H in (7.8) are the volume flow Q_p and the speed of the pump ω_r. The maps f_T and f_H are given by,

$$\begin{aligned} f_H(Q_p, \omega_r) &= \rho g \left(-a_{h2} Q_p^2 + a_{h1} Q_p \omega_r + a_{h0} \omega_r^2\right) \\ f_T(Q_p, \omega_r) &= -a_{t2} Q_p^2 + a_{t1} Q_p \omega_r + a_{t0} \omega_r^2 \ . \end{aligned}$$

A general model of a hydraulic application of a centrifugal pump is given in Section 6.3.1. Here it is argued that such a model, in most cases, can be described by the following state space model,

$$\begin{aligned} \dot{\mathbf{x}}_Q &= \mathbf{f}_A(\mathbf{x}_Q, H_p, \mathbf{d}) \\ Q_p &= h_A(\mathbf{x}_Q) \ , \end{aligned}$$

where $\mathbf{x}_Q$ is the state vector of the application model, H_p and Q_p are the pressure and volume flow of the centrifugal pump, and $\mathbf{d}$ is a vector containing some unknown input signals to the application. If it is assumed that the derivative of the states $\dot{\mathbf{x}}_Q$ equals zero during steady state operation, the steady state model becomes,

$$\begin{aligned} 0 &= \mathbf{f}_A(\mathbf{x}_Q, H_p, \mathbf{d}) \\ Q_p &= h_A(\mathbf{x}_Q) \ . \end{aligned} \tag{7.9}$$

7.1.3 The Fault Models

In Section 6.3.2 five faults are included in the centrifugal pump model. These faults are all affecting the hydraulic part of the pump. The faults are,

1. clogging inside the pump,
2. increased friction due to either rub impact or bearing faults,
3. increased leakage flow,
4. performance degradation due to cavitation,
5. dry running.

In the model of the system used here, the hydraulic part of the pump is modelled by the maps f_H, f_T and the flow measurement. Introducing the faults described above, the description of the hydraulic part of the pump becomes,

$$\begin{aligned} H_p &= f_H(Q, \omega_r) - K_f Q^2 - C_{ch} f_c - C_{dh} f_d \\ T_p &= f_T(Q, \omega_r) + \Delta B \omega_r - C_{ct} f_c - C_{dt} f_d \\ y_3 &= Q - K_l \sqrt{H_p} \ . \end{aligned}$$

In this fault model $K_f \in R_+$ represents clogging, $\Delta B \in R_+$ represents rub impact, $K_l \in R_+$ represents increased leakage flow, $f_c \in R_+$ represents cavitation and $f_d \in R_+$ represents dry runnning. The first three signals model the faults accurately, while the last two terms are linear approximations.

7.2 Structural Analysis

In this section Structural Analysis (SA) is utilized to identify subsystems, which can be used for fault detection. Moreover, the results obtained in Section 6.4, on the division of the system into two cascade connected subsystem using SA is utilized here, too. This is done to avoid too large residual expressions. The equations forming the steady state model, derived in the previous section, are collected in (7.10). Here the four motor equa-

$$
\begin{array}{lcl}
c_1 & : & -\omega_e L'_s I^e_{sq} = A_1 + V^e_{sd} \\
c_2 & : & 0 = -(R_s + R'_r) I^e_{sq} + A_2 + V^e_{sq} \\
c_3 & : & -\omega_e L'_m I^e_{mq} = -A_1 \\
c_4 & : & \omega_e L'_m I^e_{md} = -A_2 + R'_r I^e_{sq} \\
c_5 & : & 0 = T_e - B\omega_r - T_p \\
c_6 & : & \mathbf{0} = \mathbf{f}_A(\mathbf{x}_Q, H_p, \mathbf{u}_Q) \\
c_7 & : & A_1 = R'_r I^e_{md} - z_p \omega_r L'_m I^e_{mq} \\
c_8 & : & A_2 = R'_r I^e_{mq} + z_p \omega_r L'_m I^e_{md} \\
c_9 & : & T_e = \frac{3}{2} z_p L_m \left(I^e_{sq} I^e_{md} \right) \\
c_{10} & : & H_p = -a_{h2} Q_p^2 + a_{h1} Q_p \omega_r + a_{h0} \omega_r^2 \\
c_{11} & : & T_p = -a_{t2} Q_p^2 + a_{t1} Q_p \omega_r + a_{t0} \omega_r^2 \\
c_{12} & : & Q_p = h_A(\mathbf{x}_Q) \\
c_{13} & : & Y_1 = I^e_{sq} \\
c_{14} & : & Y_2 = \omega_e \\
c_{15} & : & Y_3 = H_p \\
c_{16} & : & Y_4 = Q_p
\end{array}
\tag{7.10}
$$

tions in (7.3) are split into six equations to avoid using redundant structural information in the SA.

The graph representation of the constraints in (7.10) is shown in Table 7.1. From this table it is seen that the set of constaints $\mathcal{C}_e = \{c_1, c_2, c_3, c_4, c_7, c_9, c_{13}, c_{14}\}$ forms a match on the unknown variables contained in these constraints. Therefore, this part can be considered as a subsystem, with two outputs ω_r and T_e. These outputs are denoted the connecting variables between this subsystem and the remaining parts of the system. The set of constraints $\mathcal{C}_e$ is in the following denoted the first subsystem, whereas the remaining set of constraints $\mathcal{C}_m = \{c_5, c_6, c_{10}, c_{11}, c_{12}, c_{15}, c_{16}\}$ is denoted the second subsystem. This division of the system is equivalent to the division described in Chapter 6.

In Section 7.1.3 it is argued that the faults considered in this section only affect the hydraulic part of the pump. The hydraulic part of the pump is described by f_H, f_T and the expression of the flow measurement. These expressions are given by the constraints c_{10}, c_{11}, and c_{16}, which are included in $\mathcal{C}_m$ only. Therefore, only the second subsystem $\mathcal{C}_m$ is affected by the faults considered in this chapter, meaning that only this part must

Table 7.1: The structure table of the centrifugal pump system under steady state conditions. The symbols ① show a matching for the first part of the system.

	Known						Unknown												
	Y_1	Y_2	V^e_{sd}	V^e_{sq}	Y_3	Y_4	$\mathbf{x}_Q$	$\mathbf{u}_Q$	T_p	H_p	Q_p	T_e	ω_r	I^e_{md}	I^e_{mq}	A_1	A_2	I^e_{sq}	ω_e
c_6							1	1		1									
c_{12}							1				1								
c_5									1			1	1						
c_{11}									1		1		1						
c_{10}										1	1		1						
c_{15}					1					1									
c_{16}						1					1								
c_8													1	1	1		1		
c_9												①		1				1	
c_7													①	1	1	1			
c_4														①			1	1	1
c_3															①	1			1
c_1			1													①		1	1
c_2				1													①	1	
c_{13}	1																	①	
c_{14}		1																	①

be considered when FDI is applied.

7.2.1 Calculating the Connection Variables

The SA showed that the connecting variables ω_r and T_e should be calculable using the set of constraints,

$$\mathcal{C}_e = \{c_1, c_2, c_3, c_4, c_7, c_9, c_{13}, c_{14}\} .$$

Rewriting these constraints the following expression of the speed ω_r is obtained,

$$\hat{\omega}_r = \frac{L'_m \omega_e^2 L'_s I^e_{sq} + L'_m \omega_e V^e_{sd} - R'_r R_s I^e_{sq} + R'_r V^e_{sq}}{L'_m z_p (\omega_e L'_s I^e_{sq} + V^e_{sq})} , \tag{7.11}$$

where V^e_{sd}, V^e_{sq}, $I^e_{sq} = Y_1$, and $\omega_e = Y_2$ are assumed known. The torque T_e is also obtained by rewriting $\mathcal{C}_e$ resulting in the following expression,

$$\hat{T}_e = \frac{3 z_p I^e_{sq} (I^e_{sq} R_s - V^e_{sq})}{2\omega_e} . \tag{7.12}$$

As in the above expression V^e_{sq}, $I^e_{sq} = Y_1$, and $\omega_e = Y_2$ are assumed known in the torque expression.

In the speed and torque expression (7.11) and (7.12) the voltages V^e_{sd}, V^e_{sq}, and the current I^e_{sq} are calculated using the RMS values of the supply voltage V_{rms}, supply current I_{rms}, and angle between the voltage and current ϕ, defined in Section 7.1.1. This is done using (7.5), and in the case of a Δ-connected motor (7.6).

7.2.2 Structural Analysis on the Second Subsystem

The second subsystem is described by the set,

$$\mathcal{C}_{m1} = \{c_5, c_6, c_{10}, c_{11}, c_{12}, c_{15}, c_{16}\} .$$

Beside these constraints two extra constraints are added to model the estimation of the connecting variables $\hat{\omega}_r$ and $\hat{T}_e$. These constraints are given by

$$\begin{array}{rcl} c_{17} & : & T_e = \hat{T}_e \\ c_{18} & : & \omega_r = \hat{\omega}_r \ . \end{array} \tag{7.13}$$

Table 7.2 is a representation of the graph describing the structure of the second subsystem. In this table the column at the right hand side is added to show the connection between the faults in the system and the constraints. Using SA three minimal over-

Table 7.2: The structure table of the second system. The first two columns describe the structural connection between the constraints and the known and unknown variables respectively. Whereas the last column describes the connection between the constraints and the faults in the system.

	Known				Unknown							Faults				
	Y_3	Y_4	$\hat{T}_e$	$\hat{\omega}_r$	$\mathbf{x}_Q$	$\mathbf{u}_Q$	T_p	H_p	Q_p	T_e	ω_r	K_f	K_l	ΔB	f_c	f_d
c_6					1	1		1								
c_{12}					1				1							
c_5							1			1	1					
c_{11}							1		1		1			1	1	1
c_{10}								1	1		1	1			1	1
c_{15}	1							1								
c_{16}		1							1							
c_{17}			1							1						
c_{18}				1							1		1			

constraint subsystems are identified. These are given by the following three sets,

$$\begin{array}{l} \mathcal{C}_{m1} = \{c_5, c_{11}, c_{16}, c_{17}, c_{18}\} \\ \mathcal{C}_{m2} = \{c_5, c_{10}, c_{11}, c_{15}, c_{16}, c_{17}\} \\ \mathcal{C}_{m3} = \{c_{10}, c_{15}, c_{16}, c_{18}\} \ . \end{array} \tag{7.14}$$

The connections between these sets and the faults in the system are given by

$$\begin{array}{l} \mathcal{C}_{m1} : \{K_l, \Delta B, f_c, f_d\} \\ \mathcal{C}_{m2} : \{K_f, \Delta B, f_c, f_d\} \\ \mathcal{C}_{m3} : \{K_f, K_l, f_c, f_d\} \ . \end{array} \tag{7.15}$$

7.2.3 ARR's of the Pump

The constraints c_6 and c_{12}, describing the application in which the pump is placed, are not included in any of the set of constraints $\mathcal{C}_{m1}$, $\mathcal{C}_{m2}$, and $\mathcal{C}_{m3}$. Hence, any ARR based on these sets will not be affected by the application in which the pump is placed, i.e. it will be robust with respect to the application of the pump. The next step in the development of an ARR is to eliminate all unknown variables in this set. Although it could be done by hand, here the Groebner basis algorithm is used to guarantee residual expressions that are on polynomial form. The polynomial characteristic is utilized in next section to derive an algorithm, which takes parameter variations into account. In (Staroswiecki and Comtet-Varga, 2001) the Groebner basis is also used as a part of an algorithm to obtain ARR's.

The ARR obtained using the Groebner basis algorithm on the sets $\mathcal{C}_{m1}$, $\mathcal{C}_{m2}$, and $\mathcal{C}_{m3}$ are used to establish residual expressions on the following form,

$$r_{p_i} = \mathbf{f}_{p_i}(\mathbf{y}_{p_i})^T \mathbf{a}_{p_i}(\boldsymbol{\theta}_{p_i}) \qquad i \in \{1, 2, 3\}$$

where $\boldsymbol{\theta}_{p_i}$ is the parameter vector and $\mathbf{y}_{p_i}$ is the measurement vector. In this expression both $\mathbf{a}_{p_i}(\boldsymbol{\theta})$ and $\mathbf{f}_{p_i}(\mathbf{y})$ contain polynomial functions. In the following the parameter and measurement vectors $\boldsymbol{\theta}_{p_i}$ and $\mathbf{y}_{p_i}$, and the polynomial vector functions $\mathbf{f}_{p_i}$ and $\mathbf{a}_{p_i}$ are given for each set of constraints $\mathcal{C}_{m1}$, $\mathcal{C}_{m2}$, and $\mathcal{C}_{m3}$.

ARR based on the set of constraints $\mathcal{C}_{m1}$

The set of constraints $\mathcal{C}_{m1}$ contains the following parameters and measurements described on vector form,

$$\boldsymbol{\theta}_{p_1} = \begin{pmatrix} a_{t2} & a_{t1} & a_{t0} \end{pmatrix}^T \qquad \mathbf{y}_{p_1} = \begin{pmatrix} T_e & \omega_r & Y_4 \end{pmatrix}^T .$$

The polynomial vector functions $\mathbf{f}_{p_1}$ and $\mathbf{a}_{p_1}$ are given by

$$\mathbf{a}_{p_1}(\boldsymbol{\theta}_{p_1}) = \begin{pmatrix} 1 \\ a_{t2} \\ -a_{t1} \\ -a_{t0} \end{pmatrix} \qquad \mathbf{f}_{p_1}(\mathbf{y}_{p_1}) = \begin{pmatrix} T_e - B\omega_r \\ Y_4^2 \\ Y_4\omega_r \\ w_r^2 \end{pmatrix} .$$

ARR based on the set of constraints $\mathcal{C}_{m2}$

The set of constraints $\mathcal{C}_{m2}$ contains the following parameters and measurements described on vector form,

$$\boldsymbol{\theta}_{p_2} = \begin{pmatrix} a_{h2} & a_{h1} & a_{h0} & a_{t2} & a_{t1} & a_{t0} \end{pmatrix}^T \qquad \mathbf{y}_{p_2} = \begin{pmatrix} T_e & \omega_r & Y_3 \end{pmatrix}^T .$$

The polynomial vector functions $\mathbf{f}_{p_2}$ and $\mathbf{a}_{p_2}$ are given by

$$\mathbf{a}_{p_2}(\boldsymbol{\theta}_{p_2}) = \begin{pmatrix} a_{h2}^2 \\ a_{t2}^2 \\ a_{h2}a_{t1}a_{h1} - a_{t2}a_{h1}^2 + 2a_{h2}^2a_{t0} - 2a_{h2}a_{h0}a_{t2} \\ a_1(\theta) + a_2(\theta) \\ 2a_{h2}a_{t2}a_{t0} + a_{h2}a_{t1}^2 - 2a_{h0}a_{t2}^2 - a_{h1}a_{t2}a_{t1} \\ 2a_{h2}a_{t2} \end{pmatrix},$$

where

$$\begin{aligned} a_1(\theta) &= a_{t2}(a_{h0}^2a_{t2} + a_{h0}a_{h1}a_{t1} - a_{t0}a_{h1}^2) \\ a_2(\theta) &= a_{h2}(a_{t0}^2a_{h2} + a_{t0}a_{t1}a_{h1} - a_{h0}a_{t1}^2 - 2a_{h0}a_{t2}a_{t0}) \ , \end{aligned}$$

and

$$\mathbf{f}_{p_1}(\mathbf{y}_{p_1}) = \begin{pmatrix} B^2\omega_r^2 - 2BT_e\omega_r + T_e^2 \\ Y_3^2 \\ B\omega_r^3 - T_e\omega_r^2 \\ \omega_r^4 \\ Y_3\omega_r^2 \\ -Y_3T_e + BY_3\omega_r \end{pmatrix}.$$

ARR based on the set of constraints $\mathcal{C}_{m3}$

The set of constraints $\mathcal{C}_{m3}$ contains the following parameters and measurements described on vector form,

$$\boldsymbol{\theta}_{p_3} = \begin{pmatrix} a_{h2} & a_{h1} & a_{h0} \end{pmatrix}^T \qquad \mathbf{y}_{p_3} = \begin{pmatrix} \omega_r & Y_3 & Y_4 \end{pmatrix}^T .$$

The polynomial vector functions $\mathbf{f}_{p_3}$ and $\mathbf{a}_{p_3}$ are given by

$$\mathbf{a}_{p_3}(\boldsymbol{\theta}_{p_3}) = \begin{pmatrix} -1 \\ -a_{t2} \\ a_{t1} \\ a_{t0} \end{pmatrix} \qquad \mathbf{f}_{p_3}(\mathbf{y}_{p_3}) = \begin{pmatrix} Y_3 \\ Y_4^2 \\ Y_4\omega_r \\ \omega_r^2 \end{pmatrix}.$$

7.3 The Robust FDI Algorithm

The ARR's developed in the previous section depend on the parameters describing the pump. As the application treated in this work is a real system the model parameters are not matching the real parameters exactly over the whole operating range of the pump.

Moreover, the density of the liquid is not constant due to temperature changes and impurities in the liquid. This density affects the value of the parameters in the hydraulic model of the pump given by (3.29). Therefore, parameter variations must be taken into account, for the developed algorithms to be robust and thereby usable in real applications.

7.3.1 Robustness with Respect to Parameter Variations

The residuals are in this case calculated using functions on the form $r = \mathbf{f}(\mathbf{y})^T\mathbf{a}(\boldsymbol{\theta})$ as seen in Section 7.2.3. In these equations $r = 0$ when the parameter vector $\boldsymbol{\theta} = \boldsymbol{\theta}_0$ and no fault has occured in the system. Here $\boldsymbol{\theta}_0$ is the parameter vector used in the design of the residual generators. Robustness is now formulated as the problem of handling the residual generation problem when $\boldsymbol{\theta} \in \boldsymbol{\Theta}$, where $\boldsymbol{\Theta}$ is the set of possible parameter values including $\boldsymbol{\theta}_0$. This means that $r = 0$ is not necessary fulfilled in the no fault case anymore. However, in all real life systems it is assumed that r is bounded on the set $\boldsymbol{\Theta}$.

One way to treat the parameter variation problem, sketched above, is the use of a set-valued approach, as presented in for example (Tornill et al., 2000; Idrissi et al., 2001). When using this approach a set of possible residual values is obtained. If 0 is not in this set it can be concluded that there is a fault in the system in spite of parameter variations. This is formalized in the following definition,

Definition 7.3.1 *The set of possible residual values $\mathcal{R}$ has the following properties,*

- *If the system is not affected by faults i.e. $\mathbf{e} = \mathbf{0}$ then $0 \in \mathcal{R}$.*
- *If $0 \notin \mathcal{R}$ then there are faults in the system i.e. $\mathbf{e} \neq \mathbf{0}$*

where $\mathbf{e}$ is a given fault vector and $\mathcal{R} \subset R$ is a connected set.

Now let $r = g(\mathbf{y}, \boldsymbol{\theta})$ be an ARR describing the behaviour of a given system, where $\mathbf{y}$ contains the measurements and $\boldsymbol{\theta}$ contains the parameters in the ARR. For this ARR r only equals 0 in the no fault case, if the structure and parameters of the system are known exactly. When, for such a system, parameter uncertainties are taken into account the set of possible residuals $\mathcal{R}$ defined in Definition 7.3.1 is given by the following lemma,

Lemma 7.3.1 *If the set of possible parameters $\boldsymbol{\Theta}$ is a compact set, given by*

$$\boldsymbol{\Theta} = \{\boldsymbol{\theta} | \theta_i = [\underline{\theta_i}, \overline{\theta_i}],\ i = 1, \cdots, n\}\ , \tag{7.16}$$

where $\boldsymbol{\theta} \in R^n$, and the residual function $g : \mathcal{Y} \times \boldsymbol{\Theta} \rightarrow R$ is continuous on $\boldsymbol{\Theta}$ for all $\mathbf{y} \in \mathcal{Y} \subset R^m$, then the set of possible residual values, in the no fault case, is defined by the maximum value $\overline{r}$ and minimum value $\underline{r}$ of $\mathcal{R}$. These maximum and minimum values are given by

$$\overline{r} = \max_{\boldsymbol{\theta} \in \boldsymbol{\Theta}} g(\mathbf{y}, \boldsymbol{\theta})$$
$$\underline{r} = \min_{\boldsymbol{\theta} \in \boldsymbol{\Theta}} g(\mathbf{y}, \boldsymbol{\theta})\ .$$

This is a well known fact from mathematical analysis and the proof can be found in (Apostol, 1974). Using this lemma the boundaries of $\mathcal{R}$ can be calculated. Unfortunately it is not straightforward to calculate these maximum and minimum values. However, in the case treated in this work the function g can be separated into a function of the parameters and a function of the measurements i.e. $g(\mathbf{y}, \boldsymbol{\theta}) = \mathbf{f}(\mathbf{y})^T \mathbf{a}(\boldsymbol{\theta})$. When this is the case it is easy to see that one set of boundaries on the residual set $\mathcal{R}$ is given by

$$\begin{aligned} \overline{r} \leq r_{max} &= \sum_{i=1}^{k} \max_{\boldsymbol{\theta} \in \boldsymbol{\Theta}} \left(a_i(\boldsymbol{\theta}) f_i(\mathbf{y}) \right) \\ \underline{r} \geq r_{min} &= \sum_{i=1}^{k} \min_{\boldsymbol{\theta} \in \boldsymbol{\Theta}} \left(a_i(\boldsymbol{\theta}) f_i(\mathbf{y}) \right) \ . \end{aligned}$$

From these expression it is seen that only $a_i \ i = 1, \cdots, k$ is a function of the parameters $\boldsymbol{\theta}$. The maximum and minimum of a_i can be calculated offline, leaving only a sign check of f_i to be done online. This is expressed in the following lemma.

Lemma 7.3.2 *If $r = \mathbf{f}(\mathbf{y})^T \mathbf{a}(\boldsymbol{\theta})$ where $\mathbf{a}$ and $\mathbf{f}$ are two vector functions, which are continuous on respectively $\boldsymbol{\Theta}$ and $\mathcal{Y}$, then an upper (lower) boundary of $\overline{r}$ ($\underline{r}$) is given by*

$$\overline{r} \leq r_{max} = \sum_i r_{i,max} \qquad \underline{r} \leq r_{min} = \sum_i r_{i,min} \ ,$$

where

$$\begin{aligned} r_{i,max} &= \begin{cases} f_i(\mathbf{y}) \max_{\boldsymbol{\theta} \in \boldsymbol{\Theta}} \left(a_i(\boldsymbol{\theta}) \right) & \text{if} \quad f_i(\mathbf{y}) > 0 \\ f_i(\mathbf{y}) \min_{\boldsymbol{\theta} \in \boldsymbol{\Theta}} \left(a_i(\boldsymbol{\theta}) \right) & \text{otherwise} \end{cases} \\ r_{i,min} &= \begin{cases} f_i(\mathbf{y}) \min_{\boldsymbol{\theta} \in \boldsymbol{\Theta}} \left(a_i(\boldsymbol{\theta}) \right) & \text{if} \quad f_i(\mathbf{y}) > 0 \\ f_i(\mathbf{y}) \max_{\boldsymbol{\theta} \in \boldsymbol{\Theta}} \left(a_i(\boldsymbol{\theta}) \right) & \text{otherwise} \ . \end{cases} \end{aligned}$$

The upper and lower boundaries, found using this lemma, are fast and easy to calculate online, as the hard part of the calculations can be done offline. Unfortunately, the found upper and lower boundaries are in general not very tight. However, if the residual expression $r = g(\mathbf{y}, \boldsymbol{\theta})$ is affine with respect to the parameters $\boldsymbol{\theta}$ an exact solution exists. If g is affine with respect to the parameters $\boldsymbol{\theta}$ it can be rewritten to be come,

$$r = g(\mathbf{y}, \boldsymbol{\theta}) = G_0(\mathbf{y}) + \mathbf{G}_l(\mathbf{y}) \boldsymbol{\theta} \ . \tag{7.17}$$

For an expression of this form the upper and lower boundaries can be found on an interval set $\boldsymbol{\Theta}$ using interval algebra (Boukhris et al., 1998). Using this approach the exact maximum and minimum values of (7.17) can be calculated, in the no fault case, using the following lemma.

Lemma 7.3.3 *For the parameter affine system (7.17) the maximum and minimum values of the residual set $\mathcal{R}$ can be calculated exactly, and are given by*

$$\begin{aligned}\overline{r} &= G_0(\mathbf{y}) + \mathbf{G}_l(\mathbf{y})\boldsymbol{\theta}_0 + |\mathbf{G}_l(\mathbf{y})|\,(\overline{\boldsymbol{\theta}} - \boldsymbol{\theta}_0)\\ \underline{r} &= G_0(\mathbf{y}) + \mathbf{G}_l(\mathbf{y})\boldsymbol{\theta}_0 + |\mathbf{G}_l(\mathbf{y})|\,(\underline{\boldsymbol{\theta}} - \boldsymbol{\theta}_0)\ ,\end{aligned}$$

where $\boldsymbol{\theta}_0 = \frac{1}{2}(\overline{\boldsymbol{\theta}} + \underline{\boldsymbol{\theta}})$.

This is a well-known fact from interval analysis (Boukhris et al., 1998; Moore, 1979). In the following, Lemma 7.3.2 and 7.3.3 are used to calculate an upper and a lower boundary of the residual expressions found in the previous section.

All the residual expressions derived in Section 7.2.3 are on the form

$$r = \mathbf{f}(\mathbf{y})^T\mathbf{a}(\boldsymbol{\theta})\ ,$$

where both $\mathbf{a}$ and $\mathbf{f}$ are vector functions with only polynomial nonlinearities in $\boldsymbol{\theta}$ and $\mathbf{y}$. As this is a nonlinear expression, Lemma 7.3.2 could be used to find upper and lower boundaries of the residual set. However, these upper and lower boundaries are in general far from the real maximum and minimum values of $\mathcal{R}$, which is also the case in centrifugal pumps. Therefore, the linear dependency between the parameters is extracted using a first order Taylor Series expansion of $\mathbf{a}(\boldsymbol{\theta})$. This Taylor Series expansion is given by

$$\mathbf{a}(\boldsymbol{\theta}) = \mathbf{a}(\boldsymbol{\theta}_0) + \left[\frac{\partial \mathbf{a}}{\partial \theta_i}(\boldsymbol{\theta}_0)\right](\boldsymbol{\theta} - \boldsymbol{\theta}_0) + \mathcal{O}(\boldsymbol{\theta} - \boldsymbol{\theta}_0)\ .$$

When this expression is used in the residual equation the residual is calculated by the sum of two terms $r = r_l + r_{\mathcal{O}}$. These terms are given by

$$r_l(\mathbf{y}) = \left(\mathbf{f}(\mathbf{y})^T\mathbf{a}(\boldsymbol{\theta}_0)\right) + \left(\mathbf{f}(\mathbf{y})^T\left[\frac{\partial \mathbf{a}}{\partial \theta_i}(\boldsymbol{\theta}_0)\right]\right)\tilde{\boldsymbol{\theta}} \tag{7.18a}$$

$$r_{\mathcal{O}}(\boldsymbol{\theta}, \mathbf{y}) = \mathbf{f}(\mathbf{y})^T\left(\mathcal{O}(\tilde{\boldsymbol{\theta}})\right)\ , \tag{7.18b}$$

where $\tilde{\boldsymbol{\theta}} = \boldsymbol{\theta} - \boldsymbol{\theta}_0$, and $\boldsymbol{\theta}_0$ is chosen such that $\boldsymbol{\theta}_0 = \frac{1}{2}(\overline{\boldsymbol{\theta}} - \underline{\boldsymbol{\theta}})$. It is immediately seen that (7.18a) has the same structure as (7.17), meaning that Lemma 7.3.3 can be used to calculate the maximum and minimum values of r_1 in the no fault case. This does however not form the boundaries on r because of the higher order terms $\mathcal{O}(\boldsymbol{\theta} - \boldsymbol{\theta}_0)$. The dependency on r of these terms is described by (7.18b). This expression is a nonlinear expression on the form treated in Lemma 7.3.2, which therefore gives the upper and lower boundaries on this expression.

Using interval algebra it is easy to find the boundaies of r from the boundaries of r_l and $r_{\mathcal{O}}$. This is formalized in the following algorithm, which is used for robust fault detection.

1. At each new sample $\mathbf{y}$ compute $\mathbf{f}(\mathbf{y})$, $G_0(\mathbf{y}) = \mathbf{f}(\mathbf{y})^T\mathbf{a}(\boldsymbol{\theta}_0)$ and $\mathbf{G}_l(\mathbf{y}) = \mathbf{f}(\mathbf{y})^T\left[\frac{\partial \mathbf{a}}{\partial \theta_i}(\boldsymbol{\theta}_0)\right]$.
2. Compute the maximum and minimum values $\overline{r}_l$ and $\underline{r}_l$ using Lemma (7.3.3).
3. Compute the boundaries $r_{\mho,min}$ and $r_{\mho,max}$ using Lemma 7.3.2.
4. Compute the boundaries of the residual set using,

$$\begin{aligned}\underline{r} &\geq r_{min} = \underline{r}_l + r_{\mho,min}\\ \overline{r} &\leq r_{max} = \overline{r}_l + r_{\mho,max}\end{aligned}$$

5. Compute the decision signal D using,

$$D = \begin{cases} 0 & \text{if } r_{min} \leq 0 \leq r_{max} \\ 1 & \text{otherwise} \end{cases}$$

Remark 7.3.1 *This algorithm can calculate the boundaries of the residual set of one single residual expression. However, parameter dependencies between residuals, when more than one residual is considered, are not taken into account. Therefore, the identification of incipient faults can create problems in some cases.*

Interpretation of the algorithm

The idea of the algorithm is to find the possible variation on the residual value, which can be caused by parameter divergence form the nominal parameter values. This is illustrated in Fig. 7.1.

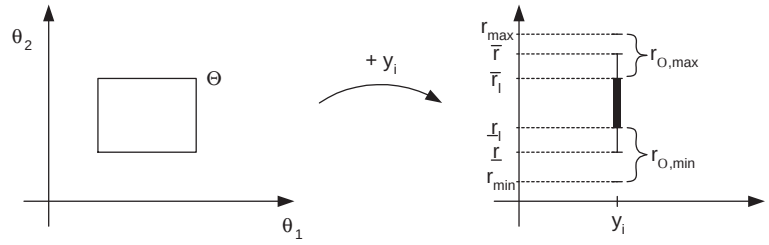

Figure 7.1: Illustration of the different boundary values in the proposed algorithm.

To the left of Fig. 7.1 the set of possible parameter values $\boldsymbol{\Theta}$ is shown. At each measurement vector $\mathbf{y}_i$ this set of parameter values is mapped into a set of possible

residual values. In the right-hand side figure of Fig. 7.1 this set is defined by $\underline{r}$, $\overline{r}$. Now considering the developed algorithm. The residual set defined by $\underline{r}_l$, $\overline{r}_l$ in Fig. 7.1 is calculated in step 2, and $r_{\mathcal{O},min}$, $r_{\mathcal{O},max}$ are calculated in step 3. These values sum up to a set defined by r_{min}, r_{max}, which is in general conservative compared to the real residual set defined by $\underline{r}$, $\overline{r}$. If $r = 0$ is not in between $\underline{r}$, $\overline{r}$ or alternative not in between r_{min}, r_{max} it is guaranteed that a fault has happened in the system.

7.4 Test Results

The final FDI algorithm is obtained by composing the steady state motor equations given in Section 7.2.1, and the ARR expressions developed in Section 7.2.3. The motor equations are used in the first subsystem to calculate the connecting variables, see Fig. 7.2. The ARR expressions are used in the second subsystem to obtain residuals for FDI. To obtain robustness in the residual generation the interval approach, described in Section 7.3, is imposed on each ARR expression. The structure of the whole FDI algorithm is depitch in Fig. 7.2.

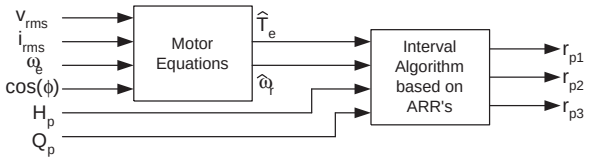

Figure 7.2: The final detection algorithm. The first part consists of (7.11) and (7.12) used for calculating the connecting variables. The second part consists of the interval algorithm described in Section 7.3.

In this algorithm the first part consists of (7.11) and (7.12), which are used for calculating the connecting variables $\hat{\omega}_r$ and $\hat{T}_e$. These calculations are based on the RMS values of the supply voltage V_{rms} and current I_{rms}, $\cos(\phi)$ where ϕ is the angle between the supply voltage and current, and the frequency of the supply voltage ω_e, see Section 7.1. The connection variables $\hat{\omega}_r$ and $\hat{T}_e$ are then, together with the flow and pressure measurement Q_p and H_p, used as input to the second subsystem, which consists of the residual generators.

This detection algorithm is tested on the same test setup as the algorithm described in Chapter 6. Meaning that it is tested on a Grundfos 1.5 (KW) CR5-10 pump placed in a tank system as depicted in Fig. 7.3. In this tank system the valve V_1 is used to model disturbances in the system. Clogging inside the pump is modelled by the valve V_c and dry running is modelled by closing V_2 and opening V_3. Rub impact is modelled by adding an extra force to the shaft and cavitation is modelled by closing valve V_2 gradually. Leakage flow is modelled by opening V_l. In the tests shown here a low

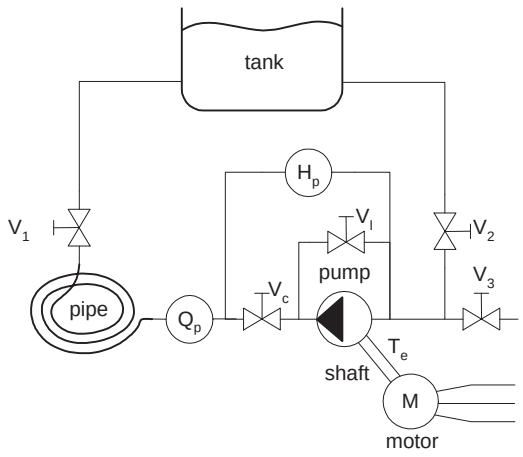

Figure 7.3: Sketch of the test setup. The measurements are the electrical quantities, the differential pressure H_p delivered by the pump and the volume flow through the pump Q_p.

bandwidth but precise flow sensor is used. This flow sensor is chosen, as this type of sensor is often used in real industrial applications.

First robustness with respect to the operating point is tested. In this test both the position of the valve V_1 and the speed of the pump are changed during operation. During the test the valve is changed in three steps from maximum opened to almost closed. The first step change is done at time 26.3 [sec] and the second step change is done at time 52.3 [sec]. The speed of the pump is changed between approximately 2030 and 2580 (rpm) each 13 [sec] during the test. The result of this test is shown in Fig. 7.4. In the three lower figures the residual sets $\mathcal{R}_{p1}$ to $\mathcal{R}_{p3}$ are shown by their boundaries at each time instant, and in the top figure the speed changes are shown. The test shows that after each transient phase, zero is included in all the three residual sets, i.e. zero is in between the residual boundaries for each residual set. This shows that the algorithm is not capable of handling transient behaviour, which was expected. More important, it shows that the algorithm is robust with respect to the operating point of the pump.

Figures 7.5 to 7.7 show test results concerning isolability of the five faults considered in this chapter. All these tests are performed with V_1 half opened and an angular speed of approximately 2350 (rpm). In each of the figures the residual sets $\mathcal{R}_{p1}$ to $\mathcal{R}_{p3}$ are shown by their boundaries in the top figure, and the decision D_{p1} to D_{p3} are shown in the bottom figure. The tests show that all the five faults considered in this chapter are detectable using the three residual sets. Moreover, comparing the decision signals it is seen that all the fault signatures given by D_{p1}, D_{p2}, and D_{p3} are distinguishable except from the cavitation and dry running fault, i.e. f_c and f_d. This was expected as

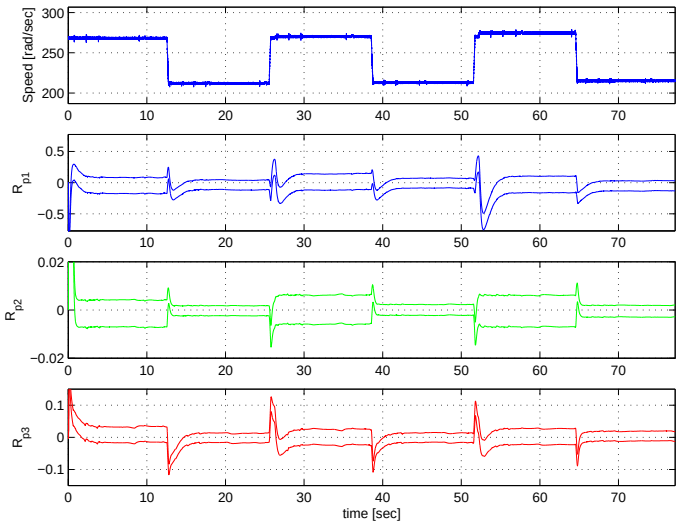

Figure 7.4: Robustness test. The top figure shows the speed steps, and the three lower figures show the residual boundaries for each of the three residual sets $\mathcal{R}_{p1}$ to $\mathcal{R}_{p3}$.

the structural analysis in Section 7.2.2 already had predicted this.

Both the appearance and the disappearance of the considered faults, except from the dry running fault f_d, are detected. From Fig. 7.7 the problem of detecting the disappearance of the dry running fault is seen. This problem is due to air bobbles in the system imposed by the dry running fault, which disturbs the flow sensor used in this test.

7.5 Discussion

The topic of this chapter is fault detection in a centrifugal pump based on steady state measurements only. Here the steady state measurements are Root Mean Square (RMS) measurement of the voltage and current, the voltage frequency, the electrical angle between the voltage and current, and the pressure and volume flow of the pump. Three residuals are derived form the steady state model of the pump, using Structural Analysis and Analytical Redundant Relations (ARR's). The faults under consideration in this chapter are only affecting the second subsystem. Hence the ARR's are only developed for this part. The connecting variables between the two subsystems are calculated using a steady state model of the motor.

Structural analysis has been used to analyse the system. As a result of this analysis the system is divided into two cascade-connected subsystems simplifying the derivation of the Analytical Redundancy Relation (ARR) considerably. The first subsystem consists of the induction motor model, and the mechanical and hydraulic parts of the pump

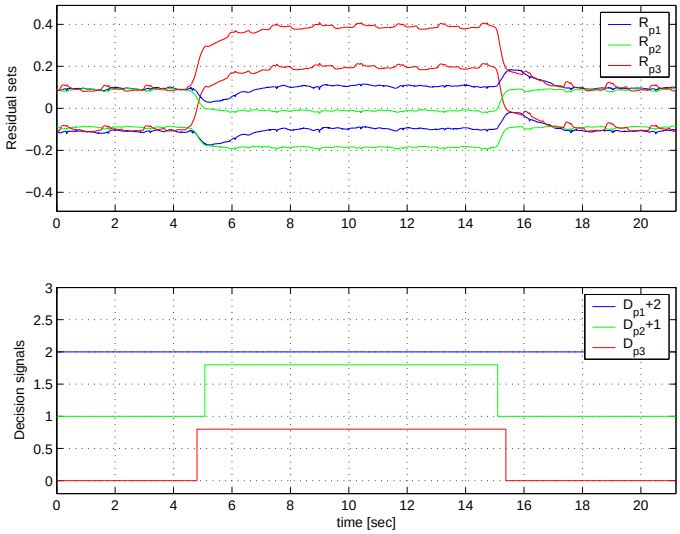

(a) Detection of the fault K_f clogging.

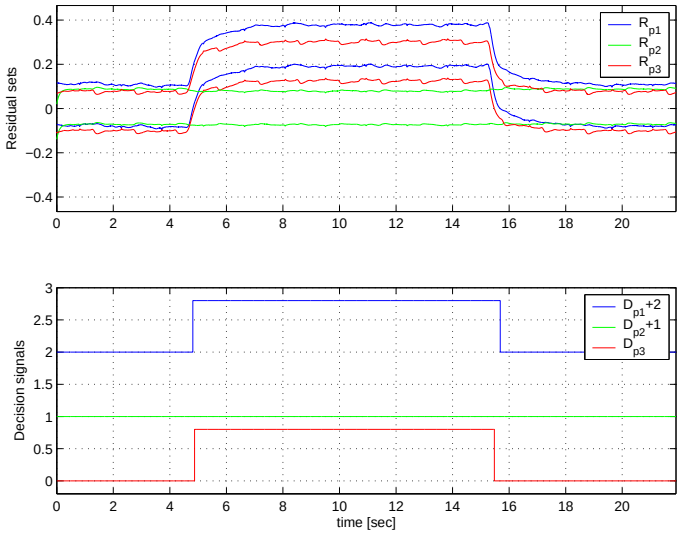

(b) Detection of the fault K_l leakage flow.

Figure 7.5: Test results. The top figures show the residual boundaries for each of the three residual sets $\mathcal{R}_1$, $\mathcal{R}_2$ and $\mathcal{R}_3$. The bottom figures show the decision signals D_1, D_2, and D_3.

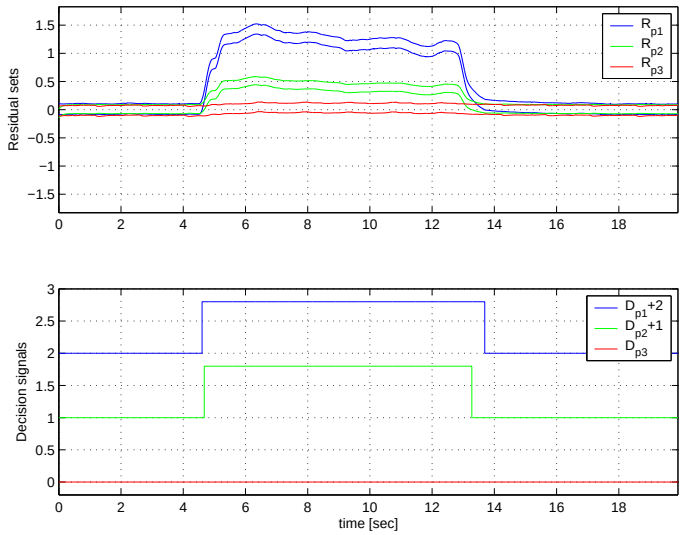

(a) Detection of the fault ΔB rub impact.

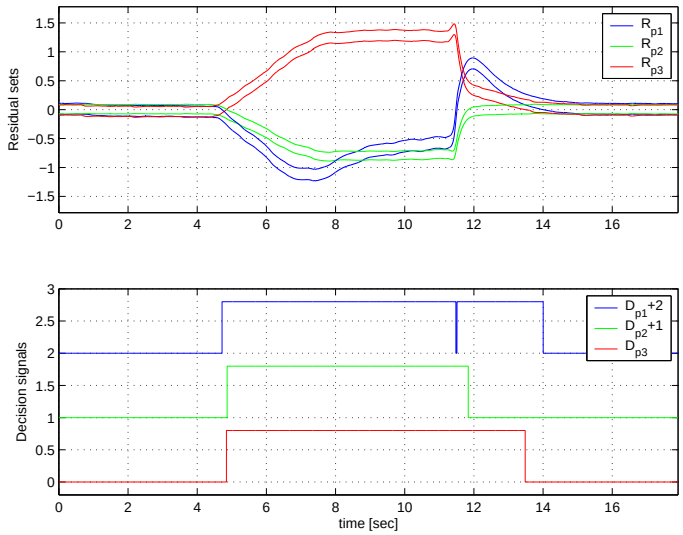

(b) Detection of the fault f_c cavitation.

Figure 7.6: Test results. The top figures show the residual boundaries for each of the three residual sets $\mathcal{R}_1$, $\mathcal{R}_2$ and $\mathcal{R}_3$. The bottom figures show the decision signals D_1, D_2, and D_3.

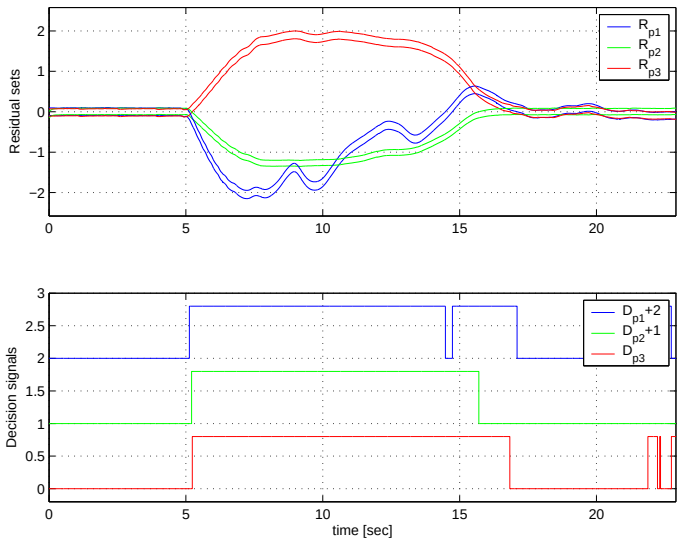

Figure 7.7: Test results showing detection of the fault f_d dry running. The top figures show the residual boundaries for each of the three residual sets $\mathcal{R}_1$, $\mathcal{R}_2$ and $\mathcal{R}_3$. The bottom figures show the decision signals D_1, D_2, and D_3.

form the second subsystem. The approach of dividing the system into two cascade-connected subsystems was also utilized in Chapter 6. Parameter variations are only considered for the second subsystem, with the drawback that the algorithm can handle only parameter variations in the hydraulic part of the pump. However, the possibility of handling parameter variations in the hydraulic part can be used to obtain a simple and logical way of setting alarm levels for a user of the system, as these can be defined directly on pump curves, as those shown in Section 3.3.5.

The residuals obtained from the ARR's are made robust with respect to parameter variations in the centrifugal pump model by using the set-valued approach. It is shown that linearization of the parameter function can be used to calculate relatively tight boundaries of the residual in the centrifugal pump case. Using the set-valued approach the set of possible residual values are changed as a function of the operating point of the pump. This could be compared to a residual with an adaptive threshold. The presented method has the advantage of connecting the physics of the pump and the set of residuals in a straightforward manner.

Chapter 8

Conclusion and Recommendations

In this thesis different aspects of Fault Detection and Identification (FDI) in centrifugal pumps were considered. Special focus was put on the robustness of the FDI algorithms. In this connection an analysis method for analysing robustness in signal-based fault detection schemes was proposed. In most model-based fault detection schemes, robustness considerations are a part of the design. Therefore, the possibilities of using these approaches on the centrifugal pump were investigated too, ending up with three new FDI algorithms. Here, a small example of connecting these algorithms into one FDI scheme is given. This example is followed by a conclusion and a number of recommendations for further research.

8.1 Algorithm Example

In the thesis four different FDI algorithms were considered. One of these was based on the signal-based approach, and the remaining three on the model-based approach. In the design of the three model-based algorithms, a subset of the following 6 faults were considered.

1. Inter-turn short circuit in the stator of the induction motor.
2. Clogging inside the pump.
3. Increased friction due to either rub impact or bearing faults.
4. Increased leakage flow.
5. Performance degradation due to cavitation.

6. Dry running.

In chapter 5 the detection and identification of the inter-turn short circuit were considered, and in Chapters 6 and 7 the remaining five faults were handled. The difference between the two algorithms in Chapters 6 and 7 lies in their ability to handle transient behaviour in the system. The algorithm derived in Chapter 6 was based on a dynamic description of the pump and was therefore able to handle transient behaviour. The algorithm derived in Chapter 7 was on the other hand based on a steady state model and therefore had inherent problems during transient phases.

Composing the algorithm derived in Chapter 5 with the FDI part of the algorithm derived in Chapter 6, the final FDI scheme is obtained. This FDI scheme is capable of detecting and identifying the 6 different faults in the centrifugal pump. The composition of the two algorithms is shown in Fig. 8.1.

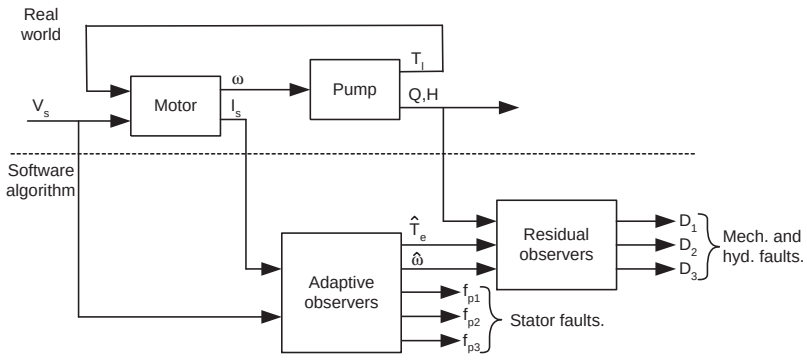

Figure 8.1: The composition of the adaptive observer, designed for inter-turn short circuit detection, and residual observers, designed for fault detection and identification in the mechanical and hydraulic part of the centrifugal pump.

In Fig. 8.1 the block denoted adaptive observer, contains the observer used for detecting stator faults. The output from this observer is the estimates of the electrical states, the speed, and the inter-turn short circuit. The estimates of the electrical states are used for calculating the torque, meaning that the adaptive observer is capable of estimating both the speed, the torque, and the inter-turn short circuit fault.

The inputs to the block, denoted residual observers in Fig. 8.1, are the measured pressure, the measured volume flow, and the estimates of the speed and torque. The output of the residual observer block is the three decision signals described in Chapter 6, meaning that the information of the mechanical and hydraulic faults are available.

In Chapter 7 residual generators, designed using the steady state model of the mechanical and hydraulic parts of the centrifugal pump, are described. These residual generators could also be used for residual generation in the block, denoted residual observer

in Fig. 8.1. However, by using these residual generators, problems will arise during transient phases.

8.2 Conclusion

The following conclusions are drawn on the accomplishments and contributions of the thesis:

- The dynamics of the centrifugal pump were considered in the development of the centrifugal pump model in Chapter 3. Two assumptions were given, under which algebraic maps can be used for describing the energy conversion from mechanical to hydraulic energy, and the pressure of the centrifugal pump. Moreover, the dynamics of the hydraulic part can be described by an added mass to the impeller, which is corresponding to the mass of the liquid inside the impeller. This means that, when the mechanical and hydraulic part of the centrifugal pump is considered, the dynamics of the pump is described by a first order system. The algebraic maps describing the energy conversion and the pressure generation are polynomial of second order. This makes the model of the system a nonlinear lumped parameter model. As the model is a lumped parameter model, it is well suited for use in model-based designs, both when it comes to control and to FDI.

- The most used methods for FDI in centrifugal pumps are, according to the state of the art analysis, presented in Chapter 2, based on the signal-based approaches. Normally robustness is not considered when FDI algorithms are derived using signal-based approaches. Therefore, it was found that a method, which can be used for robustness analysis, was needed. In Chapter 4 a combination of the Failure Mode and Effect Analysis (FMEA) and Fault Propagation Analysis (FPA) is proposed for the robustness analysis of signal-based FDI algorithms. The proposed method can be used in the design, as well as in the analysis. In addition to the robustness analysis method, an algorithm for automating one of the manual steps in the FPA was proposed. Using the improvements of the FMEA and FPA, the proposed analysis method was used to analyse different sensor configurations on the centrifugal pump. Also it was used in the design of a detection scheme, based on one particular sensor configuration. Test results on an industrial testbench showed that 3 out of 7 chosen faults could be detected in a robust manner with this sensor configuration. This showed the usability of the proposed analysis and design method. However, the result obtained in Chapters 6 and 7 showed that, using the model-based approach, 5 different faults were detected using the same sensor configuration. This shows the drawback of the signal-based approaches when used on centrifugal pumps.

- One of the faults considered in this work was the inter-turn short circuits in the windings of the induction motor driving the pump. In the state of the art analysis

in Chapter 2, it was argued, that this fault is often the initiator of a stator burnout. To understand the nature of the inter-turn short circuit fault, a dynamic model of the fault was derived in Chapter 5. A model was established for both **Y**- and Δ-connected induction motors. One remarkable result was shown by this model, namely that torque ripple should not be expected when an inter-turn short circuit has occurred. That is, if the motor is supplied with a balanced sinusoidal supply voltage, and a constant torque load. This fact was indirectly shown in the test, presented in the end of Chapter 5, as the level of oscillations in the real speed did not change when introducing the inter-turn short circuit fault.

- In Chapter 5, the model of the induction motor, including an inter-turn short circuit, was used in the derivation of an adaptive observer. In real applications, only the electrical quantities are normally available. Therefore, the derived adaptive observer was only using these quantities. The obtained observer was capable of estimating an inter-turn short circuit fault in one of the phases, the electrical states, and the speed of the induction motor simultaneously. The design of the observer was based on a dynamic model of the induction motor, with the speed assumed constant. Therefore, the observer was capable of detecting the faults during transient behaviour, when the constant speed assumption was not violated too much. This makes the algorithm very useful in real applications. Especially for induction motors supplied with a frequency converter, as transients are expected to occur frequently in these applications. The drawback of the algorithm is the need for the motor parameters, which are not always known in real life applications.

- In Chapter 3 it was shown that the model of the centrifugal pump is highly nonlinear, meaning that model-based approaches, based on nonlinear models, should be considered when the operating point of the pump is changed frequently or is unknown. This is actually the case in many centrifugal pump applications. Here, Structural Analysis (SA) was chosen as the first step in the derivation of residual generators. The only straightforward way to use the results of the SA, in order to obtain residual generators, is the derivations of Analytical Redundant Relations (ARR's). These ARR's can, and in general do, contain derivatives of the measured signals. To overcome this problem, a novel realization approach was proposed in Chapter 6. With this approach, it is possible to obtain a nonlinear state space description from the results of the SA. The obtained state space description does not include unknown variables, except for the states of the system. The approach was tested on three applications; a satellite case borrowed from (De Persis and Isidori, 2001), the induction motor, and the hydraulic part of the centrifugal pump. The realization method is based on a solution to a partial differential equation, which is the main problem with this approach. This is, however, a known problem concerning nonlinear state transformations on general nonlinear systems, as it is the case in the proposed realization approach.

- Based on the results obtained using SA and the realization approach developed in

Chapter 6, three residual observers and an ARR were derived for the centrifugal pump. Tests, on a test-bench developed particularly for this purpose, were performed, showing the capabilities of the observers and the ARR. The tests showed that the observers and the ARR were robust, with respect to changes in the operating point of the pump. Moreover, the tests showed that 5 different faults, affecting the hydraulic and mechanical parts of the pump, were detectable with this approach. This shows the superiority of the model-based approach compared to the signal-based approach, when it comes to robustness.

- In Chapter 6, the algorithm, developed for detecting faults in the mechanical and hydraulic part of the centrifugal pump, was based on a dynamic model of the system. This means that the involved signals were expected to have a bandwidth covering the dynamics of the system. These high bandwidth signals are often not available in real life centrifugal pump applications. However, low bandwidth signals are often available. Therefore, an algorithm based on a steady state model of the centrifugal pump was proposed in Chapter 7. This algorithm was shown to be able to detect 5 different faults in the mechanical and hydraulic parts of the centrifugal pump. The algorithm was made robust with respect to parameter uncertainties, using a set-valued approach. The need for only low bandwidth sensors and the robustness considerations, makes the algorithm appropriate for implementation in cost sensitive applications, where the necessary sensors already are available.

8.3 Recommendations

The following topics are not covered in this thesis, but it is believed that future investigations could be beneficial.

- In Chapter 5 an adaptive observer is designed for simultaneous estimation of the electrical states, the speed, and the inter-turn short circuit of the induction motor. In the design proposed here, the parameters of the motor are assumed known. However, an adaptive observer is used. Therefore it should be possible to find a transformation of the induction motor model, making it possible for the adaptive observer to adapt to the motor parameters. If this is possible, the proposed algorithm becomes parameter independent.
- In Chapter 5 also a Linear Matrix Inequality (LMI) approach was used for both analysis and synthesis of the observer gain in the proposed adaptive observer. It could be interesting to include the concept of LMI regions in the proposed analysis and synthesis. Hereby, it would be possible to state demands on the damping ratio in the system, as well as the convergence rate.
- In Chapter 6 a new concept, for realization of subsystems identified using Structural Analysis, was presented. This concept should be further investigated. Es-

pecially Assumption 6.2.3, stating the condition for the existence of a state space transformation, should be considered.

- In Chapter 7 a detection scheme, based on the steady state model of the pump, was proposed. Because of the steady state model, transient phases can force the residual to be different from zero, even in the no fault cases. Therefore, means for detecting these transient conditions, must be established before implementing the algorithm in real life applications.
- A set-valued approach was proposed for obtaining robustness in the residual generation in Chapter 7. This approach utilizes interval models. Extending the set-valued approach, to include interval models of each fault case, it might be possible to state which fault has happened in a robust manner. Hereby robustness is introduced in the identification of incipient faults.

Bibliography

Tom M. Apostol. *Mathematical Analysis, second edition*. Addison-Wesley Publishing Company, Inc., 1974. ISBN 0-201-00288-4.

M. Arkan, D. K. Perovic, , and P. Unsworth. Online stator fault diagnosis in induction motors. *IEE proceedings on electrical power applications, Vol. 148, No. 6*, 2001.

Neil Arthur and Jim Penman. Induction machine condition monitoring with higher order spectra. *IEEE Transaction on Industrial Electronics, Vol. 47, No. 5*, 2000.

S. Backir, S. Tnani, T. Poinot, and J. C. Trigeassou. Stator fault diagnosis in induction machines by parameter estimation. *IEEE, International Symposium on Diagnostics, Grado, Italy*, 2001.

Antonio Baldassarre, Maurizio De Lucia, and Paolo Nesi. Real-time detection of cavitation for hydraulic turbomachines. *Real-Time Imaging 4, Page 403 - 416*, 1998.

Michele Basseville and Igor V. Nikiforov. *Detection of Abrupt Changes - Theory and Application*. www.irisa.fr/sigma2/kniga/, 1998.

Alberto Bellini, Fiorenzo Filippetti, Giovanni Franceschini, Carla Tassoni, and Gerald B. Kliman. Quantitative evaluation of induction motor broken bars by means of electrical signature analysis. *IEEE Transaction on Industry Applications, Vol. 37, No. 5*, 2001.

Mohamed El Hachemi Benbouzid. A review of induction motors signature analysis as a midium for faults detection. *IEEE Transactions on industrial electronics vol. 47 no. 5*, 2000.

Gildas Besancon. Remarks on nonlinear adaptive observer design. *ELSEVIER, System & Control Letters, Vol. 41, No. 4*, 2000.

Søren Abildsten Bøgh. *Fault Tolerant Control Systems - a Development Method and Real-Life Case Study*. PhD thesis, Aalborg University, Department of Control Engineering, 1997.

Péter Bóka and Gábor Halász. Dynamic behaviour of centrifugal pumps. *Proceedings of the XXIst IAHR Symposium on Hydraulic Machinery and Systems, Lausanne*, 2002.

Mogens Blanke. Consistent design of dependable control systems. *Control Eng. Practice, Vol. 4, No. 9*, 1996.

Mogens Blanke, Michel Kinnaert, Jan Lunze, and Marcel Starowiecki. *Diagnosis and Fault-Tolerant Control*. Springer Verlag, 2003. ISBN 3-540-01056-4.

Julien Le Bleu Jr. and Ming Xu. Vibration monitoring of sealess pumps using spike energy. *Sound and Vibration, Vol. 29, No. 12*, 1995.

Austin H. Bonnett and George C. Soukup. Cause and analysis of stator and rotor failures in three-phase squirrel-cage induction motors. *IEEE Transaction on Industry Applications, Vol. 28, No. 4*, 1992.

A. Boukhris, D. Mandel, and J. Ragot. Data validation using interval algebra. *UKACC International Conference on Control, CONTROL'98*, 1998.

Fernando Briz, Michael W. Degner, Antonio Zamarron, and Juan M. Guerrero. Online stator winding fault diagnosis in inverter-fed ac machines using high-frequency signal injection. *IEEE Transactions on Industry Applications, Vol. 39, No. 4.*, 2003.

Cash, M. A., Habetler, T. G., and Kliman, G. B. Insulation failure prediction in induction machines using line-neutral voltages. *IEEE Industry Applications Conference, Thirty-Second IAS Annual Meeting, IAS '97*, 1997.

Jie Chen and R. J. Patton. *Robust Model-Based Fault Diagnosis for Dynamic Systems*. Kluwer Academic Publishers, 1999. ISBN 0-7923-8411-3.

Young Man Cho and Rajesh Rajamani. A systematic approach to adaptive observer synthesis for nonlinear systems. *IEEE Transactions on Automatic Control, Vol. 42, No. 4*, 1997.

Tommy W. S. Chow and Hong-Zhou Tan. Hos-based nonparametric and parametric methodologies for machine fault detection. *IEEE Transaction on Industrial Electronics, Vol. 47, No. 5*, 2000.

David Cox, John Little, and Donal O'Shea. *Ideals, Varieties, and Algorithms, An introduction to computational algebraic geometry and comutative algebra*. Springer-Verlag Inc., 1997. ISBN 0-387-94680-2.

Sergio M. A. Cruz and A. J. Marques Cardoso. Stator winding fault diagnosis in three-phase synchronous and asynchronous motors, by the extended park's vector approach. *IEEE Transaction on Industrial Applications, Vol. 37, No. 5*, 2001.

M. Cudina. Detection of cavitation phenomenon in centrifugal pump using audible sound. *Mechanical Systems and Signal Processing, Vol. 17, No. 6*, 2003.

Francesco Cupertino, Elisabetta de Vanna, Luigi Salvatore, and Silvio Stasi. Analysis techniques for detection of im broken rotor bars after supply disconnection. *IEEE Transactions on Industry Applications, Vol. 40, No. 2.*, 2004.

Tracy Dalton, Ron J. Patton, and J. Chen. Application of eigenstructure assignment to robust residual design for FDI. *UKACC International Conference on Control, CONTROL '96*, 1996.

Claudio De Persis and Alberto Isidori. A geometric approach to nonlinear fault detection and isolation. *IEEE Transaction on Automatic Control, Vol. 46 No. 6*, 2001.

Diego Del Gobbo, Marcello Napolitano, Parviz Famouri, and Mario Innocenti. Experimantal application of extended kalman filtering for sensor valitation. *IEEE Transactions on Control Systems Technology, Vol 9. No 2.*, 2001.

Levent Eren and Michael J. Devaney. Motor bearing damage detection via wavelet analysis of the starting current transient. *IEEE Instrumentation and Measurement Technology Conference*, 2001.

P. M. Frank and X. Ding. Survey of robust residual generation and evaluation methods in observer-based fault detection systems. *Journal of Proces Control, Vol. 7, No. 6*, 1997.

Jens Friedrichs and Günter Kosyna. Rotating cavitation in a centrifugal pump impeller of low specific speed. *Transactions of the ASME, Journal of Fluid Engineering, Vol. 124, No. 2*, 2002.

Erik Frisk and Jan Åslund. Lowering orders of derivatives in non-linear consistency relations - theory and simulation examples. Technical Report LiTH-R-2547, Dept. of Electrical Engineering, Linköping University, Sweden, 2003.

Pablo García, Fernando Briz, Michael W. Degner, and Alberto B. Diez. Diagnostics of induction machines using the zero sequence voltage. *Proceedings of the IEEE* 39^{th} *IAS Annual Meeting, Seattle, Washington*, 2004.

E. Alcorta Garcia and P. M. Frank. Deterministic nonlinear observer-based approaches to fault diagnosis: A survey. *Control Eng. practice, Vol. 5 No. 5*, 1997.

C. Gerada, K. J. Bradley, M. Sumner, P. Wheeler, S. Pickering, J. Clare, C. Whitley, and G. Towers. The implications of winding faults in induction motor drives. *Proceedings of the IEEE* 39^{th} *IAS Annual Meeting, Seattle, Washington*, 2004.

Janos J. Gertler. *Fault Detection and Diagnosis in Engineering Systems*. Marcel Dekker, Inc., 1998. ISBN 0-8247-9427-3.

Jan Tommy Gravdahl and Olav Egeland. Centrifugal compressor surge and speed control. *IEEE Transactions on Control System Technology, vol. 7, No. 5*, 1999.

S. Greitzke and C. Schmidthals. Principles and application of a diagnosis system for mechanical seals. *Pump Users International Forum 2000, Karlsruhe*, 2000.

Janati Idrissi, Olivier Adrot, and Jose Ragot. Multi-fault detection of systems with bounded uncertainties. *Proceedings of the 40th IEEE Conference on Decision and Control, Orlando, Florida USA*, 2001.

R. Isermann. Supervision fault-detection and fault-diagnosis methods - an introduction. *Control Eng. Practice, vol. 5, No. 5*, 1997.

R. Isermann and P. Balle. Trends in the application of model-based fault detection and diagnosis of technical processes. *Control Eng. Practice, vol 5, No. 5*, 1997.

Alberto Isidori. *Nonlinear Control Systems, third edition*. Springer-Verlag, 1995. ISBN 3-540-19916-0.

Roozbeh Izadi-Zamanabadi. *Fault-tolerant Supervisory Control - System Analysis and Logic Design*. PhD thesis, Aalborg University, Department of Control Engineering, 1999.

Roozbeh Izadi-Zamanabadi. Structural analysis approach for fault diagnosis and disturbance decoupling. Technical report, Institute of Electronic Systems, Aalborg Universitet, Denmark, 2001.

Roozbeh Izadi-Zamanabadi and Marcel Staroswiecki. A structural analysis method formulation on fault-tolerant control system design. *Proc. of the* 39^{th} *IEEE Conference on Decision and Control, Sydney, Austrailia*, 2000.

Bin Jiang and Marcel Staroswiecki. Adaptive observer design for robust fault estimation. *International Journal of Systems Science, Vol. 33, No. 9*, 2002.

Gojko M. Joksimovic and Jim Penman. The detection of inter-turn short circuits in the stator windings of operating motors. *IEEE Transaction on Industrial Electronics, Vol. 47, No. 5*, 2000.

Rikke Bille Jørgensen. *Development and Test of Methods for Fault Detection and Isolation*. PhD thesis, Aalborg University, Department of Control Engineering, 1995.

Carsten Skovmose Kallesøe, Vincent Cocquempot, and Roozbeh Izadi-Zamanabadi. Model based fault detection in a centrifugal pump application. *Submitted in 2004 to IEEE Transactions on Control Systems Technology*, 2004a.

Carsten Skovmose Kallesøe and Roozbeh Izadi-Zamanabadi. A realization approach for residual expressions. *Submitted to the joint 44th IEEE Conference on Decision and Control and European Control Conference ECC 2005*, 2005.

Carsten Skovmose Kallesøe, Roozbeh Izadi-Zamanabadi, Vincent Cocquempot, and Henrik Rasmussen. Model based fault diagnosis in a centrifugal pump application using structural analysis. *Proceedings of the IEEE International Conference on Control Applications, Taipei, Taiwan*, 2004b.

Carsten Skovmose Kallesøe, Henrik Rasmussen, Pierre Vadstrup, and Roozbeh Izadi-Zamanabadi. Estimation of stator winding faults in induction motors using an adaptive observer scheme. *Proceedings of the IEEE* 39^{th} *IAS Annual Meeting, Seattle, Washington*, 2004c.

Marian P. Kazmierkowski. *Automatic Control of Converter-Fed Drives*. PWN-Polish Scientific Publishers, Warszawa, 1994.

T. Kenull, G. Kosyna, and P. U. Thamsen. Diagnostics of submersible motor pumps by non-stationary signals in motorcurrent. *The 1997 ASME Fluids Engineering Division Summer Meeting, FEDSM'97*, 1997.

Hassan K. Khalil. *Nonlinear Systems*. Prentice-Hall, Inc., 2002. ISBN 0-13-067389-7.

G. B. Kliman, W. J. Premerlani, R. A. Koegl, and D. Hoeweler. A new approach to on-line turn fault detection in ac motors. *IEEE Industry Applications Conference, Thirty-First IAS Annual Meeting, IAS '96*, 1996.

D. Kollmar, D. H. Hellman, and S. Brodersen. Intelligent standardized chemical pumps, a chance for pump users? *Pump Users International Forum 2000, Karlsruhe*, 2000a.

D. Kollmar, D. H. Hellman, and F. W. Hennecke. An early failure detection system emerging from laboratory into plant. *Pump Users International Forum 2000, Karlsruhe*, 2000b.

Dragica Kostic-Perovic, Muslum Arkan, and Peter Unsworth. Induction motor fault detection by space vector angular fluctuation. *Proceedings of the IEEE* 35^{th} *IAS Annual Meeting*, 2000.

P. C. Krause, O. Wasynczuk, and S. D. Sudhoff. *Analysis of Electric Machinery*. IEEE Press, 1994.

Sang-Bin Lee, Rangarajan M. Tallam, and Thomas G. Habetler. A robust, on-line turn-fault detection technique for induction machines based on monitoring the sequence component impedance matrix. *IEEE Transactions on Power Electronics, Vol. 18, No. 3*, 2003.

Werner Leonhard. *Control of Electrical Drives*. Springer-Verlag Berlin Heidelberg New York, 1996. ISBN 3-540-13650-9.

Bo Li, Mo-Yuen Chow, Yodyium Tipsuwan, and James C. Hung. Neural-network-based motor rolling bearing fault diagnosis. *IEEE Transactions on industrial electronics vol. 47 no. 5*, 2000.

Linfan Liu and Jennie Si. Fault isolation filter design for linear systems. *Digital Avionics Systems Conference, 13th DASC., AIAA/IEEE*, 1994.

Lennart Ljung. *System Identification, Theory for the User, Second edition*. Prentice Hall Inc., 1999. ISBN 0-13-656695-2.

Henrik Lohrberg and Bernd Stoffel. Measurement of cavitation erosive aggressiveness by means of structure born noise. *IFAC 2000*, 2000.

Henrik Lohrberg, Burkart Voss, Bernd Stoffel, and Manfred Glesner. Impeller integrated measurement of cavitation erosive aggressiveness. *Mechatronic, Vol. 12, No. 8*, 2002.

Kenneth A. Loparo, M. L. Adams, Wei Lin, M. Farouk Abdel-Magied, and Nadar Afshari. Fault detection and diagnosis of rotating machinery. *IEEE Transactions on industrial electronics vol. 47 no. 5*, 2000.

Xiaogang Luo, Yuefeng Liao, Hamid A. Toliyat, Ahmed El-Antably, and Thomas A. Lipo. Multiple coupled circuit modeling of induction machines. *IEEE Transactions on Industry Applications, Vol. 31, No. 2*, 1995.

Mohammad-Ali Massoumnia, George C. Verghese, and Alan S. Willsky. Fault detection and identification. *IEEE Transactions on Automatic Control, Vol. 34, No. 3*, 1989.

R. Müller-Petersen, Th. Kenull, and G. Kosyna. Condition monitoring of pumps by motor current analysis in a field test. *Pump Users International Forum 2004, Karlsruhe*, 2004.

Ramon E. Moore. *Methods and Applications of Interval Analysis*. SIAM, Philadelphia, 1979. ISBN 0-89871-161-4.

Kent R. Nagle and Edward B. Saff. *Fundamentals of Differential Equations and Boundary Balue Problems, Second edition*. Addison-Wesley, 1996. ISBN 0-201-80879-X.

Subhasis Nandi and Hamid A. Toliyat. Novel frequency-domain-based technique to detect stator interturn faults in induction machines using stator-induced voltages after switch-off. *IEEE Transactions on Industry applications, Vol. 38, No. 1*, 2002.

G. D. Neill, R. L. Reuben, E. R. Brown, and J. A. Steel. Detection of incipient cavitation in pumps using acoustic emission. *Proceedings of the Institution of Mechanical Engineers, Vol. 211, Part E*, 1997.

D. W. Novotny and T. A. Lipo. *Vector Control and Dynamics of AC Drives*. Oxford University Press Inc., New York, 1996.

Jorge L. Parrondo, Sandra Velarde, and Carlos Santolaria. Development of a predictive maintenance system for a centrifugal pump. *Journal of Quality in Maintenance Engineering, Vol. 4, No. 3*, 1998.

R. J. Patton and J. Chen. Observer-based fault detection and isolation: Robustness and applications. *Control Eng. Practice, Vol. 5, No. 5*, 1997.

S. Perovic, P. J. Unsworth, and E. H. Higham. Fuzzy logic system to detect pump faults from motor current spectra. *IEEE, Industry Applications Conference Thirty-Sixth IAS Annual Meeting*, 2001.

Rajesh Rajamani and J. Karl Hedrick. Adaptive observers for active automotive suspensions: Theory and experiment. *IEEE Transactions on Control Systems Technology, Vol. 3, No. 1*, 1995.

Henrik Rasmussen. *Self-tuning Torque Control of Induction Motors for High Performance Applications*. PhD thesis, Aalborg University, Department of Control Engineering, 1995.

John A. Roberson and Clayton T. Crowe. *Engineering Fluid Mechanics, Fifth Edition*. Houghton Mifflin Company, 1993. ISBN 0-395-66161-7.

A. T. Sayers. *Hydraulic and Compressible flow Turbomachines*. McGraw-Hill Book Company, 1990.

Carsten Scherer and Siep Weiland. Lecture note disc course on linear matrix inequalities in control, version 2.0. Technical report, Delft University of Technology, Delft, The Netherlands, 1999. Available on the homepage of Carsten W. Scherer.

Randy R. Schoen, Thomas G. Habetler, Farrukh Lamran, and Robert G. Bartheld. Motor bearing damage detection using stator current monitoring. *IEEE Transactions on industry Applications vol. 31 no. 6*, 1995.

Mau-Hsiang Shih. Solution of the boolean markus-yamabe problem. *Advances in Applied Mathematics, Vol. 22, No. 1*, 1999.

Jason R. Stack, Ronald G. Harley, and Thomas G. Habetler. An amplitude modulation detector for fault diagnosis in rolling element bearings. *Proceedings of 28th Annual Conference of the IEEE Industrial Electronics Society*, 2002.

M. Staroswiecki. Quantitative and qualitative models for fault detection and isolation. *Mechanical Systems and Signal Processing, Vol. 14, No. 3*, 2000.

M. Staroswiecki and G. Comtet-Varga. Analytical redundancy relations for fault detection and isolation in algebraic dynamic systems. *Automatica, Vol. 37, No. 5*, 2001.

A. J. Stepanoff. *Flow Pumps, Design and Application*. John Wiley & sons, 1957. ISBN 0 471 82137 3.

Jakob Stoustrup and Henrik Niemann. Fault detection for nonlinear systems - a standard problem approach. *Proceedings of the 37th IEEE Conference on Decision & Control.*, 1998.

Jakob Stoustrup and Henrik Niemann. Fault estimation - a standard problem approach. *International Journal of Robust and Nonlinear Control, Vol. 12, No. 8*, 2002.

Karl Åström, Pedro Albertos, Mogens Blanke, Alberto Isidori, Walter Schaufelberger, and Ricardo Sanz. *Control of Complex Systems*. Springer-Verlag, 2001. ISBN 1-85233-324-3.

Charles R. Sullivan and Seth R. Sanders. Models for induction machines with magnetic saturation of the main flux path. *IEEE Transactions on Industrial Applications, Vol 31, No. 4*, 1995.

D. Surek. Pump monitoring by measurement of the case vibrations. *Pump Users International Forum 2000*, 2000.

Rangarajan M. Tallam, Thomas G. Habetler, and Ronald G. Harley. Transient model for induction machinces with stator winding turn faults. *IEEE Transactions on Industry Applications, Vol. 38, No. 3*, 2002.

Rangarajan M. Tallam, Thomas G. Habetler, and Ronald G. Harley. Stator winding turn-fault detection for closed-loop induction motor drives. *IEEE Transactions on Industry Applications, Vol. 39, No. 3*, 2003.

Jesper Sandberg Thomsen. A fault tolerant electronic steering system for a fork lift truck. Technical report, Institute of Electronic Systems, Aalborg Universitet, Denmark, 2000.

Hamid A. Toliyat, Thomas A. Lipo, and J. Coleman White. Analysis of a concentrated winding induction machine for adjustable speed drive applications part 1 (motor analysis). *IEEE Transactions on Energy Conversion, Vol 6, No. 4*, 1991.

Sebastian Tornill, Teresa Escobet, and Vicenc Puig. Fault detection using interval models. *SafeProcess '2000, IFAC, Budapest*, 2000.

Frederik C. Trutt, Joseph Sottile, and Jeffery L. Kohler. Online condition monitoring of induction motors. *IEEE Transactions on Industry Applications, Vol. 38, No. 6*, 2002.

Andrzej M. Trzynadlowski and Ewen Ritchie. Comparative investigation of diagnostic media for indiction motors, a case of rotor cage faults. *IEEE Transaction on Industrial Electronics, Vol. 47, No. 5*, 2000.

Pierre Vadstrup. Multiwinding modelling of induction motors. Technical report, Grundfos Mangement A/S, 2002. Internal technical rapport at Grunfos, not available.

E. Wiedenbrug, G. Frey, and J. Wilson. Impulse testing and turn insulation deterioration in electric motors. *IEEE Pulp and Paper Industry Technical Conference '03*, 2003.

S. Williamson and K. Mirzoian. Analysis of cage induction motors with stator windings faults. *IEEE Transactions on Power Apparatus and Systems, Vol. Pas-104, Issue. 7*, 1985.

Armin Wolfram, Dominik Fussel, Torsten Brune, and Rolf Isermann. Component-based multi-model aproach for fault detection and diagnosis of a centrifugal pump. *IEEE Proceedings of American Control Conference, ACC-2001*, 2001.

Aiping Xu and Qinghua Zhang. Nonlinear system fault diagnosis based on adaptive estimation. *Automatica, Vol. 40, No. 7*, 2004.

Zhongming Ye and Bin Wu. Online rotor bar breakage detection of three phase induction motors by wavelet packet decomposition and artificial neural network. *IEEE 32nd Annual Power Electronics Specialists Conference*, 2001.

Zhongming Ye, Bin Wu, and A. R. Sadaghian. Current signature analysis of induction motor mechanical faults by wavelet packet decomposition. *IEEE Transactions on Industrial Electronics, Vol. 50, No. 6.*, 2003.

Qinghua Zhang. A new residual generation and evaluation method for detection and isolation of faults in non-linear systems. *International Journal of Adaptive Control and Signal Processing, Vol. 14, No. 7*, 2000.

Appendix A

FMEA Tables Describing Faults in the System

This appendix contains tables describing the fault modes of the pump system. The pump system is in Chapter 4 devided into 7 components. These are,

- Electrical part of the induction motor.
- Mechanical part of the induction motor.
- Shaft.
- Hydraulic part of the centrifugal pump.
- Mechanical part of the centrifugal pump.
- Inlet of the pump.
- Outlet of the pump.

In each Section of this appendix one of the above components is analysed. This means that a FMEA table is given and that the disturbing events affecting the component are listed. The FMEA tables contain the following information; the *name of the fault mode*, the *causes of the fault*, and the *the effect of the fault*. Here, the general components, forming a centrifugal pump, are analysed. This means that no failure information of a particular product is used. This information is necessary to include risk assessment and frequency of the faults in the FMEA, and are therefore omitted here. The tables and matrices in this appendix are the results of the FMEA described in Chapter 4.

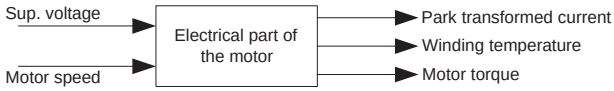

Figure A.1: The input/output structure of the electrical part of the induction motor.

A.1 Electrical part of the induction motor

The input/output structure of this part is shown in Fig. A.1, and the identified faults in the component are shown in the following FMEA table,

Electrical Part of the Motor			
	Fault Modes	Fault Causes	Possible Effects
Inputs	f_{em1} Loss of one or more phases of the supply voltage.	• Broken Fuse. • Fault on the supply cable. • poor connections.	$e_{em,i3}$ Oscillations in the length of the pack transform current. $e_{em,v1}$ Zero voltage in one or more of the phases. $e_{em,v2}$ Oscillations in the length of the pack transform voltage. $e_{em,t3}$ 1st harmonic torque oscillations.
	f_{em3} Short circuit between windings in the motor.	• Moisture or water in the motor. • Mechanical stress. • High motor temperature. • wear-out failure on the inter-turn insulation.	$e_{em,i3}$ Oscillations in the length of the pack transform current. $e_{em,T1}$ Increased temperature inside the motor.
	f_{em4} Short circuit to ground.	• Moisture or water in the motor. • Mechanical stress. • High motor temperature. • wear-out failure on the turn to ground insulation.	$e_{em,i3}$ Oscillations in the length of the pack transform current. $e_{em,i4}$ Unbalanced stator current. $e_{em,T1}$ Increased temperature inside the motor. $e_{em,t3}$ 1st harmonic torque oscillations.

Parts	f_{em5} Broken rotor bar.	• Poor production. • Mechanical stress.	$e_{em,i3}$ Oscillations in the length of the pack transform current. $e_{em,t4}$ higher harmonic torque oscillations.
	f_{em6} Eccentric air gab due to bend or misaligned motor shaft.	• Poor production. • Mechanical stress.	$e_{em,i4}$ Unbalanced stator current. $e_{em,t3}$ 1st harmonic torque oscillations.

The propagation matrix representation of the component is given by the following logical expression,

$$\mathbf{e}_{em} \leftarrow \mathbf{A}^{em}_{f_{em}} \mathbf{f}_{em} + \mathbf{A}^{em}_{dy} \mathbf{e}_{dy} \tag{A.1}$$

where the fault vector $\mathbf{f}_{em}$ and the effect vector $\mathbf{e}_{em}$ equals,

$$\mathbf{f}'_{em} = \begin{pmatrix} f_{em1} & f_{em2} & f_{em3} & f_{em4} & f_{em5} & f_{em6} \end{pmatrix}^T$$
$$\mathbf{e}_{em} = \begin{pmatrix} e_{em,i1} & e_{em,i2} & e_{em,i3} & e_{em,i4} & e_{em,v1} & e_{em,v2} \\ & & & e_{em,T1} & e_{em,t1} & e_{em,t2} & e_{em,t3} & e_{em,t4} \end{pmatrix}^T$$

A description of each fault and effect is found in the above FMEA table. The fault propargation matrix $\mathbf{A}^{em}_{f_{em}}$ in (A.1) is just a matrix representation of the connections between the faults and the effects described in the FMEA table presented in this section. The propagation matrix $\mathbf{A}^{em}_{dy}$ is defined below,

$$\mathbf{A}^{em}_{dy} = \begin{pmatrix} 0 & 1 & 0 & 0 & 0 & 0 & 0 \\ 1 & 0 & 0 & 0 & 0 & 0 & 0 \\ 0 & 0 & 1 & 0 & 0 & 0 & 0 \\ 0 & 0 & 1 & 0 & 0 & 0 & 0 \end{pmatrix}^T$$

To cover the disturbances affecting this component, the fault vector is extended with a set of disturbing events. These are,

Disturbing events	Causes	Effects
d_{em1} Unbalanced supply voltage.	• poor grid. • Fault on the supply cable. • poor connections.	$e_{em,i3}$ Oscillations in the length of the pack transform current. $e_{em,v2}$ Oscillations in the length of the pack transform voltage. $e_{em,t3}$ 1st harmonic torque oscillations.
d_{em2} Increased supply voltage.	• Changes in the supply grid. • Decreased grid load combined with too small grid for the load.	$e_{em,i1}$ Increased current.
d_{e2} Decreased supply voltage.	• Changes in the supply grid. • Increased grid load combined with too small grid for the load.	$e_{em,i2}$ Decreased current.

Including these disturbing events in the fault vector, it becomes,

$$\mathbf{f}_{em} = \left(\begin{array}{ccc} \mathbf{f}'_{em}{}^{T} & d_{em1} & d_{em2} \end{array} \right)^{T}$$

Likewise the matrix $\mathbf{A}^{em}_{f_{em}}$ is extended with rows according to the above table.

A.2 Mechanical dynamics

The input/output structure of this part is shown in Fig. A.2. As described in chapter 4

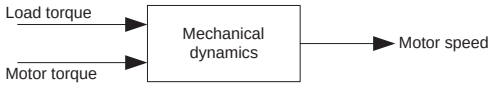

Figure A.2: The input/output structure of the part modelling the dynamics of the rotating parts of the pump.

this component is included in the analysis to cover the signal structure of the system, when building the functional model of the centrifugal pump. This means that no faults are identified in the component.

The propagation matrix representation of the component is given by the following logical expression,

$$\mathbf{e}_{dy} \leftarrow \mathbf{A}^{dy}_{em}\mathbf{e}_{em} + \mathbf{A}^{dy}_{mm}\mathbf{e}_{mm} + \mathbf{A}^{dy}_{sh}\mathbf{e}_{sh} + \mathbf{A}^{dy}_{i}\mathbf{e}_{i} + \mathbf{A}^{dy}_{mp}\mathbf{e}_{mp} \qquad \text{(A.2)}$$

The resulting effect vector $\mathbf{e}_{dy}$ in this expression is given by,

$$\mathbf{e}_{dy} = \begin{pmatrix} e_{dy,n1} & e_{dy,n2} & e_{dy,n3} & e_{dy,n4} \end{pmatrix}^T$$

where the effects in this vector are,

$$\begin{array}{ll} e_{dy,n1} & \sim \text{ Increased speed.} \\ e_{dy,n2} & \sim \text{ Decreased speed.} \\ e_{dy,n3} & \sim \text{ 1st harmonic speed oscillations.} \\ e_{dy,n4} & \sim \text{ higher harmonic speed oscillations.} \end{array}$$

The propagation matrices $\mathbf{A}_{em}^{dy}$, $\mathbf{A}_{mm}^{dy}$, $\mathbf{A}_{sh}^{dy}$, $\mathbf{A}_{i}^{dy}$, and $\mathbf{A}_{mp}^{dy}$ in (A.2) are defined below,

$$\mathbf{A}_{em}^{dy} = \begin{pmatrix} 0 & 0 & 0 & 0 & 0 & 0 & 0 & 1 & 0 & 0 & 0 \\ 0 & 0 & 0 & 0 & 0 & 0 & 0 & 0 & 1 & 0 & 0 \\ 0 & 0 & 0 & 0 & 0 & 0 & 0 & 0 & 0 & 1 & 0 \\ 0 & 0 & 0 & 0 & 0 & 0 & 0 & 0 & 0 & 0 & 1 \end{pmatrix}$$

$$\mathbf{A}_{mm}^{dy} = \begin{pmatrix} 0 & 1 & 0 & 0 & 0 & 0 & 0 \\ 1 & 0 & 0 & 0 & 0 & 0 & 0 \\ 0 & 0 & 1 & 0 & 0 & 0 & 0 \\ 0 & 0 & 0 & 1 & 0 & 0 & 0 \end{pmatrix}$$

$$\mathbf{A}_{sh}^{dy} = \begin{pmatrix} 0 & 0 & 0 & 0 & 0 & 0 & 0 & 0 & 0 \\ 0 & 0 & 0 & 0 & 0 & 0 & 0 & 0 & 0 \\ 0 & 0 & 0 & 0 & 0 & 1 & 0 & 1 & 0 \\ 0 & 0 & 0 & 0 & 0 & 0 & 1 & 0 & 1 \end{pmatrix}$$

$$\mathbf{A}_{i}^{dy} = \begin{pmatrix} 0 & 0 & 0 & 0 & 0 & 0 & 1 & 1 & 0 & 0 & 0 & 0 \\ 0 & 0 & 0 & 0 & 0 & 1 & 0 & 0 & 0 & 0 & 0 & 0 \\ 0 & 0 & 0 & 0 & 0 & 0 & 0 & 0 & 1 & 0 & 0 & 0 \\ 0 & 0 & 0 & 0 & 0 & 0 & 0 & 0 & 0 & 1 & 0 & 0 \end{pmatrix}$$

$$\mathbf{A}_{mp}^{dy} = \begin{pmatrix} 0 & 1 & 0 & 0 & 0 & 0 & 0 & 0 & 0 \\ 1 & 0 & 0 & 0 & 0 & 0 & 0 & 0 & 0 \\ 0 & 0 & 1 & 0 & 0 & 0 & 0 & 0 & 0 \\ 0 & 0 & 0 & 1 & 0 & 0 & 0 & 0 & 0 \end{pmatrix}$$

A.3 Mechanical part of the motor

The input/output structure of this part is shown in Fig. A.3, and the identified faults in the component are shown in the following FMEA table,

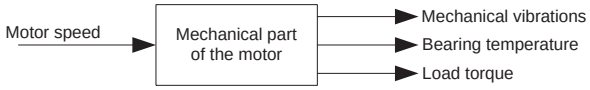

Figure A.3: The input/output structure of the mechanical part of the induction motor.

Mechanical Part of the Motor			
	Fault Modes	Fault Causes	Possible Effects
Parts	f_{mm1} Ware of the bearings in the motor.	• Ware-out faults due to a long running period. • Impurities in the bearings. • Water in the bearing oil.	$e_{mm,t4}$ higher harmonic torque oscillations. $e_{mm,T1}$ Increased bearing temperature. $e_{mm,v2}$ Increased higher harmonic vibrations.
	f_{mm2} Rub impact between the stator and the rotor due to a bend or misaligned motor shaft.	• Production fault. • Overload due to suddent blocked rotor.	$e_{mm,t1}$ Increased torque load from mechanical parts in the motor. $e_{mm,t3}$ 1st harmonic torque oscillations. $e_{mm,v1}$ Increased 1st harmonic vibrations.

The propagation matrix representation of the component is given by the following logical expression,

$$\mathbf{e}_{mm} \leftarrow \mathbf{A}^{mm}_{f_{mm}} \mathbf{f}_{mm} + \mathbf{A}^{mm}_{dy} \mathbf{e}_{dy} \tag{A.3}$$

where the fault vector $\mathbf{f}_{mm}$ and the effect vector $\mathbf{e}_{mm}$ equals,

$$\mathbf{f}_{mm} = \begin{pmatrix} f_{mm1} & f_{mm2} \end{pmatrix}^T$$

$$\mathbf{e}_{mm} = \begin{pmatrix} e_{mm,t1} & e_{mm,t2} & e_{mm,t3} & e_{mm,t4} & e_{mm,T1} & e_{mm,v1} & e_{mm,v2} \end{pmatrix}^T .$$

A description of each fault and effect is found in the above FMEA table. The fault propargation matrix $\mathbf{A}^{mm}_{f_{mm}}$ in (A.3) is just a matrix representation of the connections between the faults and the effects described in the FMEA table presented in this section. The propagation matrix $\mathbf{A}^{mm}_{dy}$ is defined below,

$$\mathbf{A}^{mm}_{dy} = \begin{pmatrix} 1 & 0 & 0 & 0 & 0 & 0 & 0 \\ 0 & 1 & 0 & 0 & 0 & 0 & 0 \\ 0 & 0 & 1 & 0 & 0 & 1 & 0 \\ 0 & 0 & 0 & 1 & 0 & 0 & 1 \end{pmatrix}^T$$

A.4 The shaft mechanics

The input/output structure of this part is shown in Fig. A.4, and the identified faults in

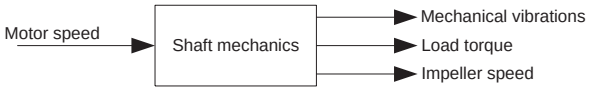

Figure A.4: The input/output structure of the shaft part.

the component are shown in the following FMEA table,

Shaft Mechanics			
	Fault Modes	Fault Causes	Possible Effects
Parts	f_{sh1} Broken shaft.		• $e_{sh,s5}$ Zero shaft speed.
	f_{sh2} Misalignment between the motor and pump.	• Overload due to sudden blocked rotor. • Fault introduced during production. • Fault introduced due to poor repair.	$e_{sh,t1}$ 1st harmonic torque oscillations. $e_{sh,v1}$ Increased 1st harmonic vibrations.
	f_{sh3} Bend shaft.	• Overload, due to for example blocked rotation.	$e_{sh,t1}$ 1st harmonic torque oscillations. $e_{sh,v1}$ Increased 1st harmonic vibrations.

The propagation matrix representation of the component is given by the following logical expression,

$$\mathbf{e}_{sh} \leftarrow \mathbf{A}^{sh}_{f_{sh}} \mathbf{f}_{sh} + \mathbf{A}^{sh}_{dy} \mathbf{e}_{dy} \tag{A.4}$$

where the fault vector $\mathbf{f}_{sh}$ and the effect vector $\mathbf{e}_{sh}$ equals,

$$\mathbf{f}_{mm} = \begin{pmatrix} f_{sh1} & f_{sh2} & f_{sh3} \end{pmatrix}^T$$

$$\mathbf{e}_{mm} = \begin{pmatrix} e_{sh,s1} & e_{sh,s2} & e_{sh,s3} & e_{sh,s4} & e_{sh,s5} & e_{mm,t1} & e_{mm,v1} \end{pmatrix}^T$$

A description of each fault and effect is found in the above FMEA table. The fault propargation matrix $\mathbf{A}^{sh}_{f_{sh}}$ in (A.4) is just a matrix representation of the connections

between faults and the effects described in the FMEA table presented in this section. The propagation matrix $\mathbf{A}_{dy}^{sh}$ is defined below,

$$\mathbf{A}_{dy}^{mm} = \begin{pmatrix} 1 & 0 & 0 & 0 & 0 & 0 & 0 \\ 0 & 1 & 0 & 0 & 0 & 0 & 0 \\ 0 & 0 & 1 & 0 & 0 & 0 & 0 \\ 0 & 0 & 0 & 1 & 0 & 0 & 0 \end{pmatrix}^T$$

A.5 Hydraulics of the Centrifugal Pump

The input/output structure of this part is shown in Fig. A.5, and the identified faults in

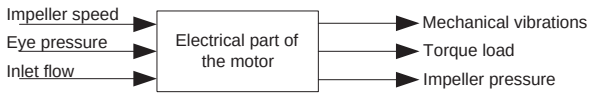

Figure A.5: The input/output structure of the part describing the hydraulics of the centrifugal pump.

the component are shown in the following FMEA table,

Hydraulics of the Centrifugal Pump			
	Fault Modes	Fault Causes	Possible Effects
Inputs	f_{i1} Dry running.	• Error in the hydraulic system in which the pump is placed.	$e_{i,h3}$ Zero pressure. $e_{i,t3}$ Zero torque load from the impeller.
	f_{i2} Impurities fixed on the impeller, causing inbalance.	• Impurities in the water.	$e_{i,h4}$ Harmonic pressure oscillations. $e_{i,t4}$ 1st harmonic torque oscillations. $e_{i,t5}$ higher harmonic torque oscillations. $e_{i,v1}$ Increased 1st harmonic vibrations. $e_{i,v2}$ Increased higher harmonic vibrations.

Parts

f_{i3} Wear of the impeller.	• Sand and other impurities in the water.	$e_{i,h2}$ Decreased pressure. $e_{i,h4}$ Harmonic pressure oscillations. $e_{i,t2}$ Decreased torque load from the impeller. $e_{i,t4}$ 1st harmonic torque oscillations. $e_{i,t5}$ higher harmonic torque oscillations. $e_{i,v1}$ Increased 1st harmonic vibrations. $e_{i,v2}$ Increased higher harmonic vibrations.
f_{i4} Blocked or partial blocked flow field inside the impeller.	• Larges obstical in the liquid.	$e_{i,h2}$ Decreased pressure. $e_{i,h4}$ Harmonic pressure oscillations. $e_{i,t2}$ Decreased torque load from the impeller. $e_{i,t4}$ 1st harmonic torque oscillations. $e_{i,t5}$ higher harmonic torque oscillations. $e_{i,v1}$ Increased 1st harmonic vibrations. $e_{i,v2}$ Increased higher harmonic vibrations.
f_{i5} Blocked impeller rotation.	• Sand and other impurities in the water.	$e_{i,h3}$ Zero pressure. $e_{i,t1}$ Increased torque load from the impeller.
f_{i6} Wear of the sealing ring.	• Long running time / normal wear. • Overheated, due to for example dry running.	$e_{i,h2}$ Decreased pressure. $e_{i,t2}$ Decreased torque load from the impeller.
f_{i7} Missing sealing ring.	• Production error.	$e_{i,h2}$ Decreased pressure. $e_{i,t2}$ Decreased torque load from the impeller.

	f_{i8} Loss of the impeller.	• Production error. • Mechanical vibrations.	$e_{i,h3}$ Zero pressure. $e_{i,t3}$ Zero torque load from the impeller.

The propagation matrix representation of the component is given by the following logical expression,

$$\mathbf{e}_i \leftarrow \mathbf{A}^i_{f_i}\mathbf{f}_i + \mathbf{A}^i_{sh}\mathbf{e}_{sh} + \mathbf{A}^i_{ip}\mathbf{e}_{ip} \tag{A.5}$$

where the fault vector $\mathbf{f}_i$ and the effect vector $\mathbf{e}_i$ equals,

$$\mathbf{f}_i = \begin{pmatrix} f_{i1} & f_{i2} & f_{i3} & f_{i4} & f_{i5} & f_{i6} & f_{i7} & f_{i8} \end{pmatrix}^T$$
$$\mathbf{e}_i = \begin{pmatrix} e_{i,h1} & e_{i,h2} & e_{i,h3} & e_{i,h4} & e_{i,h5} & e_{i,t1} & e_{i,t2} & e_{i,t3} & e_{i,t4} & e_{i,t5} & e_{i,v1} & e_{i,v2} \end{pmatrix}^T$$

A description of each fault and effect is found in the above FMEA table. The fault propargation matrix $\mathbf{A}^i_{f_i}$ in (A.5) is just a matrix representation of the connections between the faults and the effects described in the FMEA table presented in this section. The propagation matrices $\mathbf{A}^i_{sh}$ and $\mathbf{A}^i_{ip}$ are defined below,

$$\mathbf{A}^i_{sh} = \begin{pmatrix} 1 & 0 & 0 & 0 & 0 & 1 & 0 & 0 & 0 & 0 & 0 & 0 \\ 0 & 1 & 0 & 0 & 0 & 0 & 1 & 0 & 0 & 0 & 0 & 0 \\ 0 & 0 & 0 & 1 & 0 & 0 & 0 & 0 & 1 & 0 & 1 & 0 \\ 0 & 0 & 0 & 1 & 0 & 0 & 0 & 0 & 0 & 1 & 0 & 1 \\ 0 & 0 & 1 & 0 & 0 & 0 & 0 & 1 & 0 & 0 & 0 & 0 \\ 0 & 0 & 0 & 0 & 0 & 0 & 0 & 0 & 0 & 0 & 0 & 0 \\ 0 & 0 & 0 & 0 & 0 & 0 & 0 & 0 & 0 & 0 & 0 & 0 \end{pmatrix}^T$$

$$\mathbf{A}^i_{ip} = \begin{pmatrix} 0 & 0 & 1 & 0 & 0 & 0 & 0 & 1 & 0 & 0 & 0 & 0 \\ 0 & 1 & 0 & 1 & 0 & 0 & 1 & 0 & 0 & 0 & 0 & 1 \\ 0 & 0 & 0 & 0 & 1 & 0 & 0 & 0 & 0 & 0 & 0 & 0 \\ 0 & 0 & 0 & 0 & 0 & 0 & 0 & 0 & 0 & 0 & 0 & 0 \\ 0 & 0 & 0 & 0 & 0 & 0 & 0 & 0 & 0 & 0 & 0 & 0 \\ 0 & 0 & 0 & 0 & 0 & 0 & 0 & 0 & 0 & 0 & 0 & 0 \end{pmatrix}^T$$

To cover the disturbances affecting this component, the fault vector is extended with a set of disturbing events. These are,

Disturbing events	Causes	Effects
d_{i1} Decreased flow through the pump.	• Changes in the hydraulic system in which the pump is placed.	$e_{i,h1}$ Increased pressure. $e_{i,t2}$ Decreased torque load from the impeller.
d_{i2} Increased flow through the pump.	• Changes in the hydraulic system in which the pump is placed.	$e_{i,h2}$ Decreased pressure. $e_{i,t1}$ Increased torque load from the impeller.

Including these disturbing events in the fault vector, it becomes,

$$\mathbf{f}_i = \begin{pmatrix} \mathbf{f}_i'^T & d_{i1} & d_{i2} \end{pmatrix}^T$$

Likewise the matrix $\mathbf{A}^i_{f_i}$ is extended with rows according to the above table.

A.6 Mechanical Part of the Pump

The input/output structure of this part is shown in Fig. A.6, and the identified faults in

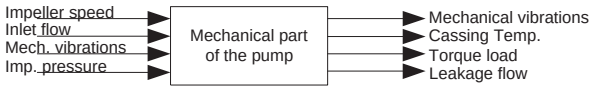

Figure A.6: The input/output structure of the part including all mechanical components in the pump, not directly involved in the pressure generation.

the component are shown in the following FMEA table,

	Mechanical Part of the Pump		
	Fault Modes	Fault Causes	Possible Effects
Inputs	f_{mp1} Dry running.	• Error in the hydraulic system in which the pump is placed.	$e_{mp,tp1}$ Increased bearing temperature.
	f_{mp2} Inlet flow equal to zero.	• Error in the hydraulic system in which the pump is placed.	$e_{mp,tp1}$ Increased bearing temperature.

Parts	f_{mp3} Ware of the bearings in the pump.	• Sand in the liquid. • Wear out due to long runing time.	$e_{mp,t3}$ 1st harmonic torque oscillations. $e_{mp,t4}$ higher harmonic torque oscillations. $e_{mp,tp1}$ Increased bearing temperature. $e_{mp,v1}$ Increased 1st harmonic vibrations.
	f_{mp4} Ware of seals.	• Over heated seals, due to for example dry running or zero flow. • Wear out due to long runing time.	$e_{mp,q1}$ Leakage flow from the pump.
	f_{mp5} Rub impact between the impeller and the cassing.	• Dirte fixed between the rotating and stationary parts of the pump. • Bend shaft due to overload, cause by for example large obsticals in the liquid.	$e_{mp,t1}$ Increased torque load from the mechanical parts of the pump. $e_{mp,t3}$ 1st harmonic torque oscillations. $e_{mp,v1}$ Increased 1st harmonic vibrations.

The propagation matrix representation of the component is given by the following logical expression,

$$\mathbf{e}_{mp} \leftarrow \mathbf{A}^{mp}_{f_{mp}}\mathbf{f}_{mp} + \mathbf{A}^{mp}_{sh}\mathbf{e}_{sh} + \mathbf{A}^{mp}_{i}\mathbf{e}_{i} \tag{A.6}$$

where the fault vector $\mathbf{f}_{mp}$ and the effect vector $\mathbf{e}_{mp}$ equals,

$$\mathbf{f}_{mp} = \begin{pmatrix} f_{mp1} & f_{mp2} & f_{mp3} & f_{mp4} & f_{mp5} \end{pmatrix}^T$$
$$\mathbf{e}_{mp} = \begin{pmatrix} e_{mp,t1} & e_{mp,t2} & e_{mp,t3} & e_{mp,t4} & e_{mp,T5} & e_{mp,v1} & e_{mp,v2} & e_{mp,q1} \end{pmatrix}^T$$

A description of each fault and effect is found in the above FMEA table. The fault propargation matrix $\mathbf{A}^{mp}_{f_{mp}}$ in (A.6) is just a matrix representation of the connections between the faults and the effects described in the FMEA table presented in this section.

The propagation matrices $\mathbf{A}_{sh}^{mp}$ and $\mathbf{A}_{i}^{mp}$ are defined below,

$$\mathbf{A}_{sh}^{mp} = \begin{pmatrix} 1 & 0 & 0 & 0 & 0 & 0 & 0 & 0 \\ 0 & 1 & 0 & 0 & 0 & 0 & 0 & 0 \\ 0 & 0 & 1 & 0 & 0 & 0 & 0 & 0 \\ 0 & 0 & 0 & 1 & 0 & 0 & 0 & 0 \\ 0 & 1 & 0 & 0 & 0 & 0 & 0 & 0 \\ 0 & 0 & 0 & 0 & 0 & 0 & 0 & 0 \\ 0 & 0 & 0 & 0 & 0 & 0 & 0 & 0 \end{pmatrix}^T$$

$$\mathbf{A}_{i}^{mp} = \begin{pmatrix} 0 & 0 & 0 & 0 & 0 & 0 & 0 & 0 \\ 0 & 0 & 0 & 0 & 0 & 0 & 0 & 0 \\ 0 & 0 & 0 & 0 & 0 & 0 & 0 & 0 \\ 0 & 0 & 0 & 0 & 0 & 1 & 1 & 0 \\ 0 & 0 & 0 & 0 & 0 & 0 & 1 & 0 \\ 0 & 0 & 0 & 0 & 0 & 0 & 0 & 0 \\ 0 & 0 & 0 & 0 & 0 & 0 & 0 & 0 \\ 0 & 0 & 0 & 0 & 0 & 0 & 0 & 0 \\ 0 & 0 & 0 & 0 & 0 & 0 & 0 & 0 \\ 0 & 0 & 0 & 0 & 0 & 0 & 0 & 0 \\ 0 & 0 & 0 & 0 & 0 & 1 & 0 & 0 \\ 0 & 0 & 0 & 0 & 0 & 0 & 1 & 0 \end{pmatrix}^T$$

A.7 Inlet Part of the Pump

The input/output structure of this part is shown in Fig. A.7, and the identified faults in

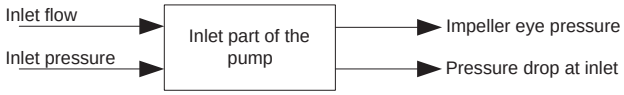

Figure A.7: The input/output structure of the part including the component forming the inlet of the pump.

the component are shown in the following FMEA table,

Inlet part of the pump			
	Fault Modes	Fault Causes	Possible Effects
Inputs	f_{ip1} Dry running.	• Application error.	$e_{ip,e1}$ The pressure at impeller eye is not defined. $e_{ip,h1}$ The pressure drop at the inlet part is not defined.
Parts	f_{ip2} Low pressure at the inlet of the pump.	• Poor dimensioned system. • Low water level in the inlet tank or well.	$e_{ip,e2}$ To low impeller eye pressure.
	f_{ip3} Opstruction of the inlet of the pump.	• Clogging in the inlet part, due to impurities in the water.	$e_{ip,e2}$ To low impeller eye pressure. $e_{ip,h2}$ The pressure drop at the inlet part is increased.

The propagation matrix representation of the component is given by the following logical expression,

$$\mathbf{e}_{ip} \leftarrow \mathbf{A}^{ip}_{f_{ip}} \mathbf{f}_{ip} \tag{A.7}$$

where the fault vector $\mathbf{f}_{ip}$ and the effect vector $\mathbf{e}_{ip}$ equals,

$$\mathbf{f}'_{ip} = \begin{pmatrix} f_{ip1} & f_{ip2} & f_{ip3} \end{pmatrix}^T$$
$$\mathbf{e}_{ip} = \begin{pmatrix} e_{ip,e1} & e_{ip,e2} & e_{ip,e3} & e_{ip,h1} & e_{ip,h2} & e_{ip,h3} \end{pmatrix}^T$$

A description of each fault and effect is found in the above FMEA table. The fault propargation matrix $\mathbf{A}^{ip}_{f_{ip}}$ in (A.7) is just a matrix representation of the connections between the faults and the effects described in the FMEA table presented in this section.

To cover the disturbances affecting this component, the fault vector is extended with a set of disturbing events. These are,

Disturbing events	Causes	Effects
d_{ip1} Decreased flow through the pump.	• Changes in the hydraulic system in which the pump is placed.	$e_{ip,h3}$ The pressure drop at the inlet part is decreased.
d_{ip2} Increased flow through the pump.	• Changes in the hydraulic system in which the pump is placed.	$e_{ip,h2}$ The pressure drop at the inlet part is increased.

d_{ip3} High frequency pressure oscillations.	• High frequency pressure noise, due to for example cavitation in valves.	$e_{ip,e3}$ High frequency pressure oscillations at the impeller eye.

Including these disturbing events in the fault vector, it becomes,

$$\mathbf{f}_{ip} = \left(\begin{array}{cccc} \mathbf{f}_{ip}'^{\,T} & d_{ip1} & d_{ip2} & d_{ip3} \end{array} \right)^T$$

Likewise the matrix $\mathbf{A}^{ip}_{f_{ip}}$ is extended with rows according to the above table.

A.8 Outlet part of the Pump

The input/output structure of this part is shown in Fig. A.8, and the identified faults in

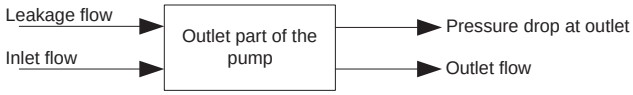

Figure A.8: The input/output structure of the part including the component forming the outlet of the pump.

the component are shown in the following FMEA table,

Outlet part of the pump			
	Fault Modes	Fault Causes	Possible Effects
Inputs	f_{op1} Dry running.	• Application error.	$e_{op,h1}$ The pressure drop at the outlet part is not defined. $e_{op,q1}$ The outlet flow is not defined.
Parts	f_{op2} Leakage on the outlet pipe.	• Waer of the outlet part.	$e_{op,q2}$ The outlet flow is descreased.
	f_{op3} Opstruction of the outlet pipe.	• Clogging in the outlet part, due to impurities in the warter.	$e_{op,h2}$ The pressure drop at the outlet part is increased.

The propagation matrix representation of the component is given by the following logical expression,

$$\mathbf{e}_{op} \leftarrow \mathbf{A}^{op}_{f_{op}} \mathbf{f}_{op} + \mathbf{A}^{op}_{mp} \mathbf{e}_{mp} \tag{A.8}$$

where the fault vector $\mathbf{f}_{op}$ and the effect vector $\mathbf{e}_{op}$ equals,

$$\mathbf{f}'_{op} = \begin{pmatrix} f_{op1} & f_{op2} & f_{op3} \end{pmatrix}^T$$
$$\mathbf{e}_{op} = \begin{pmatrix} e_{op,h1} & e_{op,h2} & e_{op,h3} & e_{op,q1} & e_{op,q2} \end{pmatrix}^T$$

A description of each fault and effect is found in the above FMEA table. The fault propargation matrix $\mathbf{A}^{op}_{f_{op}}$ in (A.8) is just a matrix representation of the connections between the faults and the effects described in the FMEA table presented in this section. The propagations matrix $\mathbf{A}^{op}_{mp}$ is defined below,

$$\mathbf{A}^{op}_{mp} = \begin{pmatrix} 0 & 0 & 0 & 0 & 0 \\ 0 & 0 & 0 & 0 & 0 \\ 0 & 0 & 0 & 0 & 0 \\ 0 & 0 & 0 & 0 & 0 \\ 0 & 0 & 0 & 0 & 0 \\ 0 & 0 & 0 & 0 & 0 \\ 0 & 0 & 0 & 0 & 0 \\ 0 & 0 & 0 & 0 & 1 \end{pmatrix}^T$$

To cover the disturbances affecting this component, the fault vector is extended with a set of disturbing events. These are,

Disturbing events	Causes	Effects
d_{ip1} Decreased flow through the pump.	• Changes in the hydraulic system in which the pump is placed.	$e_{op,h3}$ The pressure drop at the outlet part is decreased.
d_{ip2} Increased flow through the pump.	• Changes in the hydraulic system in which the pump is placed.	$e_{op,h2}$ The pressure drop at the outlet part is increased.

Including these disturbing events in the fault vector, it becomes,

$$\mathbf{f}_{op} = \begin{pmatrix} \mathbf{f}'^{\,T}_{op} & d_{op1} & d_{op2} \end{pmatrix}^T$$

Likewise the matrix $\mathbf{A}^{op}_{f_{op}}$ is extended with rows according to the above table.

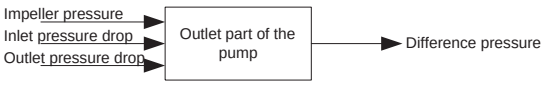

Figure A.9: The input/output structure of the part modelling the dynamics of the rotating parts of the pump.

A.9 Difference pressure

The input/output structure of this part is shown in Fig. A.9. As described in chapter 4 this component is included in the analysis to cover the signal structure of the system when building the functional model of the centrifugal pump. This means that no faults are identified in the component.

The propagation matrix representation of the component is given by the following logical expression,

$$\mathbf{e}_{dy} = \mathbf{A}_{i}^{dh}\mathbf{e}_{i} + \mathbf{A}_{ip}^{dh}\mathbf{e}_{ip} + \mathbf{A}_{op}^{dh}\mathbf{e}_{op} \tag{A.9}$$

The resulting effect vector $\mathbf{e}_{dh}$ in this expression is given by,

$$\mathbf{e}_{dh} = \begin{pmatrix} e_{dh,h1} & e_{dh,h2} & e_{dh,h3} & e_{dh,h4} & e_{dh,h5} & e_{dh,h6} \end{pmatrix}^{T}$$

where the effects in this vector are,

$e_{op,h1}$	$\sim$	Increased pressure difference across the pump.
$e_{op,h2}$	$\sim$	Decreased pressure difference across the pump.
$e_{op,h3}$	$\sim$	Zero pressure difference across the pump.
$e_{op,h4}$	$\sim$	Harmonic oscillations in the pressure difference signal.
$e_{op,h5}$	$\sim$	High frequence oscillations in the pressure difference signal.
$e_{op,h6}$	$\sim$	Pressure difference across the pump is not defined.

The propagation matrices $\mathbf{A}_i^{dh}$, $\mathbf{A}_{ip}^{dh}$, and $\mathbf{A}_{op}^{dh}$ in (A.9) are defined below,

$$\mathbf{A}_i^{dh} = \begin{pmatrix} 1 & 0 & 0 & 0 & 0 & 0 \\ 0 & 1 & 0 & 0 & 0 & 0 \\ 0 & 0 & 1 & 0 & 0 & 0 \\ 0 & 0 & 0 & 1 & 0 & 0 \\ 0 & 0 & 0 & 0 & 1 & 0 \\ 0 & 0 & 0 & 0 & 0 & 0 \\ 0 & 0 & 0 & 0 & 0 & 0 \\ 0 & 0 & 0 & 0 & 0 & 0 \\ 0 & 0 & 0 & 0 & 0 & 0 \\ 0 & 0 & 0 & 0 & 0 & 0 \\ 0 & 0 & 0 & 0 & 0 & 0 \\ 0 & 0 & 0 & 0 & 0 & 0 \end{pmatrix}^T$$

$$\mathbf{A}_{ip}^{dh} = \begin{pmatrix} 0 & 0 & 0 & 0 & 0 & 0 \\ 0 & 0 & 0 & 0 & 0 & 0 \\ 0 & 0 & 0 & 0 & 0 & 0 \\ 0 & 0 & 0 & 0 & 0 & 1 \\ 0 & 1 & 0 & 0 & 0 & 0 \\ 1 & 0 & 0 & 0 & 0 & 0 \end{pmatrix}^T$$

$$\mathbf{A}_{op}^{dh} = \begin{pmatrix} 0 & 0 & 0 & 0 & 0 & 1 \\ 0 & 1 & 0 & 0 & 0 & 0 \\ 1 & 0 & 0 & 0 & 0 & 0 \\ 0 & 0 & 0 & 0 & 0 & 0 \\ 0 & 0 & 0 & 0 & 0 & 0 \end{pmatrix}^T$$

Appendix B

Mathematical Tools

This appendix contains a short presentation of two mathematical tools used in this thesis. These are a CUSUM alogithm, and some notes on Linear Matrix Inequalities (LMI).

B.1 The CUSUM Algorithm

The cumulative sum (CUSUM) algorithm is a statistical tool to identify changes in the statistical properties of a signal. The algorithm is described in (Basseville and Nikiforov, 1998, Sec. 2.2). This presentation is based of one particular version of the CUSUM Algorithm also presented in (Basseville and Nikiforov, 1998).

The CUSUM algorithm is based on the log-likelihood ratio $ln\frac{p_{\theta_1}(y_k)}{p_{\theta_0}(y_k)}$, which can be used to measure the likelihood of two different hypotheses H_0 and H_1 described by the parameter θ, i.e.

$$\begin{aligned} H_0 &: \theta = \theta_0 \\ H_1 &: \theta = \theta_1 \end{aligned}$$

These hypotheses can be tested using a recursive algorithm called the CUSUM algorithm. One from of this algorithm is given by,

$$g_k = \begin{cases} g_{k-1} + \ln \frac{p_{\theta_1}(y_k)}{p_{\theta_0}(y_k)} & \text{if} \quad g_{k-1} + \ln \frac{p_{\theta_1}(y_k)}{p_{\theta_0}(y_k)} > 0 \\ 0 & \text{if} \quad g_{k-1} + \ln \frac{p_{\theta_1}(y_k)}{p_{\theta_0}(y_k)} \leq 0 \end{cases} \tag{B.1}$$

where $g_0 = 0$. The interpretation of the variable g_k, compared to the hypothesis H_0 and H_1, is given by the decision signal D,

$$D = \begin{cases} 1 & \text{if} \quad g_k \geq h \\ 0 & \text{otherwise} \end{cases}$$

where h is a predefined threshold value. If $D = 1$ the hypotheses H_1 is most likely to have occurred and otherwise of $D = 0$.

In this work the CUSUM algorithm is used to statistical evaluation of residual signals. Here it is assumed that the residual signals are normal distributed, meaning that their distribution is given by,

$$p_\mu(y) = \frac{1}{\sigma\sqrt{2\pi}}\, e^{-\frac{(y-\mu)^2}{2\sigma^2}}$$

where μ is the mean value of the residual. Therefore it can be deduced that $\mu = \mu_0 = 0$ in the no fault case, and $\mu = \mu_1 \neq 0$ in the faulty case. It is assumed that the variances of the residual signals are known and do not change due to faults, i.e. σ in the above expression is constant and known. When these properties are fulfilled the log-likelihood in the CUSUM algorithm (B.1) is given by,

$$\ln \frac{p_{\mu_1}(y_k)}{p_{\mu_0}(y_k)} = -\frac{(y_k - \mu_1)^2}{2\sigma^2} + \frac{y_k^2}{2\sigma^2} = -\frac{\mu_1}{\sigma^2}\left(y_k - \frac{\mu_1}{2}\right)$$

The signal g_k in the CUSUM algorithm (B.1) is bounded from below by 0. In the algorithm used in this work the signal g_k is also bounded from above by h, resulting in the following algorithm,

$$g_k = \begin{cases} 0 & \text{if} \quad g_{k-1} - \frac{\theta_1}{\sigma^2}\left(y_k - \frac{\theta_1}{2}\right) \leq 0 \\ h & \text{if} \quad g_{k-1} - \frac{\theta_1}{\sigma^2}\left(y_k - \frac{\theta_1}{2}\right) \geq h \\ g_{k-1} - \frac{\theta_1}{\sigma^2}\left(y_k - \frac{\theta_1}{2}\right) & \text{otherwise} \end{cases} \tag{B.2}$$

This algorithm is a discrete algorithm. However, only continuous systems are considered in this work. Therefore, for the sake of cosistency a continuous version of (B.2) is given below. Here $s(t) = -\frac{\mu_1}{\sigma^2}\left(y(t) - \frac{\mu_1}{2}\right)$ is used.

$$\frac{dg}{dt} = \begin{cases} 0 & \text{if} \quad (g(t) = 0 \wedge s(t) \leq 0) \vee (g(t) = h \wedge 0 \leq s(t)) \\ s(t) & \text{otherwise} \end{cases} \tag{B.3}$$

where $\wedge$ and $\vee$ denotes the logical *and* and *or* operator respectively.

B.2 Linear Matrix Inequalities

In this appendix some general remarks on Linear Matrix Inequalities (LMI)'s and there use in connection with parameter variating systems are presented. The presentation is based on (Scherer and Weiland, 1999). First the consept of LMI's is defined, followed by three proporsitions dealing with stability of parameter variating system. These proporsitions are in Section 5.2.2 used in the analysis and synthesis of the feedback gain in the proposed adaptive observer.

A LMI is an expression on the form,

$$\mathbf{F}(\mathbf{x}) = \mathbf{F}_0 + \sum_{i=1}^{m} x_i \mathbf{F}_i \prec 0 \tag{B.4}$$

where

- $\mathbf{x} = \begin{bmatrix} x_1 & x_2 & \cdots & x_m \end{bmatrix}$ is a vector of real numbers.
- $\mathbf{F}_0, \cdots, \mathbf{F}_m$ are real symmetric matrices, i.e. $\mathbf{F}_i = \mathbf{F}_i^T \in R^{n \times n}$, $i = 1, \cdots, m$ for some $n \in Z_+$.
- The inequality $\prec 0$ in (B.4) means positive definite, i.e. $\mathbf{u}^T \mathbf{F}(\mathbf{x}) \mathbf{u} < 0$ for all $\mathbf{u} \in R^n$. Equivalently, the largest eigenvalue of $\mathbf{F}(\mathbf{x})$ is negative.

This is stated in slightly more general in the following definition.

Definition B.2.1 (Linear Matrix Inequality) *(Scherer and Weiland, 1999, Sec. 1.3) A Linear Matrix Inequality (LMI) is an inequality,*

$$\mathbf{F}(\mathbf{X}) \prec 0 \tag{B.5}$$

where $\mathbf{F}$ is an affine function mapping a finit dimensional vector space $\mathcal{V}$ to the set $\mathcal{S}^n = \{\mathbf{M} \mid \mathbf{M} = \mathbf{M}^T \in R^{n \times n}\}$, $n > 0$ of real symmetric matrices.

The feasibility of the LMI defined in Definition B.2.1 denotes the existence of at least one $\mathbf{X}$ which fulfills (B.5). Likewise the LMI is infeasible if such an $\mathbf{X}$ does not exist. If an affine performance function on the form $c(\mathbf{X})$ is defined, algorithms exists which can solve the minimization problem $\min_{\mathbf{X}} c(\mathbf{X})$ constrainted by (B.5).

LMI's as defined in Definition B.2.1 can be used for checking stability of linear systems with unknown and variating parameters. Such a system is shown below,

$$\dot{\mathbf{x}} = \mathbf{A}(\boldsymbol{\delta}(t))\mathbf{x} \tag{B.6}$$

where the state matrix $\mathbf{A}(\boldsymbol{\delta}(t))$ is a function of the real valued parameter vector $\boldsymbol{\delta}$. In all physical system this parameter vector belongs to a bounded set $\boldsymbol{\Delta}$, i.e. $\boldsymbol{\delta} \in \boldsymbol{\Delta}$.

Suppose that the state matrix $\mathbf{A}(\boldsymbol{\delta}(t))$ is an affine function of the parameters, i.e. $\mathbf{A}(\boldsymbol{\delta}(t)) = \mathbf{A}_0 + \sum_{j=1}^{k} \delta_j(t)\mathbf{A}_j$ for all $\boldsymbol{\delta} \in \boldsymbol{\Delta}$, then (B.6) is refered to as an *affine parameter dependent model*. Suppose that the unknown parameters δ_j $j = 1, \cdots, k$ in this expression are bounded on an interval, i.e. $\delta_j \in [\underline{\delta}_j, \overline{\delta}_j]$. If the unknown parameters are bounded on this interval the *corners* of the uncertainty region is given by the set,

$$\boldsymbol{\Delta}_0 = \left\{ \boldsymbol{\delta} = (\delta_1, \cdots, \delta_k) \mid \delta_j \in \{\underline{\delta}_j, \overline{\delta}_j\} \right\} \tag{B.7}$$

Then the uncertainty region $\boldsymbol{\Delta} = co\{\boldsymbol{\Delta}_0\}$, where co denotes the convex hull of the generators $\boldsymbol{\Delta}_0$ (Scherer and Weiland, 1999).

The stability of (B.6), when $\mathbf{A}(\boldsymbol{\delta}(t))$ is an affine parameter dependent model, is formulated by an LMI in the following proposition.

Proposition B.2.1 *(Scherer and Weiland, 1999, Sec. 2.4) if (B.6) is an affine parameter dependent model then it is quadratically stable if and only of there exists* $\mathbf{P} \succ 0$ *such that*

$$\mathbf{A}(\boldsymbol{\delta})^T\mathbf{P} + \mathbf{P}\mathbf{A}(\boldsymbol{\delta}) \prec 0$$

for all $\boldsymbol{\delta} \in \boldsymbol{\Delta}_0$*, where* $\boldsymbol{\Delta}_\mathbf{0}$ *contains the generators of the convex hull, i.e.* $\boldsymbol{\Delta} = co\{\boldsymbol{\Delta}_0\}$.

This proposition is motivated by the Lyapunov stability criterion. When Proposition B.2.1 holds, system (B.6) is stable for arbitrary fast variations of $\boldsymbol{\delta}$. However, if the parameters are unknown and bounded on a set, but not variating Proposition B.2.1 is to restricted, i.e. system (B.6) can be stable for all $\boldsymbol{\delta} \in \boldsymbol{\Delta}$ even though Proprosition B.2.1 does not hold.

The following proposition states the stability conditions for (B.6) if the parameter vector is assumed constant, i.e. $\dot{\boldsymbol{\delta}} = 0$.

Proposition B.2.2 *(Scherer and Weiland, 1999, Page 62) If (B.6) is an affine parameter dependent model and* $\boldsymbol{\Delta} \subset R^k$ *is the uncertainty set given by* $\boldsymbol{\Delta} = co\{\boldsymbol{\Delta}_0\}$*, where* $\boldsymbol{\Delta}_0$ *is defined in (B.7), then system (B.6) is affinely quadralically stable if there exist real matrices* $\mathbf{P}_0, \cdots, \mathbf{P}_k$ *such that,*

$$\mathbf{A}(\boldsymbol{\delta})^T\mathbf{P}(\boldsymbol{\delta}) + \mathbf{P}(\boldsymbol{\delta})\mathbf{A}(\boldsymbol{\delta}) \prec 0 \qquad \forall \boldsymbol{\delta} \in \boldsymbol{\Delta}_0 \tag{B.8a}$$

$$\mathbf{P}(\boldsymbol{\delta}) \succ 0 \qquad \forall \boldsymbol{\delta} \in \boldsymbol{\Delta}_0 \tag{B.8b}$$

$$\mathbf{A}_j^T\mathbf{P}_j + \mathbf{P}_j\mathbf{A}_j \succeq 0 \qquad \textit{for } j = 1, \cdots, k \tag{B.8c}$$

Here, $\mathbf{A}(\boldsymbol{\delta}) = \mathbf{A}_0 + \sum_{j=1}^k \delta_j\mathbf{A}_j$ *and* $\mathbf{P}(\boldsymbol{\delta}) = \mathbf{P}_0 + \sum_{j=1}^k \delta_j\mathbf{P}_j$*. Moreover, in that case* $V(\mathbf{x}, \boldsymbol{\delta}) := \mathbf{x}^T\mathbf{P}(\boldsymbol{\delta})\mathbf{x}$ *is a quadratic parameter-dependent Lyapunov function for the system.*

Proposition B.2.1 states the stability conditions for system (B.6) for abitraly variating parameters $\boldsymbol{\delta} \in \boldsymbol{\Delta}$ and Proposition B.2.2 stated the stability condition for the same system when the parameters $\boldsymbol{\delta} \in \boldsymbol{\Delta}$ are constant. The following proporsition states the stability conditions in the case where the parameters are variating, but with a limet on the variation rate, i.e. $\dot{\delta}_i = \lambda_i \in [\overline{\lambda}_i, \underline{\lambda}_i]$. If each variation rate is limited to this set, the *corners* of the uncertainty region of the variations rates is given by,

$$\boldsymbol{\Lambda}_0 = \{\boldsymbol{\lambda} = (\lambda_1, \cdots, \lambda_k) \mid \lambda_i \in [\overline{\lambda}_i, \underline{\lambda}_i]\} \tag{B.9}$$

Then the uncertainty region $\boldsymbol{\Lambda} = co\{\boldsymbol{\Lambda}_0\}$ is the set of possible variation rates of the parameters $\boldsymbol{\delta}$. When the variation rates are limited on this set the following proposition states the stability conditions for system (B.6).

Proposition B.2.3 *(Scherer and Weiland, 1999, Page 64) If (B.6) is an affine parameter dependent model and* $\boldsymbol{\Delta} \subset R^k$ *is the uncertainty set given by* $\boldsymbol{\Delta} = co\{\boldsymbol{\Delta}_0\}$*, where* $\boldsymbol{\Delta}_0$

is defined in (B.7), then system (B.6) is affinely quadralically stable if there exist real matrices $\mathbf{P}_0, \cdots, \mathbf{P}_k$ *such that,*

$$\mathbf{A}(\boldsymbol{\delta})^T\mathbf{P}(\boldsymbol{\delta}) + \mathbf{P}(\boldsymbol{\delta})\mathbf{A}(\boldsymbol{\delta}) + \mathbf{P}(\boldsymbol{\lambda}) \prec \mathbf{P}_0 \qquad \forall\, \boldsymbol{\delta} \in \boldsymbol{\Delta}_0 \text{ and } \boldsymbol{\lambda} \in \boldsymbol{\Lambda}_0 \tag{B.10a}$$

$$\mathbf{P}(\boldsymbol{\delta}) \succ 0 \qquad \forall\, \boldsymbol{\delta} \in \boldsymbol{\Delta}_0 \tag{B.10b}$$

$$\mathbf{A}_j^T\mathbf{P}_j + \mathbf{P}_j\mathbf{A}_j \succeq 0 \qquad \text{for } j = 1, \cdots, k \tag{B.10c}$$

Here, $\mathbf{A}(\boldsymbol{\delta}) = \mathbf{A}_0 + \sum_{j=1}^k \delta_j \mathbf{A}_j$ *and* $\mathbf{P}(\boldsymbol{\delta}) = \mathbf{P}_0 + \sum_{j=1}^k \delta_j \mathbf{P}_j$*. Moreover, in that case* $V(\mathbf{x}, \boldsymbol{\delta}) := \mathbf{x}^T\mathbf{P}(\boldsymbol{\delta})\mathbf{x}$ *is a quadratic parameter-dependent Lyapunov function for the system.*